Winter 11-9-2023

Mechanosensitive Ion Channels as Therapeutics Targets for Osteoarthritis

Alireza Savadipour
Washington University – McKelvey School of Engineering

WASHINGTON UNIVERSITY IN ST. LOUIS

McKelvey School of Engineering
Department of Mechanical Engineering and Materials Science

Dissertation Examination Committee:
Farshid Guilak, Chair
Matthew Bersi
Spencer Lake
Simon Tang
Jessica Wagenseil

Mechanosensitive Ion Channels as Therapeutics Targets for Osteoarthritis

by

Alireza Savadipour

A dissertation presented to
the McKelvey School of Engineering
of Washington University in
partial fulfillment of the
requirements for the degree
of Doctor of Philosophy

December 2023
St. Louis, Missouri

Table of Contents

List of Figures

List of Tables

Acknowledgments

I would like to express my sincerest gratitude to my mentor, Dr. Farshid Guilak, whose continuous support, insightful guidance, and infectious enthusiasm were pivotal throughout my research journey and broader academic career. Your unwavering faith in my capabilities, coupled with the freedom you provided to explore diverse avenues, significantly contributed to my personal and professional growth. Furthermore, I am grateful for your mentorship beyond the academic sphere, including career development and support for my involvement in various extracurricular activities.

I am deeply indebted to all the members of the Guilak Lab for creating a stimulating and supportive environment that fostered creativity, collaboration, and scientific excellence. Special thanks go to Dr. Robert Nims, an invaluable collaborator on this dissertation, and also the person who trained me in the lab to become the scientist I am today. A heartfelt thank you to Bob for his relentless support, humor, and for making the lab feel like a second home. I am also grateful to the entire research team, especially Neda Rashidi, Gabi Marushack, Amanda Cimino, Jackie Garcia, Ruhang Tang, Sara Oswald, for their constructive feedback, innovative ideas, and camaraderie that made this journey both enjoyable and rewarding.

Additionally, I would like to express my gratitude to the broader research community at Washington University in St. Louis, particularly the Department of Mechanical Engineering and Materials Science, Center for Regenerative Medicine, Department of Orthopedics Surgery, and Shriners Hospital for Children, for their financial support. The research presented in this dissertation would not have been possible without the generous funding from the National

Institute of Health, Arthritis Foundation, Shriners Hospitals for Children, MNO Hospitals for Children, and the National Institutes of Health (List of Grant Numbers).

My sincere appreciation goes to my dissertation committee - Dr. Spencer Lake, Dr. Jessica Wagenseil, Dr. Simon Tang, and Dr. Matthew Bersi - for their invaluable feedback, encouragement, and guidance throughout the development of this thesis.

Beyond the professional sphere, I am eternally grateful to my friends and family for their unwavering support and belief in me throughout my academic journey. To my parents, your love and encouragement have been my pillars of strength, and I am immensely thankful for everything you have done for me. To my brother, thank you for your constant encouragement and for always being there for me, in good times and bad. Lastly, to my partner, Marianna, your love, support, and patience have been my rock, and I am incredibly fortunate to have you by my side.

In conclusion, this journey has been both challenging and rewarding, and I am deeply thankful to everyone who contributed to its success. Your support, both professional and personal, has been invaluable, and I am incredibly grateful for the opportunity to learn from and work alongside each of you.

Alireza Savadipour

Washington University in St. Louis

December 2023

Dedicated to my supportive parents and grandparents, encouraging brother, and loving partner.

ABSTRACT OF THE DISSERTATION

Mechanosensitive Ion Channels as Therapeutics Targets for Osteoarthritis

by

Alireza Savadipour

Doctor of Philosophy in Mechanical Engineering

Washington University in St. Louis, 2023

Professor Farshid Guilak, Chair

Osteoarthritis (OA) is a common degenerative joint disease characterized by the degenerative changes in joint cartilage and underlying bone. It commonly occurs in weight-bearing joints like the knees, hips, and spine but can affect any joint in the body, resulting in symptoms such as pain, stiffness, and reduced range of motion. Post-traumatic osteoarthritis (PTOA) is a subtype of OA that occurs after a joint injury, such as a fracture, dislocation, or ligament tear, causing damage to the cartilage and other joint tissues leading to OA over time. PTOA accounts for a significant proportion of all OA cases. OA is a major cause of disability worldwide and poses a significant economic burden on both individuals and healthcare systems, including direct medical costs like doctor visits, medications, and surgeries, and indirect costs like lost productivity due to absenteeism or disability. The total cost of OA is estimated to be several percent of a country's GDP. Epidemiologically, OA is one of the most common chronic diseases, affecting millions worldwide. Its prevalence increases with age and is more common in women than in men. Other risk factors include obesity, joint injury, and repetitive use of certain joints. PTOA can affect individuals of any age and is often associated with sports injuries or accidents. It is estimated that about 12% of all OA cases are post-traumatic. Despite its

prevalence and associated costs, there is no cure for OA or PTOA, and current treatments primarily focus on managing symptoms and improving joint function. These treatments include pain relievers (such as acetaminophen or nonsteroidal anti-inflammatory drugs), physical therapy, joint injections (such as corticosteroids or hyaluronic acid), and in severe cases, joint replacement surgery. However, these treatments often have limitations in terms of efficacy, side effects, and the fact that they do not stop the progression of the disease. For example, pain relievers can cause gastrointestinal issues, kidney or liver damage, and an increased risk of heart attack or stroke; injections may provide temporary relief but do not address the underlying cause of the disease, and joint replacement surgery is a major procedure with associated risks and a long recovery time. Preventive measures, such as maintaining a healthy weight, staying active, and avoiding joint injuries, can help reduce the risk of developing OA. For PTOA, prompt and appropriate treatment of joint injuries can help reduce the risk of developing OA later on. Therefore, finding new targets for drug development in OA is critically important to develop more effective and safer treatments that can stop or slow the progression of the disease, rather than just managing the symptoms.

Therefore, we first sought to investigate the role of different mechanosensors is translating different mechanical cues such as hydrostatic pressure and mechanical compression. We used primary porcine chondrocytes and either encapsulated them in agarose hydrogel or plated them on coverslip to apply hydrostatic pressure and mechanical compression on them respectively. First, we showed that TRPV1 channel is the mechanosensory of hydrostatic pressure since blocking this channel using its specific inhibitor increased the production of sGAG that was induced by hydrostatic pressure. On the other hand, we demonstrated that PIEZO1 channel, is the only channel in the PIEZO family that responds to high magnitudes of

mechanical strain and injurious loads. We also showed that PIEZO1 is sensitive to membrane tension and manipulating the membrane can regulate the sensitivity of the PIEZO1 channel to both chemical and mechanical stimuli. Additionally, we observed that PIEZO1 channel is sensitive to rate of loading, and they need intracellular and extracellular Ca^{2+} sources to be able to response to mechanical compression. Lastly, we took a novel approach and combined our experimental data with finite element modeling and determined the membrane strain threshold required for the PIEZO1 channel to get activated.

For the purpose of finding how regulating the PIEZO channels sensitivity can affect the progression of OA and PTOA, we investigated the role of polyunsaturated fatty acids including ω3 and ω6 fatty acids in regulating the functionality of the PIEZO channels. We showed that both ω3 and ω6 fatty acids were able to reduce the sensitivity of the PIEZO channels to both chemical and mechanical stimuli. Furthermore, we showed that supplementation of ω6 fatty acids increase the level of inflammatory biomarker IL-6 and senescence marker MMP3 compared to the control. However, treating the chondrocytes with ω3 decreased the level of IL-6, MMP3, and other senescence factor P53 showing the effect of ω3 fatty acids on reducing inflammation and cellular aging.

Lastly, we assessed the role of voltage gated Ca^{2+} channels (VGCCs) in regulating the PIEZO channels activity and see if the downstream effect of inhibiting the VGCCs on PIEZOs can be used as a therapeutic for OA and PTOA. We showed that blocking the L-type VGCCs activity using their specific antagonist Nifedipine can reduce the sensitivity of the PIEZO channels. However, blocking the T-type VGCCs activity using NNC-55 would significantly increase the sensitivity of the PIEZO channels. Moreover, we demonstrated that treating cartilage

explants with Nifedipine would rescue the cartilage under injury, although, blocking the T-type channels induce more cell death in an injured cartilage explant.

Overall, understanding the mechanisms by which chondrocytes respond to physiologic or pathological cartilage loading is crucial for the development of new pharmacologic therapies to treat mechanically-regulated conditions such as PTOA. Our research has shown that dietary polyunsaturated fatty acids (PUFAs) can reduce the mechanosensitivity of PIEZO channels in chondrocytes in response to deformation, thereby elucidating the role of mechanobiology in cartilage health and disease. Moreover, ω3 PUFAs were able to decrease the inflammatory and senescence markers in chondrocytes elucidating their positive effect on cell health. Additionally, we found that hypo-osmotic conditions, which may occur in early OA, can sensitize PIEZO activation of chondrocytes by increasing the apparent membrane tension. Furthermore, intracellular Ca^{2+} activation is sensitive to the rate of loading, potentially due to the viscoelasticity of the cell or membrane. Lastly, we demonstrated that inhibiting the activity of the L-type VGCCs can rescue the cartilage under injury through regulating the activity of the PIEZO channels. These findings not only provide new insights into developing future OA therapeutics but also underscore the importance of understanding the intersection of different mechanisms involved in chondrocyte mechanotransduction. This knowledge can open new pathways for the development of pharmacologic therapies to treat mechanically-regulated conditions such as PTOA.

Chapter 1: Overview of Musculoskeletal System, Diseases, Mechanics, and Mechanotransduction

Partially adapted from: Savadipour, A., Palmer, D., Ely, E. V., Collins, K. H., Garcia-Castorena, J. M., Harissa, Z., Kim, Y. S., Oestreich, A., Qu, F., Rashidi, N., Guilak, F. (2023) The role of PIEZO ion channels in musculoskeletal system. AJPCP, 324(3), C728-C740.

1.1 Articular cartilage

Articular cartilage is a specialized connective tissue that endures millions of cycles of mechanical loading annually under normal circumstances [1, 2]. It is capable of withstanding stresses as high as 18 MPa and bearing loads that exceed body weight. For example, while walking, the load applied to articular cartilage in the knee joints is three times the body weight, and this increases to 10 and 20 times the body weight while running and jumping, respectively [3, 4]. Therefore, articular cartilage must possess highly specialized mechanical properties to withstand these substantial mechanical loads. Structural degeneration of articular cartilage results in severe pain and loss of functionality. Moreover, articular cartilage is an avascular and aneural tissue [5-10], meaning it lacks blood vessels and nerves. As a result, it has a limited ability to repair itself or prevent further injury. The prevailing treatment for osteoarthritis (OA) primarily consists of painkillers that alleviate OA symptoms but do not address the underlying cause of pain, which is often the cartilage breakdown or damage that has occurred or is ongoing. Consequently, more effective therapies are needed for OA treatment, and the development of new drugs relies on a better understanding of how the tissue responds to mechanical and biological factors.

The structure and composition of articular cartilage are key to its unique mechanical properties. It is composed of water, collagen, proteoglycans, and chondrocytes. Water makes up 65-80% of its weight, while collagen, primarily type II, forms a mesh-like network that provides tensile strength and helps to distribute compressive forces [11, 12]. Proteoglycans, composed of a core protein and glycosaminoglycan (GAG) side chains, create a charged, hydrated gel that imparts compressive resistance [13-15]. Chondrocytes, the only cell type in articular cartilage, are responsible for the production and maintenance of the extracellular matrix (ECM), which includes collagen and proteoglycans [16, 17]. However, articular cartilage is not a homogeneous tissue; its properties vary from the surface to the deep layer, adapting to the mechanical demands at each depth. The superficial zone has a higher concentration of collagen fibers oriented parallel to the surface, enabling it to withstand tensile and shear forces. Meanwhile, the deep zone contains more proteoglycans and collagen fibers oriented perpendicular to the joint surface, providing resistance to compressive forces [18-21].

Chondrogenesis, the process of cartilage formation, is regulated by several genes that are crucial for the development and maintenance of articular cartilage. SOX9, a transcription factor, is a key regulator of chondrogenesis and is required for the expression of cartilage-specific genes, such as ACAN (aggrecan) and COL2A1 (collagen type II alpha 1) [22-26]. ACAN encodes aggrecan, a major proteoglycan in the cartilage ECM that provides resistance to compression. COL2A1 encodes the alpha-1 chain of type II collagen, the main collagen type in cartilage that forms the fibrillar network in the ECM. Other important genes include COMP (cartilage oligomeric matrix protein), which is involved in collagen fibril assembly and interacts with other ECM proteins, and MMPs (matrix metalloproteinases), which are involved in ECM

remodeling and degradation [27-29]. Dysregulation of these genes can lead to cartilage degradation and the development of OA.

Understanding the mechanobiology of articular cartilage is crucial for developing novel therapies for OA. Mechanical loading influences chondrocyte behavior and ECM composition, both of which are altered in OA. For instance, physiological mechanical loading promotes chondrocyte biosynthesis and maintenance of the ECM, while excessive or abnormal loading can lead to cartilage degradation and the development of OA. Hence, elucidating the mechanisms by which articular cartilage responds to mechanical and biological factors is essential for developing targeted interventions that not only alleviate pain but also address the underlying cause of cartilage breakdown and disease progression.

1.2 Mechanical loading and articular cartilage

Mechanical loading on articular cartilage is a fundamental aspect of joint function and plays a crucial role in maintaining the health and integrity of the cartilage [30-32]. Articular cartilage is a specialized connective tissue that covers the ends of bones in synovial joints, providing a smooth and lubricated surface for joint movement. It is composed of chondrocytes, which are the cells responsible for producing and maintaining the extracellular matrix (ECM), which consists of a network of collagen fibers, proteoglycans, and water.

The mechanical properties of articular cartilage are primarily determined by the composition and organization of its ECM [33, 34]. The collagen fibers provide tensile strength and resist deformation, while the proteoglycans trap water and provide resistance to compression [12, 13, 35-39]. Together, they give articular cartilage its unique biomechanical properties,

which allow it to withstand the high mechanical loads encountered during daily activities, such as walking, running, or jumping.

1.2.1 Different Types of Mechanical Loading

Compression: This is the most common type of mechanical loading experienced by articular cartilage. It occurs when two opposing forces are applied to the cartilage, causing it to deform. Compression is essential for maintaining the health and integrity of the cartilage, as it promotes the exchange of nutrients and waste products between the cartilage and the synovial fluid [30-32, 40-45]. It also stimulates chondrocytes to produce ECM components, such as collagen and proteoglycans, which are essential for maintaining the mechanical properties of the cartilage [46]. However, excessive or abnormal compression can lead to cartilage degeneration and osteoarthritis [47, 48].

Shear: This type of loading occurs when two opposing forces are applied parallel to the surface of the cartilage, causing it to deform. Shear forces are less common than compressive forces in articular cartilage but can occur during activities that involve rotational movements, such as twisting or pivoting. Shear forces can also be generated during joint instability or misalignment. Prolonged or excessive shear forces can lead to cartilage degradation and osteoarthritis [49].

Hydrostatic pressure: This is the pressure exerted by a fluid in equilibrium at a given point within the fluid, due to the force of gravity. Articular cartilage is exposed to hydrostatic pressure from the synovial fluid surrounding the joint [50]. This pressure helps to maintain the shape and volume of the cartilage during compression and is essential for maintaining the health and integrity of the cartilage [50-54].

1.2.2 Importance of Studying Mechanical Loading

Studying the effects of mechanical loading on articular cartilage is essential for several reasons:

Maintenance of Cartilage Health: Mechanical loading is crucial for maintaining the health and integrity of articular cartilage [30-32, 40-45]. It promotes the exchange of nutrients and waste products between the cartilage and the synovial fluid, stimulates chondrocytes to produce ECM components, and helps maintain the mechanical properties of the cartilage [30-32, 42-45]. Understanding how different types of mechanical loading affect cartilage health can help develop strategies to prevent cartilage degeneration and osteoarthritis.

Development of Osteoarthritis: Osteoarthritis is a degenerative joint disease characterized by the progressive loss of articular cartilage [10, 47, 48]. Abnormal mechanical loading, such as excessive or uneven compression, shear, or hydrostatic pressure, is a major risk factor for the development of osteoarthritis [10, 47, 48]. Understanding how different types of mechanical loading contribute to cartilage degradation and osteoarthritis can help develop strategies to prevent or treat this disease.

Design of Joint Replacement Implants: Joint replacement surgery is a common treatment for advanced osteoarthritis. The success of joint replacement implants depends on their ability to replicate the natural biomechanics of the joint and distribute mechanical loads evenly across the articular cartilage [55, 56]. Understanding the effects of mechanical loading on articular cartilage can help design better joint replacement implants that can reduce the risk of implant failure and improve patient outcomes.

In conclusion, mechanical loading is crucial for maintaining the health and integrity of articular cartilage and plays a significant role in the development of osteoarthritis. Understanding the effects of different types of mechanical loading on articular cartilage can provide valuable insights into the prevention and treatment of osteoarthritis and the design of joint replacement implants.

1.3 Mechanotransduction

Mechanotransduction refers to the series of events through which cells convert mechanical signals into biochemical responses. This process is crucial for several physiological functions, including cell growth, differentiation, migration, and gene expression [57-74]. It is also implicated in various pathophysiological conditions, such as cancer, cardiovascular diseases, and osteoarthritis [57, 65, 75-95].

The mechanotransduction process begins with the perception of a mechanical stimulus by mechanosensors, which are specialized proteins or protein complexes located in the cell membrane or the cytoskeleton. These mechanosensors can be ion channels, integrins, or other cell adhesion molecules, and their activation leads to a cascade of intracellular events, involving various signaling molecules and pathways, ultimately resulting in a specific cellular response.

1.3.1 Biological mechanosensors

Ion channels: These are proteins that allow ions to pass through the cell membrane in response to a mechanical stimulus. One well-known example is the Piezo channels, which are non-selective cation channels that are activated by mechanical forces, such as stretch or pressure, applied to the cell membrane [96-100]. Another example is the TRP (transient receptor potential)

channels, a family of ion channels that can be activated by various mechanical stimuli, such as stretch, osmotic stress, or shear stress [101, 102].

Integrins: These are transmembrane proteins that mediate cell adhesion to the extracellular matrix (ECM) and play a crucial role in mechanotransduction [103-106]. Integrins can sense changes in the mechanical properties of the ECM, such as stiffness or topography, and transmit these signals to the intracellular signaling machinery [103-106]. This leads to the activation of various signaling pathways, such as the focal adhesion kinase (FAK) and mitogen-activated protein kinase (MAPK) pathways, which regulate cell proliferation, migration, and differentiation [63, 103-109].

Cell adhesion molecules: Besides integrins, other cell adhesion molecules, such as cadherins and selectins, can also act as mechanosensors [62, 110-113]. Cadherins are Ca^{2+} -dependent adhesion molecules that mediate cell-cell adhesion and play a crucial role in tissue morphogenesis and maintenance [62, 110-113]. Mechanical forces applied to cadherins can induce conformational changes and activate intracellular signaling pathways, such as the β-catenin pathway, which regulates gene expression and cell proliferation [114].

Cytoskeletal proteins: The cytoskeleton, composed of actin filaments, microtubules, and intermediate filaments, plays a crucial role in cell shape, motility, and mechanical integrity [115-135]. It is also involved in mechanotransduction, as mechanical forces applied to the cell can induce conformational changes in cytoskeletal proteins, leading to the activation of various signaling pathways. For example, mechanical stretch applied to actin filaments can activate the RhoA/ROCK pathway, which regulates actin cytoskeleton remodeling and cell contractility [136-147].

Mechanotransduction is not only limited to the perception of mechanical forces by mechanosensors but also involves the conversion of these mechanical signals into biochemical responses. This involves various signaling molecules and pathways, such as protein kinases, phosphatases, GTPases, and second messengers, such as Ca^{2+} and cAMP [148-152]. These signaling molecules and pathways regulate various cellular processes, such as gene expression, cell proliferation, migration, and differentiation, in response to mechanical signals [148-152].

In conclusion, mechanotransduction is a complex process that involves various mechanosensors, signaling molecules, and pathways, and plays a crucial role in various physiological and pathophysiological conditions. Understanding the molecular mechanisms involved in mechanotransduction can provide valuable insights into the development of novel therapeutic strategies for various diseases, such as osteoarthritis.

1.4 TRP channels

Transient receptor potential (TRP) family of ion channels are nonselective cation channels that respond to various physical and chemical stimuli, such as osmotic shock, mechanical loading, shear stress, and changes in temperature [153-163]. These channels are necessary for various sensations such as touch, taste, and hearing, and are expressed in different tissues such as the brain, liver, kidney, and chondrocytes [54, 164-186]. This family of ion channels divides into several subgroups such as TRPV, TRPC, TRPA, TRPN, TRPM, TRPP, and TRPML that are phylogenetically-related and share similarities in protein structure. Further, each subgroup has several members, each of which has a unique protein structure and unique modes of channel activation. Of particular interest for the field of musculoskeletal medicine are the TRPV and TRPC subgroups members which are well documented to have mechanically-

sensitive modes of channel activation. For example, TRPV1, TRPV2, and TRPV4 channels from the TRPV subgroup are known to be sensitive to hypo-osmotic shock and mechanical loading such as stretch and shear flow [176, 187-194]. It has been previously shown that the global knockout of TRPV4 increased the risk of OA in mice on a high-fat diet, however, mice with specific cartilage knockout of TRPV4 were protected from age-related OA but not PTOA [195, 196]. Furthermore, O'Conor et al. showed that the presence of TRPV4 is necessary for mechanically-enhanced matrix production in chondrocytes [197]. Moreover, TRPV1 is an essential component in sensing burning pain and hydrostatic pressure [54, 198-204]. In the TRPC subgroup, it has been shown that the TRPC1 channel is necessary for skeletal muscle differentiation and bone formation [205, 206]. Furthermore, the TRPC3 channel has been shown to have essential roles in the function of the brain, cardiovascular, and immunity systems [207, 208]. Consequently, this family of ion channels is necessary for the homeostasis and health of the cartilage especially in the mechanotransduction of the chondrocytes.

1.5 PIEZO channels

1.5.1 Structure and function of PIEZO

PIEZO1 and PIEZO2 are multi-pass transmembrane proteins that serve as mechanosensitive cationic ion channels, directly activated by membrane stretch [209-211]. Both channels are expressed in numerous mechanosensitive tissues, with PIEZO1 found more prominently in non-sensory tissues exposed to mechanical loading, fluid pressure, and shear, and PIEZO2 found more abundantly in sensory tissues involved in touch and pain [212]. First identified in 2010 by Coste et al. as homologs of the genes Fam38a and Fam38b [209], numerous studies have since demonstrated their expression in nearly all organ systems, including

pulmonary, urinary, cardiovascular, musculoskeletal, and nervous systems, where they contribute towards tissue mechanosensation, development, and homeostasis, as well as cellular migration, differentiation, proliferation, apoptosis, and senescence.

PIEZO channels have a unique structure comprised of three subunits, each containing a curved blade with 26 transmembrane helices, which extend outwards from a central pore region with 12 transmembrane helices [210, 211, 213]. These blades are connected to the central pore by a beam domain [210, 211, 213]. The combination of the three subunits forms the large (2,547 residues and 2,822 residues for PIEZO1 and PIEZO2, respectively), propeller-like structure of the PIEZO channels [210, 211, 213]. PIEZO1 and PIEZO2 only share 42% homology, and this difference results in structural alterations between the two, with PIEZO1 containing a more dilated central pore when closed (4.5 angstroms versus 0.9 angstroms), reduced transmembrane height (140 angstroms vs 170 angstroms), and a contracted outer diameter (185 angstroms versus 280 angstroms) with more tightly spiraling blades in the clockwise direction [213, 214]. Despite these differences, PIEZO1 and PIEZO2 share a similar structure and are believed to gate in a similar manner. Studies have shown PIEZO1 responds directly to membrane stretch, while other studies have suggested that PIEZO2 may require interaction with intracellular and/or extracellular molecules to transduce membrane stretch [213-219].

Multiple studies have shown that PIEZO channels respond to various types of mechanical stimuli which induce membrane stretch, including cellular compression and tension, shear stress, and changes in substrate stiffness, as well as electrical stimuli in the form of voltage shifts [210, 212, 217, 220]. Mechanistically, research suggests that membrane stretch deforms the blade regions, with the beam domains potentially acting as a lever arm to convert this deformation into minute motions within the pore to activate the channel and allow cation influx into the cell [211,

221]. However, other studies have activated mutant PIEZO1 and PIEZO2 channels missing the proximal end of the beam domain, calling the proposed lever-like function of the beam domain into question [222]. Evidence also suggests that the blades induce some warping of the surrounding membrane, which serves to magnify local strain surrounding the channel, increasing sensitivity to membrane stretch [211, 223].

Once activated, PIEZO1 is permeable to most monovalent and divalent cations with a hydrated diameter (diameter of ion plus bound water molecules) less than the open pore diameter of ~8 angstroms. PIEZO1 displays the greatest permeability to K^+, followed by Na^+ and Cs^+, with divalent cations Ca^{2+} and Mg^{2+} exhibiting lower permeability [224]. However, PIEZO1 displays a slight selectivity preference for Ca^{2+} [209]. The high affinity of Ca^{2+} for PIEZO1 causes Ca^{2+} to travel slowly through the pore and momentarily block conductance of monovalent ions such as K^+ [224]. The ion permeability and selectivity of PIEZO2 has not been characterized as clearly, but data suggests it non-selectively conducts cations [209, 225].

The triskelion structure of PIEZO channels allows for direct activation by membrane stretch, with PIEZO1 achieving half-maximal activation at pressures of -27 ± 3.4 mmHg [221]. However, interactions with other cellular factors such as the actin cytoskeleton, extracellular matrix (ECM) proteins, integrins, and cell membrane lipid composition, as well as certain small molecules and peptides, can shift the threshold required for activation [221]. The synthetic small molecule Yoda1, as well as the more recently discovered Jedi1 and Jedi2, reduce the half-maximal activation pressure of PIEZO1 (-15.1 ± 0.9 and -16.7 ± 2.2 mmHg for Yoda1 and Jedi1, respectively) [220, 221]. Evidence suggests that these synthetic compounds alter how the beam domain transduces blade motion to the pore, encouraging activation at lower magnitudes of membrane stretch and energetically stabilizing the open channel configuration [221, 226, 227].

Despite their similar effect on PIEZO1, Jedi1 and Jedi2 do not share any structural similarity with Yoda1, with Jedi1 and Jedi2 displaying rapid activation, decay, and reversibility, while Yoda1 results in slow activation with no decay and poor reversibility [221]. A small inactive form of Yoda1, called Dooku1, may be used to antagonize the effects of Yoda1, but does not inhibit the activity of constitutive PIEZO1 channels [228].

Currently, there are no known small molecule agonists for PIEZO2, and the magnitude of stimuli required for PIEZO2 gating are still being determined [212]. Several polycationic channel inhibitors, including ruthenium red, gadolinium chloride, and GsMTx-4, effectively block PIEZO1 and PIEZO2 activation [209, 229]. Ruthenium red inhibits PIEZO1 and PIEZO2 by blocking the open pore on the extracellular side in a voltage-dependent manner [230]. Gadolinium chloride does not interact with ion channels directly, but rather binds to phospholipids and compacts the cellular membrane surrounding the ion channel to prevent opening [231]. Similarly, GsMTx-4, a peptide derived from spider venom, inserts into the outer layer of the surrounding cell membrane and interferes with its ability to transduce tension to the ion channel. Some models suggest this occurs primarily through increasing the surrounding phospholipids' deformational capacity [232], while others propose the effect is simply due to GsMTx-4 taking up space in the membrane, increasing its functional surface area to reduce tension [233].

Various mutations in PIEZO1 and PIEZO2 channels can result in a range of phenotypic effects, ranging from minor adaptations to major disease phenotypes, primarily due to how the mutation affects PIEZO activation. Here we review the contributions of PIEZO1 and PIEZO2 to the development and function of the neuro-musculoskeletal system, with examples of how dysregulation of these channels can have major consequences for tissue function. Finally, we

will discuss the potential for modulating PIEZO activity as a therapeutic strategy to treat musculoskeletal diseases and enhance tissue regeneration (Figure 1).

1.5.2 Role of PIEZO channels in cartilage and chondrocytes

Chondrocytes have been shown to require an average of 256nm cell indentation to induce a Ca^{2+} influx, and this response was significantly reduced by knocking down either Piezo1 or Trpv4 [234]. Cyclic tensile strain ranging from 3-18% deformation induced an increase in TRPV4, PIEZO1, and PIEZO2 protein levels in primary murine chondrocytes, and inhibiting these channels decreased Ca^{2+} influx at each loading magnitude [235]. Increasing substrate stiffness decreased PIEZO1 and PIEZO2 protein expression [236]. Mechanical compression of whole chondrocytes to >50% deformation via atomic force microscopy induced high levels of Ca^{2+} influx in primary porcine chondrocytes, mediated synergistically by PIEZO1 and PIEZO2 [237]. Lastly, applying one hour of cyclic loading to human chondrocytes encapsulated in polyethylene glycol (PEG) hydrogels for up to 14 days has been demonstrated to increase PIEZO1 protein expression [238].

Inflammatory damage and degeneration often associated with OA can also affect PIEZO1 expression. PIEZO1 upregulation has been shown in primary porcine chondrocytes treated with Interleukin-1α (IL-1α), which mimics similar increases in expression observed in osteoarthritic cartilage [85]. Heightened PIEZO1 expression elevated Ca^{2+} transients and loosened the f-actin network, which decreased cellular Young's Modulus [85]. Upon inhibition of PIEZO1 via GsMTx4 or depletion of PIEZO1 with PIEZO1-targeting small interfering RNA (siRNA), actin loosening was no longer observed [85]. These data suggest that PIEZO1 contributes to a pathologic feedforward mechanism by elevating Ca^{2+} transients, loosening the actin

cytoskeleton, and contributing to a pathogenetic remodeling of cartilage, contributing to the development of OA [85].

Evidence suggests that expression and activation of PIEZO1 may be linked to senescence in chondrocytes. PIEZO1 mRNA and protein levels were significantly increased in human chondrocytes induced to senescence, and hyperphysiologic strain elevated senescence pathologies such as DNA damage, enlarged cell nuclei, and increased expression of Il6, Cyclin-Dependent Kinase Inhibitor 1A (Cdkn1a/P21) and Cyclin-Dependent Kinase Inhibitor 2A (Cdkn2a/P16) in murine and human chondrocytes [239, 240]. Application of hyperphysiologic compressive loads to murine knee joints also increased the number of Cdkn1a/P21-, and Cdkn2a/P16-positive cells and decreased proteoglycan production [240]. PIEZO1 knockdown reversed senescence-related phenotypes, lowering senescence-related gene expression, ROS levels, and intracellular Ca^{2+} concentration [239]. Yoda1 treatment increased senescence phenotypes, while intracellular Ca^{2+} chelation inhibited the effects of Yoda1, indicating the importance of Ca^{2+} signaling to the development of senescence [239].

Various studies have shown that intracellular Ca^{2+} concentration, modulated by PIEZO1 and PIEZO2, plays a critical role in cell death and apoptosis as well. Hyperphysiologic compression of bovine cartilage explants induced cell death and glycosaminoglycan release [241]. Meanwhile, knocking down PIEZO1 in human chondrocytes was shown to reduce cell death induced by corticotropin-releasing factor receptor 1 antagonist [242]. Urocortin-1 (UCN), a member of the corticotropin-releasing factor family of genes, mitigated cell death and Ca^{2+} overload experienced when PIEZO1 was activated either by Yoda1 or injurious mechanical loads in porcine cartilage explants [242, 243]. Chondrocytes from patients with OA displayed reduced mRNA and protein levels of G protein coupled estrogen receptor (GPER), a key anti-apoptotic

protein. PIEZO1 knockdown increased GPER expression at mRNA and protein levels in response to 20% tensile loading [244]. PIEZO1 inhibition via GsMTx-4 has also been shown to protect against apoptosis induced by hyperphysiologic mechanical stress [245]. Recent work has also shown that PIEZO1 activation drives apoptosis and cartilage degeneration by inducing lysosome dysfunction in C57BL/6 murine chondrocytes [246]. However, these pathologies were completely abolished by knocking down PIEZO1 with siRNA or inhibiting with GsMTx-4 [246]. Mice with induced OA via destabilization of the medial meniscus were also treated with GsMTx-4, and displayed suppressed OA progression, cartilage degeneration, and apoptosis within the joint [246].

The involvement of PIEZO1 in multiple chondrocyte processes such as inflammation, senescence, and apoptosis suggests that PIEZO1 activation likely modulates gene expression. Although the mechanism by which PIEZO1 activation regulates gene expression and which genes it regulates are still being explored, it is known that PIEZO1 activation can trigger several transient cell responses such as cytoskeletal remodeling and activation of the YAP-Tafazzin (TAZ) pathway [85, 247]. Furthermore, ongoing transcriptomics work has suggested several genes may be uniquely responsive to PIEZO1, including a gene regulatory network governed by hub gene Hypoxia Inducible Factor 1 Subunit Alpha (HIF1A) [248].

Taken together, these studies highlight the important role of PIEZO channels in articular cartilage and suggest that targeting PIEZO channels to reduce inflammation, senescence, and apoptosis in response to mechanical loading has therapeutic potential. However, more studies are required to investigate the down-stream effects of modulating the activity of these channels prior to development of potential therapeutics.

1.5.3 Role of PIEZO channels in muscle

Skeletal muscle is a hierarchically organized tissue which provides stability and movement for the musculoskeletal system [249]. Each muscle is composed of bundles of fascicles, which are in turn composed of multiple myofibers [249]. Myofibers are long, multinucleated cells formed by the fusion of myoblasts during development [249]. Skeletal muscle is well-vascularized and innervated, allowing for coordinated motor activity [249]. However, when muscle tissue is damaged or degenerated, skeletal muscle must rely on skeletal muscle stem cells (MuSCs, also referred to as "satellite cells"), a population of quiescent adult stem cells within muscle fibers, for regeneration [250, 251]. Activated MuSCs proliferate and subsequently differentiate into myoblasts, which fuse to existing myofibers or generate new ones to repair damaged muscle tissue[251]. Multiple studies suggest that PIEZO1 contributes to the mechanosensation required to regulate MuSC activation and proliferation and to maintain muscle mass and prevent muscle atrophy.

Loss-of-function (LOF) studies performed using the MuSC marker Paired Box 7 (*Pax7*) to drive constitutive Cre recombinase action (a constitutive $Pax7^{Cre};Piezo1^{f/f}$ mouse line) to knock out *Piezo1* in MuSCs suggest that MuSC mechanosensation modulates the dynamics of activation and differentiation via mechanosensitive ion channel PIEZO1, with drastic effects on muscle regeneration outcomes[251, 252]. *Piezo1* knockout resulted in an 80% reduction in the number of MuSCs and dysregulation of MuSC activation in the remaining population. *Piezo1*-deficient mice also displayed reduced MuSC activation and proliferation, with most MuSCs remaining in a quiescent state[252]. Meanwhile, Yoda1 treatment prevented this shift and increased muscle regeneration. These data indicate that PIEZO1 plays a vital role in regulating and maintaining the MuSC population[251, 252].

Tamoxifen-inducible *Pax7*^{CreERT2}*;Piezo1*$^{f/f}$ mice have been used to isolate the effects of PIEZO1 on MuSCs in adult muscle tissue from the effects of *Piezo1* depletion during development. This model demonstrated that *Piezo1* knockout reduces myogenic differentiation of MuSCs as well as MuSC proliferation following muscular injury[251]. Furthermore, injured mice displayed delayed formation of myofibers and reduced myofiber diameter. Most notably, repetitive injury completely ablated the quiescent *Pax7*$^{+}$ MuSC population in *Pax7*^{CreERT2}*;Piezo1*$^{f/f}$ mice[251]. PIEZO1 inhibition also drastically reduced myoblast fusion, a later step in myogenesis following MuSC activation [253]. Conversely, treatment with Yoda1 significantly increased myoblast fusion. *Piezo1* knockdown also reduced f-actin accumulation, indicating that PIEZO1 may play a role in cytoskeletal remodeling during myoblast differentiation [253].

Evidence suggests that PIEZO1 helps maintain muscle mass and prevent muscle atrophy. Mouse limb immobilization has been correlated with a downregulation of *Piezo1*, while intramuscular injection with Yoda1 has been shown to downregulate atrophy-associated genes [254]. Similarly, tamoxifen-inducible Cre models have been used to achieve skeletal muscle-specific knockdown of *Piezo1*, resulting in decreased muscle mass, decreased intracellular Ca^{2+} and increased expression of atrophy-associated genes *Klf15* and *Il6* upon tamoxifen induction [254]. These data align well with clinical findings, such as decreased *PIEZO1* expression and increased expression of Interleukin-6 (*IL6*) and other atrophy-associated genes in the skeletal muscle of patients following cast immobilization due to bone fractures [254]. Taken together, these data demonstrate that PIEZO1 plays a vital role in the maintenance and regeneration of healthy skeletal muscle and suggest that PIEZO1 may be a key therapeutic target for muscle regeneration and treatment of muscle atrophy.

1.5.4 Role of PIEZO channels in tendon

Tendons are dense, load-bearing connective tissues that transmit muscle forces to bone. Tendons contain a hierarchical structure of type I collagen positioned in a load-bearing direction, producing a highly anisotropic tissue that is ideally suited for transmission of uniaxial tensile strain [255]. Tendons are home to a diverse and heterogenous cell population, including specialized fibroblastic populations known as tenocytes [256, 257]. Tenocytes produce ECM to maintain homeostasis in response to changing biomechanical stimuli [255]. Single-cell RNA sequencing studies have demonstrated that PIEZO1 is highly expressed in cells positive for tendon-specific markers Scleraxis (*Scx*) and Mohawk Homeobox (*Mkx*), and both inhibition and knock out studies suggest it plays key roles in transducing the loading environment of the tendon to the tenocyte, with both local and systemic effects[258-261]. Meanwhile, genotyping data has demonstrated that various gain-of-function (GOF) mutations in PIEZO1 range in effect from mild athletic advantages to severe pathologies [260-262].

Stretch induces a Ca^{2+} response via PIEZO1 activation in a strain-dependent manner in tendon explants from rat tails [261]. Shear stress alone activated a Ca^{2+} influx in rat tenocytes, indicating that shear stress from collagen fibers rubbing against one another may be the primary form of stimulus experienced by tenocytes during tendon loading. Tendon-specific, tamoxifen-inducible *Piezo1* knockout mice using *Scx* as a Cre recombinase driver ($Scx^{CreERT2};Piezo1^{f/f}$ mouse line) displayed a 40% reduction in PIEZO1 following tamoxifen injection and resulted in decreased stretch-induced Ca^{2+} influx, as well as a 10% reduction in fascicle stiffness despite no changes in fascicle diameter [261]. The incomplete knockdown of PIEZO1 reported many have been due to tendon heterogeneity, as other studies have reported multiple tenocyte populations, some of which do not express *Scx* [257]. However, stimulating wild-type fascicles with Yoda1 for

16 days *in vitro* resulted in a 4.1% increase in stiffness, which corelates well with physiological increases in tendon stiffness observed during high-strain exercise regiments of similar duration, indicating that PIEZO1 activation likely plays a key role in driving anabolic tendon stiffening [261].

PIEZO1 also modulates the exercise pressor reflex, which elevates heart rate and blood pressure via sympathetic nerve activity during skeletal muscle and tendon stretch (Mitchell, 2008 #358). Achilles' tendon stretch in rats elicited a strong exercise pressor reflex, with intra-arterial injection of GsMTx4 significantly reducing that response [258]. Intermittent muscle contraction via sciatic nerve stimulation likewise induced a strong exercise pressor reflex, which was reduced by intra-arterial injection of GsMTx4 [258]. PIEZO1 inhibition by intra-arterial injection of GsMTx4 has also been reported to reduce the exaggerated exercise pressor reflex observed in rats with induced type 1 diabetes mellitus [259]. Since GsMTx4 is a non-specific PIEZO1 inhibitor, a transient receptor potential cation (TRPC) channel-specific blocker (SKF 96365) was also used, but SKF 96365 injection did not replicate the reduced exercise pressor reflex observed following GsMTx4 injection [259]. These studies indicate that PIEZO1 may transduce muscle and tendon stretch to drive the exercise pressor reflex, and that targeted blockade of PIEZO1 in muscle and tendon may have therapeutic potential in instances of exercise pressor reflex dysregulation.

The GOF mutations of *Piezo1* which affect tendon do so primarily through increasing PIEZO1 activation. The R2482H GOF *Piezo1* mutation has been shown to result in significantly greater jumping distance and maximum running speed, compared to wild-type controls [260]. Tenocytes from both constitutive and tamoxifen-inducible $Piezo1^{R2482H}$ mice displayed higher Ca^{2+} influx and upregulation of tendon-specific marker genes compared to wild-type tenocytes, when treated with Yoda1 [260]. $Piezo1^{R2482H}$ mice had wider Achilles tendons with greatly

increased elastic limit, which resulted in increased compliance, extension, and energy storage during loading [260]. In humans, the E756del mutation in *PIEZO1* results in a similar, although milder, GOF to the R2482H mutation used in the mouse model. The frequency of E756del variants in professional sprinting, jumping, and throwing human athletes is significantly higher than that of non-athletic controls [260]. Human carriers of the E756del GOF mutation also performed better at one-legged countermovement jumps compared to individuals with typical *PIEZO1* [261]. This suggests that *PIEZO1* GOF mutations in tendon may increase athletic performance for activities requiring sudden bursts of power and may be a target for improving tendon performance.

However, certain *PIEZO* mutations affecting muscle and tendon have also shown significant pathologic effects. Mutations of *PIEZO2* have been clinically associated with arthrogryposis, a phenotype of over 300 different known disorders, characterized by multiple joint contractures [263]. Specifically, studies have implicated *PIEZO2* mutations to several subtypes of Distal Arthrogryposis (DA), a subgroup referring to patients who specifically demonstrate distal joint contractures [264-267]. Dominant GOF mutations of *PIEZO2* have been shown to result in DA type 3 (DA3/Gordon Syndrome), DA type 5 (DA5), and Marden-Walker syndrome (Delle Vedove, 2016 #368;Haliloglu, 2017 #367)[268]. Patients with DA5 suffer from distal contractures, which are accompanied by additional symptoms such as limited ocular motility and ptosis, and in some cases by pulmonary disease [268]. Certain mutations are shared between syndromes, suggesting that each of these syndromes could be a unique manifestation of the same underlying condition [268]. This further underscores the need to conduct more robust genome-wide association studies, as well as more mechanistic studies to understand how *PIEZO* mutations cause malfunction and how these defects lead to disease progression.

1.5.5 Role of PIEZO channels in bone

Bone is a mineralized connective tissue in the musculoskeletal system that provides structure to the body and permits movement. Additionally, bone supports and protects internal organs, houses bone marrow, functions as a Ca^{2+} and phosphate mineral reservoir, and acts as an endocrine organ to regulate energy metabolism [269]. Appropriate levels of mechanical loading are required for bone homeostasis, as well as for skeletal development, growth, and fracture repair [270-272]. Bone adaptation to mechanical stimuli is primarily accomplished through mechanotransduction by osteocytes, which respond to mechanical loading by producing molecules that regulate bone remodeling [273, 274]. Ion channel activation and subsequent Ca^{2+} signaling represent an early response to mechanical activation in bone-resorbing osteoclasts and bone-forming osteoblasts [275-277]. As such, evidence suggests that PIEZO1 plays a key role in the development, homeostasis, and healing of bone, modulating interactions between osteoblast and osteoclast populations to encourage anabolic bone remodeling in response to increased loading.

Several animal studies have associated *Piezo1* deficiency during development with decreased bone formation rate, decreased bone size, and increased fracture risk. Cre recombinase models utilizing Paired-Related Homeobox 1 (*Prrx1*), Bone Gamma Carboxyglutamate Protein/Osteocalcin (*Bglap*/*Ocn*), or Runx Family Transcription Factor 2 (*Runx2*) as osteoblast-specific Cre drivers have been used in multiple studies to constitutively knock out *Piezo1* ($Prrx1^{Cre};Piezo1^{f/f}$, $Ocn^{Cre};Piezo1^{f/f}$, and $Runx2^{Cre};Piezo1^{f/f}$ mouse lines, respectively) [247, 278-280]. These studies all report decreased bone mass, bone shortening, and skeletal defects [247, 278-280]. Spontaneous fractures in load-bearing distal bones were observed in mice within days of birth, indicating that PIEZO1 plays a key role in the anabolic response of osteoblasts in load-bearing bones [247, 278, 280]. *Piezo1* knockout increased differentiation of bone marrow

monocytes into osteoclasts, likely driven by decreased osteoblastic expression of several collagens, including *Col1a1* reported in $Ocn^{Cre};Piezo1^{f/f}$ mice, as well as *Col2a1*, *Col9a2*, and *Col10a1* reported in $Prrx1^{Cre};Piezo1^{f/f}$ mice [279, 280]. Osteoclast markers Cathepsin K (*Ctsk*) and Tartrate-Resistant Acid Phosphatase (*Acp5*/*Trap*) were increased in $Prrx1^{Cre};Piezo1^{f/f}$ mice, while osteoblast marker Sp7 Transcription Factor (*Sp7*) was decreased [247]. Meanwhile, a model using *Ctsk* as an osteoclast-specific Cre driver to constitutively knock out *Piezo1* ($Ctsk^{Cre};Piezo1^{f/f}$) did not show any reduction in bone mass or changes in bone resorption [280]. This suggests that PIEZO1 primarily transduces load in osteoblasts, with an indirect effect on osteoclasts via interaction between osteoblast and osteoclast populations [280]. RNA-sequencing on the developing humerus and femur tissues revealed that PIEZO1 activation in osteoblasts drives expression of Protein Phosphatase 3 Catalytic Subunit Alpha (*Ppp3ca*), which induces expression of Nuclear Factor of Activated T-Cells (*Nfat*), Yes-1 Associated Transcription Factor [225], and Catenin Beta 1 (*Ctnnb1*), which in regulates expression of Col2a1 and Col9a2 to modulate osteoclastogenesis [247]. These models suggest that *Piezo1* deficiency inhibits this pathway, shifting bone marrow monocytes towards osteoclast production and increasing bone catabolism, while also decreasing bone mass and size. These changes ultimately result in a high number of spontaneous fractures.

PIEZO1 has also been shown to regulate adult bone physiology, with inducible knock out models demonstrating decreased bone mass and increased fracture risk, without affecting bone size. Tamoxifen-inducible Cre recombinase models utilizing Collagen Type I (*Col1*) or *Ocn* as osteoblast-specific Cre drivers ($Col1^{CreERT2};Piezo1^{f/f}$ or $Ocn^{CreERT2};Piezo1^{f/f}$) were used to induce *Piezo1* knock out in adult mice. $Col1^{CreERT2};Piezo1^{f/f}$ mice displayed significantly reduced trabecular bone mass and cortical bone thickness, along with an increased osteoclast population

and reduced collagen expression following *Piezo1* knock out at 8 weeks of age [280]. Hindlimb suspension models applied to wild-type mice for 7-28 days resulted in hindlimb bone loss and increased osteoclast number [279, 280]. No further bone loss beyond that caused by the *Piezo1* knockout alone was observed when the hindlimb suspension model was applied to $Col1^{CreERT2};Piezo1^{f/f}$ mice or $Ocn^{CreERT2};Piezo1^{f/f}$ mice, indicating that PIEZO1 mediates bone resorption in the absence of loading [279, 280]. This result has also been found using Botulinum Toxin A injection to induce hindlimb paralysis in adult wild-type and constitutive *Piezo1* knock out mice utilizing Sp7 as an osteoblast-specific Cre driver ($Sp7^{CreERT2};Piezo1^{f/f}$) [247]. Clinically, PIEZO1 is also significantly reduced at the mRNA and protein level in patients with osteoporosis [279], and several single-nucleotide polymorphisms (SNPs) within *PIEZO1* are closely associated with variations in bone mineral density [281].

These studies demonstrate that PIEZO1 plays a vital role in the development and continued homeostatic maintenance of adult bone, with disruption of PIEZO1 being closely tied with disrupted bone development in immature load-bearing bones and bone loss in adult tissues. Since PIEZO1 is a critical regulator of bone mass, it may be a potential therapeutic target for osteoporosis patients and patients with bone fractures.

1.5.6 Role of PIEZO channels in disc degeneration

The intervertebral discs (IVDs) connect the vertebrae and are composed of the outer annulus fibrosus (AF), an inner gelatinous nucleus pulposus (NP), and cartilaginous endplates [282]. With degeneration, NP cells favor a catabolic state resulting in ECM destruction and apoptosis [283, 284]. PIEZO1 is expressed at the mRNA and protein level in NP cells and is overexpressed in degenerated tissue or in response to mechanical stress [285-290]. PIEZO1

contributes to inflammation, apoptosis, and transduction of changes in substrate properties which lead to senescence and understanding the role of PIEZO1 in these processes is critical to identify potential targets for treating IVD degeneration.

The activation of PIEZO1 has been shown to regulate mechanical cues to inflammatory signals in NP cells [285-287]. Inflammation is implicated in the pathogenesis of IVD degeneration, exhibited by upregulation of proinflammatory cytokines [291]. PIEZO1 signaling has been shown to activate inflammasome NLR Family Pyrin Domain Containing 3 (*NLRP3*), leading to the production of interleukin-1β (IL-1β) [286, 287, 291]. Suppressing PIEZO1 using siRNA reduced proinflammatory effects and dysfunctional metabolism, emphasizing the role of PIEZO1 in contributing to the degenerative IVD environment and its suppression as a protective tool [287].

Along with inflammation, excessive mechanical loading during IVD degeneration can induce cell apoptosis [292]. Although the exact mechanisms are unknown, studies have shown apoptosis can be promoted through altering mitochondrial membrane potential triggered by PIEZO1 activation [285-290]. The application of mechanical stretch to NP cells in monolayer led to changes in mitochondrial potential and an increased apoptotic rate [290]. Knocking down PIEZO1 via short hairpin RNA (shRNA) decreased changes in mitochondrial membrane potential and cell apoptosis [290]. Similarly, mitochondrial dysfunction and increased apoptosis has been observed after compression of human IVDs, which was partly rescued by treatment with GsMTx4 [285].

The ECM mechanical environment is a critical regulator of NP differentiation and phenotype [293, 294]. Degenerated NP tissue obtained from surgical samples display increased ECM stiffness, concurrent with overexpression of PIEZO1 [285, 288, 289]. Specifically, PIEZO1-mediated sensation of increased substrate stiffness has been linked to the accumulation of ROS,

leading to apoptosis, autophagy, and senescence [285]. Knocking down PIEZO1 in NP cells plated on stiff substrates reduced senescence, oxidative stress, and endoplasmic reticulum stress to soft substrate levels [288]. PIEZO1 activation was found to trigger senescence in stiff, degenerated NP tissue by increasing the production of periostin (POSTN) [289]. POSTN has been identified as a key player of IVD degeneration, increasing senescence and activating the Nuclear Factor Kappa B (NF-κB) signaling pathway, which in turn leads to heightened *Postn* expression [289]. This degenerative positive feedback loop was triggered by Yoda1 and blocked using GsMTx4 [289].

Taken together, PIEZO1 signaling in NP cells has been linked to the activation of intracellular pathways including inflammation, apoptosis, autophagy, and senescence— processes that drive IVD degeneration. Therefore, PIEZO1 may be an appealing therapeutic target for disc degeneration induced by inflammation and senescence. Further investigating the role of PIEZO2 in pain sensation in IVD could be another interesting path to develop effective treatments for low back pain.

Lastly, although the role of PIEZO in NP mechanotransduction has been characterized, studies have yet to determine the ion channel's role in the AF and cartilaginous endplates. Chondrocytes of the cartilaginous endplates have been shown to be mechanoresponsive [295-297]. As injurious mechanical loading signals are transduced to chondrocytes in articular cartilage via PIEZO1, it would be of interest to determine whether chondrocytes in cartilaginous endplates are similarly regulated. Similarly, cells in the AF exhibit a response to mechanical forces dependent on the magnitude, frequency, and duration of loading [298-300]. To gain a full understanding of the role of PIEZO channels in the IVD and fully harness it as a therapeutic target for low back pain, future studies may focus on the expression of PIEZO in the AF and cartilaginous end plates along with its role in regulating cells in these tissues in response to mechanical forces.

1.5.7 Role of PIEZO channels in pain

The nervous system contains multiple mechanoresponsive cell types sensitive to a wide array of signals. Noxious stimuli activate sensory neurons known as nociceptors, which are involved in a range of chronic pain conditions including peripheral neuropathies and even OA. Touch-related information is transduced by Merkel cells in the epidermis, while limb coordination is regulated by proprioceptive neurons. All these cells rely on mechanosensation via PIEZO2, implicating PIEZO2 in the processes of pain, touch, and proprioception.

PIEZO2 LOF studies have implicated PIEZO channels in mechanical pain and touch sensation, both of which affect musculoskeletal health. Neural cell *Piezo2* deletion in mice was shown to impair touch but sensitize mice to mechanical pain [301, 302]. Humans with *PIEZO2* LOF report sensitivity to noxious stimuli but insensitivity to gentle touch [301]. Mice lacking *Piezo2* in both sensory neurons and Merkel cells had a profound loss of touch sensation but had unaffected pain phenotypes, indicating distinct roles in touch and pain sensation [303]. *Piezo2* knockout abrogated Nerve Growth Factor (NGF)-induced sensitization of afferent neurons in murine bone [304]. PIEZO2 has been shown to signal through Rap Guanine Nucleotide Exchange Factor 3 (RAPGEF3/EPAC1), a cyclic AMP sensor, to induce mechanical allodynia in neuropathic and bone cancer pain [305-307]. Additionally, *Piezo2* LOF in mice attenuated mechanically stimulated pain in peripheral neuropathy [308]. Intriguingly, PIEZO1 rescued defective touch due to *Piezo2* deletion in mice, indicating that PIEZO1 may also play a role in touch [302].

PIEZO2 may also play a key role in vascular components of the synovial membrane and infrapatellar fat pad, which is known to transduce mechanical stimuli and mediate chronic pain in OA [309]. OA patients had colocalized *PIEZO1* and *PIEZO2* expression in blood vessels of the

synovial membrane and infrapatellar fat pad, compared to healthy controls, suggesting vascular remodeling may be a facet of OA progression [310]. Nociceptor-specific, *Piezo2* knockout mice are protected from NGF-induced joint pain in OA, further supporting that PIEZO2 is involved in OA joint pain [311].

In addition to the basic sensations of pain and touch, PIEZO2 is a major mechanotransducer of mammalian proprioceptors where a lack of PIEZO2 results in severely uncoordinated body movements and limb positions in mice and impaired performance on behavioral tests [312, 313]. Humans with LOF variants of *PIEZO2* had decreased joint proprioception but were still able to walk, talk and write [314]. *Piezo2* deletion in proprioceptive neurons in mice resulted in hip dysplasia and spinal malalignment, which are conditions also seen in humans with *PIEZO2* mutations [314, 315]. However, loss of *Piezo2* in osteogenic or chondrogenic lineages does not reproduce these skeletal phenotypes in mice [315]. This distinction suggests that PIEZO2 may be an indirect regulator of skeletal morphogenesis through the proprioceptive system, potentially by disturbing normal muscle activity during development.

These studies together portray PIEZO2 as an integral mechanosensor in the nervous system, transducing pain, touch, and proprioceptive signals. Further research may further resolve the role of PIEZO2 in chronic pain and allodynia-associated conditions and reveal new areas of therapeutic potential.

1.6 Potential therapeutic applications of PIEZO modulators

The broad expression and activation of PIEZO channels in neuro-musculoskeletal systems make them an attractive therapeutic target to control pain and enhance regeneration following injury [316]. Although the exact downstream cellular signaling cascades of PIEZO1 and PIEZO2 activation are still being characterized, PIEZO channels can clearly be activated by inflammation and play a key role in initiating apoptosis following high strain mechanical stress [237]. Cell death and inflammation are key processes involved in tissue regeneration after injury, and the ability to modulate these processes via PIEZO ion channels holds great therapeutic promise. However, given the broad expression of PIEZO channels, their modulation could have detrimental off-target effects and preclinical therapeutic development should consider tissue-specific delivery mechanisms.

GsMTx-4 blocks the activation of cationic stretch-activated ion channels, including PIEZO1 and PIEZO2, by changing membrane properties. Studies have shown that GsMTx-4 can decrease chondrocyte cell death following injurious loading, suggesting a potential therapeutic use for post-traumatic OA [237]. Moreover, studies have shown GsMTx-4 to be effective in slowing the progression of Duchenne muscle dystrophy, increasing the functionality of the skeletal muscles, and elevating the neurite growth [317, 318]. GsMTx-4 treatment may be a potential therapy for PIEZO related diseases; however, its side effects and toxicity to other tissues should be further evaluated.

As an alternative, several studies have suggested that the inhibition of VGCCs can reduce mechanosensitivity. Activation of mechanosensitive ion channels such as PIEZO channels has been proposed to increase intracellular cation concentration, which increases cell membrane

potential and triggers activation of VGCCs [319]. Multiple studies suggest that L-type VGCCs inhibitors reduce mechanosensitivity by decreasing the response to direct mechanical compression, stretch, and shear stress, which has been shown to protect the cartilage from degradation and OA progression [237, 319-322]. This not only demonstrates the mechanosensory nature of the VGCCs [320], but also indicates a potential link between the functionality of the voltage- and mechano-gated ion channels. Since VGCC inhibitors Verapamil and Nifedipine are FDA-approved for chest pain and high blood pressure, developing alternative musculoskeletal applications may yield novel strategies for managing PIEZO-associated diseases [322].

In addition to VGCCs, various studies have investigated the link between PIEZO channels and other mechanosensitive ion channels, including TRPV4. Activation of PIEZO channels by shear stress activated TRPV4 in murine pancreatic acinar cells [323]. Moreover, blocking the TRPV4 channel mitigated pancreatitis pathologies that occur by PIEZO channel activation [323-325]. Therefore, blocking TRPV4 instead of PIEZO channels is an alternative strategy to mitigate some PIEZO-associated pathologies. However, this also indicates that the therapeutic use of ion channel agonists or antagonists should be further evaluated in terms of their down-stream effects and modulation of other ion channels.

Instead of directly blocking PIEZO channels, specific dietary fatty acid species may be incorporated into the cell membrane to influence fluidity, stiffness, and cell signaling. Membrane lipid composition and cholesterol organization have been shown to influence PIEZO activity [326, 327]. For example, depletion of phosphoinositides from the plasma membrane inhibits PIEZO channels [328, 329]. Increased cholesterol in the plasma membrane increases stiffness and sensitizes PIEZO mechanical activation [330]. Moreover, polyunsaturated fatty acids can

also alter PIEZO channel activation to influence cellular mechanosensitivity [331]. Eicosatetraenoic acid, docosahexaenoic acid, and margaric acid mediate the PIEZO channel sensitivity to mechanical indentation, while palmitic acid and stearic acid elevate autophagy, alter the activation of NF-κB pathways, and influence differentiation and proliferation in human chondrocytes through altered PIEZO signaling [285, 332-336]. However, treating chondrocytes with lauric acid had the opposite effect and inhibited autophagy activation [285, 332, 333, 335, 336]. As such, dietary supplementation of specific fatty acid species may be a strategy to fine-tune cell membrane composition, thereby modulating PIEZO activity to restore optimal cellular mechanosensation. One clinical population that may especially benefit from PIEZO-modulating therapeutics are obese individuals. Obesogenic diets, especially those with high omega-6 content, increase OA severity in rodents and further exacerbate joint damage following injury [331, 337-341]. However, mice fed an omega-3 enriched diet and those with a transgene to convert omega-6 to omega-3 fatty acids show less severe OA pathology [331, 342-344]. Therefore, supplementation of specific fatty acids may be a preventative strategy to maintain cartilage integrity in obese individuals.

Obesity and type II diabetes are also risk factors for delayed wound healing and fracture repair [345]. Both genetically-induced [346] and diet-induced [347-349] obese mice display delayed fracture repair in part due to increased systemic inflammation and decreased vascular formation at the fracture site [346]. PIEZO1 is a key mechanosensitive ion channel in the epithelial cells of the bone vasculature, and tissue specific deletion of the Piezo1 gene in this cell population leads to impaired fracture healing [350]. Furthermore, Piezo1 is expressed in periosteal stem cells and activation of PIEZO1 with Yoda1 improves fracture healing in a tail suspension unloading mouse model [351]. Therefore, individuals with obesity or type II diabetes

who are at a higher risk for impaired fracture repair may be a clinical population that would especially benefit from PIEZO modulation of mechanically gated ion channels. However, since post-traumatic injuries are an independent risk factor for OA, additional research is necessary to determine the ideal timing of PIEZO modulation following injury for optimal fracture repair and OA prevention.

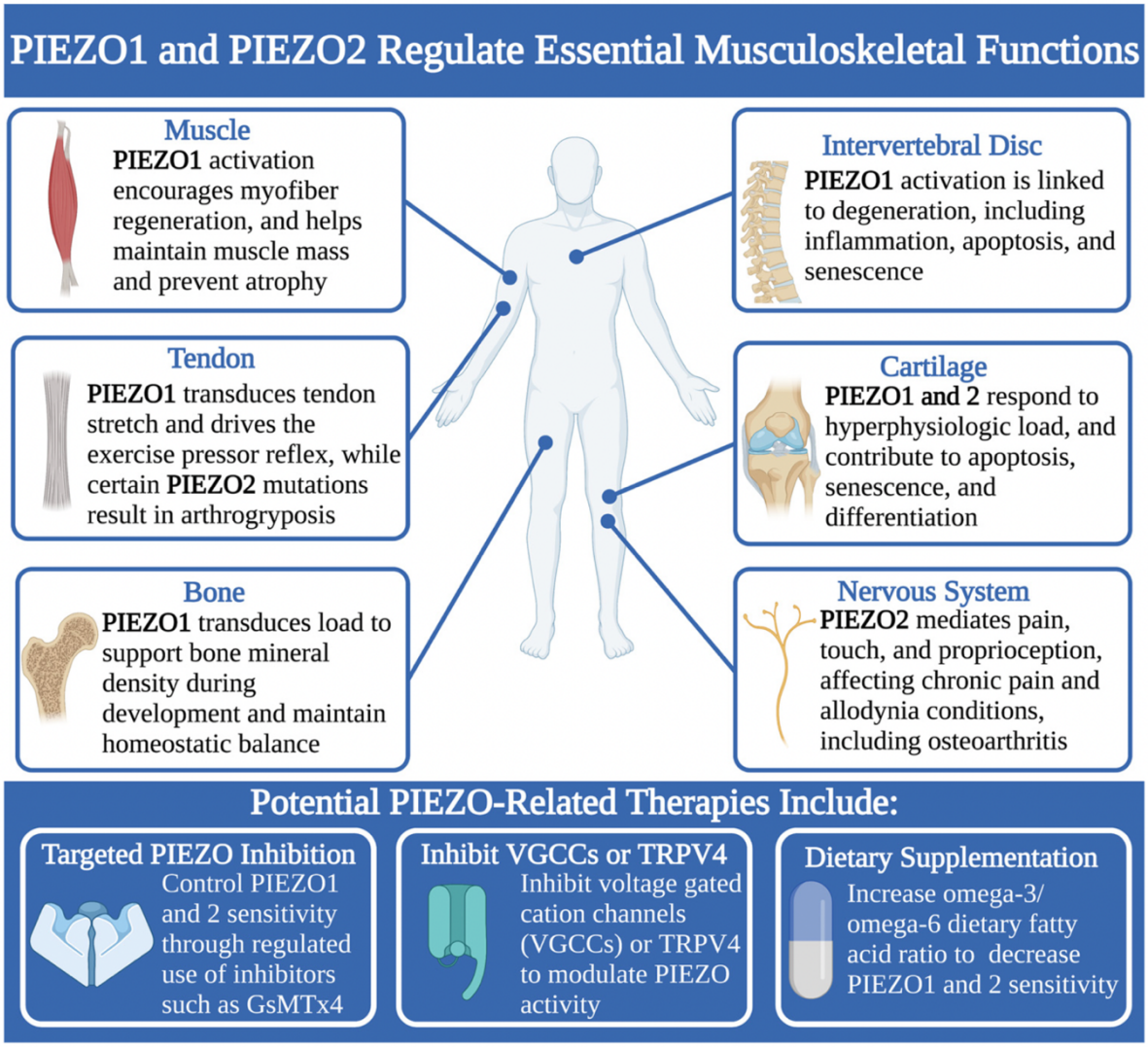

Figure 1.1 PIEZO1 and PIEZO2 play importantroles in development and function of multi-ple tissues in the musculoskeletal and nerv-ous systems, and therapeutic strategies tocontrol PIEZO1 and PIEZO2 activity includetargeted inhibition of PIEZOs or other cationchannels, and dietary supplementation.

1.7 Voltage-gated ion channels

Voltage-gated Ca^{2+} ion channels, a category of voltage-gated ion channels, enable the transit of Ca^{2+} ions (Ca^{2+}) across cell membranes when there is a shift in membrane potential. These channels have multiple subunits, with the α1 subunit forming the channel that allows Ca^{2+} ions to pass through. There are various types of voltage-gated Ca^{2+} channels, each classified according to the α1 subunit present, such as L-type, T-type, N-type, P/Q-type, and R-type channels [352-354].

1.7.1 Role in the Musculoskeletal System

In muscle contraction, voltage-gated Ca^{2+} channels are indispensable. When the membrane potential of skeletal muscle cells depolarizes, it opens the voltage-gated Ca^{2+} channels, also known as dihydropyridine receptors (DHPRs), in the t-tubules (Arikkath, 2003 #543;Bers, 1993 #549;Flucher, 2005 #548;Lazniewska, 2017 #544;Meissner, 1995 #545;Schredelseker, 2005 #546). This event leads to a physical interaction with the ryanodine receptors (RyRs) in the sarcoplasmic reticulum (SR), causing the release of stored Ca^{2+} ions from the SR into the cytoplasm (Arikkath, 2003 #543;Bers, 1993 #549;Flucher, 2005 #548;Lazniewska, 2017 #544;Meissner, 1995 #545;Schredelseker, 2005 #546). The subsequent increase in cytoplasmic Ca^{2+} concentration activates the contractile machinery, resulting in muscle contraction (Bers, 1993 #549;Meissner, 1995 #545).

Bone remodeling also involves voltage-gated Ca^{2+} channels by regulating the activity of osteoblasts and osteoclasts. The influx of Ca^{2+} through voltage-gated Ca^{2+} channels in osteoblasts triggers the release of bone morphogenetic proteins (BMPs), which promote bone

formation [319, 354-357]. Conversely, in osteoclasts, Ca^{2+} entry through voltage-gated Ca^{2+} channels activates signaling pathways that promote bone resorption [358].

1.7.2 Role in Articular Cartilage

Articular cartilage, a specialized connective tissue, covers the ends of bones in synovial joints, providing a smooth, lubricated surface for joint movement. Chondrocytes, the cells of articular cartilage, produce and maintain the extracellular matrix (ECM), composed of a network of collagen fibers, proteoglycans, and water.

Voltage-gated Ca^{2+} channels in chondrocytes participate in the synthesis and maintenance of the ECM [359-363]. The entry of Ca^{2+} through voltage-gated Ca^{2+} channels activates intracellular signaling pathways, such as the calcium-calmodulin-dependent protein kinase II (CaMKII) and protein kinase C (PKC) pathways, which regulate the synthesis of collagen and proteoglycans, key components of the ECM [363-367].

Calcium signaling via voltage-gated Ca^{2+} channels also regulates chondrocyte proliferation and differentiation [368]. For instance, Ca^{2+} entry through voltage-gated Ca^{2+} channels activates the extracellular signal-regulated kinase (ERK) pathway, promoting chondrocyte proliferation and differentiation [194, 368].

1.7.3 Synergy with Mechanosensitive Channels

In chondrocytes, mechanical loading, like compression or shear stress, can activate mechanosensitive channels, causing an influx of Ca^{2+} ions. This increase in intracellular Ca^{2+} concentration can then trigger the opening of voltage-gated Ca^{2+} channels, leading to a further influx of Ca^{2+} ions and the activation of Ca^{2+} -dependent signaling pathways [319]. Therefore,

studying the interaction between mechanosensitive channels and voltage-gated Ca^{2+} channels is essential and investigating the role of this synergy on regulating chondrocyte functions in response to mechanical loading, activating signaling pathways that regulate ECM synthesis, cell proliferation, and differentiation can open new insight in the field of mechanobiology.

All in all, understanding the role of voltage-gated Ca^{2+} channels and their interaction with mechanosensitive channels in the musculoskeletal system and articular cartilage is crucial for developing new therapeutic strategies for musculoskeletal diseases, such as osteoarthritis. Abnormal Ca^{2+} signaling via voltage-gated Ca^{2+} channels and mechanosensitive channels can lead to imbalances in ECM synthesis and degradation, altered chondrocyte proliferation and differentiation, and ultimately cartilage degeneration. Therefore, targeting these channels and their signaling pathways may offer novel approaches for preventing and treating musculoskeletal diseases.

1.8 Polyunsaturated fatty acids (PUFAs)

Fatty acids are fundamental components of dietary lipids and are crucial for human health [369, 370]. They serve as the building blocks of fats and oils, playing diverse roles ranging from energy storage to involvement in critical cellular functions [371-374]. The importance of fatty acids in human nutrition is well-acknowledged. However, it's essential to realize that not all fatty acids offer the same health benefits. The balance of different fatty acids in our diet can make a significant difference in health outcomes. Specifically, an imbalanced intake can be associated with various health issues, including obesity and diabetes [375-382].

Among the different types of fatty acids, polyunsaturated fatty acids (PUFAs) are of particular interest due to their potential health benefits [383-387]. PUFAs encompass a subgroup of fatty acids distinguished by the presence of more than one double bond in their carbon chain. They are further classified based on the position of the first double bond from the methyl end into omega-3 (ω3) and omega-6 (ω6) fatty acids.

PUFAs are pivotal for several physiological processes. They play an instrumental role in cellular metabolism, influencing energy production and consumption [383, 388, 389]. Moreover, they are essential for brain function, and their deficiency can lead to various neurological issues [390]. Given these roles, it's unsurprising that PUFAs have been explored as potential therapeutic agents. For instance, they have been used in treating cardiovascular diseases due to their ability to reduce cholesterol levels and enhance heart health [391-396].

Research has consistently highlighted the health benefits of ω3 fatty acids. These compounds, found abundantly in fish oils, have been shown to be particularly effective in reducing inflammation [397-399]. This anti-inflammatory property makes ω3 fatty acids useful in managing inflammation-associated conditions like rheumatoid arthritis (RA) [400-402]. Studies have confirmed that ω3 fatty acids can lessen inflammation and related symptoms in RA patients [400-402].

In the realm of aging, PUFAs have demonstrated the potential to modulate cholesterol levels [391-396]. This is significant since cholesterol can influence cell membrane fluidity, which in turn impacts various cellular processes [396, 403]. Importantly, the ratio of ω3 to ω6 PUFAs in our diet is critical. This balance affects cellular membrane fluidity, inflammation, and overall cellular metabolism.

The impact of PUFAs extends even to the realm of orthopedics. In the specific context of articular cartilage, which provides the cushioning in our joints, research by Curtis et al. highlighted that ω3 PUFA supplementation can reduce the expression of inflammation markers [404, 405]. Furthermore, cartilage treated with IL-1, a pro-inflammatory cytokine, showed decreased degradation when supplemented with ω3 fatty acids [404, 405]. Another study by Wu et al. showcased the protective effects of a ω3 rich diet on mouse joints [331]. Mice on this diet were more resistant to post-traumatic osteoarthritis (PTOA) after a knee injury [331].

Interestingly, recent findings have unveiled potential interactions between fatty acids and PIEZO channels, which are mechanically activated ion channels involved in various physiological processes [334, 406]. Some evidence suggests that fatty acids, particularly PUFAs, can modify the sensitivity of PIEZO channels to membrane stretching [334, 406]. This is noteworthy considering that changes in PIEZO1 expression have been observed in osteoarthritic joints.

Given these insights, it becomes evident that PUFAs, especially ω3 and ω6, can modulate PIEZO channel responses to mechanical stresses. This ability might provide a protective shield for joints against harmful loads. Consequently, a deeper understanding of the molecular mechanisms through which PUFAs exert their protective effects could be a game-changer in the quest to halt or slow osteoarthritis progression.

1.9 Osteoarthritis and post-traumatic osteoarthritis

Osteoarthritis (OA) and post-traumatic osteoarthritis (PTOA) are debilitating conditions that affect millions of people worldwide. Both are progressive degenerative joint diseases that

involve the breakdown of articular cartilage, bone remodeling, osteophyte formation, and synovial inflammation. However, PTOA specifically develops after a joint injury, such as ligament or meniscal tears, joint dislocation, or fractures.

The development and progression of OA and PTOA involve several stages. Initially, there is acute inflammation in the joint, marked by the release of pro-inflammatory cytokines like IL-1β and TNF-α, and catabolic enzymes like matrix metalloproteinases (MMPs) that degrade the extracellular matrix (ECM) of the articular cartilage [407-409]. This degradation of the cartilage matrix prompts chondrocytes, the cartilage cells, to increase the synthesis of ECM components [410]. However, the new tissue formed is often fibrocartilaginous and not as robust as the original hyaline cartilage. As the disease progresses, the cartilage becomes thin, fragmented, and fissured, exposing the underlying subchondral bone [411]. This exposure triggers increased bone remodeling, with osteoclasts resorbing bone, leading to the formation of subchondral bone cysts, and osteoblasts forming new bone, leading to osteophyte formation at the joint margins. These changes in bone structure contribute to joint pain and stiffness [412, 413].

Simultaneously, the release of cartilage ECM fragments into the synovial fluid can induce inflammation in the synovial membrane [414-416]. This synovial inflammation is characterized by synovial thickening, angiogenesis, and infiltration of inflammatory cells like macrophages and lymphocytes [414-418].

Mechanical loading and joint injury play critical roles in the onset and progression of OA and PTOA [31, 419]. Articular cartilage is designed to withstand high levels of mechanical loading during activities like walking, running, and jumping. However, abnormal loading, either

excessive or insufficient, can lead to cartilage degeneration. Excessive loading can cause acute cartilage damage and trigger catabolic and inflammatory responses, while insufficient loading can lead to cartilage atrophy due to reduced nutrient supply and mechanical stimulation [31, 44, 420-422]. Additionally, joint injuries can alter joint biomechanics, leading to abnormal loading of the articular cartilage. For example, a torn anterior cruciate ligament (ACL) can lead to increased anterior translation of the tibia and increased loading of the medial compartment of the knee, increasing the risk of PTOA [423, 424].

Preventing and managing OA and PTOA involve several strategies. Injury prevention, including the use of protective equipment and proper technique during physical activities, is crucial for preventing PTOA [425]. Weight management is important to reduce mechanical load on the joints. Physical therapy can improve joint range of motion, muscle strength, and joint biomechanics, reducing the load on the damaged cartilage and slowing disease progression [426]. Pharmacological treatments, such as nonsteroidal anti-inflammatory drugs (NSAIDs), can help reduce pain and inflammation in the early stages, although long-term use is associated with side effects [427]. Intra-articular injections of corticosteroids or hyaluronic acid can provide temporary symptom relief [428-430]. In advanced cases, surgical treatments, such as arthroscopy, osteotomy, or joint replacement, may be necessary to relieve pain and restore joint function [431-435].

In conclusion, OA and PTOA are complex diseases characterized by cartilage breakdown, bone remodeling, and synovial inflammation, with mechanical loading and joint injury playing key roles in their development and progression. Preventing joint injuries, maintaining a healthy weight, and managing symptoms with physical therapy and pharmacological treatments are essential strategies for managing these conditions.

1.10 Summary

The intricate landscape of mechanosensitive ion channels, especially PIEZO1 and PIEZO2, is at the forefront of our understanding of the neuro-musculoskeletal system. These channels, activated by mechanical stimuli, form the cornerstone of several cellular processes and have particular significance within chondrocytes – the primary cellular constituents of articular cartilage.

Starting with an examination of PIEZO channels, we delved deep into their interaction with various molecules. It is worth noting that the absence of known small molecule agonists for PIEZO2 means there is much yet to be uncovered. Current inhibitors, ranging from ruthenium red to spider venom-derived GsMTx-4, offer a tantalizing glimpse into potential avenues of modulating PIEZO activity. These interactions, combined with the spectrum of mutations in PIEZO channels, reveal a wide array of phenotypic consequences, from nuanced cellular alterations to pronounced disease phenotypes.

Chondrocytes, when under the purview of these channels, demonstrate a plethora of responses. We observed the essential role PIEZO channels play in inflammation, the onset of cellular senescence, programmed cell death (apoptosis), and the broad spectrum of gene expression. These roles are critically interwoven into the fabric of musculoskeletal health and disease.

The discussion on voltage-gated Ca^{2+} ion channels further enhanced our comprehension of the musculoskeletal system. These channels, paramount in muscle contraction and bone remodeling, exhibit a synergy with mechanosensitive channels. In the realm of articular

cartilage, the dance between these channels dictates chondrocyte functions. This interaction plays a pivotal role in modulating extracellular matrix synthesis, cellular proliferation, and differentiation.

Moreover, while the importance of fatty acids like PUFAs in nutrition is universally acknowledged, it's essential to discern that not all fatty acids confer the same health benefits. The balance of these fatty acids can significantly influence health outcomes, potentially steering the course towards diseases like obesity and diabetes.

In wrapping up, our journey through PIEZO channels, voltage-gated Ca^{2+} channels, and their significance in the musculoskeletal system underscores the potential of these channels as therapeutic targets. While our current understanding is expansive, the horizon still holds numerous secrets. Unraveling these mysteries could pave the way for groundbreaking therapeutic strategies for musculoskeletal diseases. It is an exciting time in the realm of molecular biology, and as we move forward, the detailed exploration of these channels and their downstream effects is bound to lead to innovative interventions in the healthcare landscape.

Chapter 2: Regulation of chondrocyte biosynthetic activity by dynamic hydrostatic pressure: The role of TRP channels

Partially adapted from: Savadipour, A., Nims, R. J., Katz, D. B., & Guilak, F. (2021) Regulation of chondrocyte biosynthetic activity by dynamic hydrostatic pressure: The role of TRP channels. Connective Tissue Research, 63.1 (2022): 69-81.

2.1 Abstract

Introduction: Chondrocytes perceive and respond to mechanical loading as a signal to regulate their metabolic activity. Joint loading exposes chondrocytes to multiple modes of mechanical stress, including hydrostatic pressure; however, the mechanisms by which chondrocytes sense physiologically-relevant levels of hydrostatic pressure are not well understood. We hypothesized that hydrostatic pressure is transduced to an intracellular signal through mechanosensitive ion channels on the membrane of chondrocytes. The goals of this study were to examine the effect of hydrostatic loading on the development of engineered cartilage tissue and the contribution of mechanosensitive ion channels on these hydrostatic loading effects.

Methods: Using a 3D model of porcine chondrocytes in agarose, we applied specific chemical inhibitors to determine the role of transient receptor potential (TRP) ion channels TRPV1, TRPV4, TRPC3, and TRPC1 in transducing hydrostatic pressure.

Results: Hydrostatic loading caused a frequency and magnitude-dependent decrease in sulfated glycosaminoglycans (S-GAG), without changes in DNA content. Inhibiting TRPC3 and TRPV4

decreased S-GAG content; however, only the inhibition of TRPV1 partially attenuated the hydrostatic loading-induced reduction in S-GAG content.

Conclusions: Our findings indicate that TRPV1 may serve as a transducer of hydrostatic pressure in chondrocytes, and provide further support the role of TRPV4 in regulating chondrocyte anabolism, as well as initial evidence of a role for TRPC3 in chondrogenesis. These findings add to our further understanding of the chondrocyte "channelome" and suggests that a range of ion channels are responsible for mediating the transduction of different biophysical stimuli such as hydrostatic pressure, membrane stretch, or osmotic stress.

2.2 Introduction

Osteoarthritis (OA) is a multifactorial chronic disease of multiple origins, characterized by the irreversible degradation of the articular cartilage, as well as pathologic changes in other joint tissues. The precise etiology of OA initiation and progression are not well understood, but the role of excessive and traumatic mechanical forces are implicated in OA pathogenesis due to the early onset of OA upon traumatic joint injuries [436, 437]. Under homeostatic conditions, articular cartilage undergoes millions of cycles of deformational mechanical loading every year. This tissue-scale deformational loading is transduced into distinct mechanical signals that are perceived by the chondrocytes residing within the cartilage, including direct compressive, tensile, and shear strains, as well as osmotic, electrostatic, and hydrostatic pressures that result from the mechanical deformation of the charged and hydrated cartilage tissue. While these different loading conditions are believed to be essential for tissue maintenance [438], the specific mechanotransduction mechanisms regulating each of these stimuli, and their roles in chondrocyte homeostasis remain to be determined.

Hydrostatic pressure is one of the critical mechanisms involved in the ability of articular cartilage to withstand high magnitudes of joint loading while allowing for extremely low coefficients of friction and limited tissue deformation [439-441]. During loading, the low hydraulic permeability of the cartilage tissue prevents the rapid loss of water from the tissue, resulting in the great majority of the applied load to be supported by the high water content present in the tissue, rather than being supported by the solid extracellular matrix [440-442]. This phenomenon increases in the hydrostatic pressure throughout the tissue, including the chondrocytes [443]. This pressure is subsequently lost upon the removal of the load, in effect creating a dynamic hydrostatic loading environment present during normal locomotion [444, 445]. Importantly, the role of hydrostatic pressure as a physical factor in modulating chondrocyte physiology can be isolated for study, because physiological levels of hydrostatic pressure can be applied in a uniform manner without inducing confounding physical factors such as fluid flow, electrokinetic effects, or cyclic cell deformation, due to the incompressibility of interstitial water and the extracellular matrix [446].

A number of in vitro studies have examined the effects of hydrostatic loading to cartilage tissue explants, isolated chondrocytes, and engineered cartilage tissue systems on cartilage biology as well as stem cell chondrogenesis [447-451]. In efforts to mimic the dynamic hydrostatic pressure conditions which might be experienced by chondrocytes, numerous studies have evaluated the effect of static or dynamic pressures at a range of amplitudes and frequencies. For primary chondrocytes, a wide range of catabolic and anabolic responses (or no response) have been observed under different hydrostatic pressure loading regimens [452]. Dynamic hydrostatic pressure was shown to increase the expression of cartilage matrix genes COL2A1 (type II collagen) and ACAN (aggrecan), and the critical chondrogenesis transcription factor

SOX9 but had no effect on the expression of type I collagen, suggesting the application of hydrostatic loading specifically alters matrix gene programs [453, 454]. Interestingly, the amplitude of hydrostatic pressure plays an important role in chondrocyte matrix production in the physiologic to supraphysiologic ranges of 2.5 MPa to 50 MPa [455]. These studies demonstrate the complex role that hydrostatic pressure may exert on chondrocyte physiology, while underscoring lack of detailed knowledge on the mechanisms of chondrocyte mechano-signaling.

Chondrocytes respond to mechanical loading through an array of mechanically-sensitive ion channels and receptors but understanding the contexts and activation modes for many of these mechanosensitive constituents at the molecular scale remain unresolved. Our overarching goal is to understand how mechanical loading of cartilage is deconstructed into distinct mechanical mechanisms which then act on particular mechanically-sensitive ion channels to enact and provoke unique mechano-signaling pathways that influence cartilage development, homeostasis, and disease. Chondrocytes possess a number of mechanically-sensitive ion channels include the Transient Receptor Potential (TRP) family including members TRPV1, TRPV4, TRPC1, TRPC3, TRPC6, and TRPM7 as well as the recently discovered Piezo ion channel family members PEIZO1 and PIEZO2 [171, 197, 209, 234, 235, 237, 316, 359, 361, 456-461]. To date, however, the mechanisms by which chondrocytes transduce dynamic hydrostatic pressure to an intracellular signal remain to be determined. Elucidating the role of these mechanosensitive proteins and/or organelles in the role of hydrostatic pressure-induced chondrocyte mechanotransduction is an important step towards gaining a mechanistic understanding of cartilage physiology and pathology.

The aim of this study was to investigate the role of several of the TRP family of mechanically-sensitive ion channels in hydrostatic pressure-induced chondrocyte mechanobiology. Using engineered cartilage tissue constructs we first identified the role of dynamic hydrostatic pressure frequency and amplitude on the biosynthesis of sulfated glycosaminoglycans (S-GAG), an important structural molecule synthesized in high levels and throughout life in native cartilage. Engineered cartilage constructs were cultured under

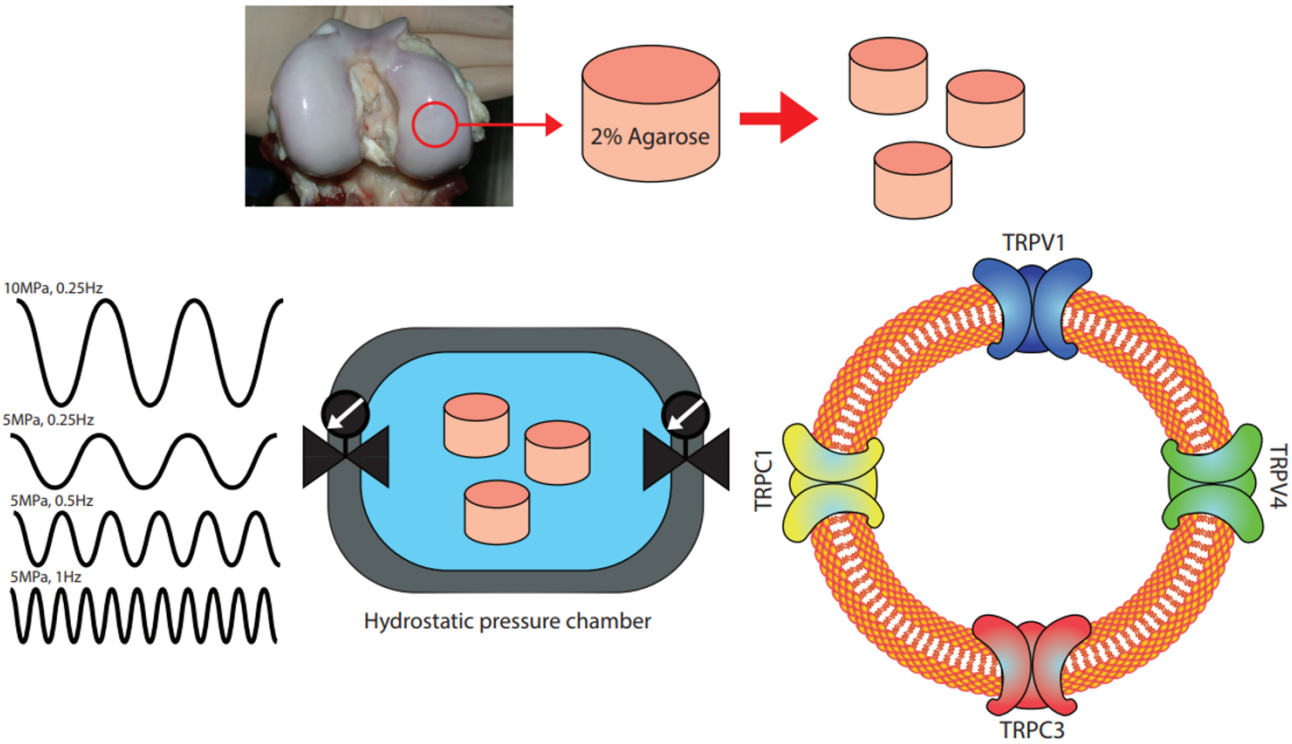

hydrostatic loading in the presence or absence of inhibitors of the ion channels TRPV1, TRPV4, TRPC3, and TRPC1 using pharmacologic inhibitors to establish the role of these mechanosensitive factors in hydrostatic pressure-induced S-GAG biosynthesis (Fig. 1).

Figure 2.1 Schematic of the experimental set up. Chondrocytes from porcine cartilage were digested and cast into an agarose scaffold to create engineered cartilage constructs. Constructs were loaded in the hydrostatic pressure chamber and tested under different loading regimens and specific TRP channel inhibitors.

2.3 Materials and Methods

2.3.1 Overall strategy

This study was performed in two sequential experiments. In experiment 1 we characterized the response to tissue engineered cartilage cast using porcine chondrocytes to different amplitudes and frequencies of hydrostatic pressure loading to identify loading regimens that alter chondrocyte metabolic activity and S-GAG accumulation in our engineered cartilage system. In experiment 2 we use the loading regimen identified from experiment 1 to test the role of several putative mechanosensitive ion channels in mediating the hydrostatic loading response using specific chemical inhibitors. For each experiment, a single batch of constructs was tested.

2.3.2 Porcine chondrocyte isolation, tissue-construct casting, and culture

The articular cartilage of porcine stifle joints was harvested on the day of the slaughter and kept in complete media at 37 °C and 5% CO2 for 2 days. Complete media was formulated with high-glucose Dulbecco's Modified Eagle Media (Gibco), 10% fetal bovine serum (Atlas), 1.5% HEPES (Gibco), 1% penicillin-streptomycin (Gibco), and 1% non-essential amino acid (Gibco). Articular cartilage was digested for 16 h with collagenase (type IV, Sigma) at 37 °C. Cells were isolated by straining through 70 μm filters, followed by counting, centrifuging and washing, and resuspending to achieve a concentration of 60 × 106 cells/ml or 120 × 106 cells/ml before encapsulating in molten agarose (4%, type VIIA, Sigma) and casting to a thickness of 2.34 mm. Cylindrical constructs were punched to create ∅3 mm × 2.34 mm constructs with a nominal final concentration of 30 or 60 × 106 cells/ml in 2% agarose. Constructs were cultured in complete media supplemented with 50 μg/mL L-ascorbic acid 2-phosphate sesquimagnesium salt and 40 μg/mL L-proline (Sigma) for the duration of the study.

2.3.3 Hydrostatic pressure loading

Hydrostatic pressure loading was performed using a Barozyme HT48 (Pressure Biosciences, South Easton, MA). Samples were loaded into individual tubes and placed in the hydrostatic pressure loading chamber for daily loading per manufacturer's protocols. Each tube contained 1.5 mL media and was loaded with 6 samples for a daily media supply of ~0.3 mL/million cells/day [462]. Samples were maintained at 37 °C and loaded for 3 h daily, 5 times per week. In experiment 1, the effects of seeding density (30 or 60 × 106 cells/ml) in engineered cartilage constructs were studied using the following hydrostatic pressure regimens: (a) 0 MPa (control), (b) 5 MPa amplitude, 0.25 Hz, (c) 5 MPa amplitude, 0.5 Hz, (d) 5 MPa amplitude, 1 Hz, and (e) 10 MPa amplitude, 0.25 Hz. Based on the results of experiment 1, the inhibitor studies of experiment 2 were treated with either 0 MPa as an unloaded control regime and 5 MPa at 0.5 Hz as a hydrostatic loading regime. For both sets of experiments (1 and 2), unloaded controls were treated in the same manner as the loaded groups but were not subjected to hydrostatic pressure.

2.3.4 Ion channels inhibitor treatments

To test the role of mechanically-sensitive ion channels to the hydrostatic pressure, we inhibited TRPV4, TRPV1, TRPC3 and TRPC1 cation channels using the selective inhibitors GSK205 (synthesized at the Duke Chemical Synthesis Facility, 10 μM), A 784168 (Tocris Bioscience, 25 nM), Pyr3 (Tocris Bioscience, 3 μM), and MRS 1845 (Tocris Bioscience, 10 μM) [197, 463-466]. Inhibitors were added 15 minutes prior to loading, and constructs were returned to base media after loading. Vehicle controls for each inhibitor were made using either deionized water or dimethyl sulfoxide (DMSO), based on the solvent necessary for inhibitor reconstitution.

Exposure to neither the inhibitors nor vehicle induced cell death (Supplemental Fig. 1). Due to the small size of the inhibitors (< 500 Da) and small tissue construct size, we supplemented inhibitors 15 minutes prior to loading which we anticipate is sufficient time for inhibitor transport within the construct.

2.3.5 Biochemical analysis

The wet weight of each construct was recorded for normalizing biochemical content measures and constructs were frozen at −20 °C until digestion. To perform biochemical assays on the engineered cartilage tissues, samples were digested in proteinase K for 16 h at 56 °C. After digestion, the remaining, undigested, agarose scaffold was pulverized and vortexed. To quantify the total amount of S-GAGs, the dimethyl methylene blue assay was performed with standards prepared from shark chondroitin sulfate (Sigma) [467]. The same assay was used to measure the amount of S-GAG release into the medium after applying the hydrostatic pressure loading. To measure cellularity of each construct, the PicoGreen fluorescent double-stranded DNA assay was used based on manufacturer's directions (Invitrogen).

2.3.6 Histology

Agarose was fixed, dehydrated, processed, embedded in paraffin, and sectioned at 8 μm thickness. Sections were stained with Safranin-O/hematoxylin using standard protocols. Brightfield images were taken at 20X magnification on a VS120 microscope (Olympus).

2.3.7 Live-Dead imaging

Constructs were stained for 30 minutes using the live/dead dye (ThermoFisher, Calcein-AM and Ethidium homodimer-1). Then the samples were imaged using a confocal microscope with the laser powers that were suggested by ThermoFisher.

2.3.8 Data analysis

Biochemical contents were normalized to tissue wet weight (converted to DNA content in μg/g tissue or S-GAG content as a mass per wet weight as a percentage, %ww) or normalized for a S-GAG content per cell (μg S-GAG per μg DNA, μg/μg) prior to analysis. For statistical analysis of the influence of different hydrostatic pressure regimens in experiment 1, a one-way ANOVA was used (α=0.05) with each loading regimen constituting an independent factor. For analyzing the effect of hydrostatic loading and inhibitors in experiment 2, a two-way ANOVA (α=0.05) was used where the effect of hydrostatic loading was one independent factor and each inhibitor was a separate independent factor. For S-GAG release, as all the constructs of each group shared the same media, we performed our calculations using standard uncertainty analysis to derive the S-GAG synthesis rate in units of μg S-GAG/d/construct. To determine this rate, regression curves were fit to cumulative μg S-GAG/sample over the time of the study. The regression of each groups provides a slope (representing the rate of S-GAG media loss in units of μg/d /construct), error (standard deviation of this rate), and degrees of freedom. Similarly, the S-GAG content within the constructs at the final time point can be used to estimate an S-GAG accumulation rate also in units of μg/d/construct. Here, we assumed a linear increase in S-GAG accumulation for each construct from day 0 to day 28 and similarly calculated a mean accumulation rate, uncertainty, and degrees of freedom. Summing the S-GAG loss rate (as

measured in the media) and S-GAG accumulation rate (as measured in the construct) provides an estimate of total S-GAG synthesis. Uncertainty propagation analysis provides an estimate of the variability of the total synthesis rate. A retention ratio was further computed as the S-GAG accumulation rate divided by the total S-GAG synthesis rate. t-test comparison between each loaded group to the control (0 MPa) and a Bonferroni p-value correction was used to assess groups significantly different than the control. For experimental reasons, select inhibitor treatments were run alongside a single vehicle control group. As our overall objective focused on detecting the effect of hydrostatic loading, the effect the select inhibitor, and the effect of their interaction, our analyses only compared an individual inhibitor treatment and its appropriate vehicle control. Therefore, several comparisons made herein share the same vehicle data.

2.4 Results

2.4.1 Experiment 1: Mechanical loading regimens influence S-GAG production

None of hydrostatic pressure regimens significantly influenced the DNA content of tissue constructs ($p=0.751$) over a long-term, 28-day culture duration (Fig. 2a). The hydrostatic loading regimen did alter S-GAG biosynthesis and accumulation in tissue engineered constructs as measured by the S-GAG content within the tissue constructs ($p<0.0001$, Fig. 2b) and S-GAG content normalized to the DNA content of each construct ($p<0.0001$, Fig. 2c). In particular, applying 5 MPa amplitude of hydrostatic loading induced a significant reduction of S-GAG content at frequencies of 0.5 and 1 Hz, but no difference in S-GAG content at 0.25 Hz when compared to unloaded, 0 MPa applied, constructs. These trends were also evident with Safrinin-O staining of histological sections of constructs after 28 days of loading (Supplemental Fig. 2). Also, the lowest amount of total S-GAG (amount released into the medium + construct) and

retention fraction was observed in the constructs that were loaded with 5MPa amplitude and the frequencies of 0.5 and 1 Hz (Fig. 2d, ,2e).2e). Moreover, the trend of S-GAG release into the medium at different time points showed that by increasing the culture duration, the amount of S-GAG diffusion into the medium will increase (Fig. 2f). Applying a higher loading amplitude, 10 MPa, at 0.25 Hz, also demonstrated a decrease in tissue construct S-GAG content compared to control, unloaded tissue constructs. Similar trends were observed in constructs seeded with 30 or 60 million cells per mL (Fig. 3). Importantly, we did not observe cell death due to hydrostatic loading (Supplemental Fig. 3). Therefore, based on our results from experiment 1, we chose a hydrostatic pressure regimen of 5 MPa at 0.5 Hz in constructs seeded with 30 million cells per mL to proceed with the inhibitor screening of experiment 2.

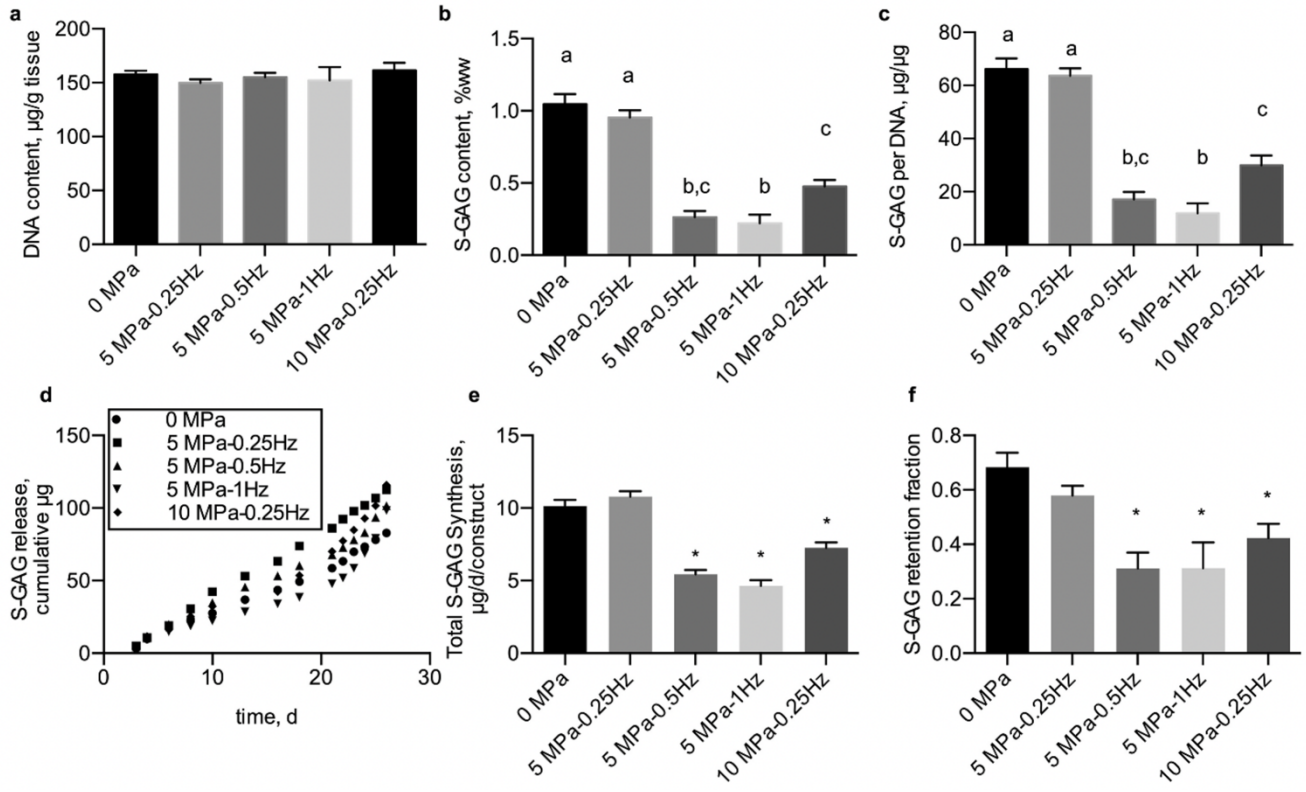

Figure 2.2 Effects of dynamic hydrostatic pressure on DNA and S-GAG content in chondrocyte-seeded agarose constructs. (a) DNA content of tissue engineered cartilage was unchanged by dynamic hydrostatic pressure, while (b) S-GAG content of tissue engineered cartilage and (c) S-GAG content normalized to DNA content were significantly reduced by hydrostatic pressure in a frequency and magnitude-dependent manner. (d) Amount of S-GAG release into the media as a function of culture duration (e) S-GAG retention fraction (f) Total S-GAG content synthesis. Groups not sharing a letter indicate statistically significant differences. n=5–6 per group. Groups with (*) are significantly different from the control (0 MPa).

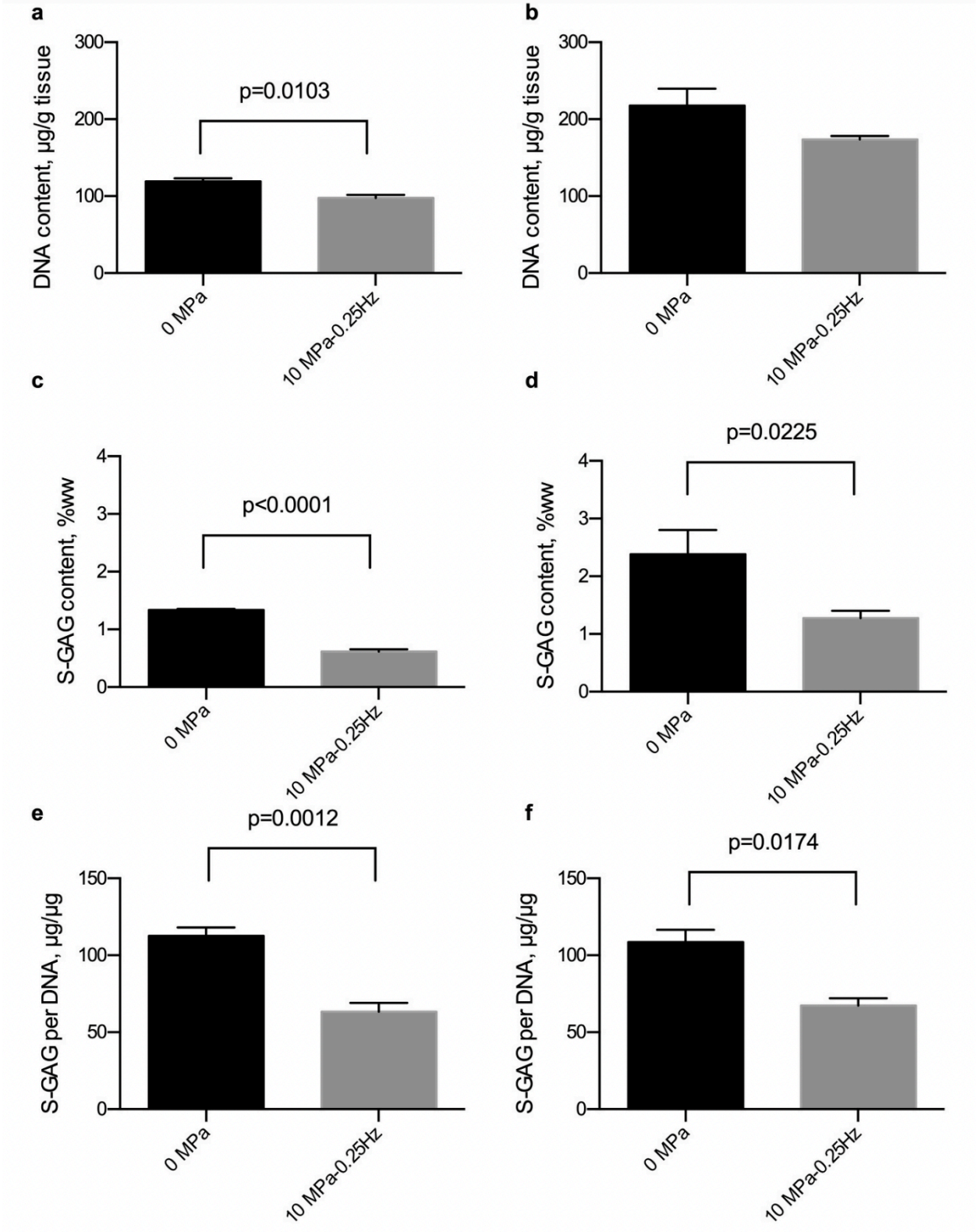
a
DNA content, µg/g tissue
300
200
100
0
p=0.0103
0 MPa
10 MPa-0.25Hz
b
DNA content, µg/g tissue
300
200
100
0
0 MPa
10 MPa-0.25Hz
c
S-GAG content, %ww
4
3
2
1
0
p<0.0001
0 MPa
10 MPa-0.25Hz
d
S-GAG content, %ww
p=0.0225
4
3
2
1
0
0 MPa
10 MPa-0.25Hz
e
S-GAG per DNA, µg/µg
p=0.0012
150
100
50
0
0 MPa
10 MPa-0.25Hz
f
S-GAG per DNA, µg/µg
p=0.0174
150
100
50
0
0 MPa
10 MPa-0.25Hz

Figure 2.3 Effects of cell density and dynamic hydrostatic pressure on DNA and S-GAG content in chondrocyte-seeded agarose constructs. (a and b) DNA content of tissue engineered cartilage was similar between loading groups for both cell densities, while (c and d) S-GAG content of tissue engineered cartilage and (e and f) S-GAG content normalized to DNA content consistently reduced by hydrostatic loading for both 30 million (n=3–5) and 60 million cell densities (n=2–3).

2.4.2 Experiment 2: Role of mechanosensitive ion channels in transducing hydrostatic pressure

MRS1845 inhibition of TRPC1 We inhibited TRPC1 activity with the inhibitor MRS 1845 (Fig. 4). After 14 days of daily hydrostatic loading, DNA content was not significantly different due to pharmacologic treatment ($p=0.055$) or loading ($p=0.92$) while S-GAG content was only significantly lower with the application of hydrostatic loading ($p=0.004$). Similarly, when S-GAG content is normalized to DNA content as a measure of S-GAG production on a cellularity basis, only the influence of hydrostatic loading was significant ($p=0.0097$).

Pyr3 inhibition of TRPC3 We inhibited TRPC3 using the inhibitor Pyr3 (Fig. 5). After 14 days of daily hydrostatic loading, DNA content was similar between all groups. S-GAG content was significantly lower with the application of hydrostatic loading ($p<0.0001$) and was lower with the Pyr3 inhibitor ($p=0.028$). When normalized to DNA content, S-GAG content was similarly reduced with the application of hydrostatic loading ($p<0.0001$) and Pyr3 inhibitor ($p=0.035$), but the interaction was not significantly altered.

GSK205 inhibition of TRPV4 We inhibited TRPV4 using the inhibitor GSK205 (Fig. 6). After 14 days of daily hydrostatic loading, DNA was lower with the treatment of GSK205. S-GAG content was significantly lower with the application of hydrostatic loading ($p<0.0001$) and with the GSK205 inhibitor treatment ($p<0.0001$). Notably, while both the non-loaded and

hydrostatic pressure treated samples supplemented with GSK205 were statistically similar ($p=0.99$), non-loaded and hydrostatic pressure loaded samples were statistically different ($p<0.0001$), consistent with the characterization from experiment 1. S-GAG content normalized to DNA content was reduced with the application of hydrostatic loading ($p=0.0005$) and GSK205 inhibitor ($p<0.0001$).

A 784168 inhibition of TRPV1 We used the inhibitor A 784168 to inhibit activity of TRPV1 (Fig. 7). After 14 days of daily hydrostatic loading, DNA was higher with the A 784168 treatment ($p=0.036$) but unaffected by loading ($p=0.397$). S-GAG content in engineered cartilage samples was significantly reduced by hydrostatic loading ($p<0.0001$) but was partially recovered by A 784168 treatment ($p=0.136$). When normalized to DNA content, engineered cartilage S-GAG content was reduced with the application of hydrostatic loading ($p<0.0001$) but not by A 784168 ($p=0.864$). By either measure of S-GAG content, the A 784168 treated group was significantly higher than the untreated group in response to hydrostatic pressure.

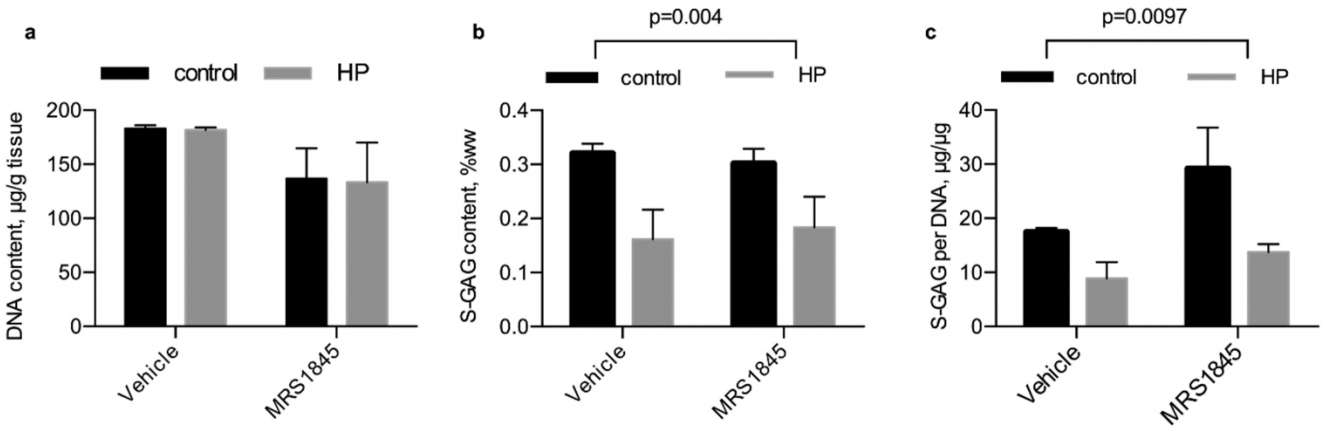

Figure 2.4 Influence of hydrostatic loading and TRPC1 inhibition with MRS 1845 on DNA and S-GAG content. (a) DNA content per tissue wet weight, (b) S-GAG content per tissue wet weight, and (c) S-GAG content per DNA content in tissue engineered cartilage. Control, no pressure; HP, hydrostatic pressure, n=5–6 per group.

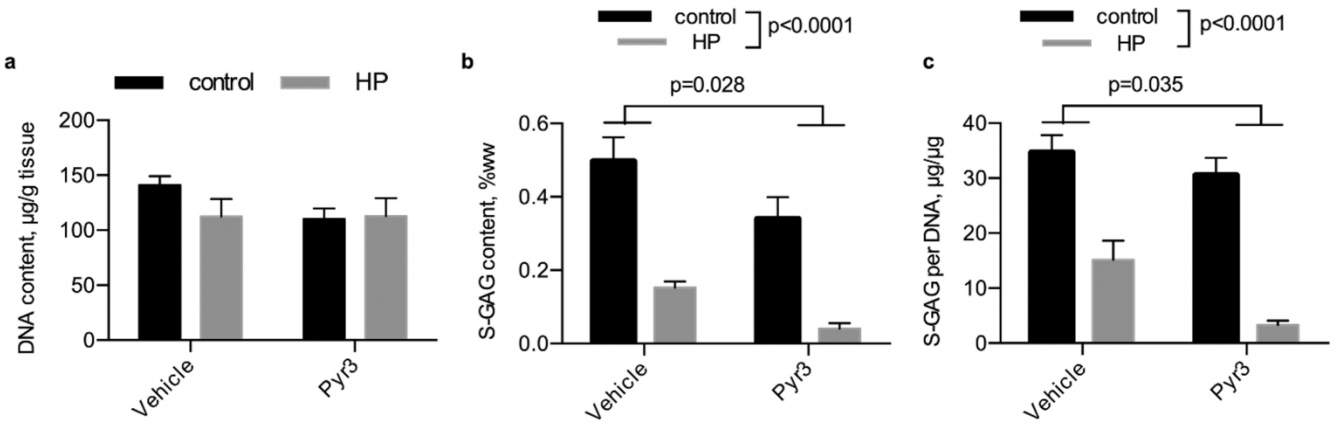

Figure 2.5 Influence of hydrostatic loading and TRPC3 inhibition with Pyr3 on DNA and S-GAG content. (a) DNA content per tissue wet weight, (b) S-GAG content per tissue wet weight, and (c) S-GAG content per DNA content in tissue engineered cartilage. Control, no pressure; HP, hydrostatic pressure, n=3–5 per group.

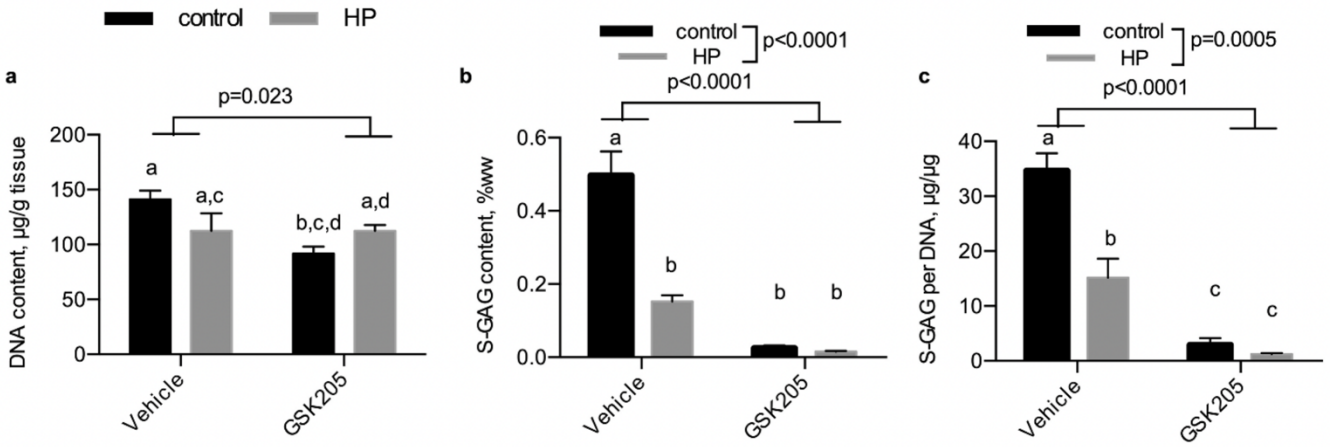

Figure 2.6 Influence of hydrostatic loading and TRPV4 inhibition with GSK205 on DNA and S-GAG content. (a) DNA content per tissue wet weight, (b) S-GAG content per tissue wet weight, and (c) S-GAG content per DNA content in tissue engineered cartilage. Control, no pressure; HP, hydrostatic pressure, n=5 per group.

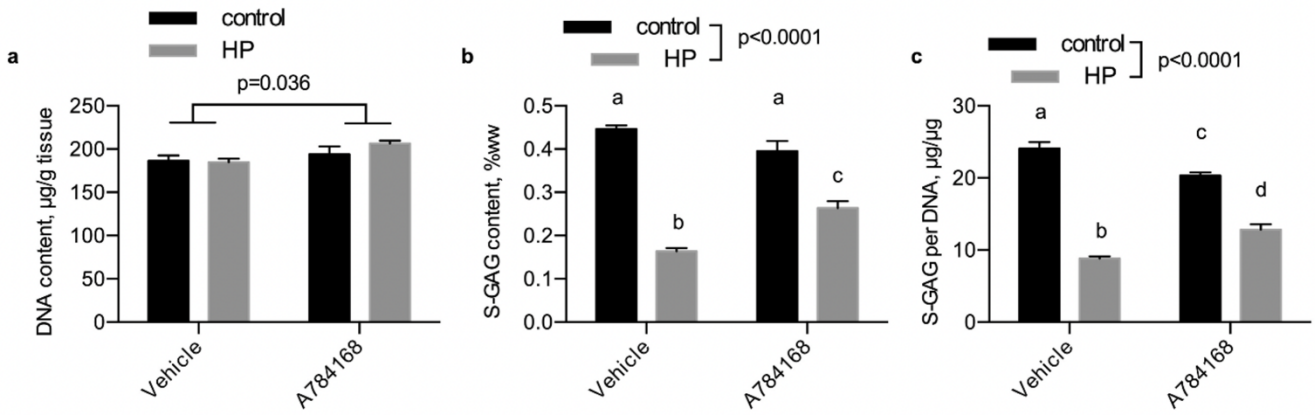

Figure 2.7 Influence of hydrostatic loading and TRPV1 inhibition with A784168 on DNA and S-GAG content. (a) DNA content per tissue wet weight, (b) S-GAG content per tissue wet weight, and (c) S-GAG content per DNA content in tissue engineered cartilage. Control, no pressure; HP, hydrostatic pressure, n=4 per group.

2.5 Discussion

In this study, we analyze the influence of hydrostatic loading on tissue engineered cartilage growth and matrix production and the role of mechanically-sensitive TRP ion channels on this response. We found that increased amplitudes (5–10 MPa) and frequencies (0.5–1 Hz) of dynamic hydrostatic loading induced a consistent response by inhibiting matrix production in our tissue engineered constructs. As mechanically-sensitive ion channels have been shown to play important roles in chondrocyte mechanobiology, we targeted several mechanically-sensitive TRP ion channels to determine if they are responsible for transduction of the signals incurred during hydrostatic pressure loading. Of the various inhibitors we used to target different ion channels, only the inhibition of TRPV1 altered the response to hydrostatic pressure. Together our results suggest that the growth modulating effect caused by hydrostatic loading may be transduced via this channel in the chondrocyte and support the notion that different ion channels are responsible

for transducing different biophysical stimuli such as hydrostatic pressure, membrane stretch, or osmotic stress.

Our results on differential HP loading regimes highlighted an interesting synthesis and retention behavior, where constructs exhibited similar S-GAG accumulation, total S-GAG synthesis, and S-GAG retention fraction characteristics. While we believe the mechanism governing differential matrix synthesis rates to be dependent on HP mechanotransduction to the cell, the finding that retention fractions are also differentially regulated by HP suggests other factors could be differentially regulated: (1) HP may also alter the synthesis of binding proteins or other molecules critical for S-GAG retention within the extracellular matrix of engineered cartilage, and/or [444] HP load may be modulating the cellular release of extracellular proteases or other molecules implicated in the loss of the extracellular matrix, and/or [444] HP load may be modulating a cellular-independent effect resulting in the loss of S-GAG, although this cellular-independent mechanism is less clear. Nims et al reported a similar level of S-GAG retention to our measurements here and speculated that S-GAG binding density may be a function of hyaluronan production into the extracellular matrix [468].

We found consistently that dynamic hydrostatic pressure inhibited S-GAG accumulation by chondrocytes in agarose; however, other studies found mixed results by applying the same loading magnitude that was used in this research depending on the duration. Parkkinen et al. also showed that in monolayer culture of bovine chondrocytes, applying the dynamic hydrostatic loading regimen that was used in our study (5MPa, 0.5Hz) for 1.5 h inhibits the S-GAG production as well, however, applying the same load to cartilage explant had the opposite effect [469]. Moreover, Jortikka et al. found that applying the aforementioned dynamic hydrostatic pressure for 20 h would significantly increase the S-GAG production in bovine chondrocytes in

monolayer culture [470]. Therefore, it appears that the duration of hydrostatic pressure loading and the culture system of chondrocytes (monolayer (2D) or hydrogel (3D, scaffolds, gels and pellet), and cartilage explants (3D)) have significant effects on the chondrocytes biosynthesis, biochemical properties and differentiation in response to hydrostatic pressure and the results can be completely different by changing any of these conditions [448, 453-455, 469-486]. For instance, collagen type II production seems to be more affected by the pressure magnitude. Dynamic hydrostatic pressure of 10 MPa at 1 Hz has the most effect on its synthesis in 2D culture [474, 482, 483], while lower levels of pressure can increase aggrecan production [474, 484]. On the other hand, in 3D culture, the constructs and the environment are more complicated, therefore, the magnitude, frequency and duration of loading could play an important role in matrix production. Even though physiological levels of hydrostatic pressure with specific durations improved matrix production, high magnitudes of it had negative effects. Increasing the magnitude of static pressure to 20 MPa - 50 MPa in resulted in a significant decrease in S-GAG and collagen production and increased cell apoptosis and the stress response gene heat shock protein 70 [455, 475, 478, 481, 487]. Interestingly, in general the cell content of our tissue constructs, as inferred by construct DNA content, did not vary with the application of hydrostatic pressure loading, suggesting the biosynthetic results at high loading pressures (10 MPa) did not induce cell death but just altered cellular metabolism. Furthermore, in our current work we have found TRPV4 and PIEZO1 mechano-sensitive channels provoke inflammatory signaling in chondrocytes [85, 468] and since high magnitudes of hydrostatic pressure inhibit growth and increase apoptosis, it is possible that these or other channels may be involved in regulating different magnitudes or frequencies of hydrostatic pressure.

We hypothesized that the response to hydrostatic pressure was mediated by one of the mechanically-sensitive TRP ion channels. Of note, only the inhibition of TRPV1 partially prevented the decrease in S-GAG accumulation caused by hydrostatic pressure. TRPV1, also known as the capsaicin receptor, was the first TRP channel to be identified and cloned and primarily serves as a sensor for heat and pain (nociception) in sensory neurons [488]. However, in other cell types, TRPV1 serves other sensing functions, alone or in combination with other mechanosensitive channels [328, 489, 490]. In particular, growing evidence suggests that TRPV1 could function as a hydrostatic pressure sensor in the eye [491], potentially through interactions with TRPV4 [198]. Further work is needed to identify the downstream pathways and potential synergistic interactions of these channels in chondrocytes [359]. Moreover, based on our results and the polymodal nature of the TRPV1 channel, future studies will be necessary to assess how mechanical versus thermal or pH activation of TRPV1 may induce different cellular signaling pathways and potentially differentially regulate chondrogenesis through TRPV1 modulation.

While we tested a number of TRP channels, it is important to note that other mechanosensitive channels such as TRPC6, TRPM7, and Piezo1/2 may be involved in a hydrostatic pressure response [492]. But there is currently a lack of commercially-available inhibitors that are selective and specific for these channels. For example, recent studies suggest that the hydrostatic response of immune cells is mediated through the Piezo-family of mechanically sensitive ion channels [493]. While the pressures they used were far below those examined in our study, and the mechanical environment used is not described (2D/3D), future studies may wish to investigate the role of Piezo ion channels in transducing hydrostatic pressure effects [209]. Additionally, the inhibitor doses we supplemented were prescribed by established

literature in alternative cell types. Future studies may focus on more complete inhibition of the hydrostatic response with inhibitor dosing-response studies and establishing how the channels are activated by a hydrostatic pressure stimuli.

In addition to the potential role of ion channels, several studies have evaluated other intracellular or downstream mechanisms in response to hydrostatic pressure. Nordberg et al. showed that LPR5 and LRP6 mRNA levels increased after applying a dynamic hydrostatic pressure of 7.5 MPa, 1 Hz, 4 hours/day for up to 14 days [479]. Furthermore, active β-catenin protein expression showed the same trend as LRP5 and increased by applying cyclic hydrostatic pressure. Knight et al. observed that both static (5 MPa) and dynamic (5 MPa, 1 Hz) of hydrostatic loading alters the actin organization and these cytoskeletal changes can be recovered after 1h of applying the pressure [494]. In addition, another study investigated the changes in the intracellular Ca^{2+} response of chondrocytes to hydrostatic pressure along with the influence of seeding duration and zonal differences [495]. Mizuno showed that applying 0.5 MPa of pressure for 5 minutes increases the Ca^{2+} levels in bovine chondrocytes, and this effect can be inhibited when the cells are treated with gadolinium, intracellular storage blocker (dantrolene), or Ca^{2+} -free medium. Moreover, this study showed that the middle zone chondrocytes are more responsive to hydrostatic pressure and had the highest Ca^{2+} influx. Lastly, it was observed that the chondrocytes that were seeded for 2 days did not have any response to hydrostatic pressure, but showed a response after 5 days of seeding.

In summary, we screened a number of TRP channels in an effort to identify the mechanism(s) by which chondrocytes respond to hydrostatic pressure. We targeted mechanosensitive TRP ion channels to evaluate their inhibition of matrix production while cultured under daily hydrostatic loading of 5 MPa at 0.5 Hz. This loading regimen was used

because it robustly inhibited S-GAG production of chondrocytes seeded in agarose gel. We hypothesized that by inhibiting mechanosensitive TRP ion channels would recover the S-GAG production present in unloaded engineered cartilage. Interestingly, inhibition of neither TRPV1, TRPV4, TRPC3, and TRPC1 completely inhibited the hydrostatic loading effects on S-GAG production in chondrocytes. The modest influence of TRPV1 suggest future studies may be well targeted on the role of TRPV1 in hydrostatic-mediated effects. Consequently, our pilot study here on the role of mechanically-sensitive TRP channels in hydrostatic pressure-mediated mechanotransduction cascade suggest only a potentially small involvement of the channels and hint to a more complex mechanosensory is involved in the hydrostatic pressure loading response on matrix production of articular cartilage. More studies are required to combine the potential mechanisms to find the actual process by which hydrostatic pressure alters the matrix synthesis in articular cartilage.

2.6 Supplemental Figures

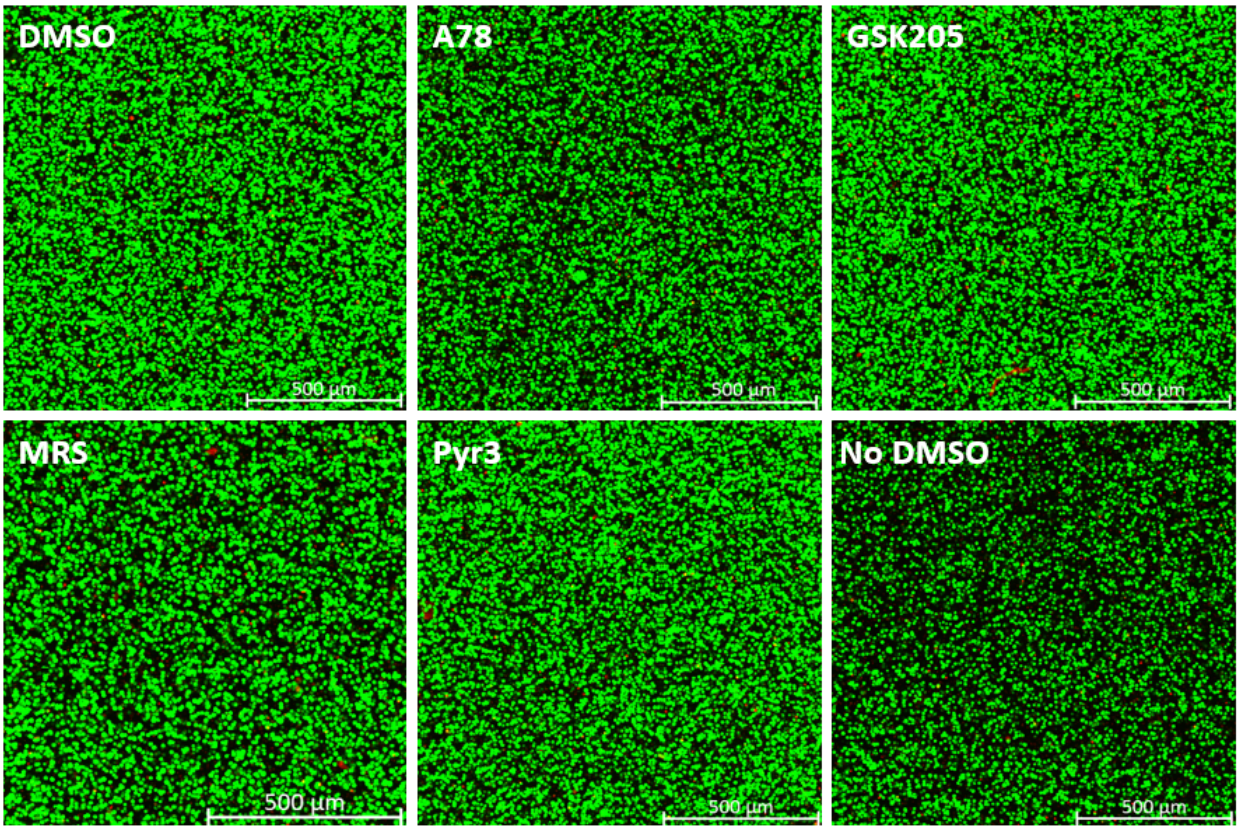

Figure S2.1 Live/dead staining of the constructs after being treated for 3 hours with different inhibitors showed that these inhibitors do not cause chondrocyte death. (DMSO: dimethyl sulfoxide; A78: TRPV1 inhibitor; GSK205: TPV4 inhibitor; MRS: TRPC1 inhibitor; Pyr3: TRPC3 inhibitor.

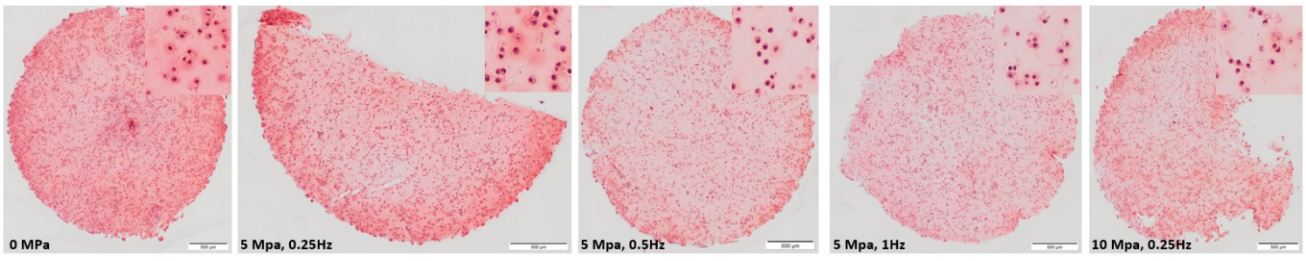

Figure S2.2 Safranin-O/hematoxylin staining of the constructs that were loaded with different hydrostatic pressure regimens. Histology and safranin-O staining reflected the quantitative S-GAG measurements made using the DMMB assay.

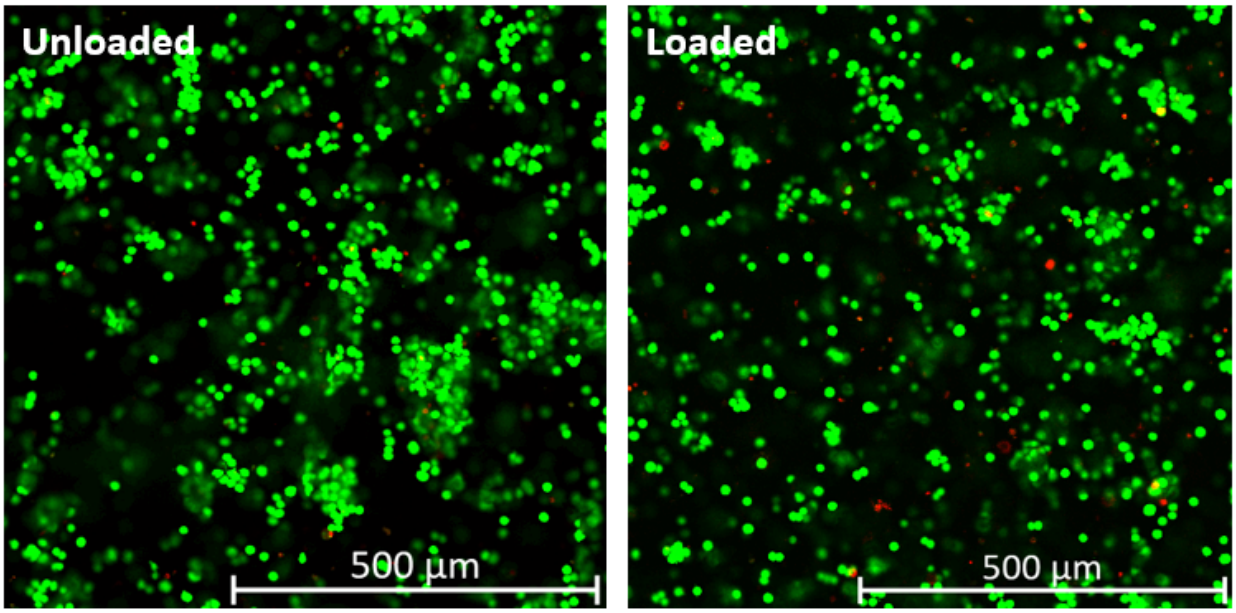

Figure S2.3 Live/dead staining of the constructs after being loaded statically by 20MPa pressure for 3 hours. Hydrostatic pressure did not cause increased cell death.

Chapter 3: Membrane Stretch as the Mechanism of Activation of PIEZO1 Ion Channels in Chondrocytes

Partially adapted from: Savadipour, A., Nims, R. J., Rashidi, N., Garcia-Castorena, J. M., Tang, R., Marushack, G. K., Oswald, S. J., Liedtke, W. B., & Guilak, F. (2023)
Membrane Stretch as the Mechanism of Activation of PIEZO1 Ion Channels in Chondrocytes.
Proceedings of the National Academy of Sciences 120.30 (2023): e2221958120

3.1 Abstract

Osteoarthritis is a chronic disease that can be initiated by altered joint loading or injury of the cartilage. The mechanically-sensitive PIEZO ion channels have been shown to transduce injurious levels of biomechanical strain in articular chondrocytes and mediate cell death. However, the mechanisms of channel gating in response to high cellular deformation and the strain thresholds for activating PIEZO channels remain unclear. We coupled studies of single-cell compression using atomic force microscopy (AFM) with finite element modeling (FEM) to identify the biophysical mechanisms of PIEZO-mediated Ca^{2+} signaling in chondrocytes. We showed that PIEZO1 and PIEZO2 are needed for initiating Ca^{2+} signaling at moderately high levels of cellular deformation, but at the highest strains, PIEZO1 functions independently of PIEZO2. Biophysical factors that increase apparent chondrocyte membrane tension, including hypo-osmotic pre-strain, high compression magnitudes, and low deformation rates, also increased PIEZO1-driven Ca^{2+} signaling. Combined AFM/FEM studies showed that 50% of chondrocytes exhibit Ca^{2+} signaling at 80-85% nominal cell compression, corresponding to a

threshold of apparent membrane finite principal strain of E=1.31, which represents a membrane stretch ratio (λ) of 1.9. Both intracellular and extracellular Ca^{2+} are necessary for the PIEZO1-mediated Ca^{2+} signaling response to compression. Our results suggest that PIEZO1-induced signaling drives chondrocyte mechanical injury due to high membrane tension, and this threshold can be altered by factors that influence membrane prestress, such as cartilage hypo-osmolarity, secondary to proteoglycan loss. These findings suggest that modulating PIEZO1 activation or downstream signaling may offer avenues for the prevention or treatment of osteoarthritis.

3.2 Introduction

Altered joint loading or joint injury increases the risk of developing post-traumatic osteoarthritis (PTOA). While the mechanisms linking injury and PTOA are not fully understood, several studies have suggested that alterations in chondrocyte physiology or even cell death due to supraphysiologic strains may be in part responsible for the initiation and progression of joint degeneration [496]. The PIEZO family of ion channels, consisting of PIEZO1 and PIEZO2, are expressed by cartilage-resident chondrocytes and respond to supraphysiologic levels of chondrocyte deformation [237]. We previously found PIEZO inhibition reduced chondrocyte death during cartilage injury, suggesting the potential of these channels as therapeutic targets for PTOA [237, 316]. While recent studies suggest that PIEZO activation is regulated by cellular membrane tension, it is unclear how whole cell deformation relates to localized membrane tension as a potential mechanism for initiating PIEZO signaling [210, 223]. Therefore, our goal was to determine the thresholds of mechanical strain that initiate cellular signaling by quantifying the physical signals that link cellular compression and PIEZO activation, in the context of chondrocyte responses to pathologic loading.

The biomechanical state of a cell, and its response to exogenous loading, is complex and depends upon interactions between the cell and the extracellular environment, including external forces, cytoskeletal proteins, cell-matrix interactions, and pericellular osmolarity, as well as intracellular conditions, including active cellular force generation, cellular stiffness, and viscoelasticity [215, 497-512]. The interface between these extracellular and intracellular conditions is the plasma membrane, where mechanosensitive ion channels, including the PIEZOs, directly respond to physical factors such as membrane stretch. Interestingly, while PIEZO activation has been attributed to increased tension in the plasma membrane, many cells, including chondrocytes, possess considerable membrane reservoirs which endow a high degree of apparent extensibility that would occur prior to an actual stretch of the membrane bilayer [513]. It is likely that membrane reservoirs would alter how externally applied forces contribute to and induce PIEZO signaling [514]. However, because of the fine structure and properties of the plasma membrane, real-time optical measurements of membrane "stretch" per se are not possible with current microscopy techniques, and thus theoretical modeling approaches can provide critical insights in our understanding of membrane mechanics [515]. Together, such a combined experimental and theoretical framework can improve our understanding of how cellular deformation modulates PIEZO mechanosensitivity.

Here, we investigated how mechanical compression induces PIEZO signaling and the implications of PIEZO signaling in cartilage injury. By coupling experimental atomic force microscopy (AFM) measurements with computational biomechanical models, we determined how bulk cellular compressive loading induces plasma membrane stretch to induce PIEZO activation. We further identified the specific roles of the osmotic environment, the magnitudes of applied force, and the rate of applied loading modulate PIEZO1 activation and observed that

PIEZO1 activation requires both intracellular and extracellular Ca^{2+} sources. Together, our findings demonstrate how PIEZO1 is activated by membrane strain and is linked to external events including applied cellular compression and extracellular factors. This understanding of the mechanisms by which chondrocytes respond to supraphysiologic loading will provide important insights into the development of new pharmacologic therapies to treat mechanically induced diseases such as PTOA.

3.3 Materials and Methods

3.3.1 Cell Culture and Sample Preparation

The knees of skeletally mature pigs (5-6 months old, mixed breeds of landrace yorkshire and duroc) were acquired on the day of slaughter from a local abattoir shop. The articular cartilage of the femoral mid-condyle was cut out and maintained in standard culture media (High glucose DMEM (Gibco, Thermo Fisher Scientific, Waltham, MA), 10% fetal bovine serum (FBS, Atlas Biologicals, Fort Collins, CO), 1.5% HEPES (Corning, Corning, NY), 1% MEM Non-essential amino acid (Corning), 1% Pen Strep (Gibco, Thermo Fisher Scientific), 0.5% L-Proline (Sigma Aldrich, St. Louis, MO)) for 1-2 days prior to digestion. The tissue was digested in pronase (Worthington Biochemical, Lakewood, NJ) dissolved in the wash media (High glucose DMEM, 1x Gentamycin (Gibco, Thermo Fisher Scientific), 1x Kanamycin (Goldbio, St. Louis, MO), 1x Fungizone (Corning)) (1320 PKU/ml media) for 1-1.5 hours. Next, the pronase-containing media was removed from the tissue, and the tissue was incubated for 3-3.5 hours with media containing 0.4% collagenase type II (Worthington Biochemical). Lastly, the cells were filtered, washed, resuspended in the growth media (10% FBS, 1.5% HEPES, 2% Pen/Strep), counted and plated on 12mm round coverslips #1.5 (Electron Microscopy Sciences, Hatfield,

PA) with the concentration of 50,000-100,000 cells/coverslip for the AFM study. For the confocal studies, the cells were plated in high resolution glass-bottom 96-well plates (Cellvis, Sunnyvale, CA). The cells were cultured for 3 days in an incubator (5% CO2, 37 °C) prior to testing. The wash and growth media osmolarity was kept at 380-400 mOsm to mitigate the physiological conditions in cartilage [516, 517].

3.3.2 Atomic Force Microscopy

Primary chondrocytes were compressed using an Atomic Force Microscope (AFM; MFP-3D Bio, Asylum Research, Santa Barbara, CA). Prior to testing, the cells were labeled with Fura2-AM dye (Invitrogen, Thermo Fisher Scientific), an intracellular Ca^{2+} sensitive dye, in media (Phenol red free DMEM, Gibco, Thermo Fisher Scientific), with 1.5% HEPES buffer (Corning), 1% Pen Strep (Gibco Thermo Fisher Scientific), 1% MEM non-essential amino acid (Corning), 1% Na Pyruvate (Corning), 1% GlutaMax (Gibco, Thermo Fisher Scientific), 0.1% L-Proline (Sigma Aldrich)) for 1-2 hrs. Chondrocytes were compressed using a tipless cantilevers with approximate stiffness of 7-13 N/m (Nanoandmore, Watsonville, CA). The stiffness of the cantilevers was measured using the thermal method provided by the manufacturer. While cells were being loaded, 340/380 nm wavelength light sources were used to capture ratiometric Ca^{2+} images. All the experiments were performed at 37°C in a hydrated environment. Cells that moved during imaging or were damaged (as noted by rapid loss of intracellular fluorescence) were not included in the analysis. The obtained AFM curves, which show the amount of indentation against the vertical displacement of the cantilever, were analyzed using a custom written MATLAB code (The Math Works, Inc, https://www.mathworks.com) to find the contact point, cell height, and cellular deformation in response to loading. Moreover, the videos of cells'

intracellular Ca^{2+} response to mechanical loading were analyzed using ImageJ software (U. S. National Institutes of Health, Bethesda, MD, https://imagej.nih.gov/ij/).

3.3.3 Confocal Microscopy

Nucleofected cells were stained for 1 hour prior to imaging using Fura red-AM (Invitrogen, Thermo Fisher Scientific) and Fluo4-AM (Invitrogen, Thermo Fisher Scientific), which are Ca^{2+} indicator dyes elucidating the changes in the level of Ca^{2+} concentration in the cell. After labeling, cells were washed and placed under a confocal microscope (LSM 880, Zeiss, Dublin, CA). The temperature during imaging was kept at 37°C to keep the environment similar to physiological conditions. After 1 minute of baseline imaging, control solution (DMSO, Sigma Aldrich) was added to the cells, and the cells were imaged for another 2 minutes. After control imaging, final concentration of 5 μM of Yoda1 was added to the cells, and the cellular response was imaged for another 2 minutes. All labeling, washing, and imaging steps were performed in iso-osmotic conditions. After imaging, the videos were analyzed in ImageJ to quantify the level of Ca^{2+} response of each cell during imaging.

3.3.4 Image Analysis

We analyzed the images from confocal and AFM experiments in ImageJ. Briefly, we exported the videos to ImageJ and divided the two channels that represent the fluo-4 and fura-red in the confocal imaging or 340 nm and 380 nm wavelength light sources that excited the fura-2 in the AFM experiment by each other to show the normalized intensity of the signal. Then, by thresholding the videos based on the staining intensity, we acquired and analyzed the shape of the cells in terms of pixel intensity throughout the whole experiment. Afterward, we normalized the mean pixel intensities to the baseline level of the signal. Finally, we reported the maximum

value of normalized pixel intensity for each cell as the intracellular Ca^{2+} response of the cell ($\Delta Fmax/F$).

To separate the responders and non-responders in the AFM studies, we performed a control test in which the cantilever was located on top of the cells, but no load was applied. Afterward, we analyzed the Ca^{2+} transient within those cells, normalized it, and calculated the mean (M) and standard deviation (SD) of the intracellular Ca^{2+} response of those cells. We considered any cellular Ca^{2+} response higher than the average of the control group plus three times the standard deviation of the mean ($\Delta Fmax/F > M + 3*SD$) that had a peak in its intracellular Ca^{2+} response trace as a responder. Therefore, any cell whose Ca^{2+} response was lower than that value or did not have a peak in its Ca^{2+} response trace was considered as a non-responder.

For the confocal experiment analysis, we analyzed the videos in ImageJ and reported the $\Delta Fmax/F$ of each cell for each experiment. We then processed these results using a custom-written MATLAB code to find the percentage of the responding cells and the average level of intracellular Ca^{2+} signaling. Using the MATLAB code, we normalized individual cell's intracellular Ca^{2+} response to Yoda1 addition to the cell's response after the DMSO addition. Then, we determined the average of the $\Delta Fmax/F$ of all the cells and reported it as the mean cellular response calculated from each video. Moreover, the MATLAB code evaluated whether the $\Delta Fmax/F$ of a cell was higher than the average of the cellular Ca^{2+} signal after DMSO addition (M´) plus five times the standard deviation of the mean (SD´) ($\Delta Fmax/F > M' + 5*SD'$). If so, we considered the cell as a responder. Finally, we reported the total number of the responders divided by the total number of the cells as the percentage of the responding cells for each video. If there were more than 4 values for the responding cells, meaning the experiment

was performed on more than 4 different animals, we reported the individual values for the percentage of the responding cell. However, if we had less than 4 values per group, we reported the average of all the results and reported a single value for the percentage of the responding cells.

3.3.5 Osmotic Treatment

Osmolarity of the media was changed by adding sucrose (Sigma Aldrich) to make either the hyper-osmotic (600 mOsm) or isosmotic (400 mOsm) solution, or by adding ultrapure 18 Megaohm water to achieve the hypo-osmotic solution (200 mOsm). The media was then filtered and used for osmotic treatments.

3.3.6 siRNA

Chondrocytes were isolated as previously described and immediately nucleofected with siRNA targeting the porcine (Sus scofra) PIEZO1 mRNA (a pool of siRNAs with the following sequence strands:

5’-CAGCGAGAUCUCGCACUCCAUCUU-3’, 5’-UACGACCUGCUGCAGCUCCUGUU-3’, and 5’-ACCCGCUGGCCAUGCAGUUCUUUU-3’ all synthesized from Dharmacon, Lafayette, CO), Piezo2 mRNA (pool of siRNAs with the following sense strands:

5’-GAUCUGCGUGGAGGACAUUUAUGUU-3’, and

5’-CGACGAAGUCGAACAGUGAGUGUU-3’all synthesized from Dharmacon), or a non-targeting construct siRNA (siNTC, Invitrogen, Thermo Fisher Scientific). Nucleofection was performed using the Lonza (Basel, Switzerland) 4D-Nucleofector according to the manufacturer’s guidelines, utilizing the ER-100 protocol. Nucleofected cells were plated on glass

coverslips, 96-well plate, or 6-well plates depending on the experiments, in FBS-containing feed media without Pen-strep. After three days of culture, cells were either collected for RT-qPCR or western blot analysis or stained for AFM or confocal imaging.

3.3.7 RNA Isolation and RT-qPCR

The cells were plated after nucleofection, and the mRNA was isolated after 3 days of culture (Norgen, Total RNA Purification Plus kit, Thorold, ON, Canada) and quantified using a NanoDrop. Afterwards, the cDNA was synthesized from mRNA (VILO Superscript Mastermix, Life Technologies, Carlsbad, CA) and real-time quantitative PCR was run using the cDNA with fast SYBR Green Master mix (Thermo Fisher Scientific). The delta delta Ct (ΔΔCt) method was used to quantify the relative expression of the genes of interest, and finally the expression levels were normalized to the ACTB mRNA levels. The sequence of the primers used are listed below.

PIEZO1: Forward 5'-GCCCCCAACGGACCTGAAGC-3'

Reverse 3'-TGCGCAGCTGGATACGCACC-5'

PIEZO2: Forward 5'-CCAGCTGGATCTGCGTGGAGG-3'

Reverse 3'-TGGTTGATCACCCCGGCGAC-5'

ACTB: Forward 5'-CACGCCATCCTGCGTCTGGA-3'

Reverse 3'-AGCACCGTGTTGGCGTAGAG-5'

3.3.8 Immunolabeling

After three days of culturing cells on round coverslips, media was washed, and cells were fixed with 4% paraformaldehyde (Electron Microscopy Sciences) for 10 minutes. Then, cells were washed with 2x Dulbecco's phosphate-buffered saline (DPBS, Gibco) followed by cell permeabilization with 0.3% Triton X-100 (Sigma) in DPBS for 5 minutes. Afterwards, 2.5% normal goat serum (Vector Laboratories, Burlingame, CA) was added for 45 minutes to block the cells. Lastly, samples were labeled with conjugated rabbit Piezo1 and Piezo2 antibodies overnight (1:25, Novus Biologicals, Littleton, CO). After immunolabeling, the cells were washed with DPBS and stored at 4°C until imaging.

3.3.9 Western Blot

To examine the effect of siRNA knockdown on PIEZO1 and PIEZO2 expression in porcine chondrocytes at protein levels, western blot analysis was performed. Protein concentration was measured using the Pierce BCA Protein Assay (Thermo Fisher Scientific) after lysing in RIPA buffer (Cell Signaling Technology, Danvers, MA) with 2.5% CHAPS (Sigma Aldrich) and protease inhibitor (Thermo Fisher Scientific). Each well of a 6% sodium dodecyl sulfate-polyacrylamide electrophoresis gel was loaded with 25 μg protein or pre-stained molecular weight markers (Thermo Fisher Scientific). The transferred polyvinylidene fluoride (PVDF) membranes were incubated overnight at 4°C with the primary antibodies: anti-PIEZO1 (1:1000, Proteintech, #15939-1-AP), anti-PIEZO2 (1:300, Alomone labs, Jerusalem, Israel, #APC-090), anti-GAPDH (1:20000, Proteintech #60004-1-Ig) for PIEZO1 knockdown, PIEZO2 knockdown, or loading control, respectively. Afterward, the membrane was incubated with HRP-conjugated secondary antibodies (1:3000, Cell Signaling Technology). Immunoblots were imaged and analyzed using the iBright FL1000 Imaging System (Thermo Fisher Scientific).

Normalized Western Blot intensity represent the signal intensity divided by the area of protein bands in arbitrary units after normalization to the signal intensity of GAPDH.

3.3.10 Chemical Inhibition of Ca^{2+} Signaling

Inhibitors were used to evaluate the effect of several factors on the mechanosensitivity of the PIEZO1 channel. We used GsMTx-4 to show that the responses to mechanical loading and different rates of loading are due to the activation of the PIEZO1 channel. We used EGTA and thapsigargin to determine the role of extracellular and intracellular Ca^{2+} sources, respectively, in the activation of the PIEZO1 channel. The concentration of each inhibitor and the duration of treatment are as follows: GsMTx-4 (20μM, 15 minutes prior to loading, Alomone Lab), EGTA (10mM, Sigma Aldrich), Thapsigargin (3μM, 30 minutes prior to loading, Sigma Aldrich).

3.3.11 Finite Element Modeling (FEBio)

To assess the mechanical influence of different loading conditions, we developed a neo-Hookean FE model of the cell during AFM compression using FEBio software (v. 2.6, www.febio.org). The model was fitted to the force/deflection AFM curves to determine the elastic modulus. Moreover, the model consisted of a homogeneous cytoplasm phase and a shell element to represent the cell membrane, both of which were fit to the same neo-Hookean model. The cell was considered to be axisymmetric in shape and have axisymmetric boundary conditions. Therefore, we modeled 1/8 of the cell to find the elastic modulus under different osmotic and mechanical conditions. The cell was considered to be incompressible ($v = 0.4999$) and a Lagrangian contact point between the cell and the cantilever was developed to enhance the quality of the contact. The apparent membrane strain was acquired from the model using the principal Lagrangian strain (E) of the membrane shell material, and the membrane tensile stretch

was calculated using the Green strain equation $\lambda = \sqrt{((2E+1))}$, where λ is the stretch ratio and E is the principal strain. The strain in the undeformed cell model (prior to compression or osmotic effects) was assumed to be zero, i.e., a stretch ratio of 1. To model osmotic shock, we used a material mixture of Neo-Hooken and cell growth along with an additional step of loading before the mechanical compression to simulate the short-term hypo-osmotic treatment.

3.3.12 Statistical Analysis

Average of the groups are presented in each plot with ±SEM. Statistical analysis was performed by student t-test, one-way, or two-way ANOVA followed by Tukey post-hoc to determine the significance between each group, $p<0.05$.

3.4 Results

3.4.1 The cooperation of PIEZO1 and PIEZO2 is dependent on the magnitude of loading

To investigate the role of PIEZO channels in chondrocyte mechanotransduction, we assessed the expression and mechanical responsiveness of the PIEZO channel family members PIEZO1 and PIEZO2 in chondrocytes. Both PIEZO1 and PIEZO2 channels were highly expressed in primary porcine chondrocytes (Fig. 1A), as we had previously found [237]. To determine cellular mechanosensitivity, we mechanically compressed isolated chondrocytes with a tipless cantilever to 500 nN at a loading rate of 1 μm/sec using atomic force microscopy (AFM) while monitoring the intracellular Ca^{2+} signaling response [237]. To determine the roles of PIEZO1 and PIEZO2 in this process, we used small interfering RNA (siRNA) to knock down PIEZO1 or PIEZO2 gene expression before measuring the intracellular Ca^{2+} signaling response of the chondrocytes to a high applied mechanical load of 500 nN. Reverse transcription

quantitative polymerase chain reaction (RT-qPCR) and western blotting confirmed the knockdown of PIEZO1 and PIEZO2 compared to the cells treated with a non-targeting control (NTC) siRNA. mRNA expression was reduced 87% for PIEZO1 ($p<0.0001$) and 72-76% for PIEZO2 ($p<0.0001$) while protein expression was reduced 67% for PIEZO1 and 61% for PIEZO2 compared to the NTC groups (Fig. 1B-C, Supplementary Fig. 1A). AFM compression of 500 nN (Fig. 1D, F) and 5 μM of Yoda1 (specific PIEZO1 agonist) pharmacologic stimulation (Fig. 1E, G) induced robust Ca^{2+} signals in the NTC-treated chondrocytes. However, PIEZO1 knockdown decreased Ca^{2+} signaling (AFM, $p<0.0005$; Confocal, $p<0.0001$) and the population of responsive cells to AFM compression or Yoda1 addition (AFM, $p<0.05$; Confocal, $p<0.0001$) (Fig. 1D-E). The same experiments were performed on cells in which PIEZO2 was knocked down using siRNA. Additionally, at loading magnitude of 100 nN, no cellular Ca^{2+} responses were observed in the NTC or P2-siRNA groups (Supplementary Fig. 1, $p=0.8398$ for Ca^{2+} response, $p=0.8524$ for percentage of the responding cells). At 300 nN force, P2-siRNA decreased chondrocyte Ca^{2+} response compared to NTC treated cells (Supplementary Fig. 1, $p<0.005$ for Ca^{2+} response, $p<0.05$ for percentage of the responding cells). At 500 nN AFM compression, however, the Ca^{2+} response and percentage of the responding cells were similar between Piezo2 knockdown and NTC-treated cells (Fig. 1F, $p=0.906$ for Ca^{2+} response, $p=0.572$ for percentage of the responding cells). These findings indicate the presence of a cooperative mechanism between PIEZO1 and PIEZO2 that is strain magnitude-dependent [237]. Furthermore, PIEZO2 knockdown significantly decreased the cellular response to the PIEZO1 agonist Yoda1 (Fig. 1G, $p=0.0046$ for Ca^{2+} response, $p=0.0037$ for percentage of the responding cells). Previous studies have shown that the response to Yoda1 is reduced in cells with PIEZO2 knock-down [518, 519]. Importantly, we further compared the levels of applied deformation and

found there were no significant differences between the NTC and P1-siRNA or P2-siRNA groups, demonstrating that the Ca^{2+} signaling changes to AFM compression were due to PIEZO1 or PIEZO2 knockdown and not alterations in the chondrocyte mechanical properties (Fig. 1D and 1F, for P1-siRNA p=0.134, and for P2-siRNA p=0.193, Supplementary Fig. 1B and 1C, p=0.6647 for 300 nN, and p=0.5541 for 100 nN). These results demonstrated that PIEZO1 and PIEZO2 interact and moderate levels of pathologic strain, but PIEZO1 serves as the primary mechanosensor at high, supraphysiologic mechanical loading, in this case 500 nN. As PIEZO1 was primarily responsible for conferring chondrocyte mechanosensitivity to high mechanical loads, we next sought to determine the relationship between the whole cell compression and apparent membrane strain as a potential mechanism for the activation of PIEZO1.

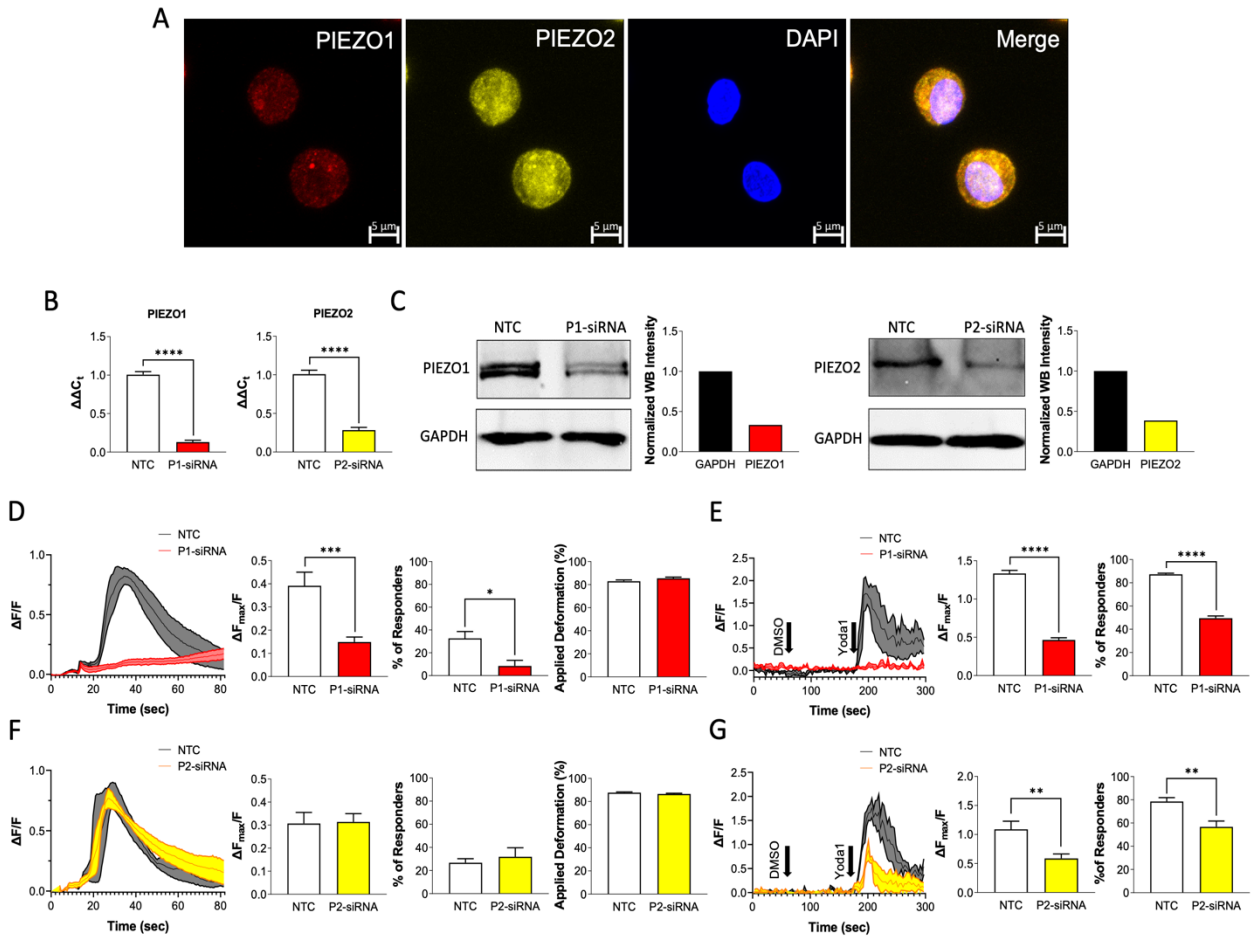

Figure 3.1 Role of PIEZO1 and PIEZO2 in primary porcine chondrocytes during mechanical or pharmacologic activation. A) Immunohistochemistry staining for PIEZO1 (red), and PIEZO2 (yellow), and DAPI (blue). Scale bar: 5 µm. B) mRNA levels of Piezo1 (P1) and Piezo2 (P2) normalized to ACTB expression level in non-targeting control (NTC) and P1-siRNA or P2-siRNA. C) Protein levels of PIEZO1 (left) and PIEZO2 (right) in NTC and P1-siRNA or P2-siRNA chondrocytes. AFM loading response of D) P1-siRNA and F) P2-siRNA cells compared to their respective NTCs showing representative cells signaling trend, normalized intracellular Ca^{2+} fluorescence intensity ΔFmax/F, the percentage of the responding cells, and deformation. Confocal imaging results of Yoda1 stimulation of E) P1-siRNA and G) P2-siRNA compared to their respective NTCs showing representative cells signaling trend, normalized intracellular Ca^{2+} fluorescence intensity ΔFmax/F, and the percentage of responding cells. Data presented as mean ± SEM. For B, n=8 samples; for D and F, percentage of responders, n=4-5 test batches, for

applied deformation and Ca^{2+} response to AFM mechanical loading, n=73-96 cells; For E and G, n=9-21 tested wells; for group comparison B, D, E, F, and G, t-test, * $p<0.05$, ** $p<0.005$, *** $p<0.001$, **** $p<0.0001$.

3.4.2 PIEZO1 mechanotransduction in chondrocytes is modulated by membrane tension

While previous studies have suggested that PIEZO1 activation is regulated by cellular membrane tension [210, 212, 216, 520], chondrocytes possess highly ruffled membranes, complicating the relationship between cellular deformation, membrane tension, and ion channel activation [215, 216, 513, 521]. Additionally, during daily activities, chondrocytes experience osmolarity changes within the range of 350-450 mOsm in healthy cartilage in the presence of all matrix components [516, 517]. We hypothesized that modes of cellular loading which increase the cell membrane tension would elevate PIEZO1 activation. To test this hypothesis, we pre-treated chondrocytes with solutions of various osmolarities to induce a cellular pre-strain before performing AFM compressive loading and monitoring PIEZO1 activation via Ca^{2+} imaging. Chondrocytes are osmotically active cells and the application of iso-osmotic (400 mOsm), hypo-osmotic (200 mOsm), or hyper-osmotic (600 mOsm) solutions were used to modulate the cellular membrane pre-strain. After 2 hours of osmotic pre-stimulation, compressive loads of 50 nN, 100 nN, 300 nN, or 500 nN were applied at the rate of 1 μm/sec to test the chondrocytes' mechanosensitivity. Chondrocytes swelled under hypo-osmotic treatment, crenated under hyper-osmotic treatment (Fig. 2A, $p<0.0001$) and were increasingly deformed at higher loads (Fig. 2B; Osmolarity, $p<0.0001$; Force, $p<0.0001$; Interaction, not significant). Intracellular Ca^{2+} signaling response was also increased at higher loads (Fig. 2C-D; Osmolarity, $p<0.0001$; Force, $p<0.0001$; Interaction, not significant) resulting in an increase in the percentage of the cells which responded (Fig. 2E; Osmolarity, $p<0.05$; Force, $p<0.05$; Interaction, not significant).

Interestingly, while cell deformation under hyper-osmotic pre-treatment was generally less than iso-osmotic pre-treatment, iso-osmotic and hypo-osmotic pre-treated chondrocytes had similar deformations (Fig. 2B; Osmolarity, $p<0.0001$; Force, $p<0.0001$; Interaction, not significant). Despite the similar deformation levels between iso-osmotic and hypo-osmotic pre-treatments, we found Ca^{2+} signaling was highest with iso-osmotic pre-treatment, particularly under 100 or 300 nN.

To investigate the relationship between osmolarity, membrane state, and membrane mechanosensitivity, we tested the hypothesis that the changes in apparent membrane strain were responsible for differences in compression-induced PIEZO1 activation and subsequent Ca^{2+} signaling among the different osmotic pre-treatments. To estimate the apparent membrane strain under these different conditions, we performed Finite Element Modeling (FEM) of the chondrocytes under AFM compression using FEBio software (http://www.febio.org/) [522]. We fit the elastic modulus to the AFM deformation and force measurements of each cell and extracted the FEM-predicted maximal apparent membrane strain to assess how membrane tension varied under the different mechanical loading conditions. We found that the chondrocyte elastic moduli were similar under iso-osmotic and hypo-osmotic pre-treatment but were significantly increased for cells under hyper-osmotic pre-treatment (Fig. 2F; Osmolarity, $p<0.0001$; Force, $p<0.0001$; Interaction, $p<0.0001$). Surprisingly, the models predicted the apparent membrane strain to be the highest under iso-osmotic pre-treatment in all loading groups compared to hypo-osmotic and hyper-osmotic pre-treatment in all loading groups (Fig. 2G; Osmolarity, $p<0.0001$; Force, $p<0.0001$; Interaction, $p<0.05$). These results suggested cells in the iso-osmotic condition experienced the highest level of membrane stretch independent of the loading magnitudes tested here. Moreover, when we plotted cellular response to the FEM-

predicted apparent membrane strain, we found cells in the iso-osmotic condition have the highest number of responding cells and level of membrane strain in all loading configurations (Fig. 2H). Since the iso-osmotic treatment groups had the most prominent Ca^{2+} response and highest levels of deformation when loaded to 50, 100, 300, and 500 nN, we used these conditions to determine the apparent membrane strain using FEM. For this group, we plotted the signaling intensity and fraction of responsive cells against the level of compression to determine the compression levels necessary to induce strong Ca^{2+} signaling and at least 50% responsive cells (Fig. 2I-K). These data show that the mean Ca^{2+} response began increasing above nominal cellular deformations of 65% (Fig. 2I), and a deformation range of ~80-85% (indicated by * in Fig. 2J) was necessary to induce signaling in 50% of compressed chondrocytes. The 80-85% range of cellular compression was shown to result in a range of apparent membrane strains (maximum principal strain E) of 1.31-1.90, which shows a tensile membrane stretch ratio (λ) of 1.9-2.19. This result indicates that stretching the membrane to 190-219% of the original dimensions (i.e., a 90-119% increase) represents the threshold of apparent membrane stretch that induces intracellular Ca^{2+} response in 50% of the cells (Fig. 2K). Interestingly, our FE model suggests that cellular compression of 65 to 75% corresponds to the high end of the toe region for the apparent membrane strain curve. In this region, a small change in deformation does not significantly affect the slope of the curve. Specifically, the FE model predicts an apparent membrane strain between 0.56 to 0.98 at the high end of the toe region. The two highest forces we tested, 300 nN and 500 nN, correspond to points where the apparent membrane strain rapidly steepens past the toe region, and experimentally, they resulted in the highest levels of cellular Ca^{2+} signaling.

Using FEM, we then determined the range of magnitudes of apparent cell membrane stretch in response to increasing levels of mechanical compression. To do so, we overlayed the average level of applied deformation that we obtained by loading the chondrocytes to 50, 100, 300, and 500 nN ± 1 standard deviation of the mean (SD) to the FEM curve (FEM-predicted apparent membrane strain against applied deformation (%)) (Fig. 2L). In this manner, we were able to determine the range of apparent membrane strain that cells underwent while being compressed to different levels. Our FEM findings predict that increasing the loading magnitude and the resulting higher levels of cellular deformation drastically increased the apparent membrane strain applied to the cell, in a nonlinear manner (Fig. 2L).

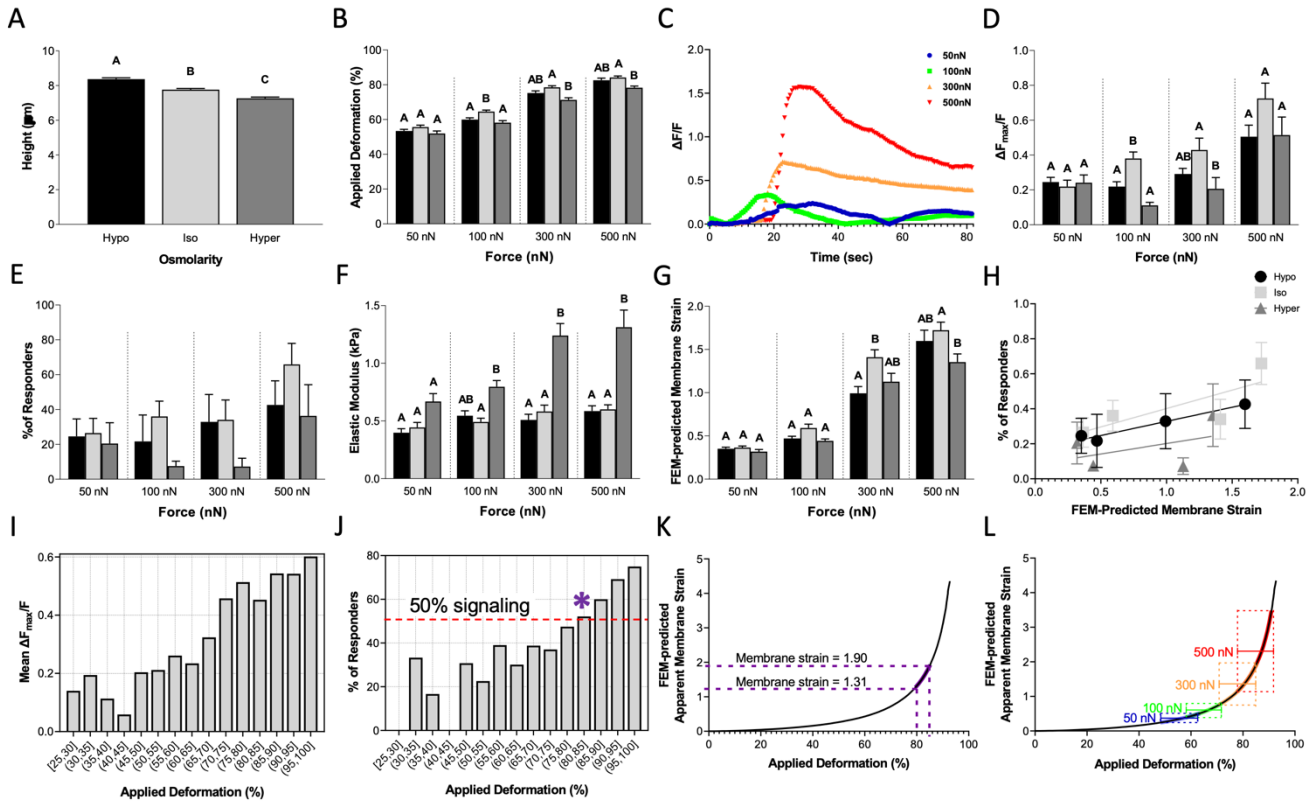

Figure 3.2 Chondrocyte intracellular Ca^{2+} response to AFM mechanical loading after long-term (2 hour) osmotic conditions, with finite element modeling (FEM) to estimate membrane strain response. A) Chondrocyte height measured by AFM for long-term osmotic conditions: hypo-osmotic (200 mOsm), iso-osmotic (400 mOsm) and hyper-osmotic (600 mOsm). B) Applied deformation (%) at different forces for each osmotic condition. C) Trend of signaling in the representative cells in iso-osmotic condition. D) AFM loading response of chondrocytes showing normalized intracellular Ca^{2+} fluorescence intensity $\Delta Fmax/F$ for each osmotic condition. E) Percentage of the responding cells to different AFM loading conditions. F) Elastic modulus (kPa) of chondrocytes calculated with FEM in each loading condition. G) FEM-predicted apparent membrane strain levels in each loading condition. H) Relation between the percentage of the responding cells and the FEM-predicted apparent membrane strain in different osmotic conditions. I) The level of mean Ca^{2+} intensity in different deformation ranges. J) The frequency of Ca^{2+} response in different deformation ranges. The * indicates the deformation range by which greater than 50% of the cells responded to the mechanical loading. K) Aligned 80-85% applied deformation range to FEM-predicted apparent membrane strain against applied deformation curve in iso-osmotic condition to determine the apparent membrane strain levels within this deformation range. L) FEM-predicted apparent membrane strain plotted against applied deformation in iso-osmotic condition with overlayed applied deformation (%) while loading the chondrocytes to 50, 100, 300, and 500 nN. Data presented as mean ± SEM. For group comparison A, one-way ANOVA with Tukey's post-hoc test, different letters indicate statistical significance, $p<0.05$, n=219-266 cells; For group comparison B, D, E, F, and G, one-way ANOVA with Tukey's post-hoc test within the groups with the same loading magnitude, different letters indicate statistical significance $p<0.05$; For B, D, E, F, and G, to find the effect of osmolarity, loading magnitude, and their interactions, two-way ANOVA with Tukey's post-hoc test was performed; n=46-67 cells for B, D, F, and G and n=4-5 test batches for E.

3.4.3 Short-term hypo-osmotic pre-treatment increased PIEZO1 mechanosensitivity

We next sought to investigate whether the signaling response following osmotic pre-treatment was time-dependent, potentially being modulated by the cellular volume regulatory response to maintain homeostasis [513, 523-527]. To investigate the short-term and long-term effects of osmotic changes on cellular volume regulation, we assessed the mechanosensitivity of chondrocytes to hypo-osmotic or iso-osmotic conditions by pre-treating them with hypo-osmotic or iso-osmotic solutions for either 30 seconds (short-term) or 2 hours (long-term) prior to mechanical compression. AFM loading to 500 nN was performed at a compression rate of 1 μm/sec. Cell height was significantly increased after hypo-osmotic pre-treatment, with cells pre-treated for 30 seconds having a higher cell height than cells pre-treated for 2 hours (Fig. 3A; Osmolarity, $p<0.005$; Treatment duration, $p<0.0001$; Interaction, not significant). There was no significant difference in cell deformation between the chondrocytes pre-treated with hypo-osmotic and iso-osmotic solutions for 2 hours (Fig. 3B; $p=0.9810$). However, there was a significant reduction in the applied deformation of the cells pre-treated with hypo-osmotic solution for 30 seconds compared to the iso-osmotic group (Fig. 3B; $p<0.0001$). There was a significant increase in Ca^{2+} signaling with 30 seconds of hypo-osmotic pre-treatment compared to the iso-osmotic and long-term hypo-osmotic treated groups (Fig. 3C-D; Osmolarity, $p<0.0001$; Treatment duration, $p<0.0001$; Interaction, $p<0.0001$). Additionally, a higher percentage of chondrocytes responded to mechanical loading after 30 seconds of hypo-osmotic pre-treatment (62%) compared to those pre-treated with iso-osmotic solution (43%) (Fig. 3E). To determine the chondrocytes membrane tension due to loading and the hypo-osmotic stress, we again used FEM to examine the chondrocyte mechanical state 30 seconds after pre-treatment. Our FEM analysis showed that the elastic moduli of chondrocytes were similar between iso-

osmotic and hypo-osmotic pre-treatment (Fig. 3F; p=0.5836). Additionally, there were no significant differences in the predicted apparent membrane strain levels between the two groups (Fig. 3G; p=0.0516). Interestingly, when we ran a model simulation to include a hypo-osmotic challenge prior to AFM compression, the apparent membrane strain level was consistently higher, despite the same level of deformation in the cells (Fig. 3H). For instance, more than 80% deformation in the iso-osmotic condition was required to reach the 1.31 maximum principal membrane strain E (which corresponds to a stretch ratio of λ=1.9) that induces intracellular Ca^{2+} response in 50% of the chondrocytes, however, less than 75% deformation is necessary to reach the same level of apparent membrane strain in the hypo-osmotic treated cells. This suggests that hypo-osmotic stress can elevate the apparent membrane strain prior to loading. In conclusion, our experimental results indicate that membrane pre-strain due to hypo-osmotic stress could increase the mechanosensitivity of chondrocytes and PIEZO1 activation. However, extended periods of pre-treatment were associated with volume recovery and reduced this hypo-osmotic sensitivity. Our FEM analysis showed that increases in cellular membrane strain during compression of hypo-osmotic pre-treated cells may sensitize PIEZO1 activation, while the recovery of cellular size back to iso-osmotic control levels after 2 hours may act to minimize the osmotically-induced membrane pre-strain. These findings suggest that changes in cellular volume regulation play a critical role in modulating chondrocyte mechanosensitivity and provide important insights into the regulation of mechanotransduction in chondrocytes.

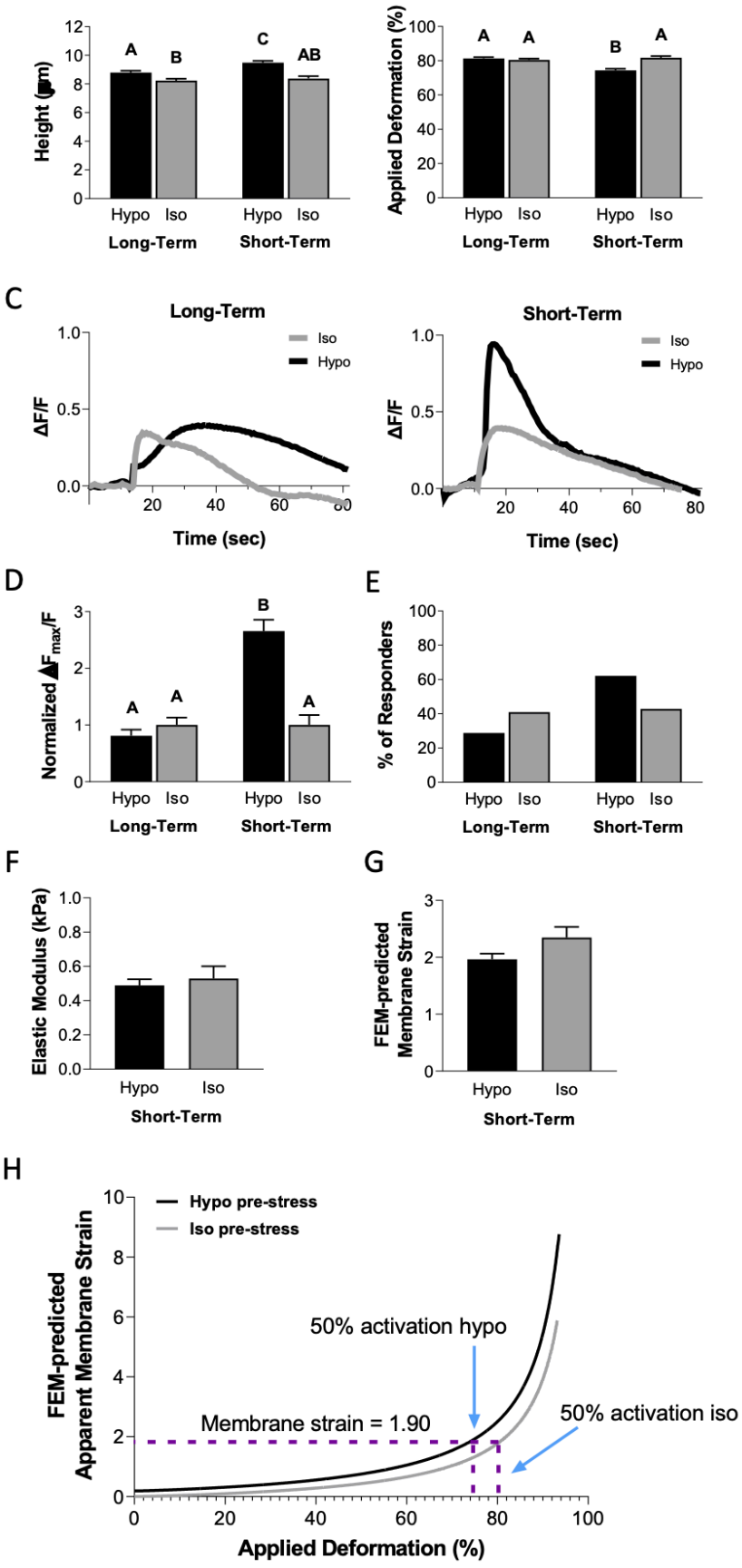
Height (μm)
A
B
C
AB
Hypo
Iso
Long-Term
Short-Term
Applied Deformation (%)
A
A
B
A
C
Long-Term
Short-Term
Iso
Hypo
ΔF/F
Time (sec)
D
Normalized ΔF max/F
E
% of Responders
F
Elastic Modulus (kPa)
G
FEM-predicted Membrane Strain
H
Hypo pre-stress
Iso pre-stress
FEM-predicted Apparent Membrane Strain
50% activation hypo
50% activation iso
Membrane strain = 1.90
Applied Deformation (%)

Figure 3.3 Chondrocyte intracellular Ca^{2+} response to AFM mechanical loading at 500 nN comparing long-term (2h) hypo-osmotic exposure and short-term (30 sec) hypo-osmotic challenge, with FEM to estimate membrane strain levels. A) Chondrocyte heights in long-term (2 hour) and short-term (30 second) exposure to hypo- (200mOsm) and iso- (400mOsm) osmotic conditions, as measured by AFM. B) Applied deformation (%) for all conditions. C) Trend of intracellular Ca^{2+} response for all conditions in representative cells. D) Intracellular Ca^{2+} fluorescence intensity $\Delta F_{max}/F$ normalized to iso-osmotic condition values. E) Percentage of responding cells for each condition. F) Elastic modulus (kPa) calculated with FEM. G) Apparent membrane strain levels calculated with FEM. H) FEM-predicted apparent membrane strain plotted against applied deformation (%) curves for iso-osmotic and hypo-osmotic challenges. Data presented as mean ± SEM. For group comparison A, B, and D, two-way ANOVA with Tukey's post-hoc test, different letters indicate statistical significance $p<0.05$, n=35-58 cells; For group comparison F and G, t-test, n=35-58 cells, no significance found.

3.4.4 Chondrocyte viscoelasticity governs PIEZO1 activation and downstream Ca^{2+} signaling

Our observations indicated that PIEZO1 activation was time- and membrane state-dependent and show that PIEZO1 activation is influenced by cellular viscoelasticity. To assess the influence of cellular viscoelastic properties on PIEZO1 mechanosensitivity, we applied 500 nN of compression at rates of 1 μm/sec, 5 μm/sec, 10 μm/sec, or 15 μm/sec under iso-osmotic conditions. Consistent with a viscoelastic material, chondrocytes experienced different levels of deformation when loaded at different rates. As the loading rate increased, the cellular deformation levels decreased significantly (Fig. 4A; $p<0.0001$), as so did the Ca^{2+} response (Fig. 4B-C; $p=0.0095$), and the percentage of cells exhibiting a Ca^{2+} response (Fig. 4D; $p=0.0015$). Therefore, these results indicate that mechanosensation via PIEZO1 activation is influenced by cellular viscoelasticity due to differences in the magnitude of cellular deformation, with

increased cellular deformations resulting in increased intracellular Ca^{2+} responses. However, when only the Ca^{2+} response of responding cells was analyzed, there was no significant effect of loading rate (Fig. 4E; p=0.3272).

While we found that Ca^{2+} signaling was dependent on the rate of loading, we were surprised to find that responsive cells exhibited similar levels of Ca^{2+} response (Fig. 4E; p=0.3272). We hypothesized that the relationship between Ca^{2+} response and viscoelasticity was driven by PIEZO1 activation and then subsequently amplified by downstream pathways. To identify the mechanosensitive origins of the loading rate sensitivity, we treated chondrocytes with varying inhibitors to either block the sources of intracellular and extracellular Ca^{2+} signaling or inhibit PIEZO1 activity before applying different rates of compressive loading. PIEZO1 was blocked using the non-specific inhibitor GsMTx-4, intracellular Ca^{2+} release was blocked using thapsagargin, and extracellular Ca^{2+} influx was blocked using EGTA (Fig. 5A-C). Notably, the inhibitors did not alter the mechanical properties of the cells, as no significant changes in cellular deformation levels were observed in response to the mechanical compression within the groups (Fig. 5A; p=0.1330-0.2051). At all rates, GsMTx-4, thapsigargin, and EGTA attenuated the intracellular Ca^{2+} response and the percentage of the responding cells (Fig. 5B-C; $p<0.0001$ for 1, 5, and 10 μm/sec; p=0.0002 for 15 μm/sec). Interestingly, when loaded at a rate of 1 μm/sec, which induces the most Ca^{2+} signaling, the non-specific PIEZO1 inhibitor GsMTx-4 significantly reduced the Ca^{2+} response while still maintaining a similar fraction of responsive cells compared to the control (Fig. 5C). Our results also indicate that PIEZO1 activation is sensitive to cellular viscoelasticity as mediated by the magnitude of overall deformation, and therefore, the subsequent increase in membrane strain. Furthermore, this data shows that both

intracellular and extracellular sources of Ca^{2+} are necessary to amplify the Ca^{2+} signaling initiated by PIEZO1 activation.

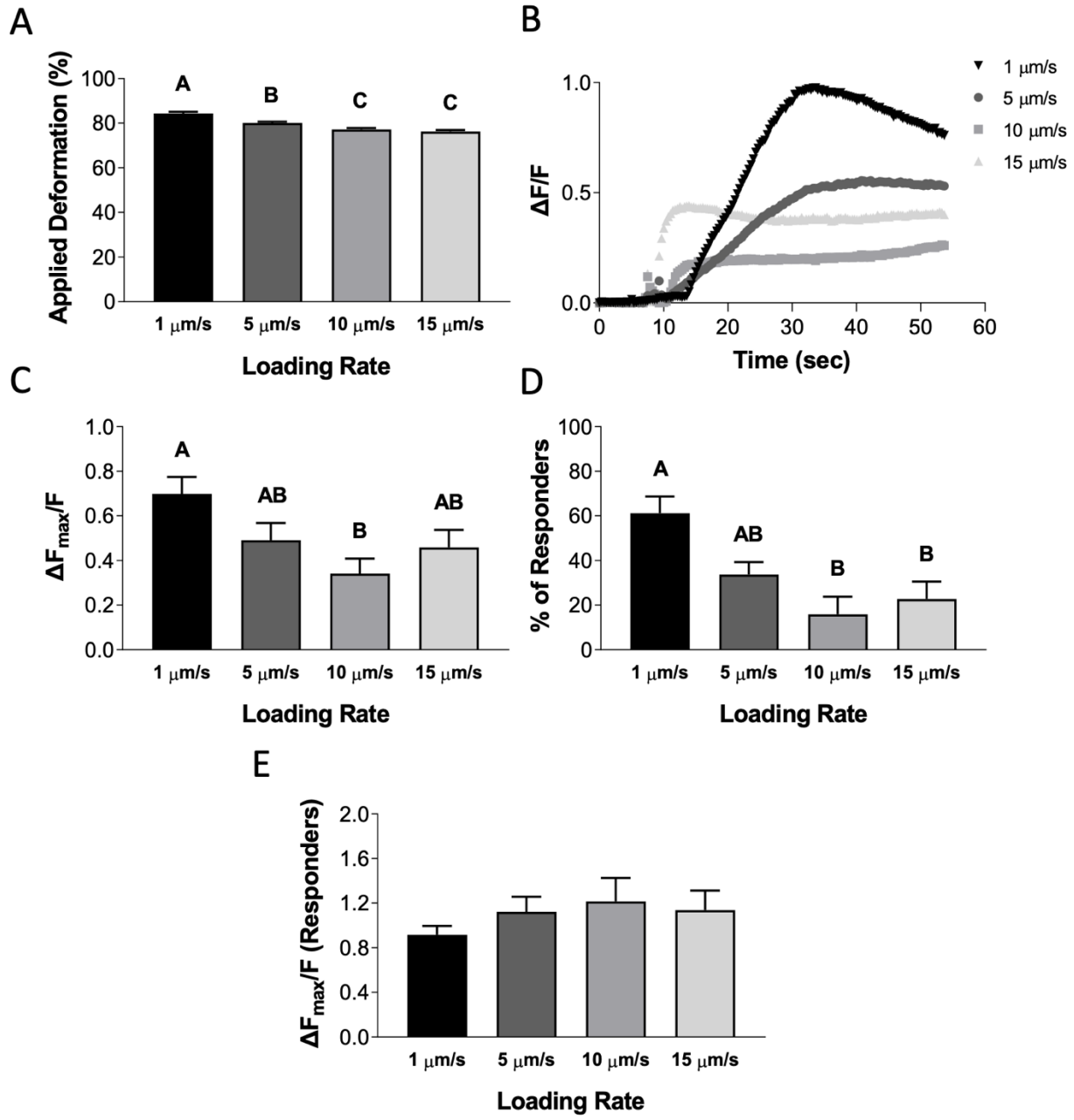

Figure 3.4 Chondrocyte Ca^{2+} response to AFM mechanical loading at different loading rates. A) Applied deformation (%) measured for each loading rate. B) Representative signaling trend for each loading rate. C) Intracellular Ca^{2+} fluorescence intensity ΔFmax/F for each loading rate. D)

Percentage of responding cells for each loading rate. E) Considering only the responding cells, intracellular Ca^{2+} fluorescence intensity ΔFmax/F for each loading rate. Data presented as mean ± SEM. For group comparison A, C, D, and E, one-way ANOVA with Tukey's post-hoc test, different letters indicate statistical significance $p<0.05$ with no significance found in E, n=51-61 cells.

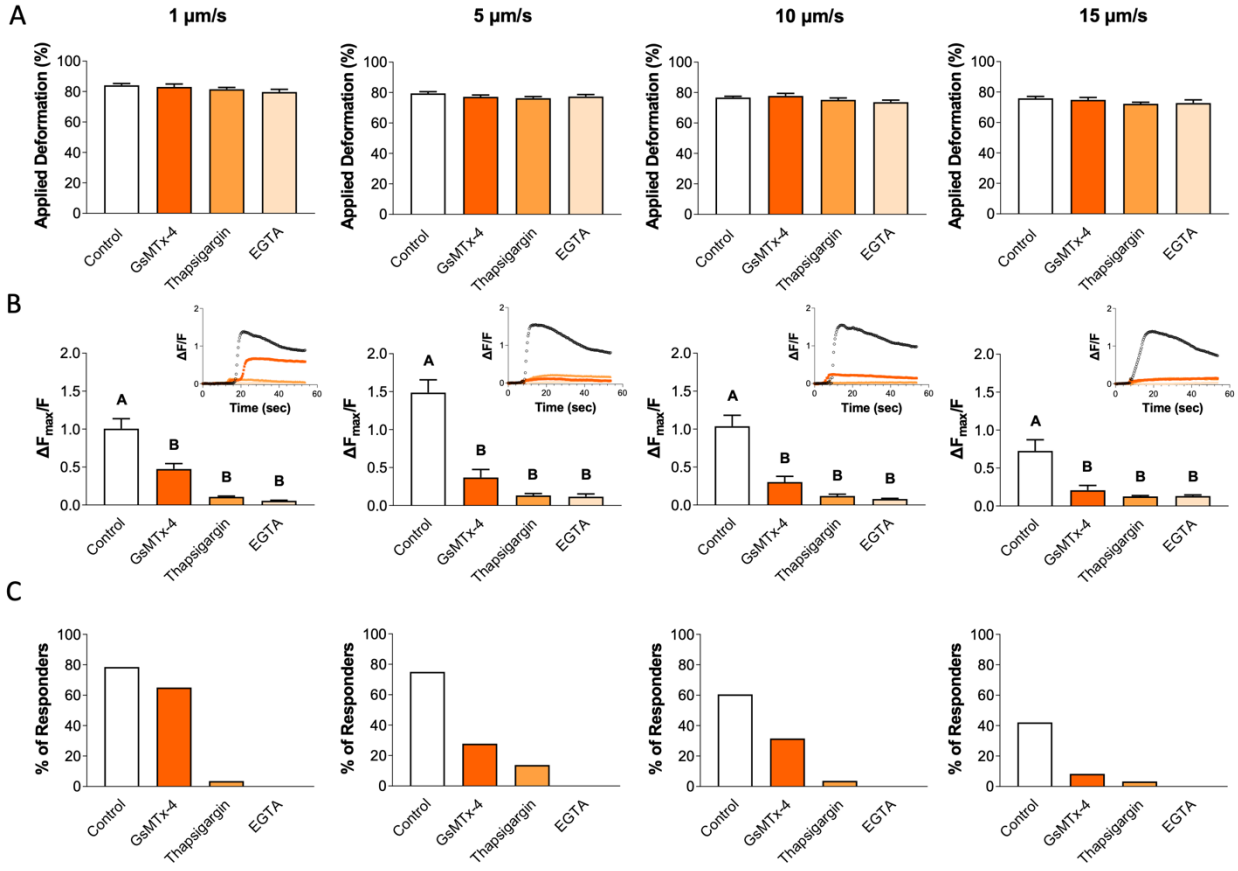

Figure 3.5 Ca^{2+} signaling of chondrocytes in response to different mechanical loading rates in the presence of PIEZO1 non-specific inhibitor GsMTx-4 and Ca^{2+} inhibitors thapsigargin and EGTA. A) Applied deformation (%). B) Intracellular Ca^{2+} fluorescence intensity ΔFmax/F, with inset showing representative signaling trends. C) Percentage of responding cells. Data presented as mean ± SEM. For group comparison A and B, one-way ANOVA with Tukey's post-hoc test, different letters indicate statistical significance $p<0.05$ with no significance found in A, n=12-42 cells.

3.5 Discussion

Our findings indicate that PIEZO activation in response to chondrocyte deformation depends on the magnitude of the apparent membrane strain that occurs as the cell is compressed and deforms (expands) laterally (Fig. 6). Specifically, we identified that supraphysiologic cellular compression leads to tensile stretch of the membrane that activates PIEZO1, and factors that influence membrane stretch can therefore modulate Ca^{2+} in response to compression. Decreasing extracellular osmolarity, increasing loading magnitude, and lowering loading rate sensitize PIEZO1 activity through increases in the apparent membrane strain, ultimately leading to increases in mechanically-induced Ca^{2+} signaling. Mechanically sensitive ion channels have been hypothesized to be activated by either strain or stress stimuli [528]. Our data support the notion that cellular deformation (i.e., strain) leads to bulging of the cell at its "equator", leading to unfolding of the extracellular plasma membrane and tensile membrane stretch that drives PIEZO1 activation. Therefore, on a cellular basis, PIEZO1 activation is driven by distortions within the plasma membrane and flattening of the membrane curvatures. More specifically, the unique shape of the PIEZO1 channel which includes multiple transmembrane domains, presence of specific amino acids within the channel, and large extracellular domain, allows PIEZO1 to be a mechanosensor for cell stretch [529, 530]. We further found that the extracellular and intracellular sources of Ca^{2+} are necessary for PIEZO1 activity but are insensitive to the rate of loading, suggesting PIEZO1 is the critical sensor of cellular deformation and thus, dependent on the viscoelastic properties of the cell.

Previous studies have suggested that PIEZO channels are activated through increased apparent membrane tension. However, the relationship between whole-cell deformation and thresholds of membrane tension required to achieve PIEZO1 activation is complex [210, 215,

216]. By combining our AFM and Ca^{2+} signaling experimental data with FEM of the whole chondrocyte's deformation, we specifically determined that an apparent membrane strain threshold of 1.31 is required for 50% probability of cellular response to mechanical compression through the PIEZO1 channel. This value suggests that large cellular deformations are required to activate the PIEZO1 channel and induce subsequent Ca^{2+} signaling in chondrocytes with high membrane ruffling. Although this threshold is considerably higher than the 2-4% area extension [531] that a phospholipid membrane can withstand, our findings are consistent with the presence of significant ruffled membrane reservoirs in chondrocytes [532]. The reservoirs enable the chondrocyte membrane to withstand this high level of apparent membrane strain without rupturing under normal physiologic levels of cartilage compression.

Furthermore, we found that increasing the loading magnitude significantly enhances the intracellular Ca^{2+} response of the chondrocytes under direct mechanical compression. This conclusion is consistent with previous findings that suggest higher magnitudes of load can unruffle more areas of the membrane [521]. Consequently, this phenomenon would expose more mechanosensitive channels to the external cues, increase membrane tension to higher levels, and increase the cellular Ca^{2+} response [237]. Previous studies have also shown that under hypo-osmotic loading, similar to levels imposed in our study, the surface area of the chondrocyte membrane can expand to 234% of the membrane surface area present under iso-osmotic conditions before the membrane ruptures, which supports our findings here [513].

Our results further described a biphasic modulation of membrane tension during cell swelling and cell crenation in activating PIEZO1. Cell crenation under hyper-osmotic stimulation and cell swelling under hypo-osmotic stimulation reduced PIEZO1 activation compared to iso-osmotic stimulation when allowed to equilibrate to the pre-treatment (i.e. the long-term treatment

regimen). Interestingly, short-term hypo-osmotic pre-treatment was necessary to induce increased PIEZO1 activation through cellular swelling, suggesting a prominent role of chondrocyte active remodeling to modulate mechanosensitivity [456, 523, 533-535]. These results demonstrate that only transient membrane pre-strain enhanced PIEZO1 response to compressive loading and that over longer durations, chondrocytes remodel and attenuate their PIEZO1 mechanosensitivity. Our FEM analysis predicted a slightly increased apparent membrane strain under iso-osmotic conditions compared to hypo-osmotic conditions owing to an increase in cellular deformation in the iso-osmotic group. As our mechanical models do not consider the active cellular remodeling under osmotic stresses, the actual apparent membrane strain is likely to be altered as the cell remodels to achieve homeostasis. Conversely, by applying a short-term hypo-osmotic stress that partially unruffles the membrane, we found that the sensitization of PIEZO1 to mechanical compression significantly increased compared to the iso-osmotic treated group. Together, these results suggest that transiently increasing the membrane tension increases PIEZO1 activation and chondrocyte mechano-response. Understanding how chondrocytes modify their mechanosensitivity in response to loading will provide valuable insights for developing refined FE models of chondrocyte mechanosensation. Furthermore, cross-talk between PIEZO1 and other chondrocyte mechanosensors may be a crucial aspect for understanding chondrocyte function under physiological and supraphysiologic loading conditions. Of note, our findings confirm and extend our previous observation of potential synergy between PIEZO1 and PIEZO2 in chondrocyte mechanosensing [237]. Consistent with previous findings, we found that Ca^{2+} signaling due to moderately high levels of cell deformation (at 300 nN) were reduced by either P1-siRNA or P2-siRNA, suggesting that PIEZO1 and PIEZO2 cooperate at these levels of membrane stretch [237]. However, at the highest levels of

loading (500 nN), P2-siRNA had no inhibitory effect, and PIEZO1 appears to function independently at this point. This important finding suggests that the synergy between PIEZO1 and PIEZO2 is dependent on the magnitude of membrane stretch.

Furthermore, we show initial evidence of PIEZO1-PIEZO2 interaction with chemical activation, as P2-siRNA reduced the Ca^{2+} response to Yoda1 (Fig. 1E, G). Because Yoda1 is a highly specific activator of PIEZO1, this finding supports the notion that PIEZO1 activation be modulated by the presence of PIEZO2 in the membrane. This finding is consistent with several previous studies that show similar trends in other cell types [518, 519]. While the mechanisms underlying these interactions remain to be determined, these findings paint a complex and expanding picture of chondrocyte mechanobiology and its underlying "channelome" [316, 361].

While osmotic loading in chondrocytes can also induce the activation of other ion channels, including transient receptor potential vanilloid-4 (TRPV4), the dynamics of activation observed in this study suggest that the response to direct loading is predominantly driven by PIEZO1. We previously demonstrated that blocking TRPV4 did not alter chondrocyte mechanosensitivity to direct compression by AFM loading [248]. Moreover, Ca^{2+} fluctuations by PIEZO1 are distinct from other mechanosensitive ion channels, characterized by different inactivation times [220, 520, 536-539]. Consequently, the downstream targets induced by PIEZO1 activation are known to differ from those induced by other mechanosensitive ion channels. Moreover, Lee et al. showed that blocking PIEZO channels using their non-specific inhibitor GsMTx-4 prior to applying a hypo-osmotic stress increased the Ca^{2+} response and the responsive cell fraction to a hypo-osmotic challenge [237], indicating a possible interaction of the PIEZO channels with TRPV4 in chondrocytes to regulate mechanosensitive currents. Additionally, we found that high cellular deformations and membrane strains are specific to

PIEZO1 activation and not sufficient to trigger PIEZO2 activation. Interestingly, applying 300 nN force to the P2-siRNA chondrocytes, which would induce a cellular deformation similar to our previous study [237], decreased the level of intracellular Ca^{2+} response in the cells, showing that the synergy between PIEZO1 and PIEZO2 exists up to a certain level of deformation. However, PIEZO1 is the only channel that responds above a certain level of mechanical deformation. Furthermore, we observed new evidence of PIEZO1/PIEZO2 interaction in the response to Yoda1, consistent with previous studies on different cell types that have suggested potential reduction in PIEZO1 activation with PIEZO2 knock-down [518, 519]. These findings support the notion of synergy between PIEZO1 and PIEZO2 and suggest that these interactions are dependent on the magnitude of deformation as well as the mode channel of activation.

Our results, showing that either chelating extracellular Ca^{2+} or inhibiting the release of intracellular Ca^{2+} blocks the whole-cell PIEZO1-induced Ca^{2+} response, support the mechanism of Ca^{2+}-induced Ca^{2+} release (CICR) downstream to PIEZO1 activation. These findings suggest that mechanical stretch initially induces a Ca^{2+} flux through the membrane, which results in greater Ca^{2+} release from intracellular storages. However, it is possible that other channels may further regulate the gating of PIEZO1 or other Ca^{2+} sources. Future studies may wish to investigate the roles of the synergy between mechanosensitive ion channels and other types of channels, such as voltage-gated Ca^{2+} permeable ion channels (VGCCs). Previous studies have suggested that the activation of a mechanosensitive channel can induce the activation of VGCCs by polarizing the membrane [319]. These studies may identify novel targets for treating PIEZO1-related pathologies.

Our findings are consistent with previous studies suggesting that cellular level mechanical strain is a primary mediator of chondrocyte death at high loads [540, 541].

Furthermore, these findings provide mechanistic insight on previous reports that have shown chondroprotective effects of media solutions with increased osmolarity [542], suggesting that altering the sequence of mechanically-induced Ca^{2+} signaling may have an influence on chondrocyte viability, and potentially, cartilage health. Additional work is needed to determine the downstream targets involved in mechanically-mediated chondrocyte death, which may include inflammatory mediators such as NF-κB [543], nitric oxide [544], and subsequent mitochondrial dysfunction [545, 546]. Furthermore, inflammatory mediators such as interleukin 1 may in turn alter the activity of mechanosensitive channels such as PIEZO1 or TRPV4 [85, 547, 548], potentially providing a positive feedback loop to exacerbate pathologic responses in chondrocytes.

Our study also revealed that the chondrocytes' mechanical properties, specifically its viscoelasticity, can influence PIEZO1 mechanosensation. To block PIEZO1 activity in these loading conditions, we used GsMTx-4, a non-specific PIEZO inhibitor [229, 549-552]. Results indicated that application of GsMTx-4 significantly decreased the response of chondrocytes to mechanical loading in all loading conditions. Moreover, the cellular Ca^{2+} response and percentage of the responders were also rate dependent even with the application of GsMTx4. The fact that GsMTx4-treated cells respond at low loading rates suggests that PIEZO1 is the primary responder to the rate of cellular deformation. Further, the finding that inhibiting extracellular Ca^{2+} sources diminished the PIEZO1 response to mechanical compression is consistent with our previous study [237]. Our finding, that PIEZO1 activity is driven by the rate of loading, opens a new perspective on how cells may use feedback control between their mechanosensors and their mechanics to maintain homeostasis. Additionally, previous studies have shown that viscoelastic effects of the extracellular environment can be sensed by TRPV4 [553, 554]. Therefore,

understanding the feedback between cell mechanics, extracellular mechanics, and these cell mechanosensors will be an important area of future research for understanding mechanically-driven disease pathogenesis. Additionally, investigating the possible variation in mechanosensitivity of the PIEZO1 channel in chondrocytes from different zones or regions in the cartilage is another important question that needs to be answered in future studies.

In summary, we found that PIEZO1 activation is driven during chondrocyte deformation by the concomitant increases in membrane tension through depleting intracellular Ca^{2+} reservoirs. Using FE models, we determined that an apparent membrane strain of 1.31 is the approximate threshold of strain which is necessary for the PIEZO1 activation with the probability of 50%. Our investigation of the different factors which play essential roles in amplifying PIEZO1 Ca^{2+} signaling demonstrated that extracellular conditions, including the osmolarity, Ca^{2+} sources, loading rate and magnitude, differentially drive PIEZO1 Ca^{2+} signaling. Future characterization of these downstream effects may offer a promising therapeutic opportunity for treating cartilage injuries. Together, our findings deconstruct the initial activation and downstream coordination of PIEZO1 signaling and establish mechanical thresholds and therapeutic entry points for treating post-traumatic osteoarthritis.

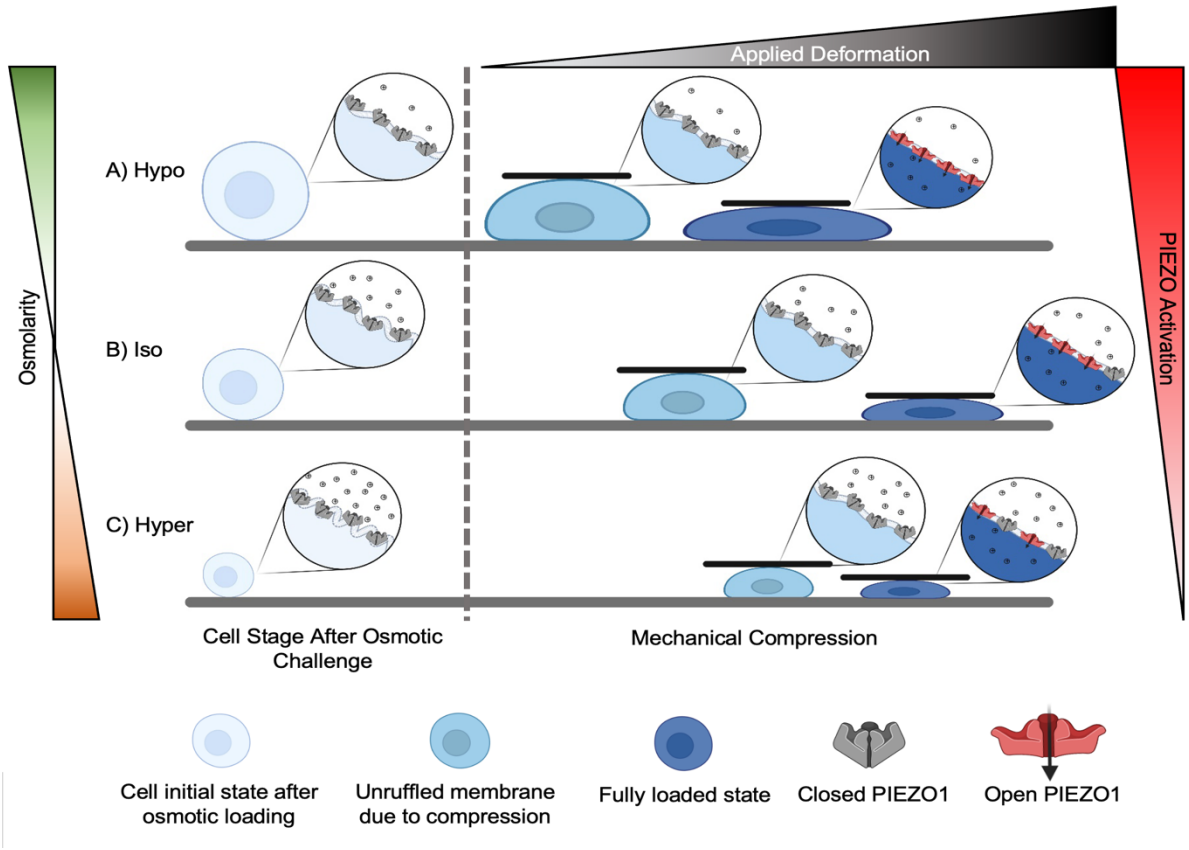

Figure 3.6 Schematic of the mechanism involved in PIEZO1 activation in response to membrane tension. As the cell is deformed and experiences tensile strains in the peripheral regions, the cell plasma membrane initially experiences unfolding. After the ruffles are unfolded, then the plasma membrane will experience local tensile strains. However, swelling of the cell with A) hypo-osmotic stress unfolds the ruffles prior to loading and exposes more PIEZO channels to the extracellular cues before mechanical compression, resulting in higher levels of intracellular Ca^{2+} signaling in the chondrocytes in response to mechanical compression compared to the B) iso-osmotically treated group. C) On the other hand, applying a hyper-osmotic stress decreases the cell size and increases membrane ruffling. Therefore, more deformation is required to unfold the membrane curvatures before inducing stretch of the plasma membrane. Consequently, the force and deformation necessary to unfold the membrane curvatures increase compared to the iso-osmotically treated group. This change results in a smaller portion of the force being dedicated to compressing the cell and decreases the sensitivity of the PIEZO channel to mechanical compression.

3.6 Supplemental Figures

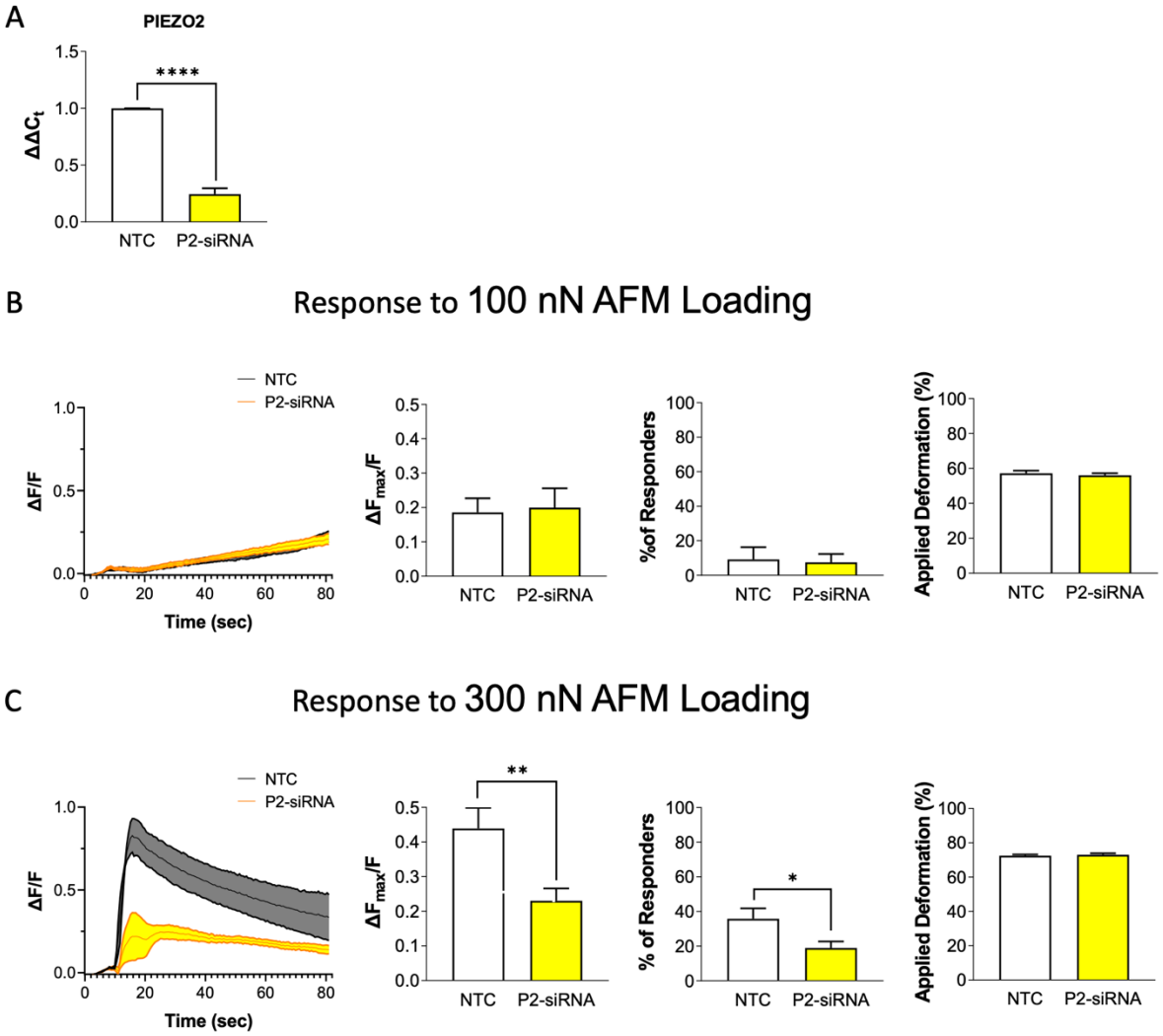

Figure S3.1 NTC and P2-siRNA chondrocyte intracellular Ca^{2+} response to 100 and 300 nN force. A) mRNA levels of PIEZO2 (P2) normalized to ACTB expression level in non-targeting control (NTC) and P2-siRNA chondrocytes, in a separate group of pigs from those in the 500 nN experiments in Figure 1. AFM loading response of P2-siRNA cells compared to their respective NTCs showing representative cells signaling trend, normalized intracellular Ca^{2+} fluorescence intensity ΔFmax/F, the percentage of the responding cells, and deformation after loading cells to B) 100 nN, and C) 300 nN. Data presented as mean ± SEM.

Chapter 4: Polyunsaturated Fatty Acids Suppress PIEZO Ion Channel Mechano-Activation in Primary Chondrocytes

4.1 Abstract

Osteoarthritis (OA) is a prevalent and debilitating joint disorder, accounting for a significant proportion of musculoskeletal diseases worldwide. This condition is hallmarked by the progressive degeneration of articular cartilage, ultimately leading to pain, stiffness, and reduced joint function. One of the critical determinants in the pathogenesis of OA is the behavior of chondrocytes, the primary cell type in cartilage. These cells undergo morphological and functional changes in response to a variety of mechanical and biochemical stimuli. As the understanding of OA's etiology evolves, polyunsaturated fatty acids (PUFAs) have emerged as potential modulators of chondrocyte behavior, presenting a novel avenue for research and therapeutic intervention.

In our study, we identified a significant role for PUFAs in regulating PIEZO activity in chondrocytes. We showed that both ω3 and ω6 fatty acids reduced the sensitivity of the chondrocytes to mechanical compression, Yoda1, and GSK101. Moreover, ω3 fatty acids showcased a remarkable capability to attenuate inflammatory and senescence markers, suggesting their potential as therapeutic agents in mitigating the adverse effects associated with OA. However, ω6 fatty acids increased the expression of IL-6 significantly. Furthermore, we showed that LA made the chondrocyte membrane more susceptible to damage in response to hypo-osmotic challenges since the membrane of the cells that were treated with LA ruptured

faster compared to the other groups after applying a hypo-osmotic shock to the cells. This finding might explain the potential exacerbation of OA symptoms with increased LA consumption.

In conclusion, our findings underscore the differential impacts of specific PUFAs on chondrocyte behavior and OA progression. While ω3 FAs exhibit protective properties, the detrimental effects of LA on chondrocyte membrane integrity warrant caution in dietary and therapeutic considerations. The implications of these results could pave the way for targeted nutritional interventions and treatments that leverage the benefits of PUFAs while minimizing potential risks.

4.2 Introduction

More than 300 million individuals suffer from osteoarthritis (OA), a painful disease marked by the degeneration of articular cartilage [555]. The origins of OA are likely varied, but heightened mechanical pressure on a joint is a known contributing factor [31]. Such pressures can stem from traumatic injuries, obesity, or even regular activities such as running and jumping [316]. In reaction to this augmented load, chondrocytes enhance the production of catabolic factors, leading to the onset of OA. The exact mechanism through which chondrocytes perceive force remains elusive, but a significant role is played by mechanosensitive cation channels [555].

PIEZO channels, a family of mechanosensitive cation channels, are present in numerous human cell types. PIEZO1 channels are predominantly found in smooth muscle cells, cardiac fibroblasts, and red blood cells, while PIEZO2 channels are abundant in proprioceptive sensory cells and Merkel cells [10, 555]. In chondrocytes, both these channels are profusely expressed

and can be stimulated by elevated membrane tension from intense mechanical stresses [48]. A study by Lee et al. and colleagues indicated that obstructing these channels could reduce chondrocyte death in cartilage explants under injury [237]. The researchers also delineated a mechanism for Ca^{2+} -driven chondrocyte damage, highlighting how Ca^{2+} influx might weaken the chondrocytes' F-actin framework, making the cell more prone to deformation harm [237]. TRPV4 is another mechanosensitive cation channel in chondrocytes, but unlike Piezo channels, it's primarily activated by osmotic stress stemming from mechanical stress [189, 456, 556-558]. In typical conditions, TRPV4 channels generate protective agents like collagen II and ACAN, but under excessive loads, these channels can spur chondrocyte apoptosis [555]. Given these findings, targeting mechanosensitive cation channels, especially Piezo channels, seems promising for OA and PTOA treatment.

One avenue being explored to alter the activity of these channels involves supplementing with poly-unsaturated fatty acid (PUFA). Embedding omega-3 fatty acids (a subtype of PUFAs) into chondrocyte membranes curbs the expression of inflammatory agents such as aggrecanases, IL-1α, and TNF-α [559]. This protective effect is also observed in live organisms; mice with a heightened omega-3 fatty acid diet showed reduced progression of OA post-knee trauma [331]. Though the exact mechanism through which omega-3 fatty acids mitigate OA symptoms remains a mystery, it's believed to relate to alterations in membrane behavior. Once embedded into the cell membrane, PUFAs lower the membrane's melting point, indicating heightened membrane fluidity, in contrast to saturated fatty acids which do the opposite [560]. Given their potential to enhance membrane fluidity and thus possibly reduce tension during mechanical stress, PUFAs are theorized to reduce the activation of mechanosensitive ion channels. However, the in vitro impact of PUFA supplementation remains ambiguous. Romero et al. and his team showed

contrasting effects on PIEZO1 activity based on the individual molecular properties of different fatty acids [334, 406]. We have previously shown that the joint of the mice on diet rich in ω3 fatty acids were protected against PTOA after an injury was applied to the knee [331]. On the other hand, we have shown that the mRNA and protein levels of PIEZO1 will increase in OA joints [85]. Consequently, we hypothesis that the PUFAs including ω3 and ω6 fatty acids can affect the sensitivity of the PIEZO channels to mechanical loading and protect the joint from injurious loads through their downstream effects on PIEZO.

In this research, we probed how fatty acid supplementation in chondrocytes might influence the response of PIEZO and TRPV4 channels to excessive mechanical stress. Using various techniques like AFM cell loading experiments, confocal microscopy, and RT-qPCR analysis, we found that PUFAs curbed the internal Ca^{2+} response to different stimuli. However, these fatty acids didn't alter chondrocyte reactions to hypo-osmotic shock, suggesting varied chondrocyte responses to different kinds of membrane tension. Lastly, we showed that ω3 fatty acids supplementation reduces inflammation and senescence biomarkers indicating their positive effect on OA and PTOA related pathologies.

4.3 Materials and Methods

4.3.1 Culturing Cells and Preparing Samples

Knees from skeletally mature pigs, aged between 5 and 6 months and of mixed breeds (landrace yorkshire and duroc), were sourced from a regional abattoir on the day of slaughter. The femoral mid-condyle's articular cartilage was extracted and preserved in a conventional culture medium consisting of High glucose DMEM (Gibco, Thermo Fisher Scientific, Waltham,

MA), 10% fetal bovine serum (FBS, Atlas Biologicals, Fort Collins, CO), 1.5% HEPES (Corning, Corning, NY), 1% MEM Non-essential amino acid (Corning), 1% Pen Strep (Gibco, Thermo Fisher Scientific), and 0.5% L-Proline (Sigma Aldrich, St. Louis, MO). This preservation lasted between 1 to 2 days before the enzymatic digestion commenced.

The cartilage tissue then underwent digestion using pronase (Worthington Biochemical, Lakewood, NJ) prepared in the wash medium that had components such as High glucose DMEM, 1x Gentamycin (Gibco, Thermo Fisher Scientific), 1x Kanamycin (Goldbio, St. Louis, MO), and 1x Fungizone (Corning), at a concentration of 1320 PKU/ml medium. This digestion lasted for about 1 to 1.5 hours. After this period, the medium containing pronase was discarded, and the tissue was then subjected to a 3 to 3.5-hour incubation with a medium that had 0.4% collagenase type II (Worthington Biochemical).

After this phase, cells were isolated, cleaned, resuspended in the growth medium which had components like 1.5% HEPES, and 1% MEM Non-essential amino acid (Corning). The cell count was taken, and then they were allocated onto 12mm round coverslips #1.5 (Electron Microscopy Sciences, Hatfield, PA) at densities ranging from 50,000 to 100,000 cells per coverslip, specifically for the AFM examination. In preparation for the confocal microscopy studies, cells were distributed in high-resolution glass-bottom 96-well plates (Cellvis, Sunnyvale, CA). These cells underwent a 3-day culturing process in an incubator set at 5% CO2 and 37 °C. The serum-free mediums were maintained at an osmolarity of 380 mOsm to emulate the physiological conditions present in cartilage, as cited in references [516, 517].

4.3.2 Atomic Force Microscopy (AFM)

Using an Atomic Force Microscope (AFM; MFP-3D Bio, Asylum Research, Santa Barbara, CA), primary chondrocytes were subjected to compression. Before experimentation, these cells were stained with the Fura2-AM dye (Invitrogen, Thermo Fisher Scientific), a dye sensitive to intracellular Ca^{2+} concentrations. The staining was done in a solution composed of Phenol red-free DMEM (Gibco, Thermo Fisher Scientific), combined with 1.5% HEPES buffer (Corning), 1% Pen Strep (Gibco Thermo Fisher Scientific), 1% MEM non-essential amino acid (Corning), 1% Na Pyruvate (Corning), 1% GlutaMax (Gibco, Thermo Fisher Scientific), and 0.1% L-Proline (Sigma Aldrich), over a period of 1-2 hours. The compression of chondrocytes was executed with tipless cantilevers, having a stiffness ranging from 7-13 N/m (Nanoandmore, Watsonville, CA). The cantilever's stiffness was ascertained using the manufacturer-provided thermal method. During cell compression, light sources of 340/380 nm wavelengths captured ratiometric Ca^{2+} images. Experiments were conducted at 37°C in moist conditions. Cells showing movement during the imaging process or those that were identified as damaged (evidenced by a quick decline in intracellular fluorescence) were excluded from the study. The video data of the intracellular Ca^{2+} response during mechanical pressure was processed through ImageJ software (U.S. National Institutes of Health, Bethesda, MD, https://imagej.nih.gov/ij/).

4.3.3 Confocal Microscopy

Ca^{2+} imaging: Cells were incubated for an hour with Ca^{2+} indicator dyes, Fura red-AM (Invitrogen, Thermo Fisher Scientific) and Fluo4-AM (Invitrogen, Thermo Fisher Scientific), which provide insights into the fluctuations of Ca^{2+} concentrations within the cell. Post-staining, cells underwent a wash and were then observed under a confocal microscope (LSM 880, Zeiss,

Dublin, CA). A temperature of 37°C was maintained during the observation to simulate physiological conditions. An initial one-minute imaging was followed by the introduction of a control solution (DMSO, Sigma Aldrich) and subsequent imaging for two more minutes. After this control phase, a final concentration of 2.5 μM of Yoda1, 1 nM of GSK101, or of water (to have an osmotic shock of -110 mOsm) was added, and cells' reactions were recorded for another two minutes. The entire process of labeling, washing, and imaging was carried out in iso-osmotic conditions. Video data post imaging was processed in ImageJ to quantify each cell's Ca^{2+} response during observation.

Live-dead imaging: The cells were stained using the live-dead kit (Invitrogen, Thermo Fisher Scientific) for 45 minutes. Afterwards, the cells were imaged under confocal to evaluate the cell death levels in response to PUFAs treatment.

Lipid droplet imaging: Cells were stained with BODIPY stain for 30 minutes to label the lipid droplets within the cells. Afterwards, a Z-stack image of cells was taken under the confocal.

Osmotic challenge imaging to measure membrane strength or sensitivity of cells to osmotic shocks: A video of chondrocytes was taken under the brightfield setup under confocal before and after osmotically shocking the cells to capture the initial and final diameter of the cells.

4.3.4 Image analysis

Image data from both confocal and AFM investigations were processed using ImageJ. Initially, the videos were imported into ImageJ, after which two distinct channels, representing the fluo-4 and fura-red for confocal imaging, or the 340 nm and 380 nm light wavelengths for the

AFM study, were isolated. The normalized intensity of the signals was displayed after channel division. The cell shapes, in terms of pixel brightness during the entire research, were acquired and evaluated by thresholding the videos according to staining intensity. Subsequently, average pixel intensities were standardized to the baseline signal level. Each cell's maximum value of normalized pixel brightness was then recorded as the cell's intracellular Ca^{2+} response ($\Delta Fmax/F$).

For AFM studies, a control assessment was done where the cantilever was positioned over the cells without exerting any pressure. The intracellular Ca^{2+} response of these cells was then assessed, standardized, and both the mean (M) and standard deviation (SD) of these responses were calculated. Cells with a Ca^{2+} response higher than the control group's average plus thrice the standard deviation ($\Delta Fmax/F > M + 3*SD$) and exhibiting a peak in their Ca^{2+} response profile were termed as responders. Cells not meeting this criterion were categorized as non-responders.

For confocal analysis, videos were processed in ImageJ, and the $\Delta Fmax/F$ for every cell in each investigation was reported. These findings were further processed using custom MATLAB software to compute the proportion of responding cells and the average level of intracellular Ca^{2+} signaling. This software facilitated the normalization of each cell's intracellular Ca^{2+} response after Yoda1 was introduced, in relation to the cell's response post DMSO addition. The average $\Delta Fmax/F$ of all cells was then determined and cited as the average cellular response derived from each video. The software also assessed if the $\Delta Fmax/F$ of a particular cell exceeded the average post DMSO addition Ca^{2+} response (M′) plus five times its standard deviation (SD′) (Yoda1: $\Delta Fmax/F > M' + 5*SD'$, GSK101: $\Delta Fmax/F > M' + 10*SD'$, Hypo-osmotic: $\Delta Fmax/F > M' + 5*SD'$). Cells meeting this criterion were termed responders. The total count of

responders divided by the total cell count was recorded as the responder percentage for each video.

To analyze the cells that underwent osmotic shock to measure their membrane strength, and responsiveness to osmotic challenges, videos that were taken from the cells before and after the application of osmotic shock were analyzed in ImageJ software to measure the initial and final diameter of the cell. Then, the change in diameter, area, and volume of the cells were determined.

To calculate the intensity and area of the lipid droplets within each cell after PUFA treatment, the Z-stack images were processed to obtain the maximum intensity projection (MIP) images. Afterwards, MIPs were analyzed in ImageJ and the intensity and area of the lipid droplets in individual cells were determined.

4.3.5 Fatty acids preparation and treatment

Amount of fatty acid (Nu-Check-Prep Inc, Elysian, MN) required to make the final concentration of 5 mM was calculated based on the density and the molecular weight of each fatty acid. Then, the fatty acids were dissolved in 100 µl of ethanol. For each 100 µl of fatty acid, 0.33 grams of bovine BSA (Sigma Aldrich) was dissolved in 4.9 ml of PBS. Afterwards, the 100 µl each fatty acid was added to 4.9 ml of BSA in a separate glass vial very slowly. Afterwards, the fatty acids were put on a shaker in an incubator for 1 hour. Lastly, the fatty acids were aliquoted in small glass vials, oxygen was removed using nitrogen gas, the vials were sealed, and stored at -20 C.

To treat the cells with fatty acids, serum-free medium with the osmolarity of 380 mOsm was used to dilute the fatty acids to reach a final concentration of 100 μM. Then, each vial of media that was supplemented with a specific fatty acid was filtered and added to the cells. The cells were then cultured for 3 days prior testing.

4.3.6 RNA extraction and RT-qPCR

After 3 days of fatty acid treatment, mRNA was harvested (Norgen, Total RNA Purification Plus kit, Thorold, ON, Canada). Briefly, cells that were seeded and treated in a 6-well plate were washed with PBS once, then 300 μl of the lysis buffer was added to each well for 10 minutes. Afterward the lysate was collected in tubes and snaped frozen in liquid nitrogen. Next, the mRNA was harvested and purified and its concentration was measured using a NanoDrop. Subsequently, cDNA was generated from the mRNA (VILO Superscript Mastermix, Life Technologies, Carlsbad, CA) and real-time quantitative PCR was performed utilizing the cDNA along with fast SYBR Green Master mix (Thermo Fisher Scientific). The delta delta Ct (ΔΔCt) approach was employed to ascertain the relative gene expression of the target genes, and ultimately, the expression levels were standardized to the ACTB mRNA levels. The primer sequences used are detailed in Table 1.

4.3.7 Statistical analysis

The mean values for each group are displayed on every graph along with the standard error of the mean (±SEM). The statistical significance between different groups was assessed using the one-way followed by a Tukey post-hoc test, with a p-value of less than 0.05 indicating statistical significance.

4.4 Results

4.4.1 PUFA treatment decreased the chondrocytes' response to mechanical compression and Yoda1 addition

We first investigated the effect of our PUFA and PA treatments on the viability of the chondrocytes. We were able to show that the 100 μM treatment of PUFAs and PA did not have any effect on cell viability (Figure S5.1). Then, we investigated the role of different PUFAs on the sensitivity of PIEZO channels in response to high magnitudes of mechanical compression and Yoda1. First, we showed that treating chondrocytes with ω6 fatty acid LA and ω3 fatty acids DHA and EPA significantly reduced the intracellular Ca^{2+} response of the cells to mechanical compression at 500 nN and loading rate of 1 μm/sec (Figure 5.1; $p < 0.0001$). However, ω6 fatty acid AA and polysaturated fatty acid PA did not have any significant effect on the mechanosensitivity of the PIEZO channels compared to the BSA group. Moreover, percentage of the responding cells to mechanical compression was between 23 to 27% in the LA, DHA, and EPA treated groups which was considerably lower than the BSA group (47%) and the cell group that was treated with AA (39.5%). Additionally, we only looked at the intracellular Ca^{2+} response of the responding cells and found that only EPA treated group had a significantly lower response compared to the BSA showing that this group is decreasing the mechanosensitivity of the PIEZO channels the most (Figure 4.1; $p = 0.0067$).

In the next experiment, we were interested in evaluating the effect of fatty acids on chondrocytes response to addition of Yoda1 using confocal microscopy. We demonstrated that all the ω3 and ω6 fatty acids were able to decrease the sensitivity of the PIEZO channels to 2.5 μM of PIEZO1 specific activator Yoda1 significantly compared to the control group (Figure 4.2;

$P < 0.0001$). Both the intracellular Ca^{2+} response and the percentage of the responding cells in the AA, LA, DHA, and EPA groups was reduced by 70 to 80% compared to the BSA group with the EPA group having the lowest amount of Ca^{2+} response and number of responding cells. Furthermore, we showed that PA-treated cells also had lower levels of intracellular Ca^{2+} response and percentage of responding cells compared to the BSA group, however, all the ω3 and ω6 groups showed significantly lower values compared to the PA group as well. Taken together, these results show that PUFAs are able to regulate the sensitivity of the PIEZO channels to both mechanical compression and Yoda1 addition.

4.4.2 PUFA treatment decreased the chondrocytes' response to GSK101 addition but did not have any effect on cellular response to hypo-osmotic shock

After observing the strong effect of PUFAs on the PIEZO channels mechanosensitivity, we became interested in investigating the influence of fatty acids on the activity of the TRPV4 channel. Therefore, we performed the same confocal microscopy experiment as before; however, instead of adding Yoda1 to the cells while imaging their intracellular Ca^{2+} response, we added 1 nM of GSK101 which is the specific activator of TRPV4. We showed that treating the chondrocytes with ω3 and ω6 fatty acids significantly lowered the percentage of responding cell and the cellular response to the addition of GSK101 compared to the BSA treated group (Figure 4.3; $p < 0.0001$). The average of the intracellular Ca^{2+} response and the percentage of responding cells were decreased by 55 to 80% compared to the control group, with EPA treated cells having the lowest levels of these readouts. We further demonstrated that the cells that were treated with the polysaturated fatty acid PA did not show any changes in the level of their Ca^{2+} response to GSK101 or percentage of the responding cells compared to the BSA group.

Since the TRPV4 channel is sensitive to hypo-osmotic challenges, we got interested in evaluating this channel's activity in response to a hypotonic shock and see how fatty acids treatment can regulate this response. Therefore, the chondrocytes that were treated with the fatty acids and were labeled with Ca^{2+} indicator dyes were imaged under a confocal microscope while undergoing a hypo-osmotic shock. We showed that the fatty acid treatment did not have any effect on the intracellular Ca^{2+} response of the cells that underwent a hypo-osmotic challenge of -110 mOms (Figure 4.4; Ca^{2+} response: $P = 0.3969$, percentage of responding cells: $p = 0.4167$). The cells that were treated with ω3 fatty acid DHA, showed the lowest level of intracellular Ca^{2+} response and percentage of responding cells compared to the BSA group. In summary, we found that PUFAs can regulate the TRPV4 channel's response to GSK101 but were not able to affect the cells' response to hypo-osmotic challenges.

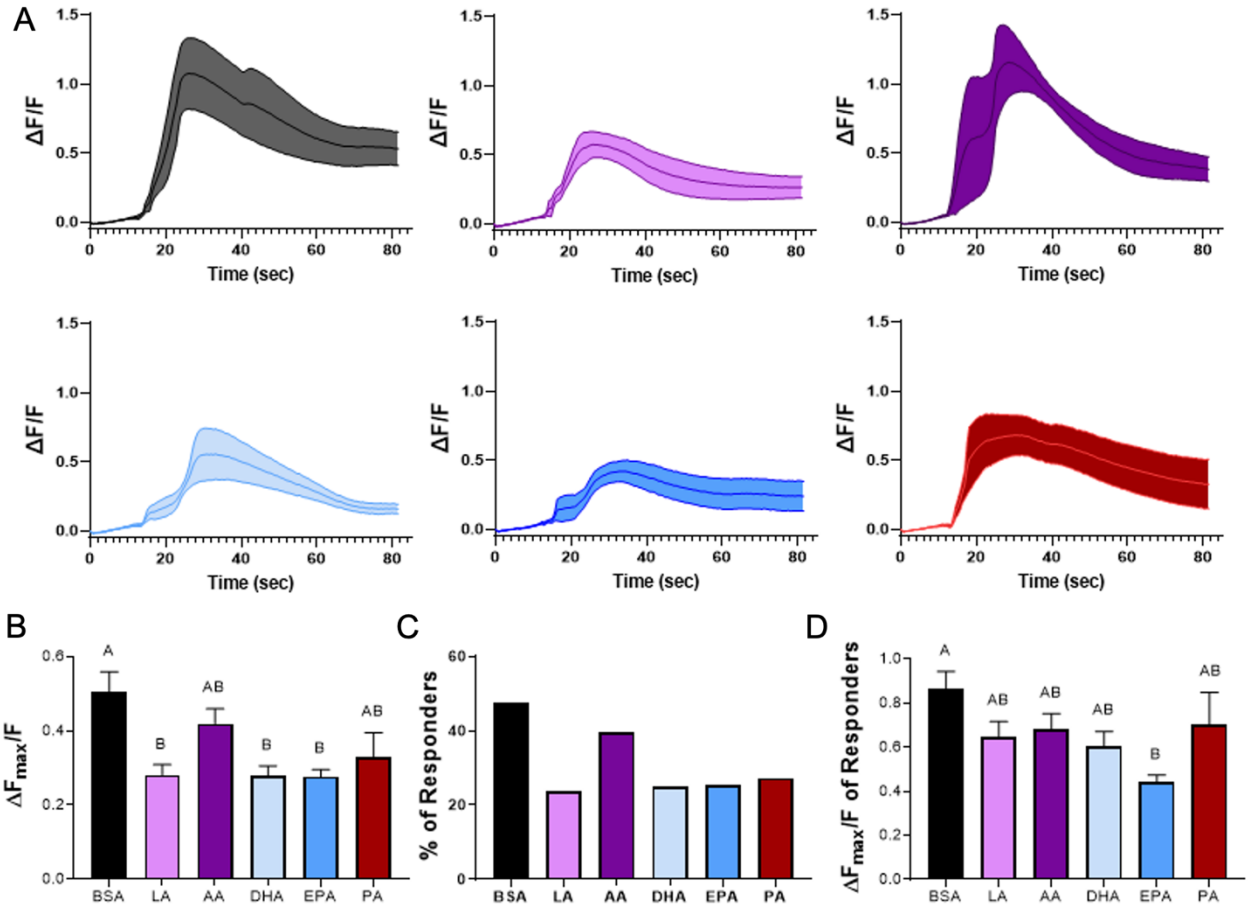

Figure 4.1 Effect of PUFAs on intracellular Ca^{2+} response of chondrocytes to mechanical compression. A) Representative signaling trend for each loading rate. B) Intracellular Ca^{2+} fluorescence intensity ΔFmax/F for each loading rate. C) Percentage of responding cells for each loading rate. D) Considering only the responding cells, intracellular Ca^{2+} fluorescence intensity ΔFmax/F for each loading rate. Data presented as mean ± SEM. For group comparison B-D, one-way ANOVA with Tukey's post-hoc test, different letters indicate statistical significance $p<0.05$, n=34-106 for B and n= for D=9-43.

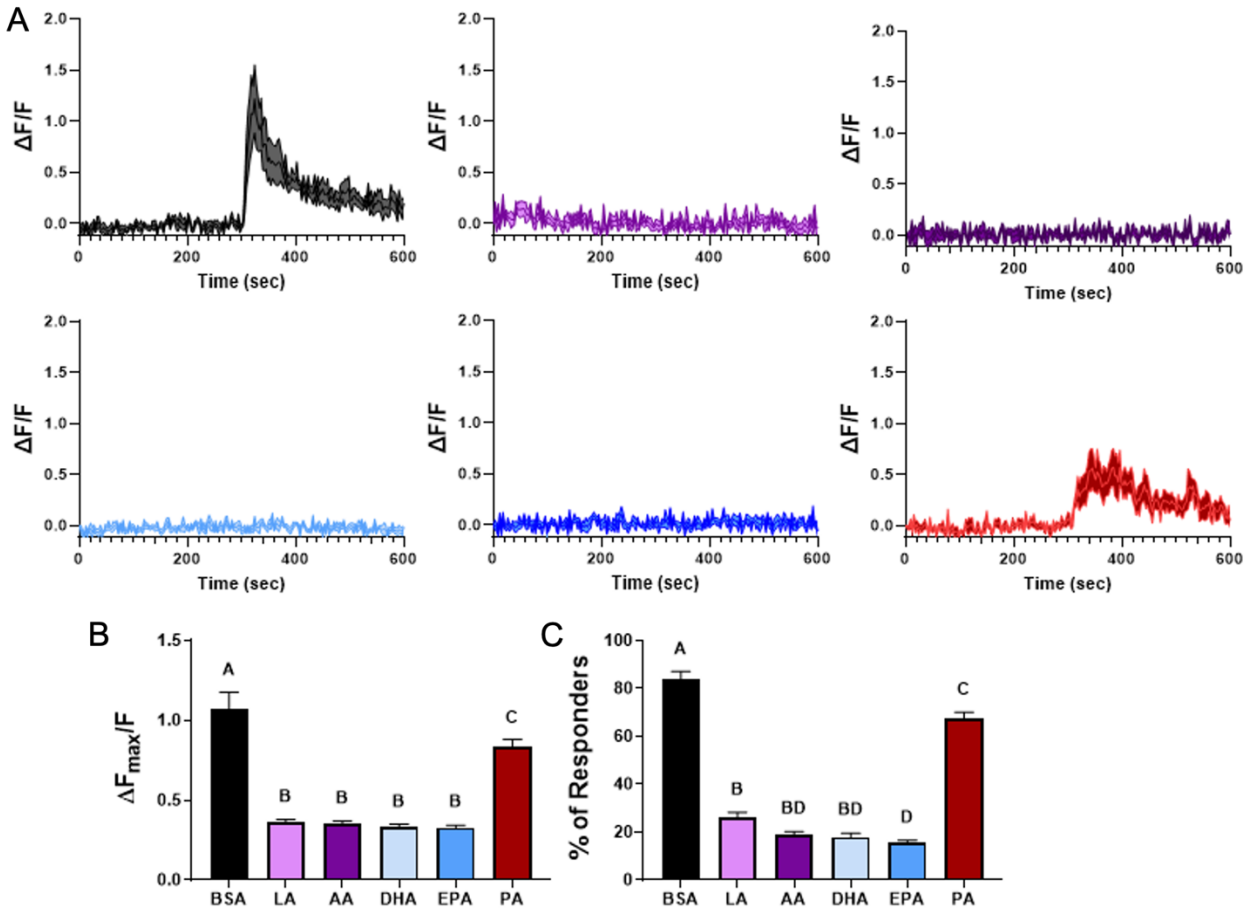

Figure 4.2 Effect of PUFAs on intracellular Ca^{2+} response of chondrocytes to Yoda1. A) Representative signaling trend for each loading rate. B) Intracellular Ca^{2+} fluorescence intensity ΔFmax/F for each loading rate. C) Percentage of responding cells for each loading rate. Data presented as mean ± SEM. For group comparison B and C, one-way ANOVA with Tukey's post-hoc test, different letters indicate statistical significance $p<0.05$, n=12-14.

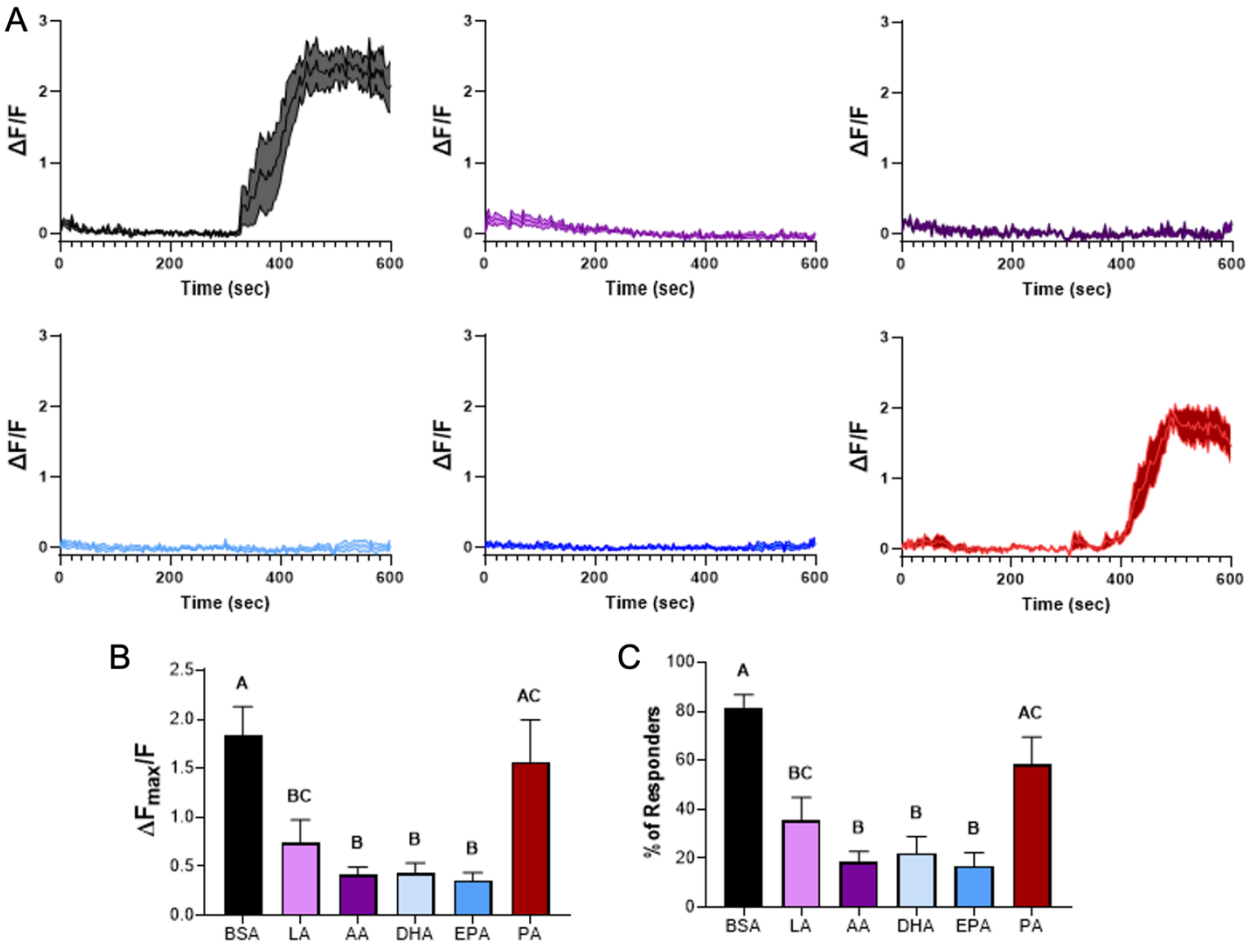

Figure 4.3 Effect of PUFAs on intracellular Ca^{2+} response of chondrocytes to GSK101. A) Representative signaling trend for each loading rate. B) Intracellular Ca^{2+} fluorescence intensity ΔFmax/F for each loading rate. C) Percentage of responding cells for each loading rate. Data presented as mean ± SEM. For group comparison B and C, one-way ANOVA with Tukey's post-hoc test, different letters indicate statistical significance $p<0.05$, n=8-10.

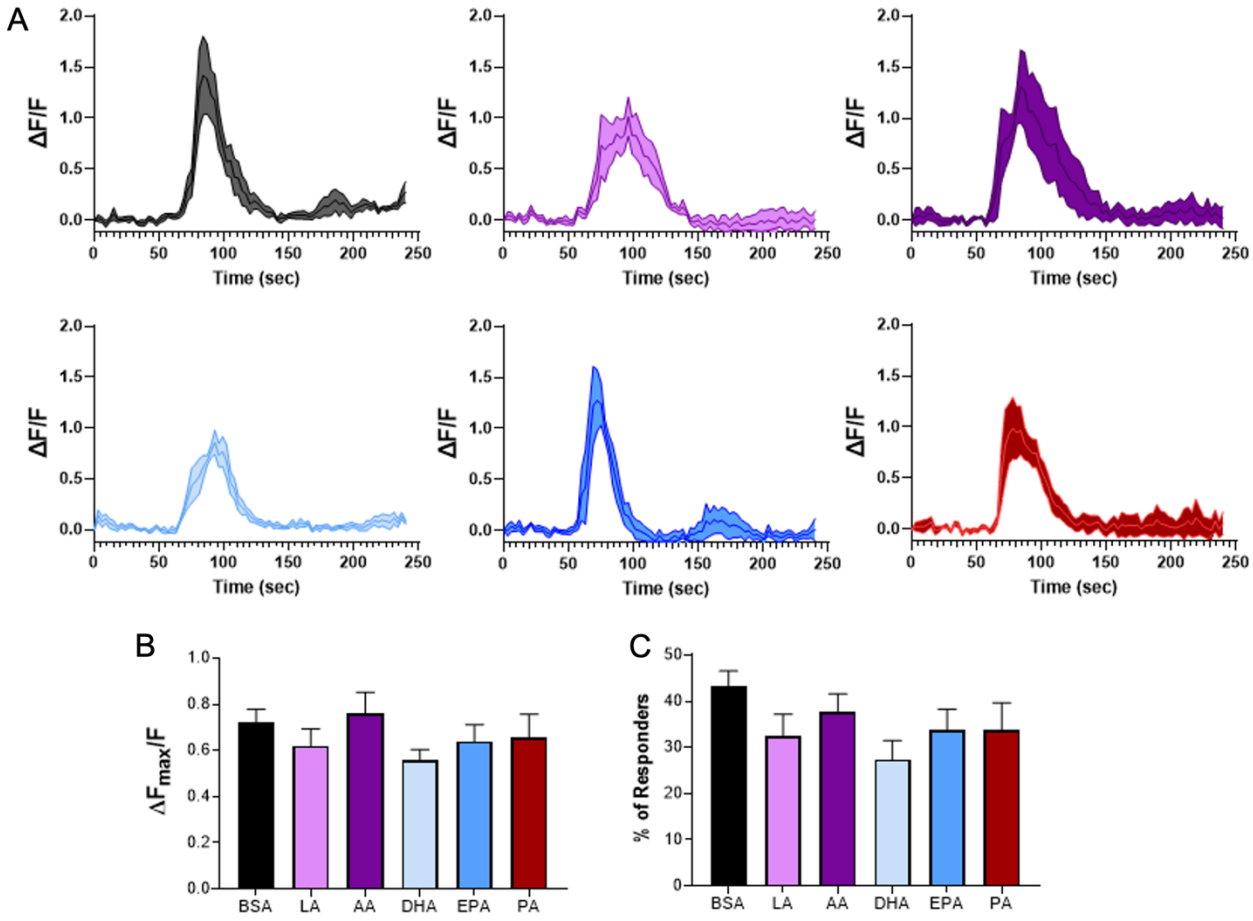

Figure 4.4 Effect of PUFAs on intracellular Ca^{2+} response of chondrocytes to hypo-osmotic shock. A) Representative signaling trend for each loading rate. B) Intracellular Ca^{2+} fluorescence intensity ΔFmax/F for each loading rate. C) Percentage of responding cells for each loading rate. Data presented as mean ± SEM. For group comparison B and C, one-way ANOVA with Tukey's post-hoc test, different letters indicate statistical significance $p<0.05$, n=13-18.

4.4.3 PUFA treatment increased the number of lipid droplets

In our previous experiments, we observed that the fatty acid treatment causes the formation of lipid droplets in the cells. Therefore, we got interested in evaluating these droplets and determine if there are any differences in the amount of lipid droplet formation between different groups of PUFAs. We demonstrated that all the fatty acid treated groups had

significantly higher lipid droplet formation (which is evaluated by measuring the area of lipid droplets within the cells), intensity, total intensity (calculated as lipid droplet area × pixel intensity), percentage of occupied cell area by lipid droplets (Figure 4.5A-D; $p < 0.0001$). However, cells treated with ω6 fatty acid LA had the largest lipid droplets indicating that LA had the most capability to form lipid droplets within the chondrocytes.

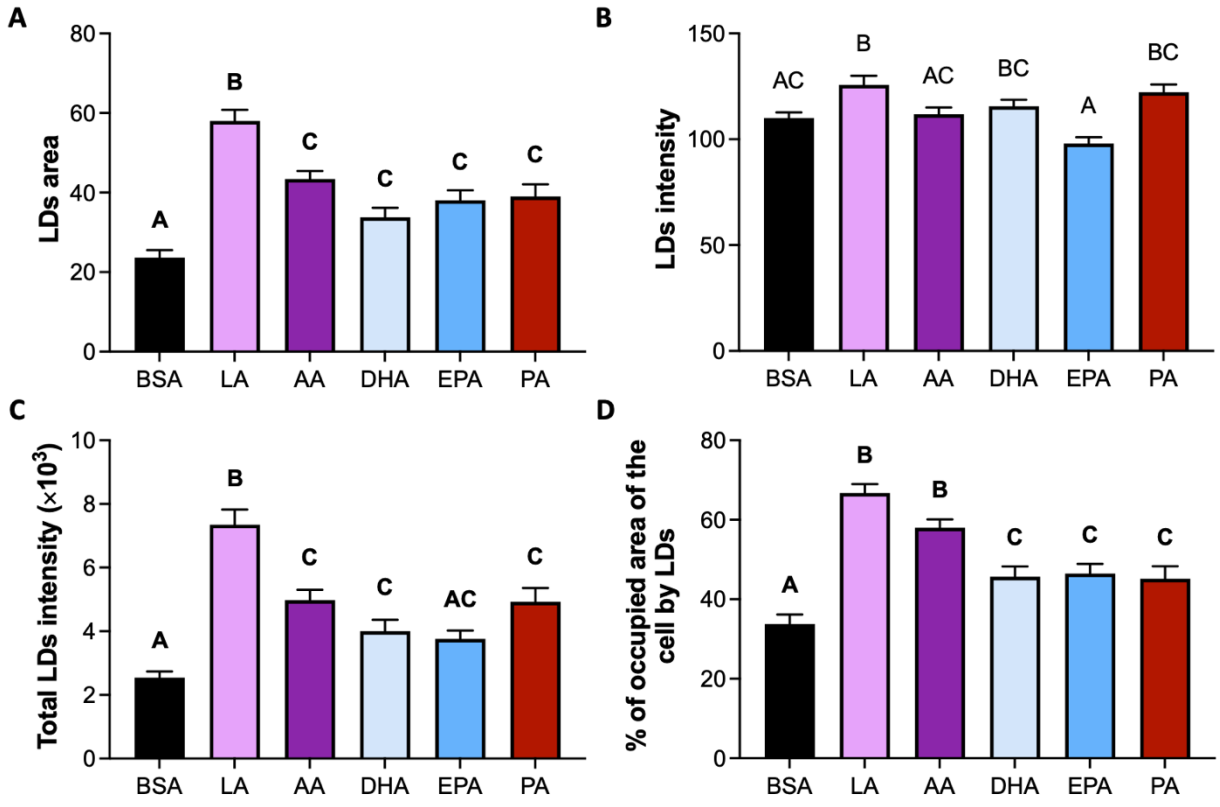

Figure 4.5 Effect of PUFAs on lipid droplet formation. A) Area of lipid droplets B) Pixel intensity of lipid droplets C) Total intensity of lipid droplets which is area of lipid droplets multiplied by their pixel intensity. D) Percentage of the cell area that is occupied by the lipid droplets. Data presented as mean ± SEM. For group comparison A-D, one-way ANOVA with Tukey's post-hoc test, different letters indicate statistical significance $p<0.05$, n=62-111.

4.4.4 The membrane of the LA-treated cells ruptured at lower diameter changes in response to a hypo-osmotic shock with no change in chondrocytes' sensitivity to osmotic challenges

We were also interested in assessing the effect of FAs on the membrane rupture in response to a hypo-osmotic challenge. We applied a hypo-osmotic shock to the cells and measured the change in cell diameter, surface area, and volume before the membrane ruptures due to the hypo-osmotic shock. We found that treating the cells with LA which is an ω6 fatty acid reduced the [percentage of change in cell diameter, surface area, and volume significantly before membrane rupture showing that the membrane of the chondrocytes treated with LA was ruptured sooner in response to the osmotic shock (Figure 4.6, $P < 0.0001$). However, treating cells with AA, DHA, EPA, and PA did not have any effect on the percentage of increase in diameter, surface area, and volume after hypo-osmotic shock.

Furthermore, we investigated the role of FAs on altering the sensitivity of the chondrocytes to different osmotic shocks. We changed the osmolarity of the cells' microenvironment by adding water or a hyper-osmotic medium to apply a final osmolarity of 180, 280, 480, and 580 mOsm (cells were cultured in iso-osmotic condition, 380 mOsm). We found no difference in the R^2 of the lines fitted to the ponder's value (normalized volume (V/V_0) against inverse osmolarity, $R^2 = 0.72\text{-}0.81$) showing that the FA treatment did not have any effect on the chondrocytes' osmotic sensitivity (Figure 4.7).

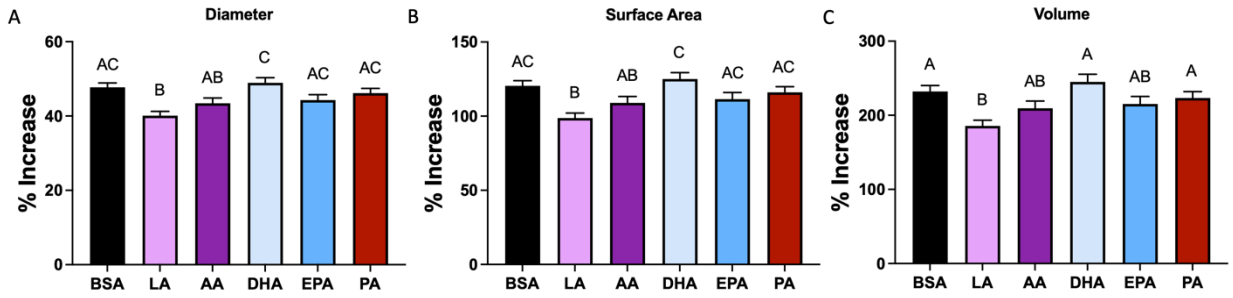

Figure 4.6 Effect of PUFAs on membrane strength. Percentage of increase in cell A) diameter, B) surface area, and C) volume before membrane rupture in the presence of PUFAs.

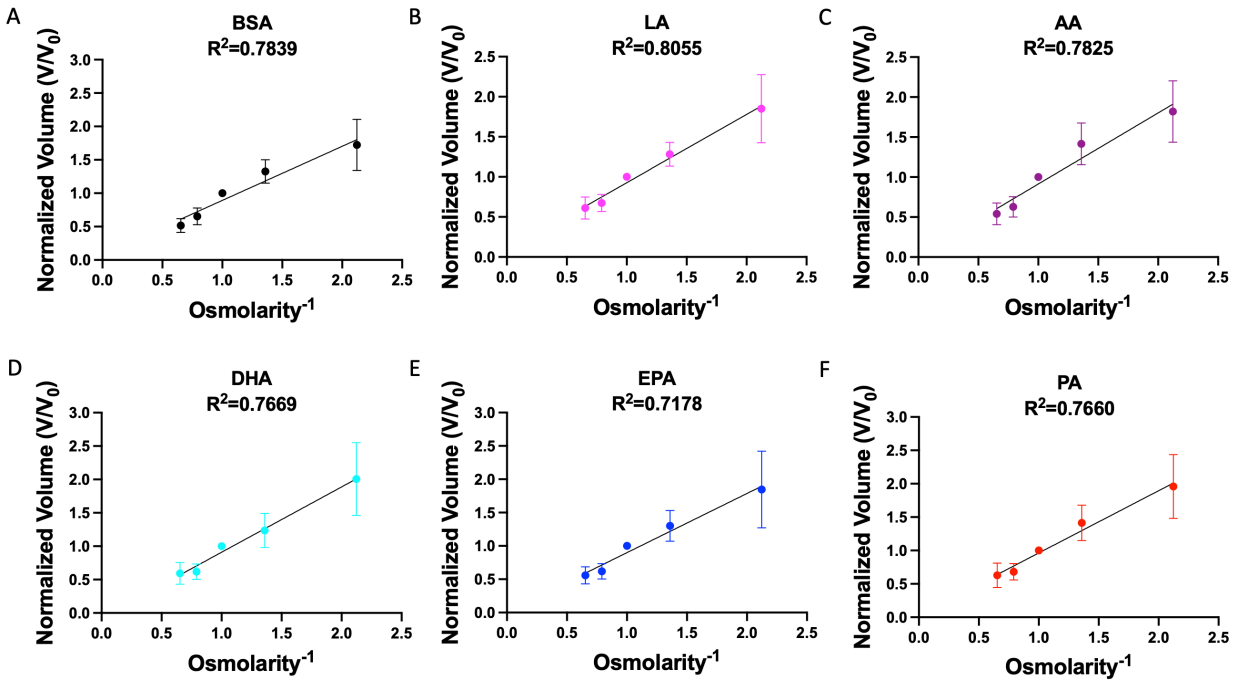

Figure 4.7 Effect of PUFAs on chondrocytes' sensitivity to osmotic shock. A) BSA, B) LA, C) AA, D) DHA, E) EPA, F) PA.

4.4.5 ω3 fatty acids decrease senescence and inflammatory markers

We further investigated the role of fatty acids on the mRNA expression of several markers. First, we wanted to see if the PUFA treatment had any effect on the expression of mechanosensitive ion channels. The RT-qPCR data showed that the PIEZO1 and PIEZO2 mRNA levels did not change after treating the chondrocytes with PUFAs compared to the BSA group (Figure 4.8A-B; A: $p = 0.0723$, B: $p = 0.1423$). However, treating the chondrocytes with ω3 fatty acids DHA and EPA, ω6 fatty acid AA, and polysaturated fatty acid PA significantly increased the mRNA expression of TRPV4 (Figure 4.8C, $P < 0.0001$). Treating the cells with ω6 fatty acid LA also had a strong effect on the mRNA expression of TRPV4 by increasing its expression by 230%, however, the statistical analysis did not detect a significant relation between LA and BSA ($p = 0.053$).

Next, we investigated the role of fatty acids in chondrogenesis markers. Our results showed that PUFAs decreased aggrecan (ACAN), collagen type II (Col2a1), and collagen type I (Col1a1), and SOX9 (Figure 4.9A-D; A: $p = 0.0045$, B: $p < 0.0001$, C: $p < 0.0088$, D: $p = 0.0109$). More specifically, ω6 fatty acid LA and ω3 fatty acid DHA reduced the mRNA expression of ACAN by 30% compared to the control, however, mRNA levels of ACAN in AA, EPA, and PA treated groups were similar to the BSA group. Moreover, all of the ω3 and ω6 treated cells showed a significant reduction in Col2a1 expression compared to the control, but PA treatment did not have any effects on Col2a1 expression. Supplementation of DHA and PA significantly reduced the expression of Col1a1 compared to the BSA group. Furthermore, treating the cells with LA, AA, and EPA also reduced the mRNA expression of Col1a1 by 8-22% however, the reduction was not significant compared to the control group. Lastly, SOX9 expression was decreased by 23% in the cells that were treated with ω3 fatty acid DHA and ω6

fatty acid AA, however, this reduction was not detected as a significant effect. Additionally, treating cells with LA, EPA, and PA did not have any effect on the mRNA levels of SOX9 in the chondrocytes.

We were also interested in evaluating the effect of fatty acids on adipogenesis markers, therefore, the mRNA levels of PPARγ, and adiponectin (ADIPOQ) were measured. None of the fatty acids had a significant effect on the expression of the adipogenesis markers (Figure 4.10A-B; A: $p = 0.2743$, B: $p = 0.2372$). AA, DHA and EPA reduced the expression of PPARγ by 53%, 27%, and 20% respectively, however this effect was not detected as a strong influence. Lastly, ω3 fatty acids DHA and EPA reduced the mRNA expression of ADIPOQ by 51% and 54% respectively, although, this reduction was not detected as a significant effect neither.

In the next step, we investigated the effect of PUFAs supplementation on inflammatory biomarkers' expression. We found that IL-1α, IL-1β, and IL-11 mRNA expressions were not impacted by the fatty acid treatments (Figure 4.11A-B, E; A: $p = 0.6767$, B: $p = 0.8338$, E: $p = 0.5339$). ω6 fatty acid LA increased the expression of IL-1α and IL-1β by 62% and 43% respectively, however, this elevation in the mRNA expression was not detected as a significant effect. IL-11 expression was reduced by both ω3 and ω6 fatty acid treatments (16-40%), but none of these reductions were strong enough to show a significant trend. On the other hand, treating the chondrocytes with PUFAs had a very strong effect on the IL-6 (Figure 4.11C, $p < 0.0001$). Supplementation of ω6 fatty acid increased the mRNA expression of IL-6 by 34-36%, although, treating the cells with ω3 fatty acids and PA, significantly reduced the IL-6 expression 34-63% indicating the strong effect of ω3 PUFAs in reducing the pro-inflammatory biomarkers. Finally, we demonstrated that the fatty acids treatment also had a strong effect on the expression

of IL-8 and all of the PUFAs increased the mRNA expression of IL-8 by 79-160% (Figure 4.11D, $p = 0.0033$).

In the last part of this study, we were interested in evaluating the effect of PUFAs on the cellular senescence. To do this, the mRNA level of 8 different senescence markers including P16, P21, P53, CCL8, MMP3, MMP12, CXCL2, and TIMP1 were measured. Fatty acid supplementation did not have any effects on the expression level of P16 (Figure 4.12A, $p = 0.5594$), P21 (Figure 4.12B, $p = 0.0641$), and CCL8 (Figure 4.12D, $p = 0.6574$). AA, DHA, and EPA reduced the P16 expression by 20-30%, DHA decreased the CCL8 expression by 30%, and AA increased the expression of CCL8 by 80%, however, none of these effects were detected as a significant trend. On the other hand, PUFAs had a significant impact on the mRNA expression level of P53 (Figure 4.12C, $p = 0.0009$), MMP3 (Figure 4.12E, $p < 0.0001$), MMP12 (Figure 4.12F, $p = 0.0003$), CXCL2 (Figure 4.12G, $p = 0.0007$), and TIMP1 (Figure 4.12H, $p = 0.0009$). P53 expression was significantly reduced with the supplementation of ω3 fatty acid DHA (27%). MMP3 expression was increased by 55% after treating the cells with ω6 fatty acid LA, however, treating the cells with ω3 fatty acids DHA and EPA, and polysaturated fatty acid PA decreased the MMP3 mRNA expression by 45-55%. MMP12 expression was significantly increased with the supplementation of both ω6 fatty acids LA and AA by 56%, although, treating the cells with DHA, EPA, and PA did not have any significant effect on the MMP12 mRNA levels. The expression of CXCL2 notably escalated by 60-67% when supplemented with both ω6 fatty acids, LA and AA, however, the administration of DHA, EPA, and PA did not yield any significant impact on the CXCL2 mRNA levels. Lastly, TIMP1 expression did not change with the supplementation of fatty acids compared to the BSA treated group, although, EPA treated group

had significantly lower level of TIMP1 expression compared to the LA and AA treated cells. All in all, these data suggest that the fatty acids have a strong effect on inflammation and cell aging.

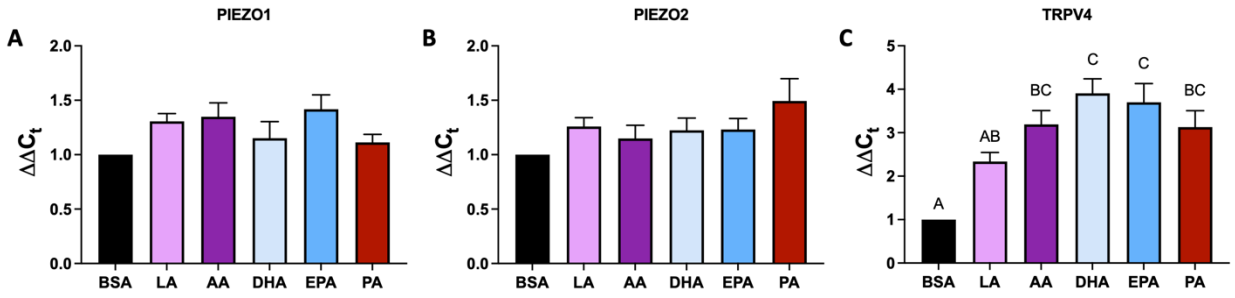

Figure 4.8 Effect of fatty acid supplementation on mRNA expression level of mechanosensitive ion channels. A) PIEZO1 B) PIEZO2 C) TRPV4. Data presented as mean ± SEM. For group comparison A-C, one-way ANOVA with Tukey's post-hoc test, different letters indicate statistical significance $p<0.05$, n=8.

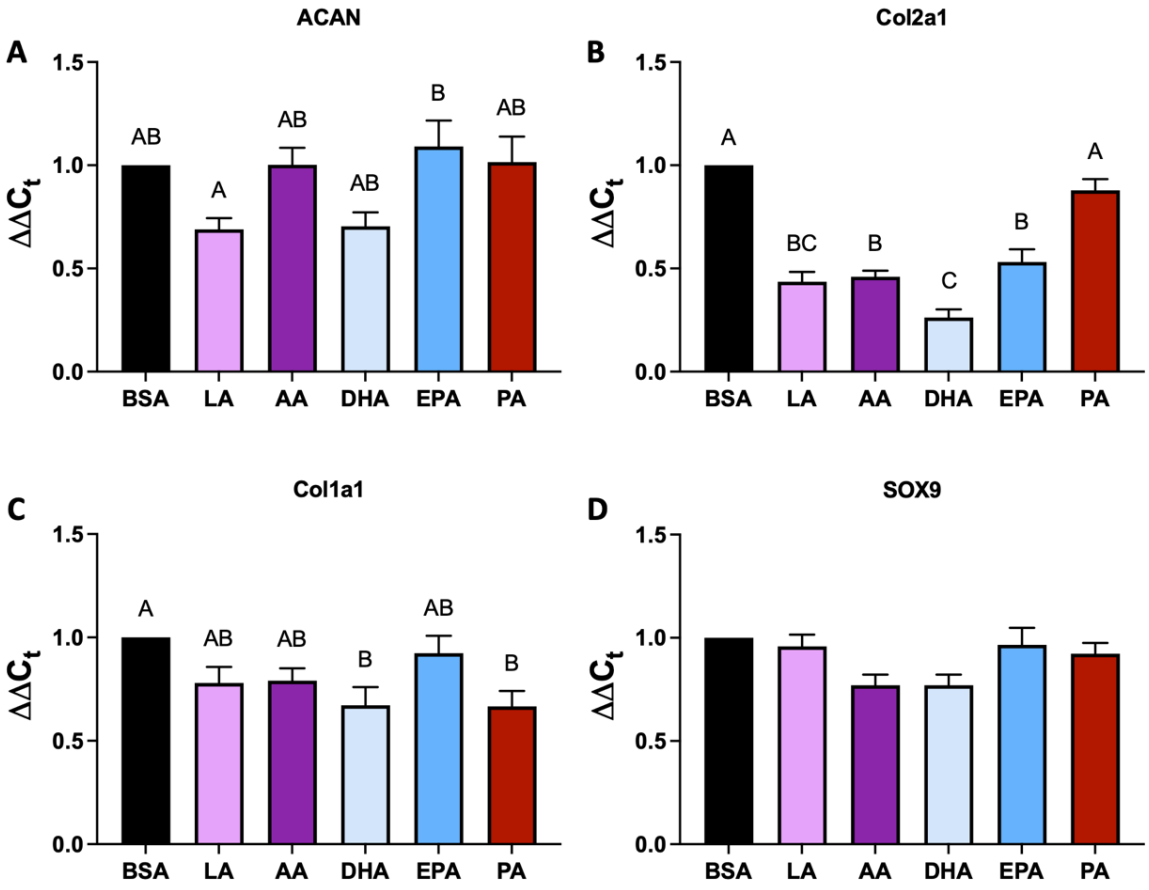

Figure 4.9 Effect of fatty acid supplementation on mRNA expression level of chondrogenesis markers. A) ACAN B) Col2a1 C) Col1a1 D) SOX9. Data presented as mean ± SEM. For group comparison A-D, one-way ANOVA with Tukey's post-hoc test, different letters indicate statistical significance $p<0.05$, n=8.

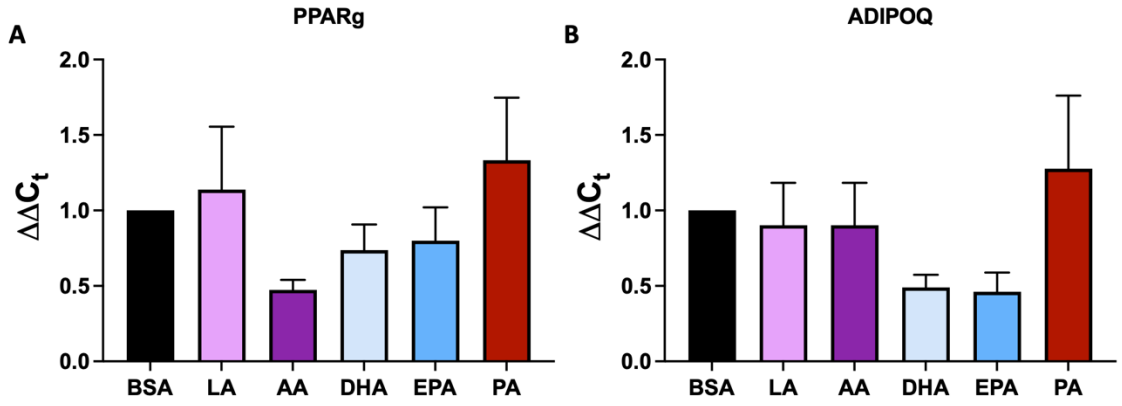

Figure 4.10 Effect of fatty acid supplementation on mRNA expression level of adipogenesis markers. A) PPARγ B) ADIPOQ. Data presented as mean ± SEM. For group comparison A-B, one-way ANOVA with Tukey's post-hoc test, different letters indicate statistical significance $p<0.05$, n=8.

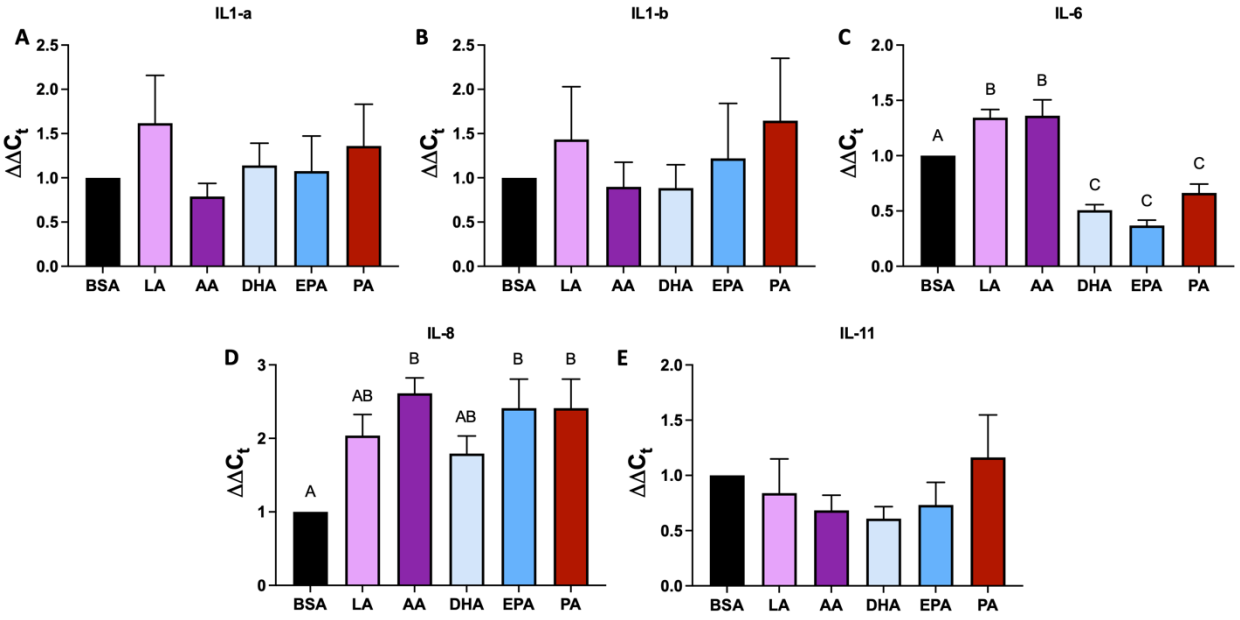

Figure 4.11 Effect of fatty acid supplementation on mRNA expression level of inflammatory biomarkers. A) IL-1α B) IL-1β C) IL-6 D) IL-8 E) IL-11. Data presented as mean ± SEM. For group comparison A-E, one-way ANOVA with Tukey's post-hoc test, different letters indicate statistical significance $p<0.05$, n=8.

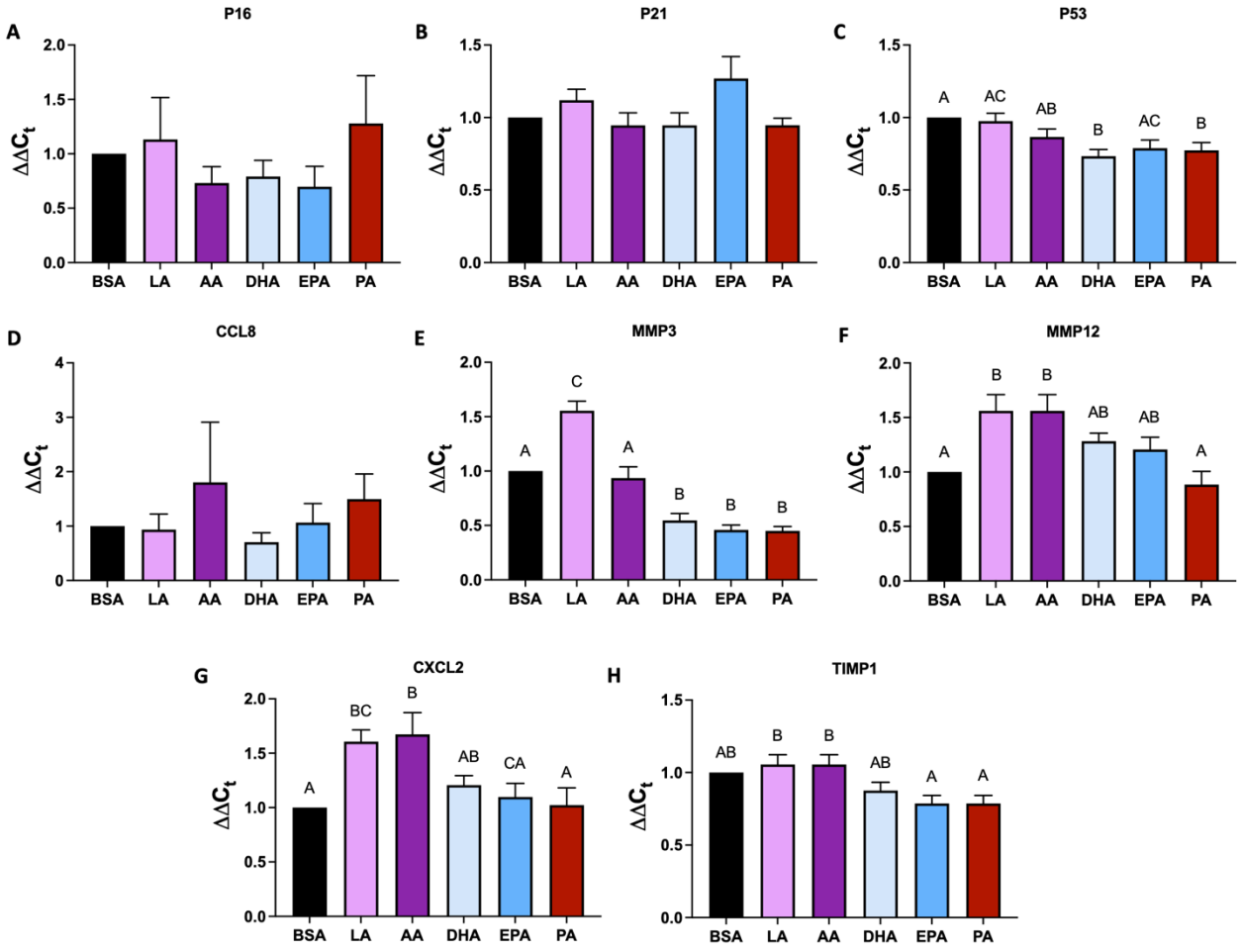

Figure 4.12 Effect of fatty acid supplementation on mRNA expression level of senescence markers. A) P16 B) P21 C) P53 D) CCL8 E) MMP3 F) MMP12 G) CXCL2 H) TIMP1. Data presented as mean ± SEM. For group comparison A-H, one-way ANOVA with Tukey's post-hoc test, different letters indicate statistical significance $p<0.05$, n=8.

Gene	Forward	Reverse
ACAN	CAGACTGTCAGATACCCCATTG	GTGTGGCAAAGAACACTTCCC
COL2a1	CTGAAAGACTGCCTCAGCCC	TTTCTGTCCCTTTGGTCCCAG
COL1a1	GACATCCCACCAGTCACCTG	TCATCGCACAACACATTGCC
SOX9	GCAAACTCTGGAGACTGCTG	TCTTCACCGACTTTCTCCGC
P16	GAATATGGTGCGCCGTCTCT	TCCTCACTAGCAACAGCACG
P21	CATGTGGACCTGTTGCTGTC	TTAGGGCTTCCTCTTGGAGA
P53	GCAGCACTAAGCGAGCACTG	TCTCGGAACATCTCGAAGCG
MMP3	TTTTGCAGTTCGAGAACACG	CATGGGCAGCAACAAGGAAT
MMP12	TCAGTCTCTCTATGGACCCCC	AACTCTCCTCTCTGGACGCT
Timp1	CGCAGCCAGGAGTTTCTCAT	GTGCAGGGAAACACTGTGCAT
CCL8	GTGCTTGCTCAGCCAGATTC	AGACCTCCTTGTCGGCTTTG
IL1a	CAGCCAACGGGAAGATTCTG	ATGGCTTCCAGGTCGTCAT
IL1b	CCTTGAAACGTGCAATGATG	TTCAAGTCCCCTGTGAGGAG
IL6	AGATGCCAAAGGTGATGCCA	ACAAGACCGGTGGTGATTCTCA
IL8	CCACACCTTTCCACCCCAAA	GTTGTTGTTGCTTCTCAGTTCTCTT
IL11	GCACGCTCAAGGTTGTTCAT	ACACCTAAAGCAGCCTCCAT
PPARγ	ATTTACACCATGCTGGCCTC	GGGCTCCATAAAGTCACCAA
ADIPOQ	ACCGTTCAGCATTCAGTGTG	AGACCGTGATGTGGAAGGAG
CXCL2	CCACTGTGACCAAACGGAAG	TGGCACTGCTCTTGTTTAGC
TRPV4	GTCATGGTCTTTGCCTTGGT	GTCCTCACTGCACACCTTCA
PIEZO1	GCCCCCAACGGACCTGAAGC	TGCGCAGCTGGATACGCACC
PIEZO2	CCAGCTGGATCTGCGTGGAGG	TGGTTGATCACCCCGGCGAC
ACTB	CACGCCATCCTGCGTCTGGA	AGCACCGTGTTGGCGTAGAG

Table 4.1 List of primers.

4.5 Discussion

In this study, we found that PIEZO1 mechano-activation is suppressed by various PUFAs. Specifically, the intracellular Ca^{2+} response and the percentage of responsive cells are significantly decreased in response to PIEZO1 agonism when cells were treated with ω3 or ω6 fatty acids. Furthermore, we showed that the high-strain mechanically-activated intracellular Ca^{2+} response was significantly decreased in cells were treated with LA, an ω6 fatty acid, and DHA or EPA, ω3 fatty acids. However, the finding that AA, an ω6 PUFA, did not reduce mechanically-activated Ca^{2+} signaling suggests that the mechanism of PIEZO activation may differ between that of Yoda1 and mechanical stimulation (Figure 2B). These results are consistent with previous study showing that PUFAs can serve to tune the PIEZO response [334, 406]; however, Romero et al found that the DHA actually reduces the inactivation of PIEZO1, unlike EPA and AA. It is important to note that the cells and the method for activating the PIEZO1 were different in Romero et al study than the ones that are used in our study which can be the reason of this difference. Moreover, Romero et al. showed that the PIEZO1 channel has different gating properties depending on the fatty acids that the cells are treated with; for example, treating N2A cells and HMVEC with Margaric Acid (MA) increased the mechanical threshold required to activate the PIEZO1 channel. In the present study, we show that AA has the ability to differentially regulate PIEZO activation depending on the mode of PIEZO stimulation (mechanical versus agonist). Our results demonstrate the composition of fatty acid supplementation can alter chondrocyte responsiveness to high mechanical strain through modulating the Piezo ion channels, therefore, our long-term goals are to determine whether fatty acid supplementation can influence the Piezo1-mediated effects, as a potential therapeutic approach for PTOA or obesity-associated OA. Moreover, we showed that LA and AA induced

the formation of large lipid droplets that take over most of the cell volume indicating that this might also be affect the sensitivity of the chondrocytes to different stimuli such as osmotic challenges. Lastly, we showed that treating the cells with ω-3 fatty acids DHA and EPA significantly reduced the expression of IL-6, however, supplementation of ω-6 fatty acids LA and AA increased the mRNA level of IL-6, showing the important role of PUFAs in regulating inflammatory markers which is also shown in different studies [404, 405, 561-564]. Curtis et al. explored the effects of dietary supplementation with ω-3 PUFAs on the metabolism of cells within synovial joint tissues. Using in vitro models of cartilage degradation and explants from normal bovine and human osteoarthritic cartilage, the researchers exposed the tissues to either ω-3 or ω-6 PUFA and then subjected them to IL-1, simulating cartilage degradation seen in arthritis. Their findings revealed that only ω3 PUFA supplementation significantly mitigated both the inflammatory and degradative facets of chondrocyte metabolism without disrupting normal tissue functions. Specifically, ω3 PUFA reduced the release of proteoglycan metabolites and suppressed the expression of certain enzymes and inflammatory mediators at the mRNA level. In contrast, other fatty acids didn't exhibit these protective effects. Hence, ω-3 PUFA may offer therapeutic advantages in slowing and reducing inflammation in degenerative joint diseases which is completely aligned with what we have observed in our study. Lastly, we investigated the role of PUFAs on cellular senescence and found that treating the chondrocytes with ω-3 fatty acids lowers the mRNA level of senescence markers MMP3 and P53 illustrating the positive effect of ω-3 PUFAs in reversing cell aging. Several studies have investigated the role of PUFAs on membrane fluidity, cholesterol levels, and aging and found that both ω-3 and ω-6 fatty acids have direct effect on all of these factors that can [396, 565]. Additionally, Petursdottir et al. showed that treating the senescence-accelerated prone 8 (SAMP8) mouse (senescence mouse

model) that have lessen ability to learn and memorize with a diet rich in DHA can increase the mouse capability to learn [566]. Consequently, PUFAs have important effect on cellular aging and inflammation and an imbalance intake of them can lead to various diseases.

Understanding the mechanisms by which chondrocytes respond to physiologic or pathological cartilage loading will provide important insights into the development of new pharmacologic therapies to treat mechanically-regulated conditions such as PTOA. Here, we showed that dietary PUFAs can reduce the mechanosensitivity of PIEZO channels in chondrocytes in response to deformation. Furthermore, supplementation of ω-3 PUFAs can reduce the inflammation and senescence levels in the cells. These findings further elucidate the positive effect of PUFAs in reducing OA and PTOA related biomarkers and the role of mechanobiology in cartilage health and disease which may provide new insights into developing future OA therapeutics.

4.6 Supplemental Figures

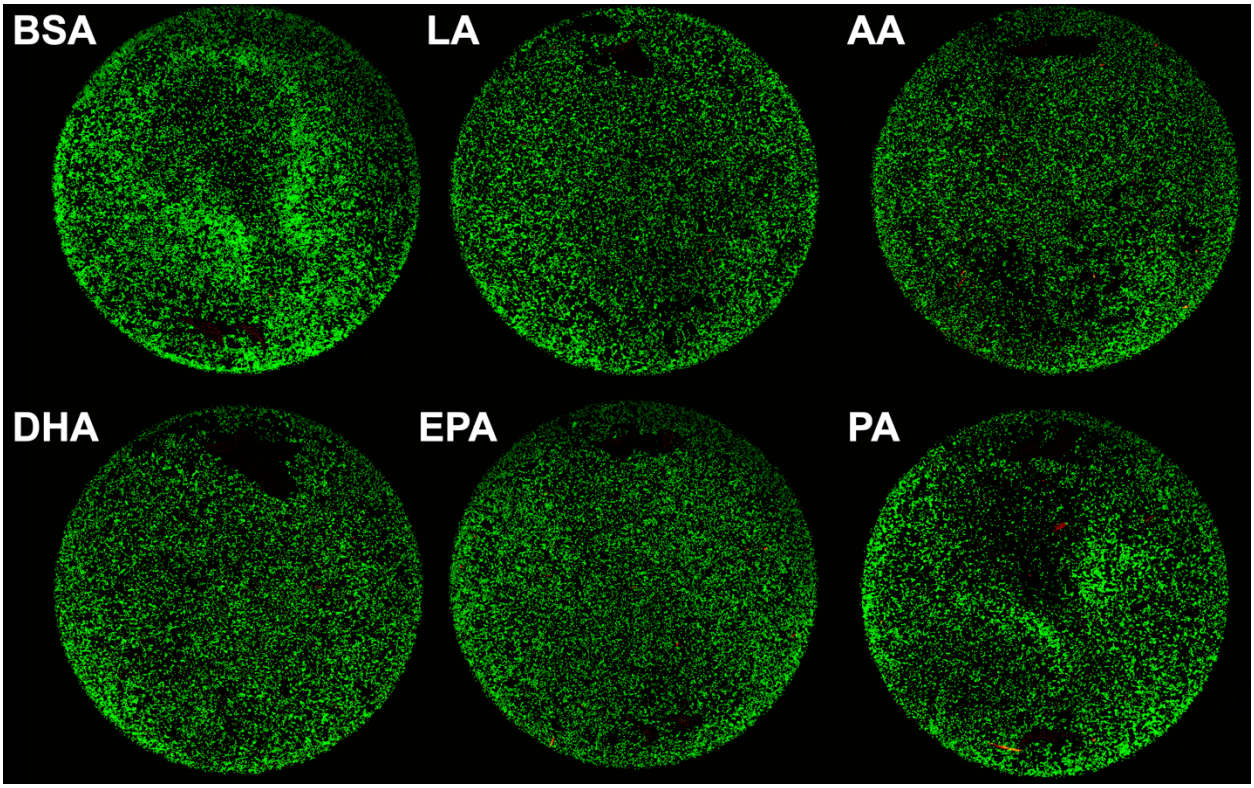

Figure S4.1 Live/dead staining of the cell after being treated for 3 days with different PUFAs showed no change chondrocyte's viability.

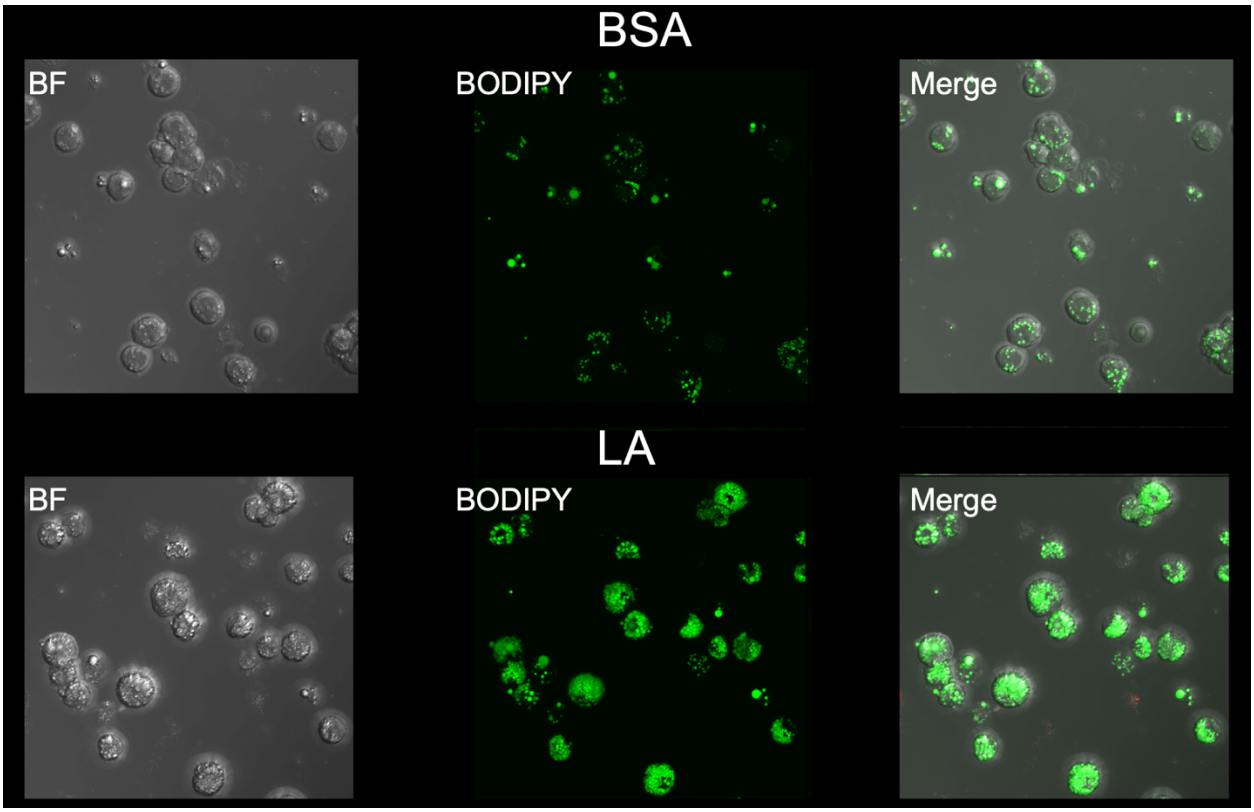

Figure S4.2 Lipid droplet formation in chondrocytes after treating the cells with BSA (Control) and LA (ω6 FA).

Chapter 5: PIEZO1 Mechanosensitivity in Chondrocytes Is Differentially Modulated by L-type and T-type Voltage-sensitive Ion Channels

5.1 Abstract

Osteoarthritis (OA), a prevalent joint disorder, affects over 300 million individuals across the globe. One of the primary triggers for this debilitating condition is the cumulative wear and tear our joints undergo from daily activities, unexpected injuries, or the burden of excess weight. Central to our understanding of OA are chondrocytes, the primary cells within our joint cartilage. These cells are sensitive to wear and tear, responding, in part, by allowing Ca^{2+} to flow into them. However, the exact mechanisms by which these cells detect and react to mechanical strains remain an area of active exploration.

In this comprehensive study, we delved deep into the interactions of certain cellular channels, namely the PIEZO1 channels and two subsets of Ca^{2+} channels (L-type and T-type VGCCs). By specifically observing their collaborative actions when the chondrocytes experience pressure, we uncovered some insightful findings. Notably, when we obstructed the function of the L-type channels using a drug named Nifedipine, the PIEZO1's activity was noticeably reduced. This led to a significant decrease in cell death, especially when the cartilage faced injurious conditions. Contrarily, impeding the T-type channels with another drug, NNC-55, caused the PIEZO1 activity to rise and resulted in a higher cell death rate when the cartilage was subjected to harm.

Expanding upon these results, it's evident that the T-type channels, which respond rapidly to minor changes, act as initial responders, setting off the reaction process in chondrocytes. In contrast, the L-type channels, which are activated by more substantial changes, exert a broader and prolonged effect on this process. Our further experiments, using a chemical agent called Yoda1, reinforced the pivotal role of L-type channels in the Ca^{2+} variations steered by PIEZO1.

The implications of our findings are vast. By demystifying the intricate mechanisms of how joint cells counteract strain, we are paving the way for innovative therapeutic interventions. Our research not only adds a valuable layer to the existing knowledge on OA's cellular dynamics but also offers a promising direction for the development of targeted treatments for osteoarthritis and related ailments. This beckons a future where joint discomfort can be better managed, offering hope to millions worldwide.

5.2 Introduction

More than 300 million individuals worldwide are afflicted by osteoarthritis (OA), a distressing condition marked by the deterioration of joint cartilage [555]. OA's causes are multifaceted, but excessive mechanical strain on joints has been identified as a significant contributor. This strain can arise from injuries, obesity, or even routine activities such as running and jumping [316]. Chondrocytes, the cells in cartilage, detect this heightened strain and react by increasing production of destructive elements and reducing regenerative ones, advancing OA. Although the precise pathway of force perception in chondrocytes remains a mystery, the influx of Ca^{2+} ions is pivotal in this mechanism [555].

Ca^{2+} ion entry into cells can happen through voltage-gated Ca^{2+} channels (VGCCs) and mechanosensitive Ca^{2+} channels. VGCCs, present in both skeletal and heart muscles, can be influenced by certain antihypertensive medications. Among the VGCCs present in chondrocytes, L-type channels stay open longer than T-type channels [567] and it has been shown that these channels have direct effect on bone formation and remodeling, osteoblast differentiation and proliferation, and mechanotransuction. Studies have suggested that VGCC-blocking drugs might offer OA relief since they have been shown to reduce chronic pain [568, 569]. One study by Takematsu and colleagues found that L-type VGCC inhibitors promoted protective markers while suppressing OA indicators in cartilage samples, possibly by influencing the Wnt/B-catenin pathway [322]. T-type VGCC inhibitors also appear beneficial against OA, although their positive effects might stem from impacts on bone-forming cells rather than chondrocytes [570]. Moreover, studies have suggested that inhibiting the L-type VGCCs using their specific inhibitor Nifedipine can reduce the cells' sensitivity to shear stress [319].

Apart from VGCCs, chondrocytes house mechanosensitive channels, notably Piezo1 and Piezo2. Piezo1 is primarily found in cells like smooth muscle and cardiac fibroblasts, while Piezo2 dominates in sensory and Merkel cells [10]. When chondrocytes face excessive mechanical strain, these channels activate [48, 555]. A study by Lee and co-authors indicated that blocking these channels might prevent chondrocyte damage following mechanical stress [237]. They posited that Ca^{2+} influx could destabilize the structural network within chondrocytes, making them prone to injury [237].

In a 2021 research, Lee et al. and team associated extreme mechanical stress, augmented Ca^{2+} ion entry through VGCCs and mechanosensitive channels, and OA development [85]. Their findings revealed that under such strain, blocking Piezo channels or VGCCs curbed Ca^{2+} entry,

even when an OA-promoting agent, IL-1α, was present [85]. Despite these insights, it remained unclear if these two channel types collaboratively influenced chondrocyte responses. On the other hand, it has been suggested that when a mechanosensitive ion channel opens, the ions will flow inside the cell, get close to the cell membrane, depolarize the membrane, and activate voltage-gated channels [319]. The fact that PIEZO channels do not have specific inhibitors, make them hard to study. However, VGCCs do have FDA approved inhibitors that are already used for heart hypertension [571, 572]. Therefore, we decided to investigate the relationship between VGCCs and PIEZO channels and determine if we could manipulate the PIEZO channels activity by inhibiting or activating different VGCCs and use the downstream effect of the VGCCs on PIEZOs as a therapeutic for OA and PTOA.

Our study delved into how blocking L-type and T-type VGCCs might alter Piezo channel reactions to mechanical strain and the potential to protect cartilage from harm. By exposing cartilage samples to varying mechanical pressures and Ca^{2+} channel blockers, we found distinct impacts of L-type VGCC inhibition on Piezo channels compared to T-type VGCCs. These discoveries shed light on chondrocyte response mechanisms and hint at the therapeutic potential of L-type VGCC inhibitors for OA.

5.3 Materials and Methods

5.3.1 Sample preparation

Culturing Cells and Preparing Samples: The femoral mid-condyle's articular cartilage was harvested from the knees of mixed breed pigs (landrace yorkshire and duroc) aged 5 to 6 months, obtained from a nearby slaughterhouse on the day of slaughter. The extracted cartilage

was stored in a standard culture medium, composed of High glucose DMEM (Gibco, Thermo Fisher Scientific, Waltham, MA), 10% fetal bovine serum (FBS, Atlas Biologicals, Fort Collins, CO), 1.5% HEPES (Corning, Corning, NY), 1% MEM Non-essential amino acid (Corning), 1% Pen Strep (Gibco, Thermo Fisher Scientific), and 0.5% L-Proline (Sigma Aldrich, St. Louis, MO), for a duration of 1 to 2 days prior to the initiation of enzymatic digestion.

The cartilage was then treated with pronase (Worthington Biochemical, Lakewood, NJ), prepared in a wash medium that included High glucose DMEM, 1x Gentamycin (Gibco, Thermo Fisher Scientific), 1x Kanamycin (Goldbio, St. Louis, MO), and 1x Fungizone (Corning), at a concentration of 1320 PKU/ml medium, for approximately 1 to 1.5 hours. Following this, the pronase-laden medium was discarded, and the tissue was incubated for an additional 3 to 3.5 hours in a medium containing 0.4% collagenase type II (Worthington Biochemical).

Subsequently, the cells were separated, cleaned, and resuspended in a growth medium containing 10% FBS, 1% Pen Strep, 1.5% HEPES, and 1% MEM Non-essential amino acid (Corning). The cell count was then determined, and they were distributed onto 12mm round coverslips #1.5 (Electron Microscopy Sciences, Hatfield, PA) at densities varying from 50,000 to 100,000 cells per coverslip, specifically for AFM analysis. For the confocal microscopy studies, cells were allocated in high-resolution glass-bottom 96-well plates (Cellvis, Sunnyvale, CA). The cells were then cultured for three days in a 5% CO2 incubator set at 37 °C. The serum-free mediums' osmolarity was adjusted to 380 mOsm to mimic the physiological conditions of cartilage, as indicated in references [516, 517].

Cartilage explants: Explants were obtained by biopsy punching 4 mm cylindrical cartilage from condyle side of the pig knees. Explants were cultured in standard cultured media

as described in the previous paragraph in a 12-well plate in a 5% CO2 incubator set at 37 °C. On the day of the test, single explants were moved to a 48-well plate for further treatment and staining.

5.3.2 Confocal microscopy

Ca^{2+} imaging: Treated cells were stained for 60 minutes using the Ca^{2+} indicator dyes, Fura red-AM (Invitrogen, Thermo Fisher Scientific) and Fluo4-AM (Invitrogen, Thermo Fisher Scientific), which help in tracking the variations in intracellular Ca^{2+} concentrations. After the staining process, the cells were rinsed and then examined using a confocal microscope (LSM 880, Zeiss, Dublin, CA) while maintaining a constant temperature of 37°C to mimic physiological conditions. The imaging process began with a baseline imaging session of one minute, followed by the addition of a control solution (DMSO, Sigma Aldrich) and another two minutes of imaging. Subsequently, a final concentration of 5 μM Yoda1 was administered to the cells, and their responses were captured for an additional two minutes. The entire procedure, which included labeling, rinsing, and imaging, was conducted under iso-osmotic conditions. After completing the imaging, the collected video data was analyzed using ImageJ software to measure the Ca^{2+} response of each individual cell during the observation period.

Explant imaging: Loaded explants were cut in half and transferred to live-dead stain in the presence of fresh inhibitors for 3 hours. Then, a Z-stack image of explants were taken under confocal to evaluate the effect of treatment and loading on the zone of death cells in the cross section of the explants.

5.3.3 Atomic Force Microscopy

The Atomic Force Microscope (AFM; MFP-3D Bio, Asylum Research, Santa Barbara, CA) was utilized to compress primary chondrocytes. Prior to the experiment, the cells were marked with Fura2-AM dye (Invitrogen, Thermo Fisher Scientific), a dye that reacts to the concentrations of intracellular Ca^{2+}. This marking process involved a mixture of Phenol red-free DMEM (Gibco, Thermo Fisher Scientific), 1.5% HEPES buffer (Corning), 1% Pen Strep (Gibco Thermo Fisher Scientific), 1% MEM non-essential amino acid (Corning), 1% Na Pyruvate (Corning), 1% GlutaMax (Gibco, Thermo Fisher Scientific), and 0.1% L-Proline (Sigma Aldrich), and lasted for 1-2 hours. Tipless cantilevers with a stiffness between 7-13 N/m (Nanoandmore, Watsonville, CA) were used for the chondrocyte compression. The thermal method, provided by the manufacturer, was employed to measure the stiffness of the cantilevers. Light sources with wavelengths of 340/380 nm were used to capture ratiometric Ca^{2+} images while the cells were being compressed. All experiments were carried out in a hydrated environment at a temperature of 37°C. Cells that exhibited movement during the imaging or appeared damaged (as indicated by a sudden decrease in intracellular fluorescence) were omitted from the analysis. The AFM curves obtained, which depicted the indentation versus the vertical displacement of the cantilever, were analyzed using a specialized MATLAB code (The Math Works, Inc, https://www.mathworks.com) to determine the point of contact, the height of the cell, and the cellular deformation in response to the applied load. Additionally, the ImageJ software (U.S. National Institutes of Health, Bethesda, MD, https://imagej.nih.gov/ij/) was used to analyze the videos of the cells' intracellular Ca^{2+} reaction to mechanical loading.

5.3.4 Explant loading

The height of the treated explants was measured and used to load them to 40, 50, 60, 70, and 80% with the loading rate of 0.5 or 1 mm/sec. After loading, the explants were cut in half and transferred to live-dead stain in the presence of the inhibitors , Yoda1 or each of the treatments' corresponding controls (DMSO or water).

5.3.5 Image analysis

Images from confocal and AFM experiments were analyzed using ImageJ. Initially, videos were imported into ImageJ, and then the two separate channels representing fluo-4 and fura-red in confocal imaging, or the 340 nm and 380 nm light wavelengths in the AFM experiment, were divided. This division resulted in the display of normalized signal intensities. Cell shapes were then acquired and analyzed by thresholding the videos based on staining intensity, throughout the experiment. Next, the mean pixel intensities were normalized to the baseline signal levels. The peak normalized pixel intensity for each cell was recorded as the intracellular Ca^{2+} response of that cell ($\Delta Fmax/F$).

In the AFM studies, a control test was conducted where the cantilever was positioned over the cells but without applying any pressure. The intracellular Ca^{2+} responses of these cells were then analyzed, normalized, and the mean (M) and standard deviation (SD) of these responses were calculated. Any cell with a Ca^{2+} response greater than the mean of the control group plus three times the standard deviation ($\Delta Fmax/F > M + 3*SD$), and that exhibited a peak in its Ca^{2+} response trace, was classified as a responder. Cells that did not meet these criteria were classified as non-responders.

For the confocal experiment analysis, videos were analyzed in ImageJ and the ΔFmax/F of each cell for every experiment was recorded. These results were then further processed using a custom MATLAB code to determine the percentage of responding cells and the average level of intracellular Ca^{2+} signaling. The MATLAB code normalized each cell's intracellular Ca^{2+} response to the addition of Yoda1, relative to the cell's response after the addition of DMSO. The mean ΔFmax/F of all cells was then calculated and reported as the mean cellular response from each video. The MATLAB code also determined whether a cell's ΔFmax/F was greater than the mean Ca^{2+} signal after DMSO addition (M´) plus ten times its standard deviation (SD´) (ΔFmax/F > M´ + 10*SD´). Cells meeting this criterion were classified as responders. The total number of responders, divided by the total number of cells, was reported as the percentage of responding cells for each video. If there were more than four values for the responding cells, meaning the experiment was conducted on more than four different animals, individual values for the percentage of responding cells were reported. However, if there were less than four values per group, the average of all results was calculated and a single value for the percentage of responding cells was reported.

To analyze the explant images, the maximum intensity projection (MIP) of each image was acquired. Afterwards, the MIP images were analyzed in ImageJ by measuring the death zone and explant thicknesses at 5 points. Then, the average of the death zone thickness measurements for each explant was divided by average of the explant thickness, and the final normalized number was reported as the death zone thickness/explant thickness.

5.3.6 Inhibitor treatment

Chondrocytes: To test the effect of different inhibitors of VGCCs on the activity of the PIEZO channels in monolayer, primary chondrocytes were treated with either Verapamil (10, 50, and 100μM, 10-20 minutes, Tocris, Bristol, United Kingdom, CaV1.x blocker), Nifedipine (10, 50, and 100μM, 10-20 minutes, Tocris, Bristol, United Kingdom, CaV1.x blocker), Diltiazem hydrochloride (50, 100, and 200μM, 10-20 minutes, Tocris, Bristol, United Kingdom, CaV1.x blocker), or NNC-55 (0.1, 1, 5 and 10μM, 10-20 minutes, Tocris, Bristol, United Kingdom, CaV3.x blocker). All of the L-type channel inhibitors were soluble in DMSO and NNC-55 was dissolved in water, therefore, for the control experiment of L-type channel inhibitors, cells were treated with DMSO, and for control experiment of T-type channel inhibitor, the cells were treated with distilled water. The AFM experiment was performed in the presence of the inhibitors since this experiment was a longer test to run unlike the confocal experiment which was a short-term experiment, and the cells were not tested in the presence of the inhibitors. Moreover, the osmolarity of the cells' environment was kept at 380 mOsm.

Cartilage explants: Explants were treated with wither Verapamil (1 mM, 2.5-3 hours prior loading and 2.5-3 hours post loading), Nifedipine (1 mM, 2.5-3 hours prior loading and 2.5-3 hours post loading), Diltiazem hydrochloride (1 mM, 2-3 hours prior loading and 2.5-3 hours post loading), NNC-55 (50 μM, 2.5-3 hours prior loading and 2-3 hours post loading), GsMTx-4 (40 μM, 2.5-3 hours prior loading and 2.5-3 hours post loading), Yoda1 (10 μM, 2.5-3 hours prior loading and 2.5-3 hours post loading). Verapamil, Nifedipine, Diltiazem hydrochloride, and Yoda1 were dissolved in DMSO, and NNC-55 and GsMTx-4 were dissolved in water. Therefore, depending on the inhibitor, DMSO or water was selected as the control treatment.

5.3.7 Statistical analysis

In every graph, the mean values for each group are illustrated, accompanied by the standard error of the mean (±SEM). To ascertain the statistical significance between the various groups, the student's t-test, or one-way ANOVA were employed, followed by the Tukey post-hoc test, considering a p-value less than 0.05 as statistically significant.

5.4 Results

5.4.1 PIEZO1 signaling is modulated by voltage-gated Ca^{2+} channels

The dependence of chondrocyte Ca^{2+} signaling under compressive loading to PIEZO1 as well as other thapsigargin-sensitive and EDTA-sensitive Ca^{2+} channels, led us to test how PIEZO1 potentially interacts with other Ca^{2+} channels to modulate the intracellular Ca^{2+} signaling response. Therefore, we investigated the role of different voltage-gated channels in modulating the functionality of the PIEZO channels. The results showed that the mechanosensitivity of the PIEZO channels was not changed in response to mechanical compression after treating the cells with Verapamil with no change in the applied deformation of bothctreated cells and control, even though the treatment effect was detected as a significant influence on deformation (Figure 5.1 A-C; A: $p = 0.0344$, B: $p = 0.6735$). However, PIEZO channels became more sensitive to Yoda1 stimulus with Verapamil treatment (Figure 5.1 D-E; D: $p < 0.0001$ E: $p < 0.0001$). Treating chondrocytes with 200 μM of Diltiazem hydrochloride significantly reduced the PIEZO channels mechanosensitivity with no change in the applied deformation. However, it did not have any effect on cells' response to Yoda1 (Figure 5.2 A-E; A: $p = 0.8722$, B: $p = 0.0053$, D: $p = 0.2669$, E: $p = 0.1296$). Treating cells with Nifedipine did

not have any effect on cellular deformation but had a significant effect on PIEZO channels responsivity to both mechanical loading and Yoda1 addition showing Nifedipine's ability of having consistent effect on PIEZO channels sensitivity (Figure 5.3 A-E; A: $p = 0.1681$, B: $p < 0.0001$, D: $p < 0.0001$, E: $p < 0.0001$). Lastly, the data showed that blocking T-type channels using NNC-55 had a subtle effect on increasing PIEZO channels mechanosensitivity and had strong effect on elevating the PIEZO channels' response to the addition of Yoda1 (Figure 5.4 A-E; A: $p = 0.3064$, B: $p = 0.1950$, D: $p < 0.0001$, E: $p < 0.0001$). Together, these results demonstrate L-type and T-type VGCC inhibition differentially modulates PIEZO1-driven Ca^{2+} signaling in chondrocytes.

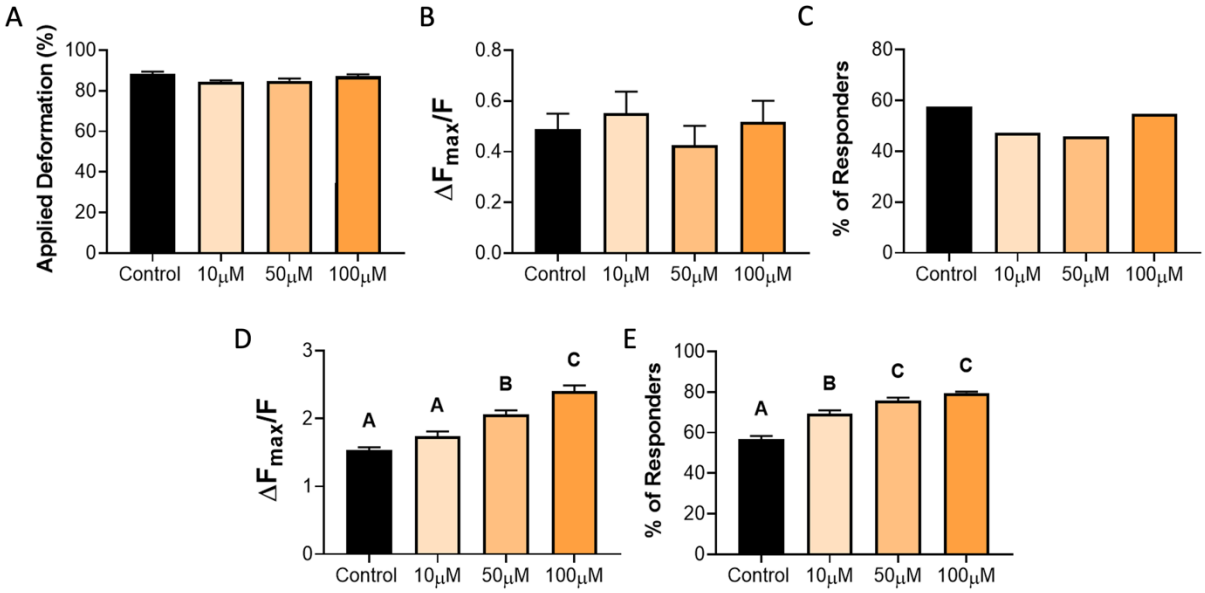

Figure 5.1 Effect of Verapamil on the PIEZO channels sensitivity. A) Applied deformation after AFM loading. B) Level of intracellular Ca^{2+} response to mechanical compression. C) Percentage of the responding cells to AFM compression. D) Level of intracellular Ca^{2+} response to Yoda1 addition. E) Percentage of the responding cells to Yoda1 addition. Data presented as mean ± SEM. For group comparison A-B and D-E, one-way ANOVA with Tukey's post-hoc test, different letters indicate statistical significance $p<0.05$, n=11-48.

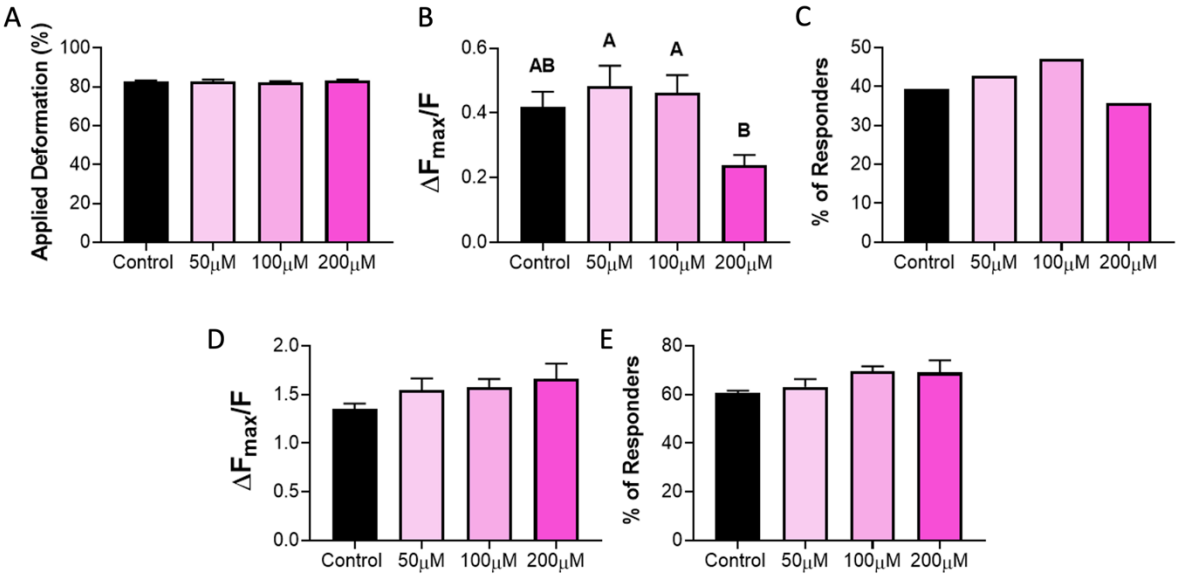

Figure 5.2 Effect of Diltiazem hydrochloride on the PIEZO channels sensitivity. A) Applied deformation after AFM loading. B) Level of intracellular Ca^{2+} response to mechanical compression. C) Percentage of the responding cells to AFM compression. D) Level of intracellular Ca^{2+} response to Yoda1 addition. E) Percentage of the responding cells to Yoda1 addition. Data presented as mean ± SEM. For group comparison A-B and D-E, one-way ANOVA with Tukey's post-hoc test, different letters indicate statistical significance $p<0.05$, n=14-80.

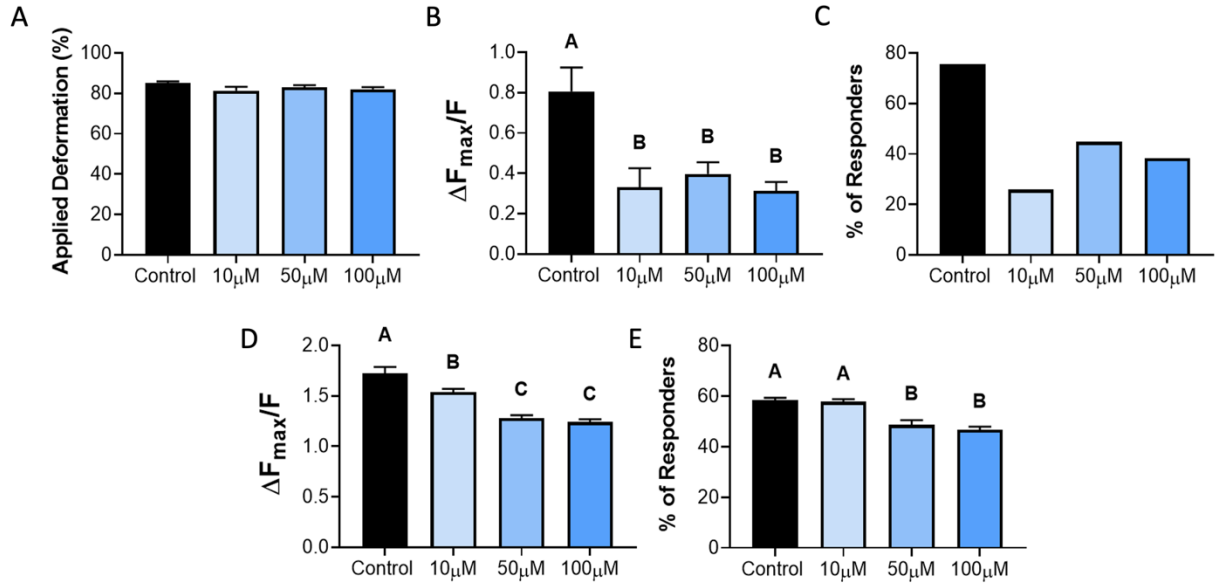

Figure 5.3 Effect of Nifedipine on the PIEZO channels sensitivity. A) Applied deformation after AFM loading. B) Level of intracellular Ca^{2+} response to mechanical compression. C) Percentage of the responding cells to AFM compression. D) Level of intracellular Ca^{2+} response to Yoda1 addition. E) Percentage of the responding cells to Yoda1 addition. Data presented as mean ± SEM. For group comparison A-B and D-E, one-way ANOVA with Tukey's post-hoc test, different letters indicate statistical significance $p<0.05$, n=13-40.

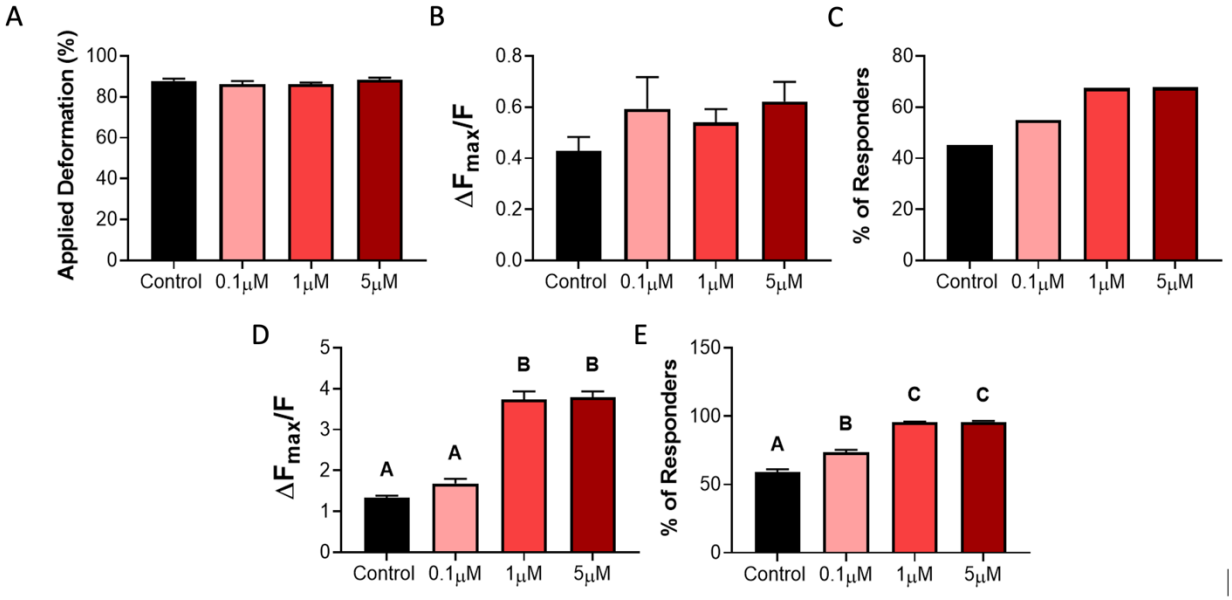

Figure 5.4 Effect of NNC-55 on the PIEZO channels sensitivity. A) Applied deformation after AFM loading. B) Level of intracellular Ca^{2+} response to mechanical compression. C) Percentage of the responding cells to AFM compression. D) Level of intracellular Ca^{2+} response to Yoda1 addition. E) Percentage of the responding cells to Yoda1 addition. Data presented as mean ± SEM. For group comparison A-B and D-E, one-way ANOVA with Tukey's post-hoc test, different letters indicate statistical significance $p<0.05$, n=10-43.

5.4.2 Loading cartilage to high levels of deformation induce cell death zone

To find a deformation magnitude that can induce cell death in cartilage explants without completely destroying the cartilage, we applied different levels of deformation with different loading rates to the cartilage explants and imaged them. Applying 80% deformation to the explants completely destroyed them and induced many fractures on the surface of the cartilage (Figure 5.5). Applying 60% deformation to the explants also induced large fractures on the surface and depth of the explants (Figure S5.1). However, applying 40-50% deformation with 0.5 and 1 mm/sec loading rate did not induce big fractures and resulted in a certain thickness where cell death was observed in the depth of the cartilage (Figure 5.6). Therefore, we chose a 50% deformation at a loading rate of 1 mm/sec for the next step of the study.

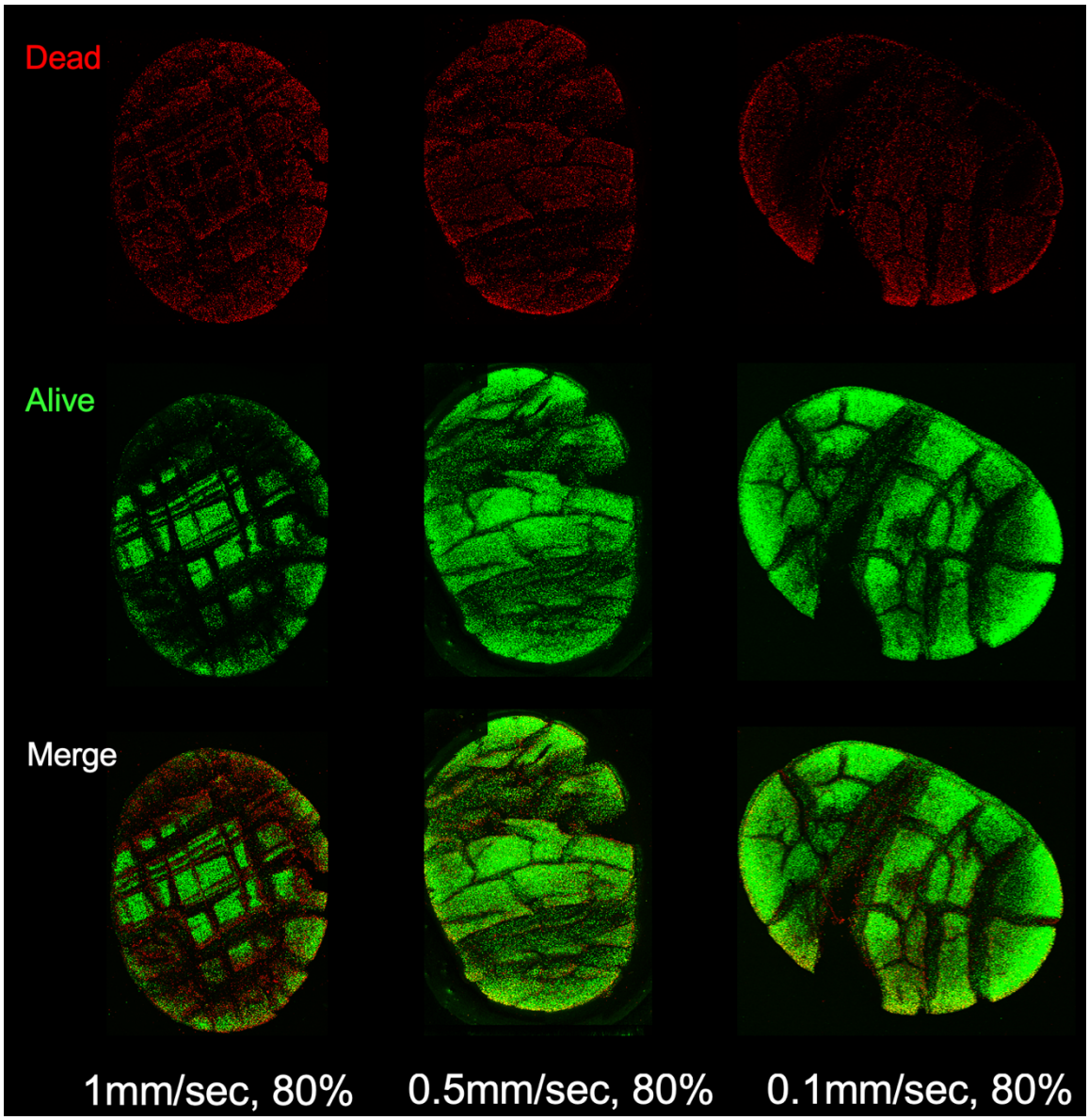

Figure 5.5 Live/dead image of the cartilage explants after being deformed to 80% of their height with the loading rate of 0.1 mm/sec, 0.5 mm/sec, 1 mm/sec.

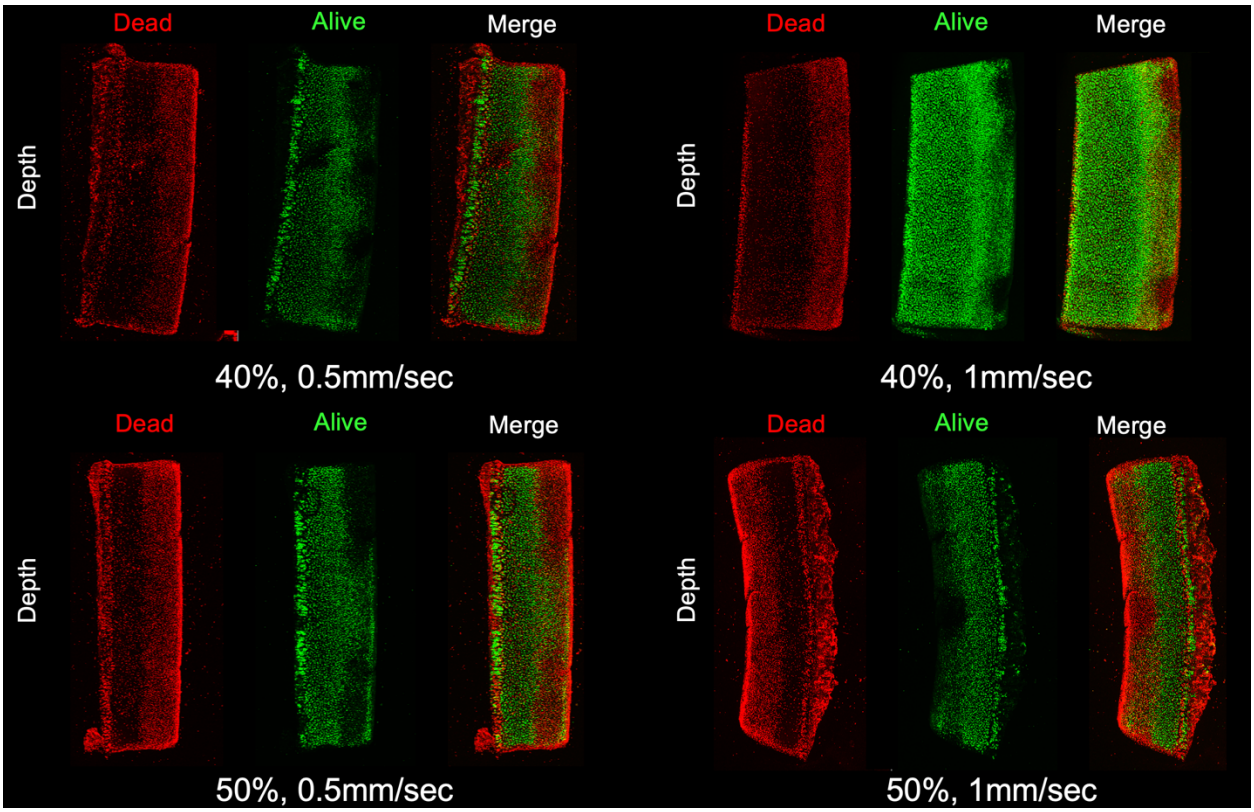

Figure 5.6 Live/dead image of the cartilage explants after being deformed to 40% and 50% of their height with the loading rate of 0.5 mm/sec, 1 mm/sec.

5.4.3 Nifedipine and NNC-55 decreased and increased the death zone respectively

To assess the effect of voltage-gated channels inhibitors, GsMTx-4, and Yoda1 on the cell death level in cartilage under injury, explants were treated with either an inhibitor or its control solution (DMSO or water, depending on the chemical). Treatment of explants with Verapamil, Diltiazem hydrochloride, Yoda1, and GsMTx-4 did not show any effect on the thickness of the death zone in the cartilage explant depth (Figure 5.7 A-D; A: $p = 0.7075$, B: $p = 0.6687$, C: $p = 0.6300$, D: $p = 0.4514$). However, cartilage explants that were treated with Nifedipine were rescued after injurious loading was applied to them (Figure 5.7 E; $p = 0.0051$). On the other hand, treating explants with the T-type channels inhibitor NNC-55 had the opposite

effect and significantly increased the thickness of the death zone in explants under injury (Figure 5.6 F; $p < 0.0001$).

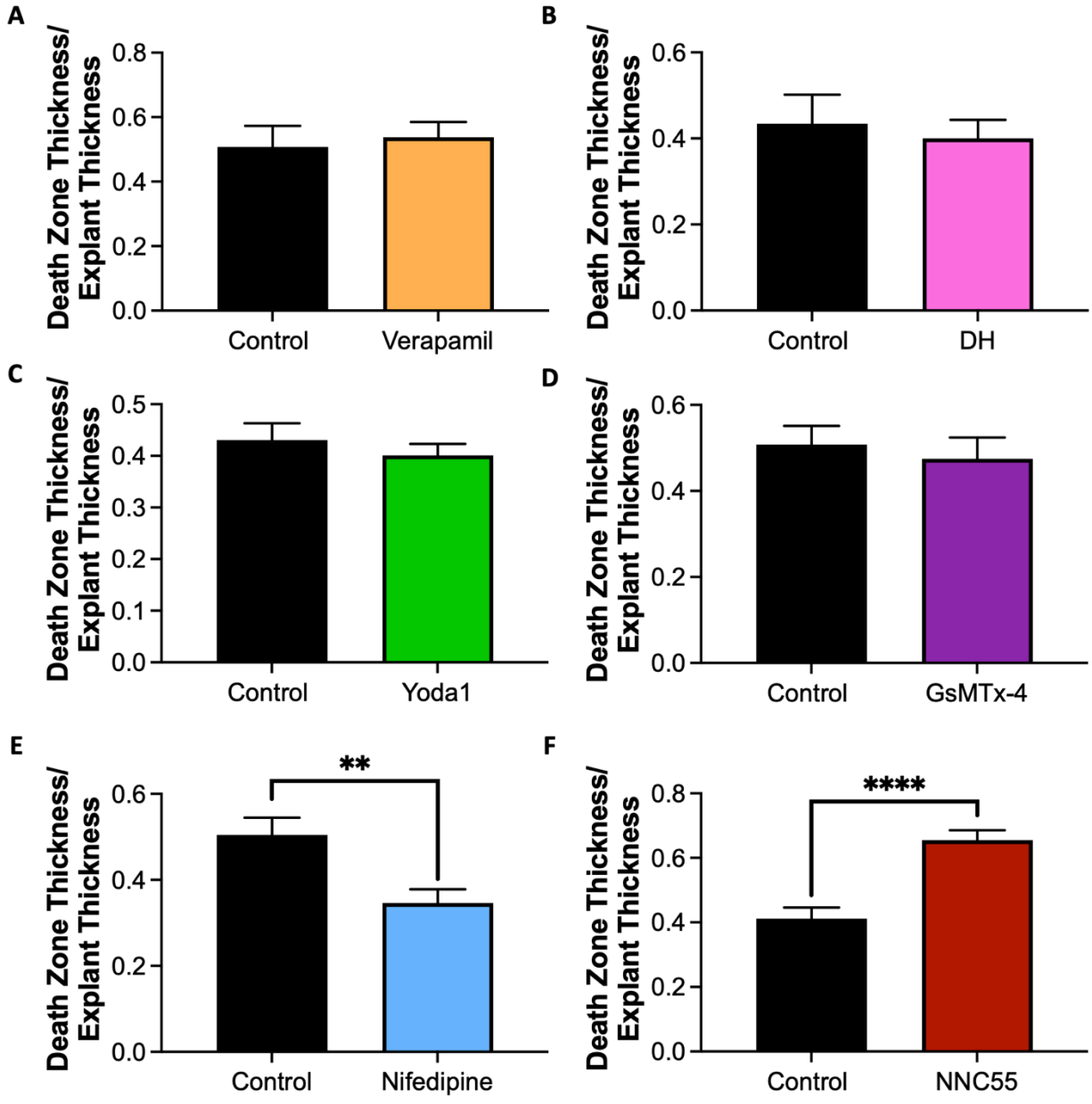

Figure 5.7 Effect of inhibitors and Yoda1 on rescuing the cartilage explant under injury from cell death. A) Verapamil B) Diltiazem Hydrochloride C) Yoda1 D) GsMTx-4 E) Nifedipine F) NNC-55. Data presented as mean ± SEM. For group comparison A-F, student t-test, * $p<0.05$, ** $p<0.005$, *** $p<0.001$, **** $p<0.0001$., n=10-43.

5.5 Discussion

In this study, we elucidated the intricate signaling mechanism in chondrocytes under high mechanical loading strains, involving PIEZO1 activation and regulation through L-type and T-type VGCCs, downstream of PIEZO1. The results were consistent between mechanical and Yoda1 stimulation of PIEZO1, indicating the role of both L-type and T-type VGCCs in modulating the PIEZO1 Ca^{2+} signaling. Previous studies have indicated that cation flux through mechanosensitive ion channels can lead to local depolarization of the cell membrane and activation of voltage-sensitive channels [319]. Our findings that blocking L-type channels decreases the PIEZO1 response to mechanical loading and Yoda1, while blocking T-type channels has the opposite effect and increases the PIEZO1 response, aligns with this understanding. It appears that the distinct activation and inactivation dynamics of L and T-type channels underpin these observations.

T-type channels are activated by slight increases (+15 mV) in membrane potential and quickly inactivated at higher potentials (+30 mV) [573]. Therefore, it is plausible that T-type channels act as early responders of PIEZO1 activation, contributing to the early phases of the Ca^{2+} response. Conversely, L-type channels are activated by larger depolarization (+30 mV), remain open longer, and carry higher currents than T-type channels but are inactivated by Ca^{2+} [574, 575]. This suggests that L-type channels are activated after T-type channels but contribute predominantly to the Ca^{2+} response. Our data supports a mechanism wherein PIEZO1 activation initiates membrane depolarization and Ca^{2+} influx, thus prompting T-type channels activation and further depolarization and Ca^{2+} influx (along with T-type inactivation). Subsequent L-type channel activation induces a robust Ca^{2+} response, which is eventually inactivated by the

feedback control of intracellular Ca^{2+}. Therefore, inhibiting L-type channels prevents the robust Ca^{2+} response induced by PIEZO1, while inhibiting T-type channels limits the early Ca^{2+} response but induces a greater L-type activation response by limiting the proportion of L-type channels that are Ca^{2+} inactivated from the T-type channel response.

Moreover, the results demonstrated that pharmacologic activation of PIEZO1 using Yoda1 further confirmed the nifedipine inhibition of L-type VGCC attenuated PIEZO1 Ca^{2+} signaling, which indicates the direct role of L-type VGCC in PIEZO1 mediated Ca^{2+} signaling. On the other hand, it was observed that the T-type inhibitor NNC55 increased chondrocyte Ca^{2+} signaling under mechanical compression and provoked a higher proportion of responsive cells while maintaining similar levels of deformation. This increase in intracellular Ca^{2+} response with Yoda1 on NNC55 treated cells further corroborates the role of T-type VGCC in the modulation of PIEZO1 Ca^{2+} signaling.

Most importantly, we demonstrated that treating cartilage explants with Nifedipine, can significantly reduce cell death in cartilage under injury. However, inhibiting the T-type channels had the complete opposite effect and increased the cell death in cartilage explants. These results, for the first time, suggest that targeting L-type channels can rescue the cartilage under injury and can be used as a therapeutic for stopping the progression of PTOA. However, further investigations about the effect of blocking L-type channels using Nifedipine to prevent PTOA in an in-vivo set up is required.

Understanding the intersection of the different mechanisms involved in chondrocyte mechanotransduction is crucial for developing new pharmacologic therapies to treat mechanically-regulated conditions such as post-traumatic osteoarthritis. The findings of this

study suggest that PIEZO1 activation leads to the subsequent activation of T-type and then L-type VGCCs, each contributing to different phases of the Ca^{2+} response. This novel insight into the role and interplay of L-type and T-type VGCCs in chondrocyte mechanotransduction and PIEZO1 Ca^{2+} signaling may pave the way for targeted interventions to modulate chondrocyte responses to mechanical stress and ultimately contribute to the development of new therapeutic strategies for osteoarthritis and other mechanically-regulated conditions.

5.6 Supplemental Figures

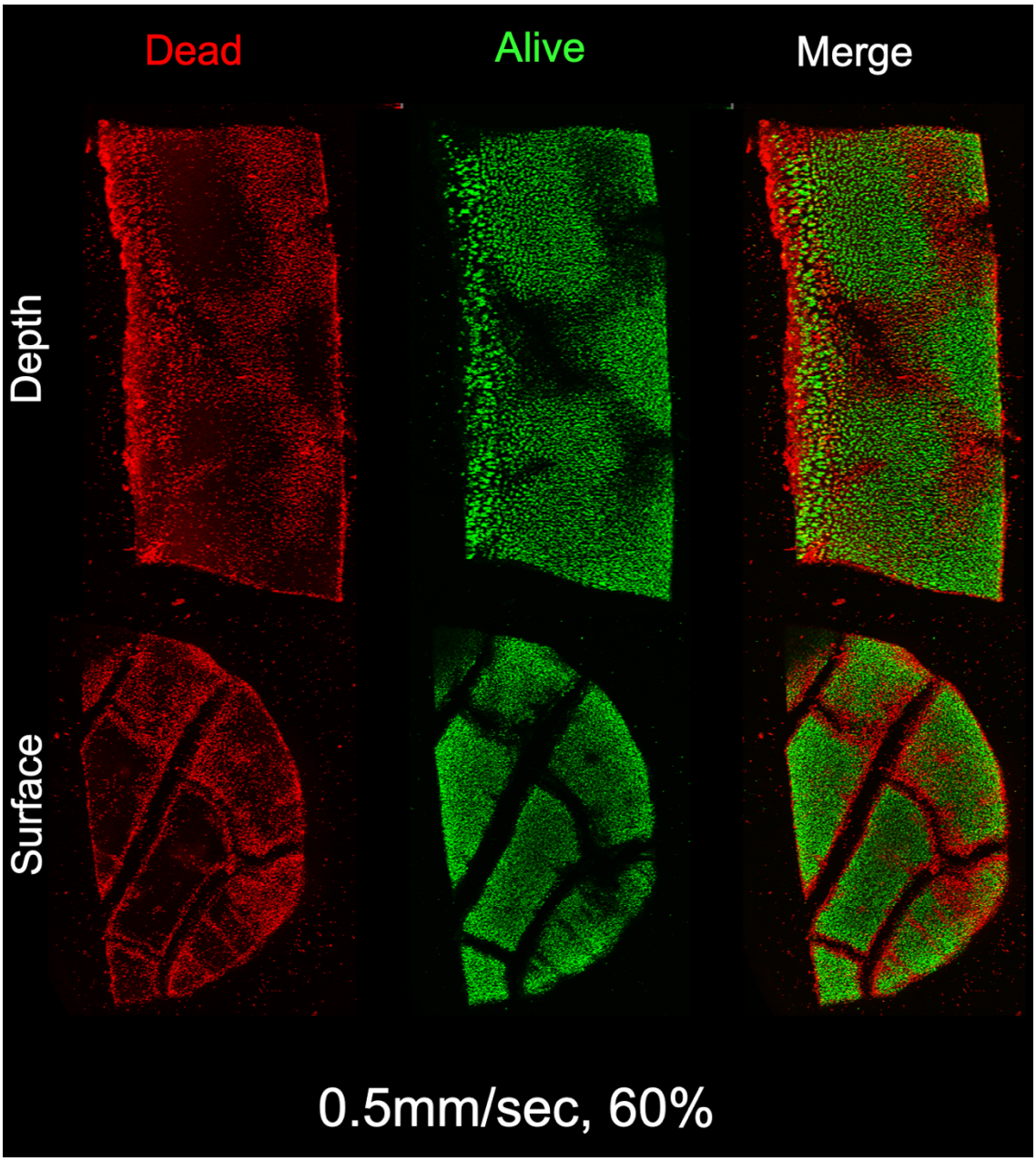

Figure S5.1 Live/dead image of the cartilage explants after being deformed to 40% and 50% of their height with the loading rate of 0.5 mm/sec, 1 mm/sec.

Chapter 6: Final Conclusions and Future Directions

Finding novel drug targets for OA and PTOA represents an unmet medical need since all the treatments for these debilitating diseases are either painkillers or anti-inflammatory drugs, and there are no treatments to stop the progression of OA and PTOA. In chapters 2 and 3, we investigated the role of different mechanosensors in transducing hydrostatic pressure and injurious compressive loading and found that TRPV1 and PIEZO1 are the mechanosensitive ion channels that can sense these types of mechanical loadings respectively. We further investigated the role of membrane tension in mechanosensitivity of the PIEZO1 channel and found that applying an osmotic challenge prior to loading the chondrocytes can alter the PIEZO1 channel sensitivity to mechanical compression. Combining the experimental data and computational modeling, we determined the membrane strain threshold that is required for the PIEZO1 channel to respond to mechanical compression with the probability of 50%. Lastly, we illustrated that changing the loading rate can affect the sensitivity of the PIEZO1 channel to mechanical compression and also both intracellular and extracellular sources of Ca^{2+} are important for the mechanosensitivity of the PIEZO1 channel.

Since the PIEZO1 channel does not have a specific inhibitor, targeting these channels as a therapeutic would involve siRNA and CRISPR methods to knock down PIEZO1. However, in chapter 4, we found that PUFAs can regulate the sensitivity of the PIEZO1 channel to both mechanical compression and Yoda1. Moreover, ω3 fatty acid treatment was able to decrease the level of inflammation and senescence in the cells indicating the important role of these PUFAs in maintaining cartilage health. Additionally, in chapter 5, we investigated the relationship between

PIEZO1 and VGCCs and found that blocking the L-type VGCCs using their specific FDA-approved inhibitor Nifedipine reduces the sensitivity of PIEZO1 channel to mechanical compression and addition of Yoda1. However, blocking the T-type VGCCs using their specific inhibitor NNC-55 had the opposite effect and elevated the PIEZO1 channel sensitivity. These results confirmed the synergy between PIEZO1 channel and VGCCs, therefore, we investigated the downstream effect that VGCCs inhibition has on PIEZO channels and assessed if this would be able to rescue the cartilage under injury. We found that blocking the L-type VGCCs using Nifedipine reduced cell death in cartilage explants under injury; however, treating the explants with T-type channel inhibitor NNC-55 had the opposite effect and increased cell death in loaded cartilage. Consequently, Nifedipine might be effective in stopping the progression of PTOA after injury.

For future studies, we need to investigate the effect of Nifedipine in vivo and see if blocking the L-type VGCCs using this specific inhibitor would rescue the cartilage under injury in mice that undergo DMM surgery. Moreover, finding novel drug delivery systems for OA and PTOA treatments is necessary. Therefore, developing cell therapy and gene therapy methods to treat PTOA and stop its progression is necessity. Furthermore, investigating the synergy between the PIEZO1 channel and other mechanosensitive ion channels can provide new and important insights into the development of new pharmacologic therapies to treat mechanically regulated conditions such as post-traumatic osteoarthritis.

References

1. Bellucci, G. and B. Seedhom, *Mechanical behaviour of articular cartilage under tensile cyclic load.* Rheumatology, 2001. **40**(12): p. 1337-1345.

2. Hayes, W. and L. Mockros, *Viscoelastic properties of human articular cartilage.* Journal of applied physiology, 1971. **31**(4): p. 562-568.

3. Adams, M.A., *The mechanical environment of chondrocytes in articular cartilage.* Biorheology, 2006. **43**(3-4): p. 537-545.

4. Armstrong, C., A. Bahrani, and D. Gardner, *In vitro measurement of articular cartilage deformations in the intact human hip joint under load.* JBJS, 1979. **61**(5): p. 744-755.

5. Attur, M., et al., *Osteoarthritis or osteoarthrosis: the definition of inflammation becomes a semantic issue in the genomic era of molecular medicine.* Osteoarthritis and Cartilage, 2002. **10**(1): p. 1-4.

6. Kheir, E. and D. Shaw, *Hyaline articular cartilage.* Orthopaedics and Trauma, 2009. **23**(6): p. 450-455.

7. Leijten, J.C., et al., *Cell sources for articular cartilage repair strategies: shifting from monocultures to cocultures.* Tissue Engineering Part B: Reviews, 2013. **19**(1): p. 31-40.

8. Mata-Miranda, M.M., et al., *Morphological, genetic and phenotypic comparison between human articular chondrocytes and cultured chondrocytes.* Histochemistry and cell biology, 2016. **146**: p. 183-189.

9. Vaish, A., et al., *Biological reconstruction of the joint: Concepts of articular cartilage regeneration and their scientific basis.* Journal of Clinical Orthopaedics and Trauma, 2022. **24**: p. 101718.

10. Savadipour, A., et al., *The role of PIEZO ion channels in the musculoskeletal system.* American Journal of Physiology-Cell Physiology, 2023. **324**(3): p. C728-C740.

11. Poole, A.R., et al., *Composition and structure of articular cartilage: a template for tissue repair.* Clinical Orthopaedics and Related Research®, 2001. **391**: p. S26-S33.

12. Sophia Fox, A.J., A. Bedi, and S.A. Rodeo, *The basic science of articular cartilage: structure, composition, and function.* Sports health, 2009. **1**(6): p. 461-468.

13. Carney, S. and H. Muir, *The structure and function of cartilage proteoglycans.* Physiological reviews, 1988. **68**(3): p. 858-910.

14. Roughley, P., *The structure and function of cartilage proteoglycans.* Eur Cell Mater, 2006. **12**(9).

15. Roughley, P.J. and E.R. Lee, *Cartilage proteoglycans: structure and potential functions.* Microscopy research and technique, 1994. **28**(5): p. 385-397.

16. Carballo, C.B., Y. Nakagawa, I. Sekiya, and S.A. Rodeo, *Basic science of articular cartilage.* Clinics in sports medicine, 2017. **36**(3): p. 413-425.

17. Peng, Z., et al., *The regulation of cartilage extracellular matrix homeostasis in joint cartilage degeneration and regeneration.* Biomaterials, 2021. **268**: p. 120555.

18. Lin, W. and J. Klein, *Recent progress in cartilage lubrication.* Advanced Materials, 2021. **33**(18): p. 2005513.

19. Qiu, F., et al., *Recent Progress in Hydrogel-Based Synthetic Cartilage: Focus on Lubrication and Load-Bearing Capacities.* Gels, 2023. **9**(2): p. 144.

20. Wei, P. and R. Bao, *Intra-articular mesenchymal stem cell injection for knee osteoarthritis: Mechanisms and clinical evidence.* International Journal of Molecular Sciences, 2022. **24**(1): p. 59.

21. Zhou, L., et al., *Functionalized hydrogels for articular cartilage tissue engineering.* Engineering, 2022. **13**: p. 71-90.

22. Akiyama, H., *Control of chondrogenesis by the transcription factor Sox9.* Modern rheumatology, 2008. **18**(3): p. 213-219.

23. Kawakami, Y., J. Rodriguez-León, and J.C.I. Belmonte, *The role of TGFβs and Sox9 during limb chondrogenesis.* Current opinion in cell biology, 2006. **18**(6): p. 723-729.

24. Smeriglio, P., et al., *TET1 directs chondrogenic differentiation by regulating SOX9 dependent activation of Col2a1 and Acan in vitro.* JBMR plus, 2020. **4**(8): p. e10383.

25. Bell, D.M., et al., *SOX9 directly regulates the type-ll collagen gene.* Nature genetics, 1997. **16**(2): p. 174-178.

26. Song, H. and K.-H. Park. *Regulation and function of SOX9 during cartilage development and regeneration*. in *Seminars in cancer biology*. 2020. Elsevier.

27. Acharya, C., et al., *Cartilage oligomeric matrix protein and its binding partners in the cartilage extracellular matrix: interaction, regulation and role in chondrogenesis.* Matrix Biology, 2014. **37**: p. 102-111.

28. Feng, Q., M. Zhu, K. Wei, and L. Bian, *Cell-mediated degradation regulates human mesenchymal stem cell chondrogenesis and hypertrophy in MMP-sensitive hyaluronic*

acid hydrogels. PLoS One, 2014. **9**(6): p. e99587.

29. Kipnes, J., et al., *Effect of cartilage oligomeric matrix protein on mesenchymal chondrogenesis in vitro.* Osteoarthritis and cartilage, 2003. **11**(6): p. 442-454.

30. Goldring, M.B. and S.R. Goldring, *Articular cartilage and subchondral bone in the pathogenesis of osteoarthritis.* Annals of the New York Academy of Sciences, 2010. **1192**(1): p. 230-237.

31. Griffin, T.M. and F. Guilak, *The role of mechanical loading in the onset and progression of osteoarthritis.* Exercise and sport sciences reviews, 2005. **33**(4): p. 195-200.

32. Sun, H.B., *Mechanical loading, cartilage degradation, and arthritis.* Annals of the New York Academy of Sciences, 2010. **1211**(1): p. 37-50.

33. Gannon, A., et al., *Postnatal changes to the mechanical properties of articular cartilage are driven by the evolution of its collagen network.* Eur Cell Mater, 2015. **29**(105): p. 121-103.

34. García-Carvajal, Z.Y., et al., *Cartilage tissue engineering: the role of extracellular matrix (ECM) and novel strategies*, in *Regenerative medicine and tissue engineering*. 2013, IntechOpen.

35. Kempson, G., H. Muir, C. Pollard, and M. Tuke, *The tensile properties of the cartilage of human femoral condyles related to the content of collagen and glycosaminoglycans.* Biochimica et Biophysica Acta (BBA)-General Subjects, 1973. **297**(2): p. 456-472.

36. Kuroda, S., et al., *Biomechanical and biochemical characteristics of the mandibular condylar cartilage.* Osteoarthritis and Cartilage, 2009. **17**(11): p. 1408-1415.

37. Ottani, V., M. Raspanti, and A. Ruggeri, *Collagen structure and functional implications.* Micron, 2001. **32**(3): p. 251-260.

38. Pastrama, M.-I., et al., *Combined enzymatic degradation of proteoglycans and collagen significantly alters intratissue strains in articular cartilage during cyclic compression.* Journal of the mechanical behavior of biomedical materials, 2019. **98**: p. 383-394.

39. Roberts, C.R., et al., *Ultrastructure and tensile properties of human tracheal cartilage.* Journal of biomechanics, 1997. **31**(1): p. 81-86.

40. Mow, V.C., M.H. Holmes, and W.M. Lai, *Fluid transport and mechanical properties of articular cartilage: a review.* Journal of biomechanics, 1984. **17**(5): p. 377-394.

41. Simon, M.R., *The role of compressive forces in the normal maturation of the condylar cartilage in the rat.* Cells Tissues Organs, 1977. **97**(3): p. 351-360.

42. Fahy, N., M. Alini, and M.J. Stoddart, *Mechanical stimulation of mesenchymal stem cells: Implications for cartilage tissue engineering.* Journal of Orthopaedic Research®, 2018. **36**(1): p. 52-63.

43. Musumeci, G., *The effect of mechanical loading on articular cartilage*. 2016, MDPI. p. 154-161.

44. Ramage, L., G. Nuki, and D. Salter, *Signalling cascades in mechanotransduction: cell–matrix interactions and mechanical loading.* Scandinavian journal of medicine & science in sports, 2009. **19**(4): p. 457-469.

45. Yokota, H., D.J. Leong, and H.B. Sun, *Mechanical loading: bone remodeling and cartilage maintenance.* Current osteoporosis reports, 2011. **9**: p. 237-242.

46. Hutton, W.C., et al., *The effect of compressive force applied to the intervertebral disc in vivo: a study of proteoglycans and collagen.* Spine, 1998. **23**(23): p. 2524-2537.

47. Martin, J.A., T. Brown, A. Heiner, and J.A. Buckwalter, *Post-traumatic osteoarthritis: the role of accelerated chondrocyte senescence.* Biorheology, 2004. **41**(3-4): p. 479-491.

48. Savadipour, A., et al., *Membrane stretch as the mechanism of activation of PIEZO1 ion channels in chondrocytes.* Proceedings of the National Academy of Sciences, 2023. **120**(30): p. e2221958120.

49. Wang, P., et al., *Fluid shear stress-induced osteoarthritis: roles of cyclooxygenase-2 and its metabolic products in inducing the expression of proinflammatory cytokines and matrix metalloproteinases.* The FASEB Journal, 2013. **27**(12): p. 4664.

50. Elder, B.D. and K.A. Athanasiou, *Hydrostatic pressure in articular cartilage tissue engineering: from chondrocytes to tissue regeneration.* Tissue Engineering Part B: Reviews, 2009. **15**(1): p. 43-53.

51. Correia, C., et al., *Dynamic culturing of cartilage tissue: the significance of hydrostatic pressure.* Tissue Engineering Part A, 2012. **18**(19-20): p. 1979-1991.

52. Meyer, E.G., C.T. Buckley, A. Steward, and D. Kelly, *The effect of cyclic hydrostatic pressure on the functional development of cartilaginous tissues engineered using bone marrow derived mesenchymal stem cells.* Journal of the mechanical behavior of biomedical materials, 2011. **4**(7): p. 1257-1265.

53. Montagne, K., et al., *High hydrostatic pressure induces pro-osteoarthritic changes in cartilage precursor cells: A transcriptome analysis.* PLoS One, 2017. **12**(8): p. e0183226.

54. Savadipour, A., R.J. Nims, D.B. Katz, and F. Guilak, *Regulation of chondrocyte biosynthetic activity by dynamic hydrostatic pressure: the role of TRP channels.* Connective tissue research, 2022. **63**(1): p. 69-81.

55. Armiento, A., M. Stoddart, M. Alini, and D. Eglin, *Biomaterials for articular cartilage tissue engineering: Learning from biology.* Acta biomaterialia, 2018. **65**: p. 1-20.

56. Butler, D.L., S.A. Goldstein, and F. Guilak, *Functional tissue engineering: the role of biomechanics.* J. Biomech. Eng., 2000. **122**(6): p. 570-575.

57. Chin, L., Y. Xia, D.E. Discher, and P.A. Janmey, *Mechanotransduction in cancer.* Current opinion in chemical engineering, 2016. **11**: p. 77-84.

58. Chiquet, M., L. Gelman, R. Lutz, and S. Maier, *From mechanotransduction to extracellular matrix gene expression in fibroblasts.* Biochimica et Biophysica Acta (BBA)-Molecular Cell Research, 2009. **1793**(5): p. 911-920.

59. Das, T., et al., *A molecular mechanotransduction pathway regulates collective migration of epithelial cells.* Nature cell biology, 2015. **17**(3): p. 276-287.

60. Hadden, W.J., et al., *Stem cell migration and mechanotransduction on linear stiffness gradient hydrogels.* Proceedings of the National Academy of Sciences, 2017. **114**(22): p. 5647-5652.

61. Hu, M., et al., *A biomimetic gelatin-based platform elicits a pro-differentiation effect on podocytes through mechanotransduction.* Scientific Reports, 2017. **7**(1): p. 43934.

62. Ingber, D.E., *Cellular mechanotransduction: putting all the pieces together again.* The FASEB journal, 2006. **20**(7): p. 811-827.

63. Iqbal, J. and M. Zaidi, *Molecular regulation of mechanotransduction.* Biochemical and biophysical research communications, 2005. **328**(3): p. 751-755.

64. Iskratsch, T., H. Wolfenson, and M.P. Sheetz, *Appreciating force and shape—the rise of mechanotransduction in cell biology.* Nature reviews Molecular cell biology, 2014. **15**(12): p. 825-833.

65. Jaalouk, D.E. and J. Lammerding, *Mechanotransduction gone awry.* Nature reviews Molecular cell biology, 2009. **10**(1): p. 63-73.

66. Li, S., N.F. Huang, and S. Hsu, *Mechanotransduction in endothelial cell migration.* Journal of cellular biochemistry, 2005. **96**(6): p. 1110-1126.

67. Lourenço, T. and M. Grãos, *Modulation of oligodendrocyte differentiation by mechanotransduction.* Frontiers in cellular neuroscience, 2016. **10**: p. 277.

68. McMurray, R.J., M.J. Dalby, and P.M. Tsimbouri, *Using biomaterials to study stem cell mechanotransduction, growth and differentiation.* Journal of tissue engineering and regenerative medicine, 2015. **9**(5): p. 528-539.

69. Moon, J.J., et al., *Role of cell surface heparan sulfate proteoglycans in endothelial cell migration and mechanotransduction.* Journal of cellular physiology, 2005. **203**(1): p. 166-176.

70. Orr, A.W., B.P. Helmke, B.R. Blackman, and M.A. Schwartz, *Mechanisms of mechanotransduction.* Developmental cell, 2006. **10**(1): p. 11-20.

71. Polacheck, W.J., et al., *Mechanotransduction of fluid stresses governs 3D cell migration.* Proceedings of the National Academy of Sciences, 2014. **111**(7): p. 2447-2452.

72. Raman, N., et al., *Mechanotransduction in mesenchymal stem cells (MSCs) differentiation: a review.* International Journal of Molecular Sciences, 2022. **23**(9): p. 4580.

73. Wang, N., *Review of cellular mechanotransduction.* Journal of physics D: Applied physics, 2017. **50**(23): p. 233002.

74. Wu, M., et al., *Effect of aging on cellular mechanotransduction.* Ageing research reviews, 2011. **10**(1): p. 1-15.

75. Broders-Bondon, F., T.H. Nguyen Ho-Bouldoires, M.-E. Fernandez-Sanchez, and E. Farge, *Mechanotransduction in tumor progression: The dark side of the force.* Journal of Cell Biology, 2018. **217**(5): p. 1571-1587.

76. Delco, M.L. and L.J. Bonassar, *Targeting calcium-related mechanotransduction in early OA.* Nature Reviews Rheumatology, 2021. **17**(8): p. 445-446.

77. Dombroski, J.A., J.M. Hope, N.S. Sarna, and M.R. King, *Channeling the force: Piezo1 mechanotransduction in cancer metastasis.* Cells, 2021. **10**(11): p. 2815.

78. Hao, J., et al., *Mechanotransduction in cancer stem cells.* Cell biology international, 2013. **37**(9): p. 888-891.

79. Jiang, W., et al., *Mechanisms linking mitochondrial mechanotransduction and chondrocyte biology in the pathogenesis of osteoarthritis.* Ageing Research Reviews, 2021. **67**: p. 101315.

80. Jutila, A.A., D.L. Zignego, W.J. Schell, and R.K. June, *Encapsulation of chondrocytes in high-stiffness agarose microenvironments for in vitro modeling of osteoarthritis mechanotransduction.* Annals of biomedical engineering, 2015. **43**: p. 1132-1144.

81. Kim, J.-H., et al., *Matrix cross-linking–mediated mechanotransduction promotes posttraumatic osteoarthritis.* Proceedings of the National Academy of Sciences, 2015. **112**(30): p. 9424-9429.

82. Knöll, R., M. Hoshijima, and K. Chien, *Cardiac mechanotransduction and implications for heart disease.* Journal of molecular medicine, 2003. **81**: p. 750-756.

83. Krajnik, A., et al., *Phosphoinositide signaling and mechanotransduction in cardiovascular biology and disease.* Frontiers in cell and developmental biology, 2020. **8**: p. 595849.

84. Lee, J.Y., et al., *YAP-independent mechanotransduction drives breast cancer progression.* Nature communications, 2019. **10**(1): p. 1848.

85. Lee, W., et al., *Inflammatory signaling sensitizes Piezo1 mechanotransduction in articular chondrocytes as a pathogenic feed-forward mechanism in osteoarthritis.* Proceedings of the National Academy of Sciences, 2021. **118**(13): p. e2001611118.

86. Li, N., et al., *Multiscale biomechanics and mechanotransduction from liver fibrosis to cancer.* Advanced Drug Delivery Reviews, 2022: p. 114448.

87. Liu, S., et al., *Mechanotherapy in oncology: Targeting nuclear mechanics and mechanotransduction.* Advanced Drug Delivery Reviews, 2023: p. 114722.

88. Liu, X., et al., *Mechanotransduction regulates inflammation responses of epicardial adipocytes in cardiovascular diseases.* Frontiers in Endocrinology, 2022. **13**: p. 1080383.

89. Lohberger, B., et al., *Mechanical exposure and diacerein treatment modulates integrin-FAK-MAPKs mechanotransduction in human osteoarthritis chondrocytes.* Cellular Signalling, 2019. **56**: p. 23-30.

90. Lyon, R.C., F. Zanella, J.H. Omens, and F. Sheikh, *Mechanotransduction in cardiac hypertrophy and failure.* Circulation research, 2015. **116**(8): p. 1462-1476.

91. Novak, C., E. Horst, and G. Mehta, *Mechanotransduction in ovarian cancer: Shearing into the unknown.* APL bioengineering, 2018. **2**(3).

92. Papavassiliou, K.A., A.N. Gargalionis, and A.G. Papavassiliou, *Polycystins, mechanotransduction and cancer development.* Journal of Cellular and Molecular Medicine, 2022. **26**(9): p. 2741.

93. Tian, G. and T. Ren, *Mechanical stress regulates the mechanotransduction and metabolism of cardiac fibroblasts in fibrotic cardiac diseases.* European Journal of Cell Biology, 2023: p. 151288.

94. Vincent, T.L., *Targeting mechanotransduction pathways in osteoarthritis: a focus on the pericellular matrix.* Current opinion in pharmacology, 2013. **13**(3): p. 449-454.

95. Wolfenson, H., B. Yang, and M.P. Sheetz, *Steps in mechanotransduction pathways that control cell morphology.* Annual review of physiology, 2019. **81**: p. 585-605.

96. Geng, J., Q. Zhao, T. Zhang, and B. Xiao, *In touch with the mechanosensitive piezo channels: structure, ion permeation, and mechanotransduction.* Current topics in membranes, 2017. **79**: p. 159-195.

97. Volkers, L., Y. Mechioukhi, and B. Coste, *Piezo channels: from structure to function.* Pflügers Archiv-European Journal of Physiology, 2015. **467**: p. 95-99.

98. Xu, X., et al., *Piezo channels: Awesome mechanosensitive structures in cellular mechanotransduction and their role in bone.* International Journal of Molecular Sciences, 2021. **22**(12): p. 6429.

99. Young, M., A.H. Lewis, and J. Grandl, *Physics of mechanotransduction by Piezo ion channels.* Journal of General Physiology, 2022. **154**(7).

100. Zhang, M., et al., *Trpv4 and piezo channels mediate the mechanosensing of chondrocytes to the biomechanical microenvironment.* Membranes, 2022. **12**(2): p. 237.

101. Patel, A., et al., *Canonical TRP channels and mechanotransduction: from physiology to disease states.* Pflügers Archiv-European Journal of Physiology, 2010. **460**: p. 571-581.

102. Yin, J. and W.M. Kuebler, *Mechanotransduction by TRP channels: general concepts and specific role in the vasculature.* Cell biochemistry and biophysics, 2010. **56**: p. 1-18.

103. Katsumi, A., A.W. Orr, E. Tzima, and M.A. Schwartz, *Integrins in mechanotransduction.* Journal of Biological Chemistry, 2004. **279**(13): p. 12001-12004.

104. Ross, T.D., et al., *Integrins in mechanotransduction.* Current opinion in cell biology, 2013. **25**(5): p. 613-618.

105. Schwartz, M.A., *Integrins and extracellular matrix in mechanotransduction.* Cold Spring Harbor perspectives in biology, 2010. **2**(12): p. a005066.

106. Sun, Z., S.S. Guo, and R. Fässler, *Integrin-mediated mechanotransduction.* Journal of Cell Biology, 2016. **215**(4): p. 445-456.

107. Burkholder, T.J., *Mechanotransduction in skeletal muscle.* Frontiers in bioscience: a journal and virtual library, 2007. **12**: p. 174.

108. Davis, M.J., et al., *Integrins and mechanotransduction of the vascular myogenic response.* American Journal of Physiology-Heart and Circulatory Physiology, 2001. **280**(4): p. H1427-H1433.

109. Urciuoli, E. and B. Peruzzi, *Involvement of the FAK network in pathologies related to altered mechanotransduction.* International Journal of Molecular Sciences, 2020. **21**(24): p. 9426.

110. Alberts, B., et al., *Cell-cell adhesion*, in *Molecular Biology of the Cell. 4th edition*. 2002, Garland Science.

111. Gumbiner, B.M., *Cell adhesion: the molecular basis of tissue architecture and morphogenesis.* Cell, 1996. **84**(3): p. 345-357.

112. Panorchan, P., et al., *Single-molecule analysis of cadherin-mediated cell-cell adhesion.* Journal of cell science, 2006. **119**(1): p. 66-74.

113. Priest, A.V., O. Shafraz, and S. Sivasankar, *Biophysical basis of cadherin mediated cell-cell adhesion.* Experimental cell research, 2017. **358**(1): p. 10-13.

114. Hinck, L., I.S. Näthke, J. Papkoff, and W.J. Nelson, *β-catenin: a common target for the regulation of cell adhesion by Wnt-1 and Src signaling pathways.* Trends in biochemical sciences, 1994. **19**(12): p. 538-542.

115. Ausmees, N., J.R. Kuhn, and C. Jacobs-Wagner, *The bacterial cytoskeleton: an intermediate filament-like function in cell shape.* Cell, 2003. **115**(6): p. 705-713.

116. Bouchet, B.P. and A. Akhmanova, *Microtubules in 3D cell motility.* Journal of cell science, 2017. **130**(1): p. 39-50.

117. Bugyi, B. and M.-F. Carlier, *Control of actin filament treadmilling in cell motility.* Annual review of biophysics, 2010. **39**: p. 449-470.

118. Cheng, F. and J.E. Eriksson, *Intermediate filaments and the regulation of cell motility during regeneration and wound healing.* Cold Spring Harbor perspectives in biology, 2017. **9**(9): p. a022046.

119. Eriksson, J.E., et al., *Introducing intermediate filaments: from discovery to disease.* The Journal of clinical investigation, 2009. **119**(7): p. 1763-1771.

120. Goldman, R.D., et al., *The function of intermediate filaments in cell shape and cytoskeletal integrity.* The Journal of cell biology, 1996. **134**(4): p. 971-983.

121. Hawkins, T., M. Mirigian, M.S. Yasar, and J.L. Ross, *Mechanics of microtubules.* Journal of biomechanics, 2010. **43**(1): p. 23-30.

122. Kaverina, I. and A. Straube. *Regulation of cell migration by dynamic microtubules*. in *Seminars in cell & developmental biology*. 2011. Elsevier.

123. Kelemen, G.H., *Intermediate filaments supporting cell shape and growth in bacteria.* Prokaryotic Cytoskeletons: Filamentous Protein Polymers Active in the Cytoplasm of Bacterial and Archaeal Cells, 2017: p. 161-211.

124. Kerr, J.P., et al., *Detyrosinated microtubules modulate mechanotransduction in heart and skeletal muscle.* Nature communications, 2015. **6**(1): p. 8526.

125. Ketene, A.N., et al., *Actin filaments play a primary role for structural integrity and viscoelastic response in cells.* Integrative Biology, 2012. **4**(5): p. 540-549.

126. Laly, A.C., et al., *The keratin network of intermediate filaments regulates keratinocyte rigidity sensing and nuclear mechanotransduction.* Science Advances, 2021. **7**(5): p. eabd6187.

127. Lyons, J.S., et al., *Microtubules tune mechanotransduction through NOX2 and TRPV4 to decrease sclerostin abundance in osteocytes.* Science signaling, 2017. **10**(506): p. eaan5748.

128. Malivert, A., et al., *FERONIA and microtubules independently contribute to mechanical integrity in the Arabidopsis shoot.* PLoS biology, 2021. **19**(11): p. e3001454.

129. Matis, M., *The mechanical role of microtubules in tissue remodeling.* BioEssays, 2020. **42**(5): p. 1900244.

130. Pallari, H.-M. and J.E. Eriksson, *Intermediate filaments as signaling platforms.* Science's STKE, 2006. **2006**(366): p. pe53-pe53.

131. Pollard, T.D. and G.G. Borisy, *Cellular motility driven by assembly and disassembly of actin filaments.* Cell, 2003. **112**(4): p. 453-465.

132. Pollard, T.D. and J.A. Cooper, *Actin, a central player in cell shape and movement.* science, 2009. **326**(5957): p. 1208-1212.

133. Romet-Lemonne, G. and A. Jégou, *Mechanotransduction down to individual actin filaments.* European journal of cell biology, 2013. **92**(10-11): p. 333-338.

134. Sanghvi-Shah, R. and G.F. Weber, *Intermediate filaments at the junction of mechanotransduction, migration, and development.* Frontiers in cell and developmental biology, 2017. **5**: p. 81.

135. van Bodegraven, E.J. and S. Etienne-Manneville, *Intermediate filaments from tissue integrity to single molecule mechanics.* Cells, 2021. **10**(8): p. 1905.

136. Alenghat, F.J. and D.E. Ingber, *Mechanotransduction: all signals point to cytoskeleton, matrix, and integrins.* Science's STKE, 2002. **2002**(119): p. pe6-pe6.

137. Harris, A.R., P. Jreij, and D.A. Fletcher, *Mechanotransduction by the actin cytoskeleton: converting mechanical stimuli into biochemical signals.* Annual review of biophysics, 2018. **47**: p. 617-631.

138. Li, Z., et al., *Leptin activates RhoA/ROCK pathway to induce cytoskeleton remodeling in nucleus pulposus cells.* International Journal of Molecular Sciences, 2014. **15**(1): p. 1176-1188.

139. Ohashi, K., S. Fujiwara, and K. Mizuno, *Roles of the cytoskeleton, cell adhesion and rho signalling in mechanosensing and mechanotransduction.* The journal of biochemistry, 2017. **161**(3): p. 245-254.

140. Sauzeau, V., I.M. Berenjeno, C. Citterio, and X.R. Bustelo, *A transcriptional cross-talk between RhoA and c-Myc inhibits the RhoA/Rock-dependent cytoskeleton.* Oncogene, 2010. **29**(26): p. 3781-3792.

141. Schwarz, U.S. and M.L. Gardel, *United we stand–integrating the actin cytoskeleton and cell–matrix adhesions in cellular mechanotransduction.* Journal of cell science, 2012. **125**(13): p. 3051-3060.

142. Shafrir, Y. and G. Forgacs, *Mechanotransduction through the cytoskeleton.* American Journal of Physiology-Cell Physiology, 2002. **282**(3): p. C479-C486.

143. Tang, L., et al., *RhoA/ROCK signaling regulates smooth muscle phenotypic modulation and vascular remodeling via the JNK pathway and vimentin cytoskeleton.* Pharmacological research, 2018. **133**: p. 201-212.

144. Uray, I.P. and K. Uray, *Mechanotransduction at the plasma membrane-cytoskeleton interface.* International journal of molecular sciences, 2021. **22**(21): p. 11566.

145. Wang, N., J.P. Butler, and D.E. Ingber, *Mechanotransduction across the cell surface and through the cytoskeleton.* Science, 1993. **260**(5111): p. 1124-1127.

146. Xu, B., et al., *RhoA/ROCK, cytoskeletal dynamics, and focal adhesion kinase are required for mechanical stretch-induced tenogenic differentiation of human mesenchymal stem cells.* Journal of cellular physiology, 2012. **227**(6): p. 2722-2729.

147. Xue, Y., et al., *Methamphetamine reduces expressions of tight junction proteins, rearranges F-actin cytoskeleton and increases the blood brain barrier permeability via the RhoA/ROCK-dependent pathway.* Biochemical and biophysical research communications, 2019. **509**(2): p. 395-401.

148. DeOre, B.J., P.P. Partyka, F. Fan, and P.A. Galie, *CD44 mediates shear stress mechanotransduction in an in vitro blood-brain barrier model through small GTPases RhoA and Rac1.* The FASEB Journal, 2022. **36**(5): p. e22278.

149. Johnson, G.P., et al., *Mesenchymal stem cell mechanotransduction is cAMP dependent and regulated by adenylyl cyclase 6 and the primary cilium.* Journal of Cell Science, 2018. **131**(21): p. jcs222737.

150. Kuo, J.C., *Mechanotransduction at focal adhesions: integrating cytoskeletal mechanics in migrating cells.* Journal of cellular and molecular medicine, 2013. **17**(6): p. 704-712.

151. Lammerding, J., R.D. Kamm, and R.T. Lee, *Mechanotransduction in cardiac myocytes.* Annals of the New York Academy of Sciences, 2004. **1015**(1): p. 53-70.

152. Marjoram, R., E. Lessey, and K. Burridge, *Regulation of RhoA activity by adhesion molecules and mechanotransduction.* Current molecular medicine, 2014. **14**(2): p. 199-208.

153. Castillo, K., et al., *Thermally activated TRP channels: molecular sensors for temperature detection.* Physical biology, 2018. **15**(2): p. 021001.

154. Clapham, D.E., *TRP channels as cellular sensors.* Nature, 2003. **426**(6966): p. 517-524.

155. Huang, J., X. Zhang, and P.A. McNaughton. *Modulation of temperature-sensitive TRP channels*. in *Seminars in cell & developmental biology*. 2006. Elsevier.

156. Inoue, R., Z. Jian, and Y. Kawarabayashi, *Mechanosensitive TRP channels in cardiovascular pathophysiology.* Pharmacology & therapeutics, 2009. **123**(3): p. 371-385.

157. Kuipers, A.J., J. Middelbeek, and F.N. van Leeuwen, *Mechanoregulation of cytoskeletal dynamics by TRP channels.* European journal of cell biology, 2012. **91**(11-12): p. 834-846.

158. Liedtke, W., *Role of TRPV ion channels in sensory transduction of osmotic stimuli in mammals.* Experimental physiology, 2007. **92**(3): p. 507-512.

159. Lin, S.-Y. and D.P. Corey, *TRP channels in mechanosensation.* Current opinion in neurobiology, 2005. **15**(3): p. 350-357.

160. Nadezhdin, K.D., et al., *Structural mechanism of heat-induced opening of a temperature-sensitive TRP channel.* Nature structural & molecular biology, 2021. **28**(7): p. 564-572.

161. Voets, T., *TRP channels and thermosensation.* Mammalian Transient Receptor Potential (TRP) Cation Channels: Volume II, 2014: p. 729-741.

162. Voets, T., et al., *The principle of temperature-dependent gating in cold-and heat-sensitive TRP channels.* Nature, 2004. **430**(7001): p. 748-754.

163. Yue, Z., et al., *Role of TRP channels in the cardiovascular system.* American Journal of Physiology-Heart and Circulatory Physiology, 2015. **308**(3): p. H157-H182.

164. Aroke, E.N., et al., *Taste the pain: the role of TRP channels in pain and taste perception.* International journal of molecular sciences, 2020. **21**(16): p. 5929.

165. Chatzigeorgiou, M., et al., *Specific roles for DEG/ENaC and TRP channels in touch and thermosensation in C. elegans nociceptors.* Nature neuroscience, 2010. **13**(7): p. 861-868.

166. Chinigò, G., H. Castel, O. Chever, and D. Gkika, *TRP channels in brain tumors.* Frontiers in Cell and Developmental Biology, 2021. **9**: p. 617801.

167. Christensen, A.P. and D.P. Corey, *TRP channels in mechanosensation: direct or indirect activation?* Nature Reviews Neuroscience, 2007. **8**(7): p. 510-521.

168. Çiğ, B., S. Derouiche, and L.-H. Jiang, *Emerging roles of TRP channels in brain pathology*. 2021, Frontiers Media SA. p. 705196.

169. Corey, D.P., *New TRP channels in hearing and mechanosensation.* Neuron, 2003. **39**(4): p. 585-588.

170. Cuajungco, M.P., C. Grimm, and S. Heller, *TRP channels as candidates for hearing and balance abnormalities in vertebrates.* Biochimica et Biophysica Acta (BBA)-Molecular Basis of Disease, 2007. **1772**(8): p. 1022-1027.

171. Gavenis, K., et al., *Expression of ion channels of the TRP family in articular chondrocytes from osteoarthritic patients: changes between native and in vitro propagated chondrocytes.* Molecular and cellular biochemistry, 2009. **321**: p. 135-143.

172. Hsu, Y.-J., J.G. Hoenderop, and R.J. Bindels, *TRP channels in kidney disease.* Biochimica et Biophysica Acta (BBA)-Molecular Basis of Disease, 2007. **1772**(8): p. 928-936.

173. Krupkova, O., J. Zvick, and K. Wuertz-Kozak, *The role of transient receptor potential channels in joint diseases.* European cells & materials, 2017. **34**: p. 180-201.

174. Lieben, L. and G. Carmeliet, *The involvement of TRP channels in bone homeostasis.* Frontiers in endocrinology, 2012. **3**: p. 99.

175. Liu, Y., Y. Lyu, L. Zhu, and H. Wang, *Role of TRP Channels in Liver-Related Diseases.* International Journal of Molecular Sciences, 2023. **24**(15): p. 12509.

176. Martinac, B. and C. Cox, *Mechanosensory transduction: focus on ion channels.* Reference Module in Life Sciences; Elsevier: Amsterdam, The Netherlands, 2017: p. 9780128096338082000.

177. Moran, M.M., H. Xu, and D.E. Clapham, *TRP ion channels in the nervous system.* Current opinion in neurobiology, 2004. **14**(3): p. 362-369.

178. Nilius, B., G. Owsianik, T. Voets, and J.A. Peters, *Transient receptor potential cation channels in disease.* Physiological reviews, 2007. **87**(1): p. 165-217.

179. Qamar, S., M. Vadivelu, and R. Sandford, *TRP channels and kidney disease: lessons from polycystic kidney disease.* Biochemical Society Transactions, 2007. **35**(1): p. 124-128.

180. Roper, S.D., *TRPs in taste and chemesthesis.* Mammalian Transient Receptor Potential (TRP) Cation Channels: Volume II, 2014: p. 827-871.

181. Rychkov, G.Y. and G.J. Barritt, *Expression and function of TRP channels in liver cells.* Transient Receptor Potential Channels, 2011: p. 667-686.

182. Sawamura, S., et al., *TRP Channels in the Brain.* Neurobiology of TRP channels, 2017.

183. Sun, Y., et al., *TRPA channels distinguish gravity sensing from hearing in Johnston's organ.* Proceedings of the National Academy of Sciences, 2009. **106**(32): p. 13606-13611.

184. Uzieliene, I., P. Bernotas, A. Mobasheri, and E. Bernotiene, *The role of physical stimuli on calcium channels in chondrogenic differentiation of mesenchymal stem cells.* International journal of molecular sciences, 2018. **19**(10): p. 2998.

185. Vennekens, R., A. Menigoz, and B. Nilius, *TRPs in the brain.* Reviews of Physiology, Biochemistry and Pharmacology, Vol. 163, 2012: p. 27-64.

186. Wang, R., S. Tu, J. Zhang, and A. Shao, *Roles of TRP channels in neurological diseases.* Oxidative Medicine and Cellular Longevity, 2020. **2020**.

187. Hdud, I.M., A. Mobasheri, and P.T. Loughna, *Effect of osmotic stress on the expression of TRPV4 and BKCa channels and possible interaction with ERK1/2 and p38 in cultured equine chondrocytes.* American Journal of Physiology-Cell Physiology, 2014. **306**(11): p. C1050-C1057.

188. Li, W., et al., *Calcium signaling of primary chondrocytes and ATDC5 chondrogenic cells under osmotic stress and mechanical stimulation.* Journal of Biomechanics, 2022. **145**: p. 111388.

189. McNulty, A.L., H.A. Leddy, W. Liedtke, and F. Guilak, *TRPV4 as a therapeutic target for joint diseases.* Naunyn-Schmiedeberg's archives of pharmacology, 2015. **388**: p. 437-450.

190. Mergler, S., et al., *Thermosensitive transient receptor potential channels in human corneal epithelial cells.* Journal of cellular physiology, 2011. **226**(7): p. 1828-1842.

191. Son, A., et al., *TRPM3/TRPV4 regulates Ca2+-mediated RANKL/NFATc1 expression in osteoblasts.* Journal of molecular endocrinology, 2018. **61**(4): p. 207-218.

192. Wang, L., et al., *ATP release from mast cells by physical stimulation: a putative early step in activation of acupuncture points.* Evidence-Based Complementary and Alternative Medicine, 2013. **2013**.

193. Zhang, K., et al., *The mechanosensory and mechanotransductive processes mediated by ion channels and the impact on bone metabolism: A systematic review.* Archives of Biochemistry and Biophysics, 2021. **711**: p. 109020.

194. Zhao, Z., et al., *Mechanotransduction pathways in the regulation of cartilage chondrocyte homoeostasis.* Journal of cellular and molecular medicine, 2020. **24**(10): p. 5408-5419.

195. O'conor, C.J., T.M. Griffin, W. Liedtke, and F. Guilak, *Increased susceptibility of Trpv4-deficient mice to obesity and obesity-induced osteoarthritis with very high-fat diet.* Annals of the rheumatic diseases, 2013. **72**(2): p. 300-304.

196. O'Conor, C.J., et al., *Cartilage-specific knockout of the mechanosensory ion channel TRPV4 decreases age-related osteoarthritis.* Scientific reports, 2016. **6**(1): p. 29053.

197. O'conor, C.J., et al., *TRPV4-mediated mechanotransduction regulates the metabolic response of chondrocytes to dynamic loading.* Proceedings of the National Academy of Sciences, 2014. **111**(4): p. 1316-1321.

198. Delamere, N.A., et al., *Signaling between TRPV1/TRPV4 and intracellular hydrostatic pressure in the mouse lens.* Investigative ophthalmology & visual science, 2020. **61**(6): p. 58-58.

199. Iftinca, M., M. Defaye, and C. Altier, *TRPV1-targeted drugs in development for human pain conditions.* Drugs, 2021. **81**(1): p. 7-27.

200. Jara-Oseguera, A., S.A. Simon, and T. Rosenbaum, *TRPV1: on the road to pain relief.* Current molecular pharmacology, 2008. **1**(3): p. 255-269.

201. Riera, C.E., et al., *TRPV1 pain receptors regulate longevity and metabolism by neuropeptide signaling.* Cell, 2014. **157**(5): p. 1023-1036.

202. Sappington, R.M. and D.J. Calkins, *Contribution of TRPV1 to microglia-derived IL-6 and NFκB translocation with elevated hydrostatic pressure.* Investigative ophthalmology & visual science, 2008. **49**(7): p. 3004-3017.

203. Sappington, R.M., T. Sidorova, D.J. Long, and D.J. Calkins, *TRPV1: contribution to retinal ganglion cell apoptosis and increased intracellular Ca2+ with exposure to hydrostatic pressure.* Investigative ophthalmology & visual science, 2009. **50**(2): p. 717-728.

204. Szallasi, A. and M. Sheta, *Targeting TRPV1 for pain relief: limits, losers and laurels.* Expert opinion on investigational drugs, 2012. **21**(9): p. 1351-1369.

205. Gailly, P., *TRP channels in normal and dystrophic skeletal muscle.* Current opinion in pharmacology, 2012. **12**(3): p. 326-334.

206. Zanou, N., et al., *Role of TRPC1 channel in skeletal muscle function.* American Journal of Physiology-Cell Physiology, 2010. **298**(1): p. C149-C162.

207. Tiapko, O. and K. Groschner, *TRPC3 as a target of novel therapeutic interventions.* Cells, 2018. **7**(7): p. 83.

208. Woo, J.S., D.H. Kim, P.D. Allen, and E.H. Lee, *TRPC3-interacting triadic proteins in skeletal muscle.* Biochemical Journal, 2008. **411**(2): p. 399-405.

209. Coste, B., et al., *Piezo1 and Piezo2 are essential components of distinct mechanically activated cation channels.* Science, 2010. **330**(6000): p. 55-60.

210. Lin, Y.-C., et al., *Force-induced conformational changes in PIEZO1.* Nature, 2019. **573**(7773): p. 230-234.

211. Saotome, K., et al., *Structure of the mechanically activated ion channel Piezo1.* Nature, 2018. **554**(7693): p. 481-486.

212. Wu, J., A.H. Lewis, and J. Grandl, *Touch, tension, and transduction–the function and regulation of Piezo ion channels.* Trends in biochemical sciences, 2017. **42**(1): p. 57-71.

213. Wang, L., et al., *Structure and mechanogating of the mammalian tactile channel PIEZO2.* Nature, 2019. **573**(7773): p. 225-229.

214. Zhao, Q., et al., *Structure and mechanogating mechanism of the Piezo1 channel.* Nature, 2018. **554**(7693): p. 487-492.

215. Cox, C.D., et al., *Removal of the mechanoprotective influence of the cytoskeleton reveals PIEZO1 is gated by bilayer tension.* Nature communications, 2016. **7**(1): p. 10366.

216. Lewis, A.H. and J. Grandl, *Mechanical sensitivity of Piezo1 ion channels can be tuned by cellular membrane tension.* Elife, 2015. **4**: p. e12088.

217. Moroni, M., et al., *Voltage gating of mechanosensitive PIEZO channels.* Nature communications, 2018. **9**(1): p. 1096.

218. Shin, K.C., et al., *The Piezo2 ion channel is mechanically activated by low-threshold positive pressure.* Scientific Reports, 2019. **9**(1): p. 6446.

219. Syeda, R., et al., *Piezo1 channels are inherently mechanosensitive.* Cell reports, 2016. **17**(7): p. 1739-1746.

220. Syeda, R., et al., *Chemical activation of the mechanotransduction channel Piezo1.* Elife, 2015. **4**: p. e07369.

221. Wang, Y., et al., *A lever-like transduction pathway for long-distance chemical-and mechano-gating of the mechanosensitive Piezo1 channel.* Biophysical Journal, 2018. **114**(3): p. 113a-114a.

222. Taberner, F.J., et al., *Structure-guided examination of the mechanogating mechanism of PIEZO2.* Proceedings of the National Academy of Sciences, 2019. **116**(28): p. 14260-14269.

223. Haselwandter, C.A. and R. MacKinnon, *Piezo's membrane footprint and its contribution to mechanosensitivity.* Elife, 2018. **7**: p. e41968.

224. Gnanasambandam, R., C. Bae, P.A. Gottlieb, and F. Sachs, *Ionic selectivity and permeation properties of human PIEZO1 channels.* PloS one, 2015. **10**(5): p. e0125503.

225. Wang, F., et al., *Mechanosensitive ion channel Piezo2 is important for enterochromaffin cell response to mechanical forces.* The Journal of physiology, 2017. **595**(1): p. 79-91.

226. Botello-Smith, W.M., et al., *A mechanism for the activation of the mechanosensitive Piezo1 channel by the small molecule Yoda1.* Nature communications, 2019. **10**(1): p. 4503.

227. Wijerathne, T.D., A.D. Ozkan, and J.J. Lacroix, *Yoda1's energetic footprint on Piezo1 channels and its modulation by voltage and temperature.* Proceedings of the National Academy of Sciences, 2022. **119**(29): p. e2202269119.

228. Evans, E.L., et al., *Yoda1 analogue (D ooku1) which antagonizes Y oda1-evoked activation of P iezo1 and aortic relaxation.* British journal of pharmacology, 2018. **175**(10): p. 1744-1759.

229. Bae, C., F. Sachs, and P.A. Gottlieb, *The mechanosensitive ion channel Piezo1 is inhibited by the peptide GsMTx4.* Biochemistry, 2011. **50**(29): p. 6295-6300.

230. Coste, B., et al., *Piezo proteins are pore-forming subunits of mechanically activated channels.* Nature, 2012. **483**(7388): p. 176-181.

231. Ermakov, Y.A., K. Kamaraju, K. Sengupta, and S. Sukharev, *Gadolinium ions block mechanosensitive channels by altering the packing and lateral pressure of anionic lipids.* Biophysical journal, 2010. **98**(6): p. 1018-1027.

232. Suchyna, T.M., et al., *Bilayer-dependent inhibition of mechanosensitive channels by neuroactive peptide enantiomers.* Nature, 2004. **430**(6996): p. 235-240.

233. Gnanasambandam, R., et al., *GsMTx4: mechanism of inhibiting mechanosensitive ion channels.* Biophysical journal, 2017. **112**(1): p. 31-45.

234. Rocio Servin-Vences, M., M. Moroni, G.R. Lewin, and K. Poole, *Direct measurement of TRPV4 and PIEZO1 activity reveals multiple mechanotransduction pathways in chondrocytes.* elife, 2017. **6**: p. e21074.

235. Du, G., et al., *Roles of TRPV4 and piezo channels in stretch-evoked Ca2+ response in chondrocytes.* Experimental Biology and Medicine, 2020. **245**(3): p. 180-189.

236. Du, G., W. Chen, L. Li, and Q. Zhang, *The potential role of mechanosensitive ion channels in substrate stiffness-regulated Ca2+ response in chondrocytes.* Connective Tissue Research, 2022. **63**(5): p. 453-462.

237. Lee, W., et al., *Synergy between Piezo1 and Piezo2 channels confers high-strain mechanosensitivity to articular cartilage.* Proceedings of the National Academy of Sciences, 2014. **111**(47): p. E5114-E5122.

238. Xie, M., et al., *Dynamic loading enhances chondrogenesis of human chondrocytes within a biodegradable resilient hydrogel.* Biomaterials Science, 2021. **9**(14): p. 5011-5024.

239. Ren, X., et al., *High expression of Piezo1 induces senescence in chondrocytes through calcium ions accumulation.* Biochemical and Biophysical Research Communications, 2022. **607**: p. 138-145.

240. Zhang, H., et al., *Mechanical overloading promotes chondrocyte senescence and osteoarthritis development through downregulating FBXW7.* Annals of the rheumatic diseases, 2022. **81**(5): p. 676-686.

241. Imgenberg, J., et al., *Estrogen reduces mechanical injury-related cell death and proteoglycan degradation in mature articular cartilage independent of the presence of the superficial zone tissue.* Osteoarthritis and Cartilage, 2013. **21**(11): p. 1738-1745.

242. Lawrence, K.M., et al., *Chondroprotection by urocortin involves blockade of the mechanosensitive ion channel Piezo1.* Scientific Reports, 2017. **7**(1): p. 5147.

243. Jones, R.C., et al., *Urocortin-1 is chondroprotective in response to acute cartilage injury via modulation of Piezo1.* International Journal of Molecular Sciences, 2022. **23**(9): p. 5119.

244. Sun, Y., et al., *G protein coupled estrogen receptor attenuates mechanical stress-mediated apoptosis of chondrocyte in osteoarthritis via suppression of Piezo1.* Molecular Medicine, 2021. **27**(1): p. 96.

245. Li, X., et al., *Mechanism of the Piezo1 protein-induced apoptosis of the chondrocytes through the MAPK/ERK1/2 signal pathway.* Zhonghua yi xue za zhi, 2016. **96**(31): p. 2472-2477.

246. He, Z., et al., *Excessive mechanical stress mediated Piezo1 activation regulates lysosomal membrane permeabilization-induced chondrocyte apoptosis in mouse osteoarthritis model.* 2022.

247. Zhou, T., et al., *Piezo1/2 mediate mechanotransduction essential for bone formation through concerted activation of NFAT-YAP1-ß-catenin.* Elife, 2020. **9**: p. e52779.

248. Nims, R.J., et al., *A synthetic mechanogenetic gene circuit for autonomous drug delivery in engineered tissues.* Science Advances, 2021. **7**(5): p. eabd9858.

249. Mukund, K. and S. Subramaniam, *Skeletal muscle: A review of molecular structure and function, in health and disease.* Wiley Interdisciplinary Reviews: Systems Biology and Medicine, 2020. **12**(1): p. e1462.

250. Bernareggi, A., et al., *The state of the art of Piezo1 channels in skeletal muscle regeneration.* International Journal of Molecular Sciences, 2022. **23**(12): p. 6616.

251. Peng, Y., et al., *Mechano-signaling via Piezo1 prevents activation and p53-mediated senescence of muscle stem cells.* Redox Biology, 2022. **52**: p. 102309.

252. Ma, N., et al., *Piezo1 regulates the regenerative capacity of skeletal muscles via orchestration of stem cell morphological states.* Science advances, 2022. **8**(11): p. eabn0485.

253. Ortuste Quiroga, H.P., et al., *Fine-tuning of Piezo1 expression and activity ensures efficient myoblast fusion during skeletal myogenesis.* Cells, 2022. **11**(3): p. 393.

254. Hirata, Y., et al., *A Piezo1/KLF15/IL-6 axis mediates immobilization-induced muscle atrophy.* The Journal of Clinical Investigation, 2022. **132**(10).

255. Thorpe, C.T. and H.R. Screen, *Tendon structure and composition.* Metabolic influences on risk for tendon disorders, 2016: p. 3-10.

256. Buschmann, J. and G.M. Bürgisser, *Biomechanics of tendons and ligaments: tissue reconstruction and regeneration*. 2017: Woodhead Publishing.

257. Kendal, A.R., et al., *Multi-omic single cell analysis resolves novel stromal cell populations in healthy and diseased human tendon.* Scientific reports, 2020. **10**(1): p. 13939.

258. Copp, S.W., J.S. Kim, V. Ruiz-Velasco, and M.P. Kaufman, *The mechano-gated channel inhibitor GsMTx4 reduces the exercise pressor reflex in decerebrate rats.* The Journal of physiology, 2016. **594**(3): p. 641-655.

259. Grotle, A.-K., et al., *GsMTx-4 normalizes the exercise pressor reflex evoked by intermittent muscle contraction in early stage type 1 diabetic rats.* American Journal of Physiology-Heart and Circulatory Physiology, 2021. **320**(4): p. H1738-H1748.

260. Nakamichi, R., et al., *The mechanosensitive ion channel PIEZO1 is expressed in tendons and regulates physical performance.* Science translational medicine, 2022. **14**(647): p. eabj5557.

261. Passini, F.S., et al., *Shear-stress sensing by PIEZO1 regulates tendon stiffness in rodents and influences jumping performance in humans.* Nature biomedical engineering, 2021. **5**(12): p. 1457-1471.

262. McMillin, M.J., et al., *Mutations in PIEZO2 cause Gordon syndrome, Marden-Walker syndrome, and distal arthrogryposis type 5.* The American Journal of Human Genetics, 2014. **94**(5): p. 734-744.

263. HALL, J.G., *Genetic aspects of arthrogryposis.* Clinical Orthopaedics and Related Research (1976-2007), 1985. **194**: p. 44-53.

264. Bamshad, M., L.B. Jorde, and J.C. Carey, *A revised and extended classification of the distal arthrogryposes.* American journal of medical genetics, 1996. **65**(4): p. 277-281.

265. Hall, J., S. Reed, and G. Greene, *The distal arthrogryposes: delineation of new entities–review and nosologic discussion.* American journal of medical genetics, 1982. **11**(2): p. 185-239.

266. Ma, S., et al., *Excessive Mechanotransduction in Sensory Neurons Causes Joint Contractures in a Mouse Model of Arthrogryposis.* bioRxiv, 2022: p. 2022.06. 07.495164.

267. Masingue, M., et al., *A novel nonsense PIEZO2 mutation in a family with scoliosis and proprioceptive defect.* Neuromuscular Disorders, 2019. **29**(1): p. 75-79.

268. Mitchell, J.H. and S.A. Smith, *Unravelling the mysteries of the exercise pressor reflex at the cellular level.* The Journal of Physiology, 2008. **586**(Pt 13): p. 3025.

269. Du, Y., et al., *Endocrine regulation of extra-skeletal organs by bone-derived secreted protein and the effect of mechanical stimulation.* Frontiers in Cell and Developmental Biology, 2021. **9**: p. 778015.

270. Morgan, E.F., et al., *Mechanotransduction and fracture repair.* The Journal of bone and joint surgery. American volume, 2008. **90**(Suppl 1): p. 25.

271. Rolfe, R.A., et al., *Identification of mechanosensitive genes during skeletal development: alteration of genes associated with cytoskeletal rearrangement and cell signalling pathways.* BMC genomics, 2014. **15**(1): p. 1-23.

272. Watanabe-Takano, H., et al., *Mechanical load regulates bone growth via periosteal Osteocrin.* Cell reports, 2021. **36**(2).

273. Bonewald, L.F., *The amazing osteocyte.* Journal of bone and mineral research, 2011. **26**(2): p. 229-238.

274. Florencio-Silva, R., et al., *Biology of bone tissue: structure, function, and factors that influence bone cells.* BioMed research international, 2015. **2015**.

275. Mikuni-Takagaki, Y., K. Naruse, Y. Azuma, and A. Miyauchi, *The role of calcium channels in osteocyte function.* JOURNAL OF MUSCULOSKELETAL AND NEURONAL INTERACTIONS, 2002. **2**(3): p. 252-255.

276. Rawlinson, S., A. Pitsillides, and L. Lanyon, *Involvement of different ion channels in osteoblasts' and osteocytes' early responses to mechanical strain.* Bone, 1996. **19**(6): p. 609-614.

277. Yu, K., et al., *Mechanical loading disrupts osteocyte plasma membranes which initiates mechanosensation events in bone.* Journal of Orthopaedic Research®, 2018. **36**(2): p. 653-662.

278. Hendrickx, G., et al., *Piezo 1 inactivation in chondrocytes impairs trabecular bone formation.* Journal of Bone and Mineral Research, 2021. **36**(2): p. 369-384.

279. Sun, W., et al., *The mechanosensitive Piezo1 channel is required for bone formation.* Elife, 2019. **8**: p. e47454.

280. Wang, L., et al., *Mechanical sensing protein PIEZO1 regulates bone homeostasis via osteoblast-osteoclast crosstalk.* Nature Communications, 2020. **11**(1): p. 282.

281. Bai, W.-Y., et al., *Identification of PIEZO1 polymorphisms for human bone mineral density.* Bone, 2020. **133**: p. 115247.

282. Walter, B., et al., *Form and function of the intervertebral disc in health and disease: a morphological and stain comparison study.* Journal of anatomy, 2015. **227**(6): p. 707-716.

283. Buckwalter, J., *Aging and degeneration of the human intervertebral disc. Spine (Phila Pa 1976). 1995; 20 (11): 1307–14*. Epub 1995/06/01. https://doi. org/10.1097/00007632-199506000-00022 PMID: 7660243.

284. Dou, Y., et al., *Intervertebral disk degeneration: the microenvironment and tissue engineering strategies.* Frontiers in bioengineering and biotechnology, 2021. **9**: p. 592118.

285. Shi, S., et al., *Excessive mechanical stress-induced intervertebral disc degeneration is related to Piezo1 overexpression triggering the imbalance of autophagy/apoptosis in human nucleus pulpous.* Arthritis Research & Therapy, 2022. **24**(1): p. 1-11.

286. Sun, Y., et al., *Piezo1 activates the NLRP3 inflammasome in nucleus pulposus cell-mediated by Ca2+/NF-κB pathway.* International Immunopharmacology, 2020. **85**: p. 106681.

287. Sun, Z., et al., *Single impact injury of vertebral endplates without structural disruption, initiates disc degeneration through Piezo1 mediated inflammation and metabolism dysfunction.* Spine, 2022. **47**(5): p. E203.

288. Wang, B., et al., *Mechanosensitive ion channel Piezo1 activated by matrix stiffness regulates oxidative stress-induced senescence and apoptosis in human intervertebral disc degeneration.* Oxidative Medicine and Cellular Longevity, 2021. **2021**.

289. Wu, J., et al., *Self-amplifying loop of NF-κB and periostin initiated by PIEZO1 accelerates mechano-induced senescence of nucleus pulposus cells and intervertebral disc degeneration.* Molecular Therapy, 2022. **30**(10): p. 3241-3256.

290. Yang, Q., et al., *Study on the mechanism of excessive apoptosis of nucleus pulposus cells induced by shRNA-Piezo1 under abnormal mechanical stretch stress.* Journal of Cellular Biochemistry, 2019. **120**(3): p. 3989-3997.

291. Molinos, M., et al., *Inflammation in intervertebral disc degeneration and regeneration.* Journal of the Royal Society Interface, 2015. **12**(104): p. 20141191.

292. Vergroesen, P.-P., et al., *Mechanics and biology in intervertebral disc degeneration: a vicious circle.* Osteoarthritis and cartilage, 2015. **23**(7): p. 1057-1070.

293. Gilchrist, C.L., E.M. Darling, J. Chen, and L.A. Setton, *Extracellular matrix ligand and stiffness modulate immature nucleus pulposus cell-cell interactions.* PloS one, 2011. **6**(11): p. e27170.

294. Navaro, Y., et al., *Matrix stiffness determines the fate of nucleus pulposus–derived stem cells.* Biomaterials, 2015. **49**: p. 68-76.

295. Ariga, K., et al., *Mechanical Stress-Induced Apoptosis of Endplate Chondrocytes in Organ-Cultured Mouse Intervertebral Discs: An: Ex Vivo: Study.* Spine, 2003. **28**(14): p. 1528-1533.

296. Xu, H.-g., et al., *Intermittent cyclic mechanical tension-induced calcification and downregulation of ankh gene expression of end plate chondrocytes.* Spine, 2012. **37**(14): p. 1192-1197.

297. Xu, H.-g., et al., *Intermittent cyclic mechanical tension promotes endplate cartilage degeneration via canonical Wnt signaling pathway and E-cadherin/β-catenin complex cross-talk.* Osteoarthritis and Cartilage, 2016. **24**(1): p. 158-168.

298. Abbott, R.D., A.K. Howe, H.M. Langevin, and J.C. Iatridis, *Live free or die: Stretch-induced apoptosis occurs when adaptive reorientation of annulus fibrosus cells is restricted.* Biochemical and biophysical research communications, 2012. **421**(2): p. 361-366.

299. Gilbert, H.T., J.A. Hoyland, A.J. Freemont, and S.J. Millward-Sadler, *The involvement of interleukin-1 and interleukin-4 in the response of human annulus fibrosus cells to cyclic tensile strain: an altered mechanotransduction pathway with degeneration.* Arthritis research & therapy, 2011. **13**(1): p. 1-12.

300. Tisherman, R., et al., *NF-κB signaling pathway in controlling intervertebral disk cell response to inflammatory and mechanical stressors.* Physical Therapy, 2016. **96**(5): p. 704-711.

301. Szczot, M., et al., *PIEZO2 mediates injury-induced tactile pain in mice and humans.* Science translational medicine, 2018. **10**(462): p. eaat9892.

302. Zhang, M., et al., *Mechanically activated piezo channels mediate touch and suppress acute mechanical pain response in mice.* Cell Reports, 2019. **26**(6): p. 1419-1431. e4.

303. Ranade, S.S., et al., *Piezo2 is the major transducer of mechanical forces for touch sensation in mice.* Nature, 2014. **516**(7529): p. 121-125.

304. Nencini, S., et al., *Piezo2 knockdown inhibits noxious mechanical stimulation and NGF-induced sensitization in A-delta bone afferent neurons.* Frontiers in Physiology, 2021. **12**: p. 644929.

305. Eijkelkamp, N., et al., *A role for Piezo2 in EPAC1-dependent mechanical allodynia.* Nature communications, 2013. **4**(1): p. 1682.

306. Luo, Z., et al., *Extracellular ATP and cAMP signaling promote Piezo2-dependent mechanical allodynia after trigeminal nerve compression injury.* Journal of Neurochemistry, 2022. **160**(3): p. 376-391.

307. Ni, K., et al., *Dorsal root ganglia NR2B-mediated Epac1-Piezo2 signaling pathway contributes to mechanical allodynia of bone cancer pain.* Oncology Letters, 2021. **21**(4): p. 1-8.

308. Ferrari, L.F., O. Bogen, P. Green, and J.D. Levine, *Contribution of Piezo2 to endothelium-dependent pain.* Molecular pain, 2015. **11**: p. s12990-015-0068-4.

309. Fontanella, C.G., et al., *Mechanical behavior of infrapatellar fat pad of patients affected by osteoarthritis.* Journal of Biomechanics, 2022. **131**: p. 110931.

310. Emmi, A., et al., *Infrapatellar fat pad-synovial membrane anatomo-fuctional unit: microscopic basis for Piezo1/2 mechanosensors involvement in osteoarthritis pain.* Frontiers in Cell and Developmental Biology, 2022. **10**: p. 886604.

311. Obeidat, A.M., et al., *Piezo2 expressing nociceptors mediate mechanical sensitization in experimental osteoarthritis.* Nature Communications, 2023. **14**(1): p. 2479.

312. Florez-Paz, D., K.K. Bali, R. Kuner, and A. Gomis, *A critical role for Piezo2 channels in the mechanotransduction of mouse proprioceptive neurons.* Scientific Reports, 2016. **6**(1): p. 25923.

313. Woo, S.-H., et al., *Piezo2 is the principal mechanotransduction channel for proprioception.* Nature neuroscience, 2015. **18**(12): p. 1756-1762.

314. Chesler, A.T., et al., *The role of PIEZO2 in human mechanosensation.* New England Journal of Medicine, 2016. **375**(14): p. 1355-1364.

315. Assaraf, E., et al., *Piezo2 expressed in proprioceptive neurons is essential for skeletal integrity.* Nature communications, 2020. **11**(1): p. 3168.

316. Lee, W., F. Guilak, and W. Liedtke, *Role of piezo channels in joint health and injury.* Current topics in membranes, 2017. **79**: p. 263-273.

317. Jacques-Fricke, B.T., et al., *Ca2+ influx through mechanosensitive channels inhibits neurite outgrowth in opposition to other influx pathways and release from intracellular stores.* Journal of Neuroscience, 2006. **26**(21): p. 5656-5664.

318. Ward, C.W., F. Sachs, E.D. Bush, and T.M. Suchyna, *GsMTx4-D provides protection to the D2. mdx mouse.* Neuromuscular Disorders, 2018. **28**(10): p. 868-877.

319. Hara, M., et al., *Calcium influx through a possible coupling of cation channels impacts skeletal muscle satellite cell activation in response to mechanical stretch.* American Journal of Physiology-Cell Physiology, 2012. **302**(12): p. C1741-C1750.

320. Efremov, A.K., et al., *Application of piconewton forces to individual filopodia reveals mechanosensory role of L-type Ca2+ channels.* Biomaterials, 2022. **284**: p. 121477.

321. Takahashi, K., et al., *L-type calcium channel modulates mechanosensitivity of the cardiomyocyte cell line H9c2.* Cell Calcium, 2019. **79**: p. 68-74.

322. Takamatsu, A., et al., *Verapamil protects against cartilage degradation in osteoarthritis by inhibiting Wnt/β-catenin signaling.* PloS one, 2014. **9**(3): p. e92699.

323. Swain, S.M., et al., *TRPV4 channel opening mediates pressure-induced pancreatitis initiated by Piezo1 activation.* The Journal of clinical investigation, 2020. **130**(5): p. 2527-2541.

324. Romac, J.M.-J., et al., *Piezo1 is a mechanically activated ion channel and mediates pressure induced pancreatitis.* Nature communications, 2018. **9**(1): p. 1715.

325. Swain, S.M., J.M. Romac, S.R. Vigna, and R.A. Liddle, *Piezo1-mediated stellate cell activation causes pressure-induced pancreatic fibrosis in mice.* JCI insight, 2022. **7**(8).

326. Ridone, P., et al., *Disruption of membrane cholesterol organization impairs the activity of PIEZO1 channel clusters.* Journal of General Physiology, 2020. **152**(8): p. e201912515.

327. Xiao, B., *Levering mechanically activated piezo channels for potential pharmacological intervention.* Annual review of pharmacology and toxicology, 2020. **60**: p. 195-218.

328. Borbiro, I., D. Badheka, and T. Rohacs, *Activation of TRPV1 channels inhibits mechanosensitive Piezo channel activity by depleting membrane phosphoinositides.* Science signaling, 2015. **8**(363): p. ra15-ra15.

329. Narayanan, P., et al., *Myotubularin related protein-2 and its phospholipid substrate PIP2 control Piezo2-mediated mechanotransduction in peripheral sensory neurons.* Elife, 2018. **7**: p. e32346.

330. Qi, Y., et al., *Membrane stiffening by STOML3 facilitates mechanosensation in sensory neurons.* Nature communications, 2015. **6**(1): p. 8512.

331. Wu, C.-L., et al., *Dietary fatty acid content regulates wound repair and the pathogenesis of osteoarthritis following joint injury.* Annals of the rheumatic diseases, 2015. **74**(11): p. 2076-2083.

332. Han, Y., et al., *Mechanosensitive ion channel Piezo1 promotes prostate cancer development through the activation of the Akt/mTOR pathway and acceleration of cell cycle.* International journal of oncology, 2019. **55**(3): p. 629-644.

333. Jin, Y., et al., *Functional role of mechanosensitive ion channel Piezo1 in human periodontal ligament cells.* The Angle Orthodontist, 2015. **85**(1): p. 87-94.

334. Romero, L.O., et al., *Dietary fatty acids fine-tune Piezo1 mechanical response.* Nature communications, 2019. **10**(1): p. 1200.

335. Sekar, S., et al., *Saturated fatty acids promote chondrocyte matrix remodeling through reprogramming of autophagy pathways.* Nutrition, 2018. **54**: p. 144-152.

336. Zhong, M., Y. Komarova, J. Rehman, and A.B. Malik, *Mechanosensing Piezo channels in tissue homeostasis including their role in lungs.* Pulmonary Circulation, 2018. **8**(2): p. 2045894018767393.

337. Collins, K., et al., *High-fat/high-sucrose diet-induced obesity results in joint-specific development of osteoarthritis-like degeneration in a rat model.* Bone & Joint Research, 2018. **7**(4): p. 274-281.

338. Collins, K.H., et al., *Response to diet-induced obesity produces time-dependent induction and progression of metabolic osteoarthritis in rat knees.* Journal of Orthopaedic Research, 2016. **34**(6): p. 1010-1018.

339. Griffin, T.M., et al., *Diet-induced obesity differentially regulates behavioral, biomechanical, and molecular risk factors for osteoarthritis in mice.* Arthritis research & therapy, 2010. **12**: p. 1-18.

340. Harasymowicz, N.S., A. Dicks, C.L. Wu, and F. Guilak, *Physiologic and pathologic effects of dietary free fatty acids on cells of the joint.* Annals of the New York Academy of Sciences, 2019. **1440**(1): p. 36-53.

341. Wu, C.-L., K.A. Kimmerling, D. Little, and F. Guilak, *Serum and synovial fluid lipidomic profiles predict obesity-associated osteoarthritis, synovitis, and wound repair.* Scientific reports, 2017. **7**(1): p. 44315.

342. Cordingley, D.M. and S.M. Cornish, *Omega-3 fatty acids for the management of osteoarthritis: A narrative review.* Nutrients, 2022. **14**(16): p. 3362.

343. Kimmerling, K.A., et al., *Transgenic conversion of ω-6 to ω-3 polyunsaturated fatty acids via fat-1 reduces the severity of post-traumatic osteoarthritis.* Arthritis Research & Therapy, 2020. **22**: p. 1-10.

344. Xie, Y., et al., *Docosahexaenoic acid inhibits bone remodeling and vessel formation in the osteochondral unit in a rat model.* Biomedicine & Pharmacotherapy, 2019. **114**: p. 108811.

345. Jiao, H., E. Xiao, and D.T. Graves, *Diabetes and its effect on bone and fracture healing.* Current osteoporosis reports, 2015. **13**: p. 327-335.

346. Gao, F., T.-R. Lv, J.-C. Zhou, and X.-D. Qin, *Effects of obesity on the healing of bone fracture in mice.* Journal of orthopaedic surgery and research, 2018. **13**: p. 1-8.

347. Brown, M.L., et al., *Delayed fracture healing and increased callus adiposity in a C57BL/6J murine model of obesity-associated type 2 diabetes mellitus.* PloS one, 2014. **9**(6): p. e99656.

348. Figeac, F., et al., *Impaired bone fracture healing in type 2 diabetes is caused by defective functions of skeletal progenitor cells.* Stem Cells, 2022. **40**(2): p. 149-164.

349. Khajuria, D.K., et al., *Aberrant structure of fibrillar collagen and elevated levels of advanced glycation end products typify delayed fracture healing in the diet-induced obesity mouse model.* Bone, 2020. **137**: p. 115436.

350. Chen, P., et al., *Mechanosensitive Piezo1 in endothelial cells promotes angiogenesis to support bone fracture repair.* Cell Calcium, 2021. **97**: p. 102431.

351. Liu, Y., et al., *Mechanosensitive Piezo1 is crucial for periosteal stem cell-mediated fracture healing.* International Journal of Biological Sciences, 2022. **18**(10): p. 3961.

352. Catterall, W.A., *Voltage-gated calcium channels.* Cold Spring Harbor perspectives in biology, 2011. **3**(8): p. a003947.

353. Guy, H.R. and F. Conti, *Pursuing the structure and function of voltage-gated channels.* Trends in neurosciences, 1990. **13**(6): p. 201-206.

354. Wright, C.S., A.G. Robling, M.C. Farach-Carson, and W.R. Thompson, *Skeletal functions of voltage sensitive calcium channels.* Current osteoporosis reports, 2021. **19**: p. 206-221.

355. Barry, E., *Expression of mRNAs for the α 1 Subunit of Voltage-Gated Calcium Channels in Human Osteoblast-Like Cell Lines and in Normal Human Osteoblasts.* Calcified tissue international, 2000. **66**: p. 145-150.

356. Sun, X., V. Kishore, K. Fites, and O. Akkus, *Osteoblasts detect pericellular calcium concentration increase via neomycin-sensitive voltage gated calcium channels.* Bone, 2012. **51**(5): p. 860-867.

357. Tan, Y.z., et al., *L-type voltage-gated calcium channels in stem cells and tissue engineering.* Cell Proliferation, 2019. **52**(4): p. e12623.

358. Miyauchi, A., et al., *Osteoclast cytosolic calcium, regulated by voltage-gated calcium channels and extracellular calcium, controls podosome assembly and bone resorption.* The Journal of cell biology, 1990. **111**(6): p. 2543-2552.

359. Barrett-Jolley, R., R. Lewis, R. Fallman, and A. Mobasheri, *The emerging chondrocyte channelome.* Frontiers in physiology, 2010. **1**: p. 135.

360. Li, X., et al., *Millimeter wave promotes the synthesis of extracellular matrix and the proliferation of chondrocyte by regulating the voltage-gated K+ channel.* Journal of bone and mineral metabolism, 2014. **32**: p. 367-377.

361. Mobasheri, A., et al., *The chondrocyte channelome: A narrative review.* Joint Bone Spine, 2019. **86**(1): p. 29-35.

362. Sugimoto, T., et al., *Voltage-gated ionic channels in cultured rabbit articular chondrocytes.* Comparative Biochemistry and Physiology Part C: Pharmacology, Toxicology and Endocrinology, 1996. **115**(3): p. 223-232.

363. Xu, J., W. Wang, C. Clark, and C. Brighton, *Signal transduction in electrically stimulated articular chondrocytes involves translocation of extracellular calcium through voltage-gated channels.* Osteoarthritis and cartilage, 2009. **17**(3): p. 397-405.

364. Boileau, C., et al., *PD-0200347, an α2δ ligand of the voltage gated calcium channel, inhibits in vivo activation of the Erk1/2 pathway in osteoarthritic chondrocytes: a PKCα dependent effect.* Annals of the rheumatic diseases, 2006. **65**(5): p. 573-580.

365. Steward, A., D. Kelly, and D. Wagner, *The role of calcium signalling in the chondrogenic response of mesenchymal stem cells to hydrostatic pressure.* Eur Cell Mater, 2014. **28**: p. 358-371.

366. Varga, Z., et al., *Switch of voltage-gated K+ channel expression in the plasma membrane of chondrogenic cells affects cytosolic Ca2+-oscillations and cartilage formation.* PloS one, 2011. **6**(11): p. e27957.

367. Zhang, K., et al., *Mechanosensory and mechanotransductive processes mediated by ion channels in articular chondrocytes: Potential therapeutic targets for osteoarthritis.* Channels, 2021. **15**(1): p. 339-359.

368. Atsuta, Y., R.R. Tomizawa, M. Levin, and C.J. Tabin, *L-type voltage-gated Ca2+ channel CaV1. 2 regulates chondrogenesis during limb development.* Proceedings of the National Academy of Sciences, 2019. **116**(43): p. 21592-21601.

369. Calder, P.C., *Functional roles of fatty acids and their effects on human health.* Journal of parenteral and enteral nutrition, 2015. **39**: p. 18S-32S.

370. Williams, C.M. *Dietary fatty acids and human health*. in *Annales de zootechnie*. 2000. EDP Sciences.

371. Calder, P.C., *The relationship between the fatty acid composition of immune cells and their function.* Prostaglandins, Leukotrienes and Essential Fatty Acids, 2008. **79**(3-5): p. 101-108.

372. De Carvalho, C.C. and M.J. Caramujo, *The various roles of fatty acids.* Molecules, 2018. **23**(10): p. 2583.

373. Lochner, M., L. Berod, and T. Sparwasser, *Fatty acid metabolism in the regulation of T cell function.* Trends in immunology, 2015. **36**(2): p. 81-91.

374. Rozanna, D., et al., *Fatty acids as phase change materials (PCMs) for thermal energy storage: a review.* International journal of green energy, 2005. **1**(4): p. 495-513.

375. Arner, P., *Insulin resistance in type 2 diabetes: role of fatty acids.* Diabetes/metabolism research and reviews, 2002. **18**(S2): p. S5-S9.

376. Bergman, R.N. and M. Ader, *Free fatty acids and pathogenesis of type 2 diabetes mellitus.* Trends in Endocrinology & Metabolism, 2000. **11**(9): p. 351-356.

377. Berry, E.M., *Dietary fatty acids in the management of diabetes mellitus.* The American journal of clinical nutrition, 1997. **66**(4): p. 991S-997S.

378. Boden, G., *Obesity and free fatty acids.* Endocrinology and metabolism clinics of North America, 2008. **37**(3): p. 635-646.

379. D'Angelo, S., M.L. Motti, and R. Meccariello, *ω-3 and ω-6 polyunsaturated fatty acids, obesity and cancer.* Nutrients, 2020. **12**(9): p. 2751.

380. Group, A.S.C., *Effects of n− 3 fatty acid supplements in diabetes mellitus.* New England Journal of Medicine, 2018. **379**(16): p. 1540-1550.

381. Karpe, F., J.R. Dickmann, and K.N. Frayn, *Fatty acids, obesity, and insulin resistance: time for a reevaluation.* Diabetes, 2011. **60**(10): p. 2441-2449.

382. Wyne, K.L., *Free fatty acids and type 2 diabetes mellitus.* The American journal of medicine, 2003. **115**(8): p. 29-36.

383. Kapoor, B., et al., *Dietary polyunsaturated fatty acids (PUFAs): Uses and potential health benefits.* Current Nutrition Reports, 2021. **10**: p. 232-242.

384. Minihane, A.M. and J. Lovegrove, *Health benefits of polyunsaturated fatty acids (PUFAs)*, in *Improving the fat content of foods*. 2006, Elsevier. p. 107-140.

385. Ruxton, C., S. Reed, M. Simpson, and K. Millington, *The health benefits of omega-3 polyunsaturated fatty acids: a review of the evidence.* Journal of human nutrition and dietetics: the official journal of the British Dietetic Association, 2007. **20**(3): p. 275-285.

386. Ruxton, C., S.C. Reed, M. Simpson, and K. Millington, *The health benefits of omega-3 polyunsaturated fatty acids: a review of the evidence.* Journal of human nutrition and dietetics, 2004. **17**(5): p. 449-459.

387. Zárate, R., et al., *Significance of long chain polyunsaturated fatty acids in human health.* Clinical and translational medicine, 2017. **6**: p. 1-19.

388. Flachs, P., M. Rossmeisl, M. Bryhn, and J. Kopecky, *Cellular and molecular effects of n− 3 polyunsaturated fatty acids on adipose tissue biology and metabolism.* Clinical science, 2009. **116**(1): p. 1-16.

389. Wiktorowska-Owczarek, A., M. Berezinska, and J.Z. Nowak, *PUFAs: structures, metabolism and functions.* Adv Clin Exp Med, 2015. **24**(6): p. 931-941.

390. Bazinet, R.P. and S. Layé, *Polyunsaturated fatty acids and their metabolites in brain function and disease.* Nature reviews neuroscience, 2014. **15**(12): p. 771-785.

391. Abdelhamid, A.S., et al., *Polyunsaturated fatty acids for the primary and secondary prevention of cardiovascular disease.* The Cochrane database of systematic reviews, 2018. **2018**(7).

392. Ander, B.P., C.M. Dupasquier, M.A. Prociuk, and G.N. Pierce, *Polyunsaturated fatty acids and their effects on cardiovascular disease.* Experimental & Clinical Cardiology, 2003. **8**(4): p. 164.

393. Hibbeln, J.R. and N. Salem Jr, *Dietary polyunsaturated fatty acids and depression: when cholesterol does not satisfy.* The American journal of clinical nutrition, 1995. **62**(1): p. 1-9.

394. Ntambi, J.M., *Regulation of stearoyl-CoA desaturase by polyunsaturated fatty acids and cholesterol.* Journal of lipid research, 1999. **40**(9): p. 1549-1558.

395. Ravnskov, U., *The questionable role of saturated and polyunsaturated fatty acids in cardiovascular disease.* Journal of clinical epidemiology, 1998. **51**(6): p. 443-460.

396. Yehuda, S., S. Rabinovitz, R.L. Carasso, and D.I. Mostofsky, *The role of polyunsaturated fatty acids in restoring the aging neuronal membrane.* Neurobiology of aging, 2002. **23**(5): p. 843-853.

397. Hao, W., et al., *ω-3 fatty acids suppress inflammatory cytokine production by macrophages and hepatocytes.* Journal of pediatric surgery, 2010. **45**(12): p. 2412-2418.

398. Maroon, J.C. and J.W. Bost, *ω-3 Fatty acids (fish oil) as an anti-inflammatory: an alternative to nonsteroidal anti-inflammatory drugs for discogenic pain.* Surgical neurology, 2006. **65**(4): p. 326-331.

399. Yan, Y., et al., *Omega-3 fatty acids prevent inflammation and metabolic disorder through inhibition of NLRP3 inflammasome activation.* Immunity, 2013. **38**(6): p. 1154-1163.

400. Bahadori, B., et al., *ω-3 Fatty Acids Infusions as Adjuvant Therapy in Rheumatoid Arthritis.* Journal of Parenteral and Enteral Nutrition, 2010. **34**(2): p. 151-155.

401. Gioxari, A., A.C. Kaliora, F. Marantidou, and D.P. Panagiotakos, *Intake of ω-3 polyunsaturated fatty acids in patients with rheumatoid arthritis: A systematic review and meta-analysis.* Nutrition, 2018. **45**: p. 114-124. e4.

402. Ruggiero, C., et al., *Ω-3 polyunsaturated fatty acids and immune-mediated diseases: inflammatory bowel disease and rheumatoid arthritis.* Current pharmaceutical design, 2009. **15**(36): p. 4135-4148.

403. Mukerjee, S., A.S. Saeedan, M.N. Ansari, and M. Singh, *Polyunsaturated fatty acids mediated regulation of membrane biochemistry and tumor cell membrane integrity.* Membranes, 2021. **11**(7): p. 479.

404. Curtis, C.L., et al., *Effects of n-3 fatty acids on cartilage metabolism.* Proceedings of the Nutrition Society, 2002. **61**(3): p. 381-389.

405. Curtis, C.L., et al., *Pathologic indicators of degradation and inflammation in human osteoarthritic cartilage are abrogated by exposure to n-3 fatty acids.* Arthritis & Rheumatism: Official Journal of the American College of Rheumatology, 2002. **46**(6): p. 1544-1553.

406. Romero, L.O., et al., *A dietary fatty acid counteracts neuronal mechanical sensitization.* Nature communications, 2020. **11**(1): p. 2997.

407. Bedingfield, S.K., et al., *Top-down fabricated microplates for prolonged, intra-articular matrix metalloproteinase 13 siRNA nanocarrier delivery to reduce post-traumatic osteoarthritis.* ACS nano, 2021. **15**(9): p. 14475-14491.

408. Han, P.-f., et al., *Contribution of IL-1β, 6 and TNF-α to the form of post-traumatic osteoarthritis induced by "idealized" anterior cruciate ligament reconstruction in a porcine model.* International immunopharmacology, 2018. **65**: p. 212-220.

409. Lieberthal, J., N. Sambamurthy, and C.R. Scanzello, *Inflammation in joint injury and post-traumatic osteoarthritis.* Osteoarthritis and cartilage, 2015. **23**(11): p. 1825-1834.

410. Akkiraju, H. and A. Nohe, *Role of chondrocytes in cartilage formation, progression of osteoarthritis and cartilage regeneration.* Journal of developmental biology, 2015. **3**(4): p. 177-192.

411. Buckwalter, J.A., H.J. Mankin, and A.J. Grodzinsky, *Articular cartilage and osteoarthritis.* Instructional Course Lectures-American Academy of Orthopaedic Surgeons, 2005. **54**: p. 465.

412. Goldring, S.R. and M.B. Goldring, *Changes in the osteochondral unit during osteoarthritis: structure, function and cartilage–bone crosstalk.* Nature Reviews Rheumatology, 2016. **12**(11): p. 632-644.

413. Sharma, A.R., S. Jagga, S.-S. Lee, and J.-S. Nam, *Interplay between cartilage and subchondral bone contributing to pathogenesis of osteoarthritis.* International journal of molecular sciences, 2013. **14**(10): p. 19805-19830.

414. Ghosh, P., *The role of hyaluronic acid (hyaluronan) in health and disease: interactions with cells, cartilage and components of synovial fluid.* Clinical and experimental rheumatology, 1994. **12**(1): p. 75-82.

415. Goldring, M.B. and M. Otero, *Inflammation in osteoarthritis.* Current opinion in rheumatology, 2011. **23**(5): p. 471.

416. Haraden, C.A., et al., *Synovial fluid biomarkers associated with osteoarthritis severity reflect macrophage and neutrophil related inflammation.* Arthritis research & therapy, 2019. **21**(1): p. 1-9.

417. De Lange-Brokaar, B.J., et al., *Synovial inflammation, immune cells and their cytokines in osteoarthritis: a review.* Osteoarthritis and cartilage, 2012. **20**(12): p. 1484-1499.

418. Sanchez-Lopez, E., et al., *Synovial inflammation in osteoarthritis progression.* Nature Reviews Rheumatology, 2022. **18**(5): p. 258-275.

419. Du, G., et al., *Abnormal mechanical loading induces cartilage degeneration by accelerating meniscus hypertrophy and mineralization after ACL injuries in vivo.* The American journal of sports medicine, 2016. **44**(3): p. 652-663.

420. Jørgensen, A.E.M., M. Kjær, and K.M. Heinemeier, *The effect of aging and mechanical loading on the metabolism of articular cartilage.* The Journal of rheumatology, 2017. **44**(4): p. 410-417.

421. Nicodemus, G. and S. Bryant, *Mechanical loading regimes affect the anabolic and catabolic activities by chondrocytes encapsulated in PEG hydrogels.* Osteoarthritis and cartilage, 2010. **18**(1): p. 126-137.

422. Takahashi, I., T. Matsuzaki, H. Kuroki, and M. Hoso, *Disuse atrophy of articular cartilage induced by unloading condition accelerates histological progression of osteoarthritis in a post-traumatic rat model.* Cartilage, 2021. **13**(2_suppl): p. 1522S-1529S.

423. Racine, J. and R.K. Aaron, *Post-traumatic osteoarthritis after ACL injury.* RI Med J, 2014. **97**(11): p. 25-28.

424. Wang, L.-J., et al., *Post-traumatic osteoarthritis following ACL injury.* Arthritis research & therapy, 2020. **22**(1): p. 1-8.

425. Whittaker, J.L. and E.M. Roos, *A pragmatic approach to prevent post-traumatic osteoarthritis after sport or exercise-related joint injury.* Best Practice & Research Clinical Rheumatology, 2019. **33**(1): p. 158-171.

426. Michlovitz, S.L., B.A. Harris, and M.P. Watkins, *Therapy interventions for improving joint range of motion: a systematic review.* Journal of Hand Therapy, 2004. **17**(2): p. 118-131.

427. Sok, D., et al., *NSAIDs Reduce Therapeutic Efficacy of Mesenchymal Stromal Cell Therapy in a Rodent Model of Posttraumatic Osteoarthritis.* The American Journal of Sports Medicine, 2022. **50**(5): p. 1389-1398.

428. Deloney, M., et al., *Hyaluronic Acid-Binding, Anionic, Nanoparticles Inhibit ECM Degradation and Restore Compressive Stiffness in Aggrecan-Depleted Articular Cartilage Explants.* Pharmaceutics, 2021. **13**(9): p. 1503.

429. Faust, H.J., et al., *A hyaluronic acid binding peptide-polymer system for treating osteoarthritis.* Biomaterials, 2018. **183**: p. 93-101.

430. Huebner, K.D., N.G. Shrive, and C.B. Frank, *Dexamethasone inhibits inflammation and cartilage damage in a new model of post-traumatic osteoarthritis.* Journal of orthopaedic research, 2014. **32**(4): p. 566-572.

431. Lützner, C., et al., *Total knee arthroplasty in post-traumatic osteoarthritis is more challenging, but results in similar patient satisfaction–An analysis of 1646 cases.* The Knee, 2022. **39**: p. 116-123.

432. Murtha, A.S., A.E. Johnson, J.A. Buckwalter, and J.C. Rivera, *Total knee arthroplasty for posttraumatic osteoarthritis in military personnel under age 50.* Journal of Orthopaedic Research, 2017. **35**(3): p. 677-681.

433. Sanchis-Alfonso, V. and J.L. Koh, *Joint-preserving osteotomies for isolated patellofemoral osteoarthritis: alternatives to arthroplasty.* American journal of orthopedics (Belle Mead, NJ), 2017. **46**(3): p. 139-145.

434. Scott, C., et al., *Total knee arthroplasty following tibial plateau fracture: a matched cohort study.* The Bone & Joint Journal, 2015. **97**(4): p. 532-538.

435. Vasso, M., et al., *Intraarticular injection of microfragmented adipose tissue plus arthroscopy in isolated primary patellofemoral osteoarthritis is clinically effective and not affected by age, BMI, or stage of osteoarthritis.* Journal of Orthopaedics and Traumatology, 2022. **23**(1): p. 1-10.

436. Goldring, M., *Potential Mechanisms of PTOA: Inflammation In: Olson SA, Guilak F, editors. Post-Traumatic Arthritis: Pathogenesis, Diagnosis and Treatment*. 2015, New York: Springer.

437. Olson, S.A. and F. Guilak, *Arthritis that develops after joint injury: Is it post-traumatic arthritis or post-traumatic osteoarthritis?* Post-Traumatic Arthritis: Pathogenesis, Diagnosis and Management, 2015: p. 3-6.

438. Guilak, F. and C.T. Hung, *Physical regulation of cartilage metabolism.* Basic Orthopaedic Biomechanics. Philadelphia: Lippincott-Raven, 2005: p. 259-300.

439. Armstrong, C. and V.C. Mow, *Variations in the intrinsic mechanical properties of human articular cartilage with age, degeneration, and water content.* JBJS, 1982. **64**(1): p. 88-94.

440. Ateshian, G.A., *The role of interstitial fluid pressurization in articular cartilage lubrication.* Journal of biomechanics, 2009. **42**(9): p. 1163-1176.

441. Park, S., R. Krishnan, S.B. Nicoll, and G.A. Ateshian, *Cartilage interstitial fluid load support in unconfined compression.* Journal of biomechanics, 2003. **36**(12): p. 1785-1796.

442. Soltz, M.A. and G.A. Ateshian, *Interstitial fluid pressurization during confined compression cyclical loading of articular cartilage.* Annals of biomedical engineering, 2000. **28**: p. 150-159.

443. Mow, V., N. Bachrach, L. Setton, and F. Guilak, *Stress, strain, pressure and flow fields in articular cartilage and chondrocytes*, in *Cell mechanics and cellular engineering*. 1994, Springer. p. 345-379.

444. Hodge, W., et al., *Contact pressures in the human hip joint measured in vivo.* Proceedings of the National Academy of Sciences, 1986. **83**(9): p. 2879-2883.

445. Krishnan, R., M. Kopacz, and G.A. Ateshian, *Experimental verification of the role of interstitial fluid pressurization in cartilage lubrication.* Journal of orthopaedic research, 2004. **22**(3): p. 565-570.

446. Bachrach, N.M., V.C. Mow, and F. Guilak, *Incompressibility of the solid matrix of articular cartilage under high hydrostatic pressures.* Journal of biomechanics, 1998. **31**(5): p. 445-451.

447. Angele, P., et al., *Cyclic hydrostatic pressure enhances the chondrogenic phenotype of human mesenchymal progenitor cells differentiated in vitro.* Journal of orthopaedic research, 2003. **21**(3): p. 451-457.

448. Finger, A.R., et al., *Differential effects on messenger ribonucleic acid expression by bone marrow–derived human mesenchymal stem cells seeded in agarose constructs due to ramped and steady applications of cyclic hydrostatic pressure.* Tissue engineering, 2007. **13**(6): p. 1151-1158.

449. Nordberg, R.C., J.C. Bodle, and E.G. Loboa, *Mechanical stimulation of adipose-derived stem cells for functional tissue engineering of the musculoskeletal system via cyclic hydrostatic pressure, simulated microgravity, and cyclic tensile strain.* Adipose-Derived Stem Cells: Methods and Protocols, 2018: p. 215-230.

450. Pattappa, G., et al., *Cells under pressure–the relationship between hydrostatic pressure and mesenchymal stem cell chondrogenesis.* eCells & Materials, 2019. **2019**(37): p. 360-381.

451. Puetzer, J., et al., *The effects of cyclic hydrostatic pressure on chondrogenesis and viability of human adipose-and bone marrow-derived mesenchymal stem cells in three-dimensional agarose constructs.* Tissue Engineering Part A, 2013. **19**(1-2): p. 299-306.

452. Hodder, E., F. Guppy, D. Covill, and P. Bush, *The effect of hydrostatic pressure on proteoglycan production in articular cartilage in vitro: a meta-analysis.* Osteoarthritis and Cartilage, 2020. **28**(8): p. 1007-1019.

453. Kawanishi, M., et al., *Redifferentiation of dedifferentiated bovine articular chondrocytes enhanced by cyclic hydrostatic pressure under a gas-controlled system.* Tissue engineering, 2007. **13**(5): p. 957-964.

454. Miyanishi, K., et al., *Dose-and time-dependent effects of cyclic hydrostatic pressure on transforming growth factor-β3-induced chondrogenesis by adult human mesenchymal stem cells in vitro.* Tissue engineering, 2006. **12**(8): p. 2253-2262.

455. Hall, A., J. Urban, and K. Gehl, *The effects of hydrostatic pressure on matrix synthesis in articular cartilage.* Journal of orthopaedic research, 1991. **9**(1): p. 1-10.

456. Phan, M.N., et al., *Functional characterization of TRPV4 as an osmotically sensitive ion channel in porcine articular chondrocytes.* Arthritis & Rheumatism: Official Journal of the American College of Rheumatology, 2009. **60**(10): p. 3028-3037.

457. Qian, N., et al., *TRPM7 channels mediate spontaneous Ca2+ fluctuations in growth plate chondrocytes that promote bone development.* Science Signaling, 2019. **12**(576): p. eaaw4847.

458. Sambale, M., J. Intemann, T. Pap, and J. Sherwood, *A homeostatic role for transient receptor potential cation channel (TRPC1) in articular cartilage.* Osteoarthritis and Cartilage, 2019. **27**: p. S175.

459. Sherwood, J., et al., *Activation of the transient receptor potential cation channel TRPC6 is required for chondrocyte phenotypic stability.* Osteoarthritis and Cartilage, 2016. **24**: p. S152-S153.

460. Szűcs Somogyi, C., et al., *Polymodal transient receptor potential vanilloid (TRPV) ion channels in chondrogenic cells.* International journal of molecular sciences, 2015. **16**(8): p. 18412-18438.

461. 正木勉, *Molecular Medicine Reports.* (No Title).

462. Nims, R.J., et al., *Matrix production in large engineered cartilage constructs is enhanced by nutrient channels and excess media supply.* Tissue Engineering Part C: Methods, 2015. **21**(7): p. 747-757.

463. Cui, M., et al., *TRPV1 receptors in the CNS play a key role in broad-spectrum analgesia of TRPV1 antagonists.* Journal of Neuroscience, 2006. **26**(37): p. 9385-9393.

464. Kanju, P., et al., *Small molecule dual-inhibitors of TRPV4 and TRPA1 for attenuation of inflammation and pain.* Scientific reports, 2016. **6**(1): p. 26894.

465. Koenig, S., et al., *A TRPC3 blocker, ethyl-1-(4-(2, 3, 3-trichloroacrylamide) phenyl)-5-(trifluoromethyl)-1H-pyrazole-4-carboxylate (Pyr3), prevents stent-induced arterial remodeling.* Journal of Pharmacology and Experimental Therapeutics, 2013. **344**(1): p. 33-40.

466. Paez, P.M., et al., *Modulation of canonical transient receptor potential channel 1 in the proliferation of oligodendrocyte precursor cells by the golli products of the myelin basic protein gene.* Journal of Neuroscience, 2011. **31**(10): p. 3625-3637.

467. Farndale, R.W., D.J. Buttle, and A.J. Barrett, *Improved quantitation and discrimination of sulphated glycosaminoglycans by use of dimethylmethylene blue.* Biochimica et Biophysica Acta (BBA)-General Subjects, 1986. **883**(2): p. 173-177.

468. Nims, R.J., et al., *Synthesis rates and binding kinetics of matrix products in engineered cartilage constructs using chondrocyte-seeded agarose gels.* Journal of biomechanics, 2014. **47**(9): p. 2165-2172.

469. Parkkinen, J., et al., *Effects of cyclic hydrostatic pressure on proteoglycan synthesis in cultured chondrocytes and articular cartilage explants.* Archives of biochemistry and biophysics, 1993. **300**(1): p. 458-465.

470. Jortikka, M.O., et al., *The role of microtubules in the regulation of proteoglycan synthesis in chondrocytes under hydrostatic pressure.* Archives of biochemistry and biophysics, 2000. **374**(2): p. 172-180.

471. Elder, B.D. and K.A. Athanasiou, *Synergistic and additive effects of hydrostatic pressure and growth factors on tissue formation.* PloS one, 2008. **3**(6): p. e2341.

472. Elder, B.D. and K.A. Athanasiou, *Effects of temporal hydrostatic pressure on tissue-engineered bovine articular cartilage constructs.* Tissue engineering Part A, 2009. **15**(5): p. 1151-1158.

473. Elder, S., K. Fulzele, and W. McCulley, *Cyclic hydrostatic compression stimulates chondroinduction of C3H/10T1/2 cells.* Biomechanics and modeling in mechanobiology, 2005. **3**: p. 141-146.

474. Ikenoue, T., et al., *Mechanoregulation of human articular chondrocyte aggrecan and type II collagen expression by intermittent hydrostatic pressure in vitro.* Journal of orthopaedic research, 2003. **21**(1): p. 110-116.

475. Lammi, M.J., et al., *Expression of reduced amounts of structurally altered aggrecan in articular cartilage chondrocytes exposed to high hydrostatic pressure.* Biochemical Journal, 1994. **304**(3): p. 723-730.

476. Luo, Z. and B. Seedhom, *Light and low-frequency pulsatile hydrostatic pressure enhances extracellular matrix formation by bone marrow mesenchymal cells: an in-vitro study with special reference to cartilage repair.* Proceedings of the Institution of Mechanical Engineers, Part H: Journal of Engineering in Medicine, 2007. **221**(5): p. 499-507.

477. Miyanishi, K., et al., *Effects of hydrostatic pressure and transforming growth factor-β 3 on adult human mesenchymal stem cell chondrogenesis in vitro.* Tissue engineering, 2006. **12**(6): p. 1419-1428.

478. Nakamura, S., et al., *Hydrostatic pressure induces apoptosis of chondrocytes cultured in alginate beads.* Journal of orthopaedic research, 2006. **24**(4): p. 733-739.

479. Nordberg, R.C., et al., *LRP receptors in chondrocytes are modulated by simulated microgravity and cyclic hydrostatic pressure.* PloS one, 2019. **14**(10): p. e0223245.

480. Parkkinen, J.J., et al., *Influence of short-term hydrostatic pressure on organization of stress fibers in cultured chondrocytes.* Journal of orthopaedic research, 1995. **13**(4): p. 495-502.

481. Parkkinen, J.J., et al., *Altered Golgi apparatus in hydrostatically loaded articular cartilage chondrocytes.* Annals of the rheumatic diseases, 1993. **52**(3): p. 192-198.

482. Smith, R.L., et al., *In vitro stimulation of articular chondrocyte mRNA and extracellular matrix synthesis by hydrostatic pressure.* Journal of orthopaedic research, 1996. **14**(1): p. 53-60.

483. Smith, R.L., et al., *Time-dependent effects of intermittent hydrostatic pressure on articular c on rocyte type II collagen and aggrecan mRNA expression.* J. Rehabil. Res. Dev, 2000. **37**: p. 153-161.

484. Suh, J.-K., et al., *Intermittent sub-ambient interstitial hydrostatic pressure as a potential mechanical stimulator for chondrocyte metabolism.* Osteoarthritis and Cartilage, 1999. **7**(1): p. 71-80.

485. Toyoda, T., B.B. Seedhom, J. Kirkham, and W.A. Bonass, *Upregulation of aggrecan and type II collagen mRNA expression in bovine chondrocytes by the application of hydrostatic pressure.* Biorheology, 2003. **40**(1, 2, 3): p. 79-85.

486. Toyoda, T., et al., *Hydrostatic pressure modulates proteoglycan metabolism in chondrocytes seeded in agarose.* Arthritis & Rheumatism, 2003. **48**(10): p. 2865-2872.

487. Xu, T., G. Xu, Z. Gu, and H. Wu, *Role of endoplasmic reticulum stress pathway in hydrostatic pressure-induced apoptosis in rat mandibular condylar chondrocytes.* Molecular and cellular biochemistry, 2017. **429**: p. 23-31.

488. Caterina, M.J., et al., *The capsaicin receptor: a heat-activated ion channel in the pain pathway.* Nature, 1997. **389**(6653): p. 816-824.

489. Grundy, L., et al., *TRPV1 enhances the afferent response to P2X receptor activation in the mouse urinary bladder.* Scientific reports, 2018. **8**(1): p. 197.

490. Ohtsuki, T., et al., *Mechanical strain attenuates cytokine-induced ADAMTS9 expression via transient receptor potential vanilloid type 1.* Experimental cell research, 2019. **383**(2): p. 111556.

491. Sappington, R.M., et al., *Activation of transient receptor potential vanilloid-1 (TRPV1) influences how retinal ganglion cell neurons respond to pressure-related stress.* Channels, 2015. **9**(2): p. 102-113.

492. Zhao, R., et al., *Cell sensing and decision-making in confinement: The role of TRPM7 in a tug of war between hydraulic pressure and cross-sectional area.* Science advances, 2019. **5**(7): p. eaaw7243.

493. Solis, A.G., et al., *Mechanosensation of cyclical force by PIEZO1 is essential for innate immunity.* Nature, 2019. **573**(7772): p. 69-74.

494. Knight, M., T. Toyoda, D. Lee, and D. Bader, *Mechanical compression and hydrostatic pressure induce reversible changes in actin cytoskeletal organisation in chondrocytes in agarose.* Journal of biomechanics, 2006. **39**(8): p. 1547-1551.

495. Mizuno, S., *A novel method for assessing effects of hydrostatic fluid pressure on intracellular calcium: a study with bovine articular chondrocytes.* American Journal of Physiology-Cell Physiology, 2005. **288**(2): p. C329-C337.

496. Pountos, I. and P.V. Giannoudis, *Modulation of cartilage's response to injury: can chondrocyte apoptosis be reversed?* Injury, 2017. **48**(12): p. 2657-2669.

497. Ateshian, G.A., K.D. Costa, and C.T. Hung, *A theoretical analysis of water transport through chondrocytes.* Biomechanics and modeling in mechanobiology, 2007. **6**(1-2): p. 91-101.

498. Eleswarapu, S.V., N.D. Leipzig, and K.A. Athanasiou, *Gene expression of single articular chondrocytes.* Cell and tissue research, 2007. **327**(1): p. 43-54.

499. Han, S.-K., R. Madden, Z. Abusara, and W. Herzog, *In situ chondrocyte viscoelasticity.* Journal of biomechanics, 2012. **45**(14): p. 2450-2456.

500. Koay, E.J., G. Ofek, and K.A. Athanasiou, *Effects of TGF-β1 and IGF-I on the compressibility, biomechanics, and strain-dependent recovery behavior of single chondrocytes.* Journal of biomechanics, 2008. **41**(5): p. 1044-1052.

501. Koay, E.J., A.C. Shieh, and K.A. Athanasiou, *Creep indentation of single cells.* J. Biomech. Eng., 2003. **125**(3): p. 334-341.

502. Lee, J.K., et al., *Tension stimulation drives tissue formation in scaffold-free systems.* Nature materials, 2017. **16**(8): p. 864-873.

503. Leipzig, N.D. and K.A. Athanasiou, *Static compression of single chondrocytes catabolically modifies single-cell gene expression.* Biophysical journal, 2008. **94**(6): p. 2412-2422.

504. Ofek, G., et al., *Biomechanics of single chondrocytes under direct shear.* Biomechanics and modeling in mechanobiology, 2010. **9**: p. 153-162.

505. Ofek, G., R.M. Natoli, and K.A. Athanasiou, *In situ mechanical properties of the chondrocyte cytoplasm and nucleus.* Journal of biomechanics, 2009. **42**(7): p. 873-877.

506. Ofek, G., D.C. Wiltz, and K.A. Athanasiou, *Contribution of the cytoskeleton to the compressive properties and recovery behavior of single cells.* Biophysical journal, 2009. **97**(7): p. 1873-1882.

507. Shieh, A. and K. Athanasiou, *Dynamic compression of single cells.* Osteoarthritis and cartilage, 2007. **15**(3): p. 328-334.

508. Shieh, A.C. and K.A. Athanasiou, *Principles of cell mechanics for cartilage tissue engineering.* Annals of biomedical engineering, 2003. **31**: p. 1-11.

509. Shieh, A.C., E.J. Koay, and K.A. Athanasiou, *Strain-dependent recovery behavior of single chondrocytes.* Biomechanics and modeling in mechanobiology, 2006. **5**(2-3): p. 172-179.

510. Trickey, W.R., G.M. Lee, and F. Guilak, *Viscoelastic properties of chondrocytes from normal and osteoarthritic human cartilage.* Journal of Orthopaedic Research, 2000. **18**(6): p. 891-898.

511. Trickey, W.R., T.P. Vail, and F. Guilak, *The role of the cytoskeleton in the viscoelastic properties of human articular chondrocytes.* Journal of Orthopaedic Research, 2004. **22**(1): p. 131-139.

512. Van Donkelaar, C. and W. Wilson, *Mechanics of chondrocyte hypertrophy.* Biomechanics and modeling in mechanobiology, 2012. **11**: p. 655-664.

513. Guilak, F., G.R. Erickson, and H.P. Ting-Beall, *The effects of osmotic stress on the viscoelastic and physical properties of articular chondrocytes.* Biophysical journal, 2002. **82**(2): p. 720-727.

514. Nourse, J.L. and M.M. Pathak. *How cells channel their stress: Interplay between Piezo1 and the cytoskeleton*. in *Seminars in cell & developmental biology*. 2017. Elsevier.

515. Carpenter, E.P., K. Beis, A.D. Cameron, and S. Iwata, *Overcoming the challenges of membrane protein crystallography.* Current opinion in structural biology, 2008. **18**(5): p. 581-586.

516. Mang, T., S. Lindemann, and A. Gigout, *Increasing the medium osmolarity reduces the inflammatory status of human OA chondrocytes and increases their responsiveness to GDF-5.* International Journal of Molecular Sciences, 2020. **21**(2): p. 531.

517. Sieber, S., et al., *Importance of osmolarity and oxygen tension for cartilage tissue engineering.* BioResearch Open Access, 2020. **9**(1): p. 106-115.

518. Dalghi, M.G., et al., *Functional roles for PIEZO1 and PIEZO2 in urothelial mechanotransduction and lower urinary tract interoception.* JCI insight, 2021. **6**(19).

519. Parsonage, G., et al., *Improved PIEZO1 agonism through 4-benzoic acid modification of Yoda1.* British Journal of Pharmacology, 2023. **180**(16): p. 2039-2063.

520. Beech, D.J. and A.C. Kalli, *Force sensing by piezo channels in cardiovascular health and disease.* Arteriosclerosis, thrombosis, and vascular biology, 2019. **39**(11): p. 2228-2239.

521. Moo, E.K. and W. Herzog, *Unfolding of membrane ruffles of in situ chondrocytes under compressive loads.* Journal of Orthopaedic Research, 2017. **35**(2): p. 304-310.

522. Maas, S.A., B.J. Ellis, G.A. Ateshian, and J.A. Weiss, *FEBio: finite elements for biomechanics.* 2012.

523. Bush, P.G. and A.C. Hall, *Regulatory volume decrease (RVD) by isolated and in situ bovine articular chondrocytes.* Journal of cellular physiology, 2001. **187**(3): p. 304-314.

524. Bush, P.G. and A.C. Hall, *The osmotic sensitivity of isolated and in situ bovine articular chondrocytes.* Journal of Orthopaedic Research, 2001. **19**(5): p. 768-778.

525. Bush, P.G. and A.C. Hall, *The volume and morphology of chondrocytes within non-degenerate and degenerate human articular cartilage.* Osteoarthritis and cartilage, 2003. **11**(4): p. 242-251.

526. Bush, P.G., P.D. Hodkinson, G.L. Hamilton, and A.C. Hall, *Viability and volume of in situ bovine articular chondrocytes—changes following a single impact and effects of medium osmolarity.* Osteoarthritis and cartilage, 2005. **13**(1): p. 54-65.

527. Bush, P.G., C.A. Parisinos, and A.C. Hall, *The osmotic sensitivity of rat growth plate chondrocytes in situ; clarifying the mechanisms of hypertrophy.* Journal of cellular physiology, 2008. **214**(3): p. 621-629.

528. Martinac, B., *Mechanosensitive ion channels: molecules of mechanotransduction.* Journal of cell science, 2004. **117**(12): p. 2449-2460.

529. Fang, X.-Z., et al., *Structure, kinetic properties and biological function of mechanosensitive Piezo channels.* Cell & bioscience, 2021. **11**: p. 1-20.

530. Li, W., N. Gao, and M. Yang, *The structural basis for sensing by the Piezo1 protein.* Current Topics in Membranes, 2017. **79**: p. 135-158.

531. Evans, E.A., R. Waugh, and L. Melnik, *Elastic area compressibility modulus of red cell membrane.* Biophysical Journal, 1976. **16**(6): p. 585-595.

532. Moo, E.K., et al., *The properties of chondrocyte membrane reservoirs and their role in impact-induced cell death.* Biophysical journal, 2013. **105**(7): p. 1590-1600.

533. Erickson, G.R., L.G. Alexopoulos, and F. Guilak, *Hyper-osmotic stress induces volume change and calcium transients in chondrocytes by transmembrane, phospholipid, and G-protein pathways.* Journal of biomechanics, 2001. **34**(12): p. 1527-1535.

534. Lewis, R., C.H. Feetham, and R. Barrett-Jolley, *Cell volume regulation in chondrocytes.* Cellular Physiology and Biochemistry, 2011. **28**(6): p. 1111-1122.

535. Wang, Z., et al., *The rate of hypo-osmotic challenge influences regulatory volume decrease (RVD) and mechanical properties of articular chondrocytes.* Osteoarthritis and cartilage, 2015. **23**(2): p. 289-299.

536. Gottlieb, P.A. and F. Sachs, *Piezo1: properties of a cation selective mechanical channel.* Channels, 2012. **6**(4): p. 214-219.

537. Nilius, B., J. Prenen, and G. Owsianik, *Irritating channels: the case of TRPA1.* The Journal of physiology, 2011. **589**(7): p. 1543-1549.

538. Nilius, B., et al., *TRPV4 calcium entry channel: a paradigm for gating diversity.* American Journal of Physiology-Cell Physiology, 2004. **286**(2): p. C195-C205.

539. Nilius, B., H. Watanabe, and J. Vriens, *The TRPV4 channel: structure-function relationship and promiscuous gating behaviour.* Pflügers Archiv, 2003. **446**: p. 298-303.

540. Argote, P.F., et al., *Chondrocyte viability is lost during high-rate impact loading by transfer of amplified strain, but not stress, to pericellular and cellular regions.* Osteoarthritis and cartilage, 2019. **27**(12): p. 1822-1830.

541. Guilak, F., A. Ratcliffe, and V.C. Mow, *Chondrocyte deformation and local tissue strain in articular cartilage: a confocal microscopy study.* Journal of Orthopaedic Research, 1995. **13**(3): p. 410-421.

542. Amin, A.K., et al., *Osmolarity influences chondrocyte death in wounded articular cartilage.* JBJS, 2008. **90**(7): p. 1531-1542.

543. Berke, I.M., et al., *NF-κB-mediated effects on behavior and cartilage pathology in a non-invasive loading model of post-traumatic osteoarthritis.* Osteoarthritis and cartilage, 2021. **29**(2): p. 248-256.

544. Prince, D.E. and J.K. Greisberg, *Nitric oxide-associated chondrocyte apoptosis in trauma patients after high-energy lower extremity intra-articular fractures.* Journal of Orthopaedics and Traumatology, 2015. **16**: p. 335-341.

545. Buckwalter, J.A., et al., *The roles of mechanical stresses in the pathogenesis of osteoarthritis: implications for treatment of joint injuries.* Cartilage, 2013. **4**(4): p. 286-294.

546. Delco, M.L., E.D. Bonnevie, L.J. Bonassar, and L.A. Fortier, *Mitochondrial dysfunction is an acute response of articular chondrocytes to mechanical injury.* Journal of Orthopaedic Research®, 2018. **36**(2): p. 739-750.

547. Pritchard, S. and F. Guilak, *Effects of interleukin-1 on calcium signaling and the increase of filamentous actin in isolated and in situ articular chondrocytes.* Arthritis & Rheumatism: Official Journal of the American College of Rheumatology, 2006. **54**(7): p. 2164-2174.

548. Pritchard, S., B.J. Votta, S. Kumar, and F. Guilak, *Interleukin-1 inhibits osmotically induced calcium signaling and volume regulation in articular chondrocytes.* Osteoarthritis and cartilage, 2008. **16**(12): p. 1466-1473.

549. Guo, J., et al., *Trends in piezo channel research over the past decade: a bibliometric analysis.* Frontiers in Pharmacology, 2021. **12**: p. 668714.

550. Haliloglu, G., et al., *Recessive PIEZO2 stop mutation causes distal arthrogryposis with distal muscle weakness, scoliosis and proprioception defects.* Journal of human genetics, 2017. **62**(4): p. 497-501.

551. John, L., et al., *The Piezo1 cation channel mediates uterine artery shear stress mechanotransduction and vasodilation during rat pregnancy.* American Journal of Physiology-Heart and Circulatory Physiology, 2018. **315**(4): p. H1019-H1026.

552. Suchyna, T.M., *Piezo channels and GsMTx4: Two milestones in our understanding of excitatory mechanosensitive channels and their role in pathology.* Progress in biophysics and molecular biology, 2017. **130**: p. 244-253.

553. Lee, H.-p., R. Stowers, and O. Chaudhuri, *Volume expansion and TRPV4 activation regulate stem cell fate in three-dimensional microenvironments.* Nature communications, 2019. **10**(1): p. 529.

554. Liu, A., et al., *Tunable fast relaxation in imine-based nanofibrillar hydrogels stimulates cell response through TRPV4 activation.* Biomacromolecules, 2020. **21**(9): p. 3745-3755.

555. Gao, W., H. Hasan, D.E. Anderson, and W. Lee, *The role of mechanically-activated ion channels Piezo1, Piezo2, and TRPV4 in chondrocyte mechanotransduction and mechano-therapeutics for osteoarthritis.* Frontiers in Cell and Developmental Biology, 2022. **10**: p. 885224.

556. Liedtke, W., *TRPV4 plays an evolutionary conserved role in the transduction of osmotic and mechanical stimuli in live animals.* The Journal of physiology, 2005. **567**(1): p. 53-58.

557. Liedtke, W., *TRPV4 as osmosensor: a transgenic approach.* Pflügers Archiv, 2005. **451**: p. 176-180.

558. Liedtke, W., D.M. Tobin, C.I. Bargmann, and J.M. Friedman, *Mammalian TRPV4 (VR-OAC) directs behavioral responses to osmotic and mechanical stimuli in Caenorhabditis elegans.* Proceedings of the National Academy of Sciences, 2003. **100**(suppl_2): p. 14531-14536.

559. Curtis, C.L., et al., *n-3 fatty acids specifically modulate catabolic factors involved in articular cartilage degradation.* Journal of Biological Chemistry, 2000. **275**(2): p. 721-724.

560. Ibarguren, M., D.J. López, and P.V. Escribá, *The effect of natural and synthetic fatty acids on membrane structure, microdomain organization, cellular functions and human health.* Biochimica et Biophysica Acta (BBA)-Biomembranes, 2014. **1838**(6): p. 1518-1528.

561. Calder, P., *Polyunsaturated fatty acids and inflammation.* Biochemical Society Transactions, 2005. **33**(2): p. 423-427.

562. Calder, P. and R. Grimble, *Polyunsaturated fatty acids, inflammation and immunity.* European journal of clinical nutrition, 2002. **56**(3): p. S14-S19.

563. Calder, P.C., *Polyunsaturated fatty acids, inflammation, and immunity.* Lipids, 2001. **36**(9): p. 1007-1024.

564. Calder, P.C., *Polyunsaturated fatty acids and inflammation.* Prostaglandins, leukotrienes and essential fatty acids, 2006. **75**(3): p. 197-202.

565. Janssen, C.I. and A.J. Kiliaan, *Long-chain polyunsaturated fatty acids (LCPUFA) from genesis to senescence: the influence of LCPUFA on neural development, aging, and neurodegeneration.* Progress in lipid research, 2014. **53**: p. 1-17.

566. Petursdottir, A.L., et al., *Effect of dietary n-3 polyunsaturated fatty acids on brain lipid fatty acid composition, learning ability, and memory of senescence-accelerated mouse.* The Journals of Gerontology Series A: Biological Sciences and Medical Sciences, 2008. **63**(11): p. 1153-1160.

567. Shah, K., et al., *Calcium channels in the heart: Disease states and drugs.* Cells, 2022. **11**(6): p. 943.

568. Lee, S., *Pharmacological inhibition of voltage-gated Ca2+ channels for chronic pain relief.* Current neuropharmacology, 2013. **11**(6): p. 606-620.

569. Zamponi, G.W., et al., *Role of voltage-gated calcium channels in ascending pain pathways.* Brain research reviews, 2009. **60**(1): p. 84-89.

570. Srinivasan, P.P., et al., *Inhibition of T-type voltage sensitive calcium channel reduces load-induced OA in mice and suppresses the catabolic effect of bone mechanical stress on chondrocytes.* PLoS One, 2015. **10**(5): p. e0127290.

571. McTavish, D. and E.M. Sorkin, *Verapamil: An updated review of its pharmacodynamic and pharmacokinetic properties, and therapeutic use in hypertension.* Drugs, 1989. **38**(1): p. 19-76.

572. Sorkin, E., S. Clissold, and R. Brogden, *Nifedipine: a review of its pharmacodynamic and pharmacokinetic properties, and therapeutic efficacy, in ischaemic heart disease, hypertension and related cardiovascular disorders.* Drugs, 1985. **30**: p. 182-274.

573. Lee, J.-H., et al., *Cloning and expression of a novel member of the low voltage-activated T-type calcium channel family.* Journal of Neuroscience, 1999. **19**(6): p. 1912-1921.

574. Kohlmeier, K.A., et al., *Dual orexin actions on dorsal raphe and laterodorsal tegmentum neurons: noisy cation current activation and selective enhancement of Ca2+ transients mediated by L-type calcium channels.* Journal of neurophysiology, 2008. **100**(4): p. 2265-2281.

575. Rossier, M.F., M.M. Burnay, M.B. Vallotton, and A.M. Capponi, *Distinct functions of T- and L-type calcium channels during activation of bovine adrenal glomerulosa cells.* Endocrinology, 1996. **137**(11): p. 4817-4826.